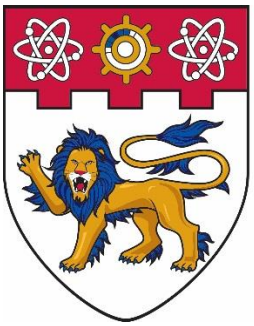

NANYANG TECHNOLOGICAL UNIVERSITY
SINGAPORE

LIGNOCELLULOSIC BIOMASS REFORM FOR CO-PRODUCING GREEN CHEMICALS AND GREEN HYDROGEN

LEE LI QUAN
Interdisciplinary Graduate Programme
AEBC/NEWRI
2023

LIGNOCELLULOSIC BIOMASS REFORM FOR CO-PRODUCING GREEN CHEMICALS AND GREEN HYDROGEN

LEE LI QUAN

Interdisciplinary Graduate Programme
AEBC/NEWRI

A thesis submitted to the Nanyang Technological University in partial fulfillment of the requirement for the degree of
Doctor of Philosophy

2023

Statement of Originality

I hereby certify that the work embodied in this thesis is the result of original research, is free of plagiarised materials, and has not been submitted for a higher degree to any other University or Institution.

26-Jul-2023

. . . . . .

Date

. . . . . .

Lee Li Quan

Supervisor Declaration Statement

I have reviewed the content and presentation style of this thesis and declare it is free of plagiarism and of sufficient grammatical clarity to be examined. To the best of my knowledge, the research and writing are those of the candidate except as acknowledged in the Author Attribution Statement. I confirm that the investigations were conducted in accord with the ethics policies and integrity standards of Nanyang Technological University and that the research data are presented honestly and without prejudice.

26-Jul-2023

. . . . . .

Date

. . . . . .

Assoc. Prof Li Hong

Authorship Attribution Statement

This thesis contains material from 2 papers published in the following peer-reviewed journal in which I am listed as an author.

Chapter 2 (Sections 2.5.1 to 2.5.3) is published as Li Quan Lee, Zi Iun Lai and Hong Li, Electroreforming of Biomass for Value-Added Products. *Micromachines* 12(11), 1405. (2021). DOI: 10.3390/mi12111405.

The contributions of the co-authors are as follows:

- Prof Li Hong offered the initial project guidance and revised the drafts of the manuscript.
- I prepared and revised the manuscript drafts together with Mr. Lai Zi Iun.

Chapter 3 is published as Li Quan Lee, Hu Zhao, Tian Yee Lim, Ge Junyu, Ovi Lian Ding, Wen Liu and Hong Li, Green Hydrogen Generation Assisted by Electroreforming of Raw Sugarcane Bagasse Waste. *Green Chemistry* 25(19), 7707-7720 (2023). DOI: 10.1039/D3GC01603J

The contributions of the co-authors are as follows:

- Prof Li Hong offered the initial project guidance and revised the drafts of the manuscript.
- I prepared the manuscript drafts with Dr Zhao Hu. Prof Liu and Dr Ding revised and reviewed the manuscript.
- I designed the study with Prof Li Hong and conducted the laboratory work at the School of Mechanical and Aerospace Engineering (MAE) and Advanced Environmental Biotechnology & Bioprocesses (AEBC) in Nanyang Environment and Water Research Institute (NEWRI). I also performed the data analysis.
- All product characterization, including sample preparation, was conducted by me in the AEBC lab at NEWRI and Nuclear Magnetic

Resonance (NMR) Facility at School of Chemistry, Chemical Engineering and Biotechnology (CCEB)

- Dr Zhao Hu assisted in Scanning electron microscopy (SEM), X-ray diffraction (XRD) and X-ray photoelectron (XPS) spectroscopies at Facility for Analysis, Characterization, Testing and Simulation (FACTS).
- Dr Ge Junyu assisted in Transmission electron microscopy (TEM) at FACTS.
- Mr Lim Tian Yee performed the life cycle assessment study under supervision of Prof Liu.

Chapter 4 is published as Li Quan Lee, Hu Zhao, Ge Junyu, Yan Zhou and Hong Li, Valorization of Paulownia wood to green chemicals and green hydrogen, *Accepted on 11-Dec-2023, Green Chemistry.* DOI: 10.1039/D3GC03458E

The contributions of the co-authors are as follows:

- Prof Li Hong offered the initial project guidance and revised the drafts of the manuscript.
- I prepared the manuscript drafts. Prof Zhou Yan and Dr Zhao Hu revised and reviewed the manuscript.
- I designed the study with Prof Li Hong and conducted the laboratory work at the School of Mechanical and Aerospace Engineering (MAE) and Advanced Environmental Biotechnology & Bioprocesses (AEBC) in Nanyang Environment and Water Research Institute (NEWRI). I also performed the data analysis.
- All product characterization, including sample preparation, was conducted by me in the AEBC lab at NEWRI and Nuclear Magnetic Resonance (NMR) Facility at School of Chemistry, Chemical Engineering and Biotechnology (CCEB)
- Dr Zhao Hu assisted in SEM, XRD and XPS spectroscopies at FACTS.
- Dr Ge Junyu assisted in TEM at FACTS.

26-Jul-2023

. . . . . .

Date

. . . . . .

Lee Li Quan

Acknowledgement

This Thesis would not have been possible without the assistance of the following individuals. I am very thankful and would like to express my sincere gratitude to them.

First, I would like to thank my supervisor, Assoc. Professor Li Hong, Colin for his guidance, patience, and support. I am very fortunate to be able to contribute and work on this project under the supervision of Professor Li. In addition, I would like to convey my gratitude to my Co-Supervisor, Assoc Prof. Zhou Yan and mentor, Assoc Prof. Su Pei-Chen as part of the thesis advisory committee as well as their valuable experience and insights.

Secondly, I am also grateful to my research group members for their guidance and assistance throughout my entire PhD journey - Dr. Zhao Hu, Dr. Koh See Wee, Dr. Ge Junyu, Mr. Fei Jipeng, Mr. Tan Jun Yan, Mr. Ao Qing Shuo, Dr. Ao Kelong, Dr. Sun Zi Xu, Dr. Hong Wei, Dr. Yao Mengqi, Ms. Li Ying and Mr. Li Chenchen. Furthermore, I would like to express gratitude towards the laboratory managers - Mr. Ho Kar Kiat and Ms. Juliana Sng from MAE innovation lab, Ms. Ong Qian Mei and Ms. Emily Mar'atusalihat from AEBC lab, NEWRI for their kind guidance on the operation of various equipment, safety guidance, resource arrangement and research assistance. I also want to acknowledge the FYP students that are also actively involved in part of the research project. I would also like to thank Ms Goh Ee Ling (CCBE) and the NEWRI analytic team (Dr. Lv Yunbo, Ms Lam Mei Shan, Mr. She Ka Keng and Ms Tan Kuan Yi) for their assistance in equipment training and guidance for product characterization tests.

This research would not been made possible if without the funding support from Agency for Science, Technology and Research (A*STAR) and the NTU research scholarship under NEWRI IGS-Sustainable Earth.

Finally, I would like to express my heartfelt appreciation to my family, friends, classmates and colleagues for their kind support and understanding during this period.

Table of Contents

Acknowledgement ..... **i**

Table of Contents ..... **ii**

Figure Captions ..... **v**

Table Captions ..... **x**

Abbreviations ..... **xi**

Abstract ..... **xiii**

Chapter 1: Introduction **1**

1.1 Challenges and strategies for efficient green sustainable hydrogen production 1

1.2 Raw fast-growing plant biomass reforming to value-added products 4

1.3 Motivation and objectives of thesis 8

1.4 Organization of Thesis 9

Chapter 2: Literature review **10**

2.1 Photosynthetic pathways of plants 10

2.1.1 Sugarcane and its chemical composition 12

2.1.2 Paulownia and its chemical composition 14

2.1.3 Cellulose 18

2.1.4 Hemicellulose 22

2.1.5 Lignin 23

2.2 Plant Biomass Pretreatment methods 25

2.2.1 Physical 28

2.2.2 Biological 30

2.2.3 Other solvent(s)/methods 30

2.2.4 Combinational methods 33

2.2.4.1 Catalytic Mechanochemical 33

2.2.4.2 Thermochemical 37

2.2.4.3 Microwave-assisted dilute acid hydrothermal 43

2.3 Water Electrolysis 46

2.4 Hybrid electrolysis 49

2.5 Electroforming of lignocellulosic biomass 51

2.5.1 Electroreforming at the anode 57

2.5.1.1 Cellulose 57

2.5.1.2 Glucose 62

2.5.1.3 Other Biomass Derivatives 67

2.5.2 Electroreforming at cathode 71

2.5.3 Evolution of Hydrogen Coupled with Biomass Electroreforming 71
2.5.3.1 Glucose Electrooxidation Coupled with Green Hydrogen Generation 72
2.5.3.2 5-HMF Electrooxidation Coupled with Green Hydrogen Generation 77
2.6 Perspectives and research gaps 80
Chapter 3: Raw biomass electroreforming to formic acid 84
3.1 Experimental section 86
3.1.1 Materials 86
3.1.2 Synthesis of electrocatalysts 86
3.1.3 Pretreatment of sugarcane bagasse waste 87
3.1.4 Electrochemical reforming of HSCB and sugars/organic acids 88
3.1.5 Solar-driven Electrooxidation of HSCB 90
3.1.6 SCB and electrocatalyst characterization 90
3.1.7 Product analysis 91
3.1.8 Life cycle assessment 93
3.2 Results and discussion 96
3.2.1 Preparation of the anode and cathode 96
3.2.2 Pretreatment and electrooxidation of SCB 105
3.2.3 Electrooxidation of mono/disaccharides and intermediates 115
3.2.4 Solar-driven electroreforming of HSCB 126
3.2.5 Life cycle assessment 128
3.3 Summary 131
Chapter 4: Valorization of Paulownia wood to valuable green chemicals 133
4.1 Experimental section 136
4.1.1 Materials 136
4.1.2 Pretreatment of Paulownia wood 137
4.1.3 Thermo-alkaline treatment of HPW and sugars to lactate 139
4.1.4 Electroforming of HPW to formate 139
4.1.5 Solar-driven Electrooxidation of HPW 140
4.1.6 Paulownia wood and electrocatalyst characterization 140
4.1.7 Product analysis 141
4.2 Results and discussion 144
4.2.1 Pretreatment of Paulownia wood to sugar 144
4.2.2 Thermo-alkaline treatment to lactate 156
4.2.3 Electroreforming to Formate 160
4.2.4 Solar-driven electroreforming of HPW 167
4.3 Summary 169
4.4 Effect of CNT on microwave-assisted hydrothermal for cellulose conversion to glucose 170

Chapter 5: Overall outlook and future work 173
5.1 Overall outlook 173
5.2 Recommendations for future work..... 176
References..... 181

Figure Captions

Figure 1 Global sugarcane and sugarcane bagasse production in 2020. Top 7 countries and Southeast Asia with their – (a) sugarcane production and (b) estimated sugarcane humid bagasse waste generated. 4
Figure 2 Global Distribution of Paulownia Trees. (Highlighted regions in orange). 7
Figure 3 Comparison between plant and man-made pillar structures. 15
Figure 4 Simplified diagram of plant cell wall structure. (a) Middle lamella, primary and secondary wall (b) Primary wall layer, (c) Secondary wall layer. 16
Figure 5 Simplified 2D representation of cell wall composition of Non-grass Angiosperms. 17
Figure 6 (a) Chemical structure of cellulose consists of cellobiose with reducing and nonreducing ends (b) crystalline and amorphous regions in cellulose microfibrils. 20
Figure 7 Chemical structure of glucuronoxylan. 23
Figure 8 Chemical structure of lignin from Beech. 23
Figure 9 Primary precursors of lignin – (a) p-coumaryl alcohol, (b) coniferyl alcohol, and (c) sinapyl alcohol. 25
Figure 10 Role of mechanical treatment for lignocellulosic polymers. 29
Figure 11 (a) Heating profiles in conventional and microwave heating. Microwave-assisted continuous-flow reactor – (b) experimental setup, and (c) schematic illustration. 44
Figure 12 Three types of water electrolysis systems and their operating principles. 47
Figure 13 (a) Mechanism of HER and, (b) OER electrocatalysis in alkaline media. 49
Figure 14 Anodic reaction of specific organics to value-added chemicals with their LSV plots of Ni_2S_2/NF at scan rate of 2 mV s^{-1} in 1 M KOH with/without 10 mM organic species 51
Figure 15 General mechanism of electron transfer for organic transformation and substrate oxidation equations. 53
Figure 16 Cellulose, glucose and its derivatives. 56
Figure 17 (a) Microscopic images before (i) and after (ii) dissolution. (b) X-ray diffraction of cellulose before (i) and after (ii) dissolution. (c) cyclic voltammogram (vs. Ag/AgCl) of cellulose ball milled to average particle size of 100 nm (i), 500 nm (ii) (e) FTIR scans of cellulose before dissolution (i), after dissolution (ii) and after oxidation (iii). 58
Figure 18 Proposed cellulose oxidation mechanism on electrode surface in alkali media in CV cycle. 59
Figure 19 (a) SEM image of pretreated CA. (b) SEM of 10 nm Au/CA. (c) Magnified SEM of 10 nm Au/CA. (d) XRD results of 10 nm Au/CA and 50 nm Au/CA electrodes. (e) High performance liquid chromatography results of products using 10 nm Au/CA electrodes. 60
Figure 20 (a) CVs (vs. SCE) of 0.5 M sulfuric acid (i) and 0.5 M sulfuric acid with 10 g L^{-1} cellulose (ii). (b) Decrease in DP over time at 30 mA cm^{-2}. (c) Decrease in DP over time without applied current 62
Figure 21 Proposed cellulose depolymerization mechanism in acidic media. 62
Figure 22 Nano MnO_2/Ti electrocatalysts in flow-through cells for glucaric acid (GA) and gluconic acid (GLA) production from glucose. 64
Figure 23 (a) TEM image of AuNP capped with decanethiolate monolayer shell (for deposition on electrode). (b) Change in current ratios across time with gold nanoparticles in alkali medium (i), bulk gold in alkali medium (ii), gold nanoparticles in neutral medium (iv). (c) Plots of electrolysis products with 2 nm AuNP in 0.1 M NaOH, 0.01 M glucose, at different potentials (vs. Ag/AgCl); total current efficiency of all products (i), gluconolactone (ii), oxalate (iii), glyconate (iv), formate (v). 67

Figure 24 (a) LSV scan in 2-electrode cell without and with 0.5 M glucose in 10 M KOH, iron phosphide anode. (b) Amount of hydrogen theoretically calculated and collected at 1.9 V, 10 M KOH with and without 0.5 M glucose. 72
Figure 25 (a) TEM of Pd_3Au_7/C (b) SEM of Co-Ni alloy. (c) SEM of $Co_{0.5}$ $Ni_{0.5}(OH)_2$. (d) SEM of Ni-MoS_2. 74
Figure 26 (a) SEM image of $Fe_{0.1}CoSe_2$/CC. (b) LSV for anodic glucose oxidation, 1 M KOH, 0.5 M glucose with different electrodes. (c) LSV for cathodic hydrogen evolution, 0.5 M H_2SO_4. 76
Figure 27 (a) SEM image of carbon pellet. (b) Hydrogen production over days, from carbon oxidation contribution (COC) or oxygen evolution, with a carbon electrode. (c) Hydrogen production under similar conditions with a nitrogen-doped carbon electrode. 76
Figure 28 Schematic diagram of coupled formate and green hydrogen generation from raw sugarcane bagasse. 85
Figure 29 (a) LSV of nickel foam (Ni-F), cobalt foam (Co-F), iron foam (Fe-F) and *hp*-Ni in HSCB. Bare Ni Foam (b) SEM image, (c) zoom-in SEM image of region in image (b). *hp*-Ni (d) SEM image, (e) zoom-in SEM image of region in image (d). (f) XRD of *hp*-Ni After 12 hours. glucose electrooxidation (red), as synthesized (green) and cubic Ni standard from JCPDS card No. 0004-0850 (black). 96
Figure 30 *hp*-Ni – (a) SEM image used for EDS analysis; *hp*-Ni EDS – (b) combined layered image of the detected elements, (c) oxygen element mapping image, (d) nickel element mapping image, (e) EDS spectrum of area in image (a). XPS spectra of (f) full survey spectra, (g) Ni 2p states, and (h) O 1s states of As synthesized *hp*-Ni electrode after activation (black spectra) and Post EO HSCB for 4 h at 1.58 V vs RHE. (red spectra). 98
Figure 31 HR-TEM images of nanoparticles from (a) As synthesized *hp*-Ni, showing the d-spacing of 0.206 and 0.167 nm of fcc Ni (111) and (200) planes, respectively. The d-spacing of 0.221 nm corresponds to NiO (111) plane; (b) Post EO HSCB *hp*-Ni, showing the d-spacing of 0.209 and 0.230 nm of NiOOH (105) and $Ni(OH)_2$ (111) planes, respectively. 100
Figure 32 LSV of Bare NF (black curve) vs *hp*-Ni (blue curve) – (a) in 1 M KOH (b) with addition of 0.1 M Glucose; and (c) their corresponding Tafel slopes in HSCB. 101
Figure 33 Electrochemical active surface area measurements. CV curves of – (a) Ni-F, (b) Fe-F, (c) Co-F, and (d) *hp*-Ni collected in 1.0 M KOH solution at the non-Faradaic region with different scan rates. (e) Linear-fitted scan rate dependence of the current density difference at the open circuit potential; LSV of Co-F, Fe-F and Ni-F and *hp*-Ni as working anode in – (f) 1.0 M KOH solution, (g) 0.1 M Glucose in 1.0 M KOH solution. 102
Figure 34 Ni_2P cathode – (a) SEM image; Ni_2P EDS – (b) combined layered image of the detected elements, (c) phosphorus element mapping image, (d) nickel element mapping image, (e) EDS spectrum of area in image (a). 104
Figure 35 Pretreatment of SCB. (a) RSCB rough cut to smaller pieces (Left: Before drying, Right: after overnight drying); (b)Total TOC% comprising of solid, liquid, and lost components of SCB before HT (Hydrothermal), 1-step HT and 2-Step HT; (c) HPLC chromatograms and (d) ^{1}H NMR spectrums of RSCB after dilute H_2SO_4 hydrothermal process (Black: 1-Step Hydrothermal (HT), Red: 2-Step HT) with maleic acid as internal standard; (e) ^{1}H NMR spectrum of dissolved products from residue of HSCB by mild alkaline treatment. 105
Figure 36 (a) LSV of *hp*-Ni working anode (black curve: background 1.0 M KOH, red curve: HSCB adjusted to pH 13.8 (equivalent to pH of 1.0 M KOH); (b) Tafel plots derived from current–potential curves obtained of *hp*-Ni electrode at scan rate 5 mV s^{-1} in the presence of 1.0 M KOH (black), 0.1 M Glucose (red) and HSCB (green). HSCB electrooxidation at 1.58 V vs

RHE with (c) Tafel plot derived from a current–potential curve obtained of *hp*-Ni electrode at scan rate 5 mV s^{-1} of HSCB and (d) Chronoamperometric plot of HSCB electrooxidation in 1.0 M KOH for 5 hours. 107
Figure 37 HSCB electrooxidation at 1.58 V vs RHE with (a) Effect of applied charges on products yield% (oxalic acid, acetic acid and formic acid) and TOC %; (b) HPLC chromatograms of products at different electrooxidation intervals; Electrooxidation of mixture of various saccharides with (c) HPLC chromatograms at different intervals at 1.58 V vs RHE and (d) Effect of charges on product yield. 111
Figure 38 Glucose electrooxidation tests. (a) LSV of *hp*-Ni working anode (black curve: background 1 M KOH, red curve: 0.1 M glucose in 1 M KOH), (b) Nyquist plots in 1 M KOH at 1.58 V vs. RHE; (c) LSV of Ni_2P cathode anode (black curve: background 1M KOH, red curve: 0.1 M Glucose in 1 M KOH), (d) 3 consecutive runs with 0.1 M glucose in 1 M KOH at constant potential at 1.58 V vs RHE; € Effect of charges on formic acid yield % and glucose conversion% at 1.58 V vs. RHE. 115
Figure 39 HPLC chromatograms of Glucose electrooxidation at – (a) 0 V vs RHE, (b)1.30 V vs RHE, (c)1.48 V vs RHE, (d) 1.58 V vs RHE, (e) 2.00 V vs RHE, and (f) Effect of applied charges on products yield% (oxalic acid, acetic acid and formic acid) and TOC % of (e). 118
Figure 40 EO of Intermediates – (a) Fructose; (b) Glycolic acid; (c) Lactic acid; and EO of possible intermediates – (d) Gluconic acid; (e) Glucaric acid salt; (f) Tartaric acid. 120
Figure 41 Proposed reaction pathway of xylose / glucose to formic acid, and other products. 121
Figure 42 Glucose electrooxidation tests (a) Effect of charges on product analysis (oxalic acid, acetic acid and formic acid and TOC % at 1.58 V vs RHE; Comparison of glucose oxidation reaction at 1.48 V vs RHE, 1.58 V vs RHE and AWE at 1.80 V vs RHE on: (b) ratio of H_2 to O_2 gas products and (c) H_2 Faradaic efficiency 122
Figure 43 Xylose electrooxidation tests. (a) LSV of *hp*-Ni working anode (blue curve: background 1 M KOH, red curve: 0.1 M glucose in 1 M KOH), Inset: Nyquist plots in 1 M KOH at 1.58 V vs. RHE; (b) Effect of charges on formic acid yield % and xylose conversion% at 123
Figure 44 ^{1}H NMR spectrums of Before and After EO of monosaccharaides – (a) glucose; (b) xylose; (c) arabinose (Black curve: Before EO, Red curve: After EO); and HPLC chromatographs of Before and After EO of disaccharides – (d) sucrose; (e) cellobiose. 125
Figure 45 Solar photovoltaic HSCB-reforming process – (a) Experimental setup; Real-time monitoring of (b) Schematic diagram; (c) Gas flow rate with accumulated volume; (d) Voltage with Current density; (e) Effect of applied charges on products yield% (oxalic acid 126
Figure 46 Life cycle assessment of the SCB Process in terms of carbon emission, showing (a) Carbon emission per tonne of SCB processed by SCB upcycling and conventional SCB management processes. For electro-reforming processes, the sources of electricity and heat 128
Figure 47 Flowchart of upcycling process of raw sugarcane bagasse to end products (Main products in green) 129
Figure 48 Sankey diagram showing breakdown of the total carbon emission allocated to individual process component for the upcycling of SCB in the PV_MW heat scenario. 131
Figure 49 Schematic diagram of valorization of Paulownia wood to green chemicals – Dilute acid microwave-assisted hydrothermal of Paulownia wood powder to simple sugars followed by: (A) Thermo-alkaline treatment in microwave to lactate; (B) Electro-reforming to f 134
Figure 50 Paulownia wood sticks in pristine condition and after cutting and milling into cubes and powder, respectively 137

Figure 51 Microwave heating of 3 settings Ramp 200 °C, Hold 180 °C and 160 °C – (a) Temperature profiles; (b) Power profiles; (c) Energy consumption. 138
Figure 52 Optimization of microwave hydrothermal parameters to obtain highest total sugar yields from Paulownia wood – (a) Effect of concentration of H_2SO_4 on sugar yield at 180 °C and 30 min. ^{1}H NMR spectra of microwave-assisted hydrothermal of Paulownia wood f 144
Figure 53 Optimization of microwave hydrothermal parameters to obtain highest total sugar yields from Paulownia wood – (a) Effect of temperature on sugar yield with 300 micron particle size; (b) ^{1}H NMR spectrum of MHT at 200 °C (c) Effect of particles size on 147
Figure 54 FE-SEM images of Paulownia wood (PW) before MHT at different magnifications: (a) 80 ×, (d) 100,000 ×; and Paulownia wood of 300 microns (PW300) at different magnifications: (b) 80 ×, (e) 100,000 ×; and Paulownia wood of less than 100 microns (PW100) and Paulownia wood of less than 100 microns (PW100) at different magnifications: (c) 80 ×, (f) 100,000 ×. 149
Figure 55 FE-SEM images of Post xylose extraction (Post X) at different magnifications – (a) 80 ×, (b) 100,000 ×, (c) color-enhanced image of (b) with pores circled in yellow; (d) 1000 ×; (e) color-enhanced image of (d) with lignin highlighted in orange and cellulose in green, and (f) close-up image of (e)..... 150
Figure 56 XRD patterns of reference samples cellulose, hemicellulose (xylan) and lignin in comparison to Paulownia wood samples before and after MHT (Post xylose and glucose-xylose extractions)..... 151
Figure 57 Study of glucose conversion from cellulose residue after optimized MHT. (a) Effect of acid concentration, heating mode and temperature (a Product yield based on moles of carbon from cellulose residue from after MHT); (b) Consecutive MHT cycles of cellulose residue with glucose recovery and yield based on initial cellulose content in residue, and glucose selectivity was calculated based on measured liquid TOC. (*Yellow star indicates the selected condition for cellulose residue conversion). 152
Figure 58 FE-SEM images of post xylose-glucose extraction (Post XG) at - a) magnification of 80 ×, b) 650 ×. c) color-enhanced image of dotted blue area in image (b) with small, clustered size particles (blue). d) magnification of 10,000 × of surface of cluster and e) close-up image of (d); f) color-enhanced image of dotted purple area in image (e) with lignin nanospheres (orange) with diameters ranging from 5 to 50 nm on lignin agglomeration (purple)..... 153
Figure 59 (a) Cellulose control study - Influence of acid concentrations and microwave set temperatures (180 and 200 °C) on product yield and dissolved TOC, Inset: shows the zoom-in of products of less than 1% *calculated based on moles of carbon of initial cellulose); (b) Comparison of 180 °C hold 30 min (optimized MHT), 200 °C ramp 30 min (cellulose-residue conversion) and their total combined sugar yield for paulownia wood MHT with glucose and xylose selectivity. [a] Product selectivity based on measured liquid TOC)..... 154
Figure 60 Monosaccharides conversion to lactic acid in 1 M NaOH at 25 °C and 70 °C (a) HPLC chromatograms of glucose to lactic acid by conventional oven incubation; (b) HPLC chromatograms of xylose to lactic acid by conventional oven incubation; (c) Overall sugar 157
Figure 61 Lactic acid production from HPW – (a) Effect of lactic acid yield% at 50 and 70 °C at different microwave duration; (b) ^{1}H NMR spectrum of pretreated Paulownia wood to lactic acid at 70 °C, 120 min (c) HPLC chromatograms of product at various durations 158
Figure 62 Formic acid production from HPW – (a) Positive sweep LSV of *hp*-Ni working anode (black curve: background 1 M KOH, red curve: HPW), Inset: Nyquist plots in 1 M KOH at 1.58 V vs. RHE; (b) HPLC chromatograms of reactants and products; 160
Figure 63 Proposed reaction pathway of xylose/glucose to lactic acid (path A) and to formic acid (Path B). 164

Figure 64 (a) XRD spectra of *hp*-Ni – (red) Post electrooxidation (EO) of HPW, (black) As synthesized, and (blue) cubic Ni standard from JCPDS card No. 0004-0850. XPS spectra of (b) Ni 2p states, (c) O 1s state, and (d) full survey spectra of Activated *hp*-Ni..... 166
Figure 65 Solar reforming to formic acid from HPW – (a) Overall schematic diagram, (b) Voltage and current density against time plot, (c) Gas airflow rate and accumulated volume with time plot; (d) Effect of charges to liquid products and conversion of glucose and xylose from HPW; (e) Gas products composition at different solar reforming time intervals. 167
Figure 66 (a) Faradaic efficiency at the anode (black curve: OER, red curve: POR); (b) LSV of Ni_2P cathode anode. (black curve: background 1 M KOH, red curve: 0.1 M Glucose in 1 M KOH, and blue curve: HPW)..... 168
Figure 67 CNT study of cellulose MHT in water – (a) Temperature profile with different amount of CNT, (b) Energy consumption and energy saving at 180 °C; and in dilute H_2SO_4 - (c) Energy consumption and energy saving at 180 °C and 200 °C, (d) Effect of CNT on liquid products yield % and TOC%. (Product yield % and TOC % calculated based on moles of carbon of initial cellulose)..... 171

Table Captions

Table 1 Summary of Pretreatment methods of lignocellulosic biomass. 26
Table 2 Dilute acid hydrothermal conversion of different feedstock to sugar. 40
Table 3 Anodic oxidation of lignocellulosic biomass - lignin and hemicellulose..... 55
Table 4 Studies investigating electroreforming of cellulose and its derivatives at the anode.. 69
Table 5 Studies investigating evolution of hydrogen coupled with biomass electroreforming.78
Table 6 Utilities used, and their corresponding global warming potential assumed in LCA... 93
Table 7 Flow inventory of the SCB upcycling process, as modelled in LCA..... 95
Table 8 Energy efficiency comparison of AWE and HSCB electroreforming. 108
Table 9 Anodic oxidation of lignocellulosic biomass. 113
Table 10 Comparison of oven and microwave-assisted hydrothermal method on Paulownia wood to yield equivalent sugar yield (glucose and xylose). 156

Abbreviations

^{1}H	Proton
3D	Three dimensional
5-HMF	5-hydroxymethylfurfural
AFEX	Ammonia fiber explosion
ATP	Adenosine 5′-triphosphate
AWE	Alkaline water splitting
b	Tafel slope
C^{-}	Carbon radical
$C_{\#}$	Carbon, # represent number of
C_4mmCl	1-butyl-3-methylimidazolium chloride
CA	Chronoamperometry
CA	Carbon aerogel
CAM	Crassulacean acid metabolism
CC	Carbon cloth
Cdl	Double layer capacitance
CNT	Carbon Nanotubes
CV	Cyclic voltammetry
D_2O	Deuterium oxide
Da	Dalton
DC	Direct current
DP	Degree of polymerization
DW	Dried wood
E	Electrical potential
ECSA	Electrochemical surface area
EDS	Energy dispersive spectroscopy
EIS	Electrochemical impedance spectra
[EMIM]Cl	1-ethyl-3-methylimidazolium chloride
EO	Electrooxidation
FA	Formic acid
FCC	Face-centered cubic
FDCA	2,5-furandicarboxylic acid
FESEM	Field-Emission scanning electron microscopy
FTIR	Fourier transform infrared imaging
G	Guaicyl
GA	Glucaric acid
GC-TCD	Gas chromatography-thermal conductivity detector
GOR	Glucose electrooxidation reaction
GLA	Gluconic acid
Gts	Giga tonnes
gVS	gram of Volatile Solids
GWP	Global warming potential
H	*p*-Hydroxyphenyl
HAc	Acetic acid
HER	Hydrogen evolution reaction
HHV	Higher heating value
HMF	Hydroxymethylfurfural
HPLC	High-Performance Liquid Chromatography

HPW	Hydrolysate of Paulownia Wood
HRTEM	High resolution transmission electron microscopy
HSCB	Hydrolysate of Sugar cane bagasse
HT	Hydrothermal
***hp*-Ni**	Hierarchically porous nickel
Hz	Hertz
IC	Inorganic carbon
ILs	Ionic liquids
IPCC	Intergovernmental panel on climate change
j	Current density
OER	Oxygen evolution reaction
PEM	Proton exchange membrane
Pa	Pascal
PEP	Phosphoenolpyruvate
PGA	Phosphoglyceric acid
PV	Photovoltaics
LA	Levulinic acid
LCA	Life cycle assessment
LSV	Linear sweep voltammetry
MHT	Microwave Hydrothermal Treatment
MMT	Millions of metric tons
MW	Megawatts
N-CNT	Nitrogen-doped carbon nanotubes
Ni-F	Nickel foam
NMR	Nuclear magnetic resonance
NMMO	N-methylmorpholine N-oxide
NP	Nanoparticles
NS	Nanosheet
pH	Power of hydrogen
POR	Paulownia oxidation reaction
ppm	parts per million
Redox	Reduction-oxidation
RHE	Reversible hydrogen electrode
RID	Refractive Index detector
RSCB	Raw sugar cane bagasse
RuBisCO	Ribulose bisphosphate carboxylase/oxygenase
RuBP	Ribulose 1,5-bisphosphate
S	Syringyl
SCB	Sugar cane bagasse
SEM	Scanning electron microscopy
SPORL	Sulfite pretreatment to overcome recalcitrance of Lignocellulose
t/ha	Metric tons per hectare
TEM	Transmission electron microscopy
TOC	Total organic carbon
UV	Ultraviolet
VFA	Volatile fatty acid
wt	Weight
XRD	X-ray diffraction spectroscopy
XPS	X-ray photoelectron spectroscopy

Abstract

Climate change and fossil fuel depletion are intertwined global challenges that necessitate urgent action and lead to the sustainability shift towards low-carbon biofuels, renewable energy, and clean hydrogen fuel, as well as green chemicals. High purity hydrogen can be generated from water electrolysis but is hindered by inefficient oxygen evolution reaction (OER) and the possible explosive mixture of oxygen and hydrogen under the condition of partial loading and membrane degradation. There is a widespread effort to replace OER with the more favorable electrooxidation of small organic molecules. Although value-added products can be generated, the production of these organics is process-intensive and costly. Most importantly, they lack the abundance necessary to meet the requirements of a hydrogen economy.

Abundant raw biomass with annual production of billions of tons in nature are promising alternatives to these small organics. Significantly, biomass reforming via electrooxidation (to replace OER) could close the carbon cycle and promote a circular economy. However, the complex structure of raw biomass poses challenges, limiting processability. Consequently, these biomass materials are conventionally used as fuel for electricity generation. Thermal process-based energy extraction, especially without proper carbon capture and storage, inevitably leads to CO_2 emission and the underutilization of biomass. Therefore, from both resources recovery and carbon abatement perspectives, it is critical to develop advanced electro-refinery system for biomass valorisation. To overcome the low processability of raw biomass, highly efficient pretreatment methods were developed and thoroughly investigated.

In this thesis, fast-growing plant species were featured as promising biomass for reforming due to their rapid carbon fixation within short timeframe. Their fast growth

rate also accompanies with a shorter lifespan; hence they release carbon back into the atmosphere only after a short period of storage, rendering advanced carbon storage and utilization crucial. Reforming of biomass from fast-growing plant species not only produces green commodity chemicals and hydrogen fuels but also holds promising potential for climate change mitigation. Sugarcane bagasse (food waste) and Paulownia (non-food waste), as two representative fast-growing plant species due to their high abundance in Asia.

In the first work, abundant sugarcane bagasse agricultural waste was investigated with a facile hydrothermal pretreatment to recover soluble mono/oligosaccharides feedstock for subsequent green hydrogen and valuable chemicals production by electroreforming. Having suppressed oxygen evolution and thus avoiding hydrogen-oxygen mixture formation, the electroreforming process was directly driven by photovoltaic electricity. Characterizations using SEM, TEM, XRD, and XPS revealed abundant active sites on the hierarchical porous nickel catalyst acts as a highly active and robust electrocatalyst for SCB electroreforming. Organic acid salts, primarily formate, comprised 63% of the total yield of valuable chemical products. The reaction pathways were thoroughly investigated with complete electrooxidation of the possible mono-/disaccharides and intermediates. Finally, life cycle assessment highlights that the electroreforming upcycling process driven by photovoltaic and waste heat contributes 8–20% less greenhouse gases compared to conventional waste management methods.

In the second work, wood waste from fast-growing Paulownia was processed using the energy-saving, microwave-assisted hydrothermal method. The optimal sugar yield (100% xylose and 17% glucose) with minimal acid usage and energy consumption was achieved by coupling mechanochemical size shrinking and microwave hydrothermal treatment. The sugars were further reformed to valuable chemicals via two approaches:

1) mild thermo-alkaline conversion to produce high-value lactate and 2) hybrid electrolysis to generate high-purity formate and green hydrogen. Remarkably high glucose yields were recovered, reaching 45% in one cycle and 90% in five cycles, rendering the cellulose-rich residue suitable for commercial bioethanol production Alternatively, the produced glucose can also be converted to formate with a yield of up to 90%. Finally, the feasibility of directly driving hybrid electrolysis of the pretreated wood biomass waste was confirmed, showcasing a sustainable way to cogenerate formate and green hydrogen.

Overall, this thesis has validated the high feasibility of valorization of raw lignocellulose biomass, enabling safe and low-carbon production of green hydrogen and green chemicals. This contributes to reducing reliance on fossil fuels and potentially paves the way for decarbonization efforts and sustainable development initiatives.

Chapter 1: Introduction

1.1 Challenges and strategies for efficient green sustainable hydrogen production

Ever since industrial revolution, the atmospheric concentration of carbon dioxide has been rising extensively and reaching dangerous levels. [1] The main cause is from the major mankind activities such as fossil fuels combustion which leads to the emission of CO_2, one of the major greenhouses. This causes global warming and leads to climate change, that melts snow caps and results in floods. [2, 3] In 2019, an Intergovernmental Panel on Climate Change (IPCC) special report established several conditions required to restrict global temperature rise to 1.5 °C above pre-industrial levels. By 2030, carbon emissions would need to be halved, and by 2050, the net carbon released into the atmosphere must be zero. [4] Worryingly, according to IPCC's 6th assessment report [5], Earth is perilously close to breaching the 1.5 °C goal by 2030. Limiting temperature rise will require extensive effort, but inaction could result in a sea level rise of 180 cm by 2100 that could lead to USD 27 trillion in damages per year. [6] With additional temperature rise, considerable increase in heat-related mortality can be expected, with warmer and poorer regions experiencing a disproportionate burden. [7] Consequently, water stress and food shortages could increase in frequency and severity. [8, 9] The window for intervening is open but rapidly dwindling. [10]

However, another pressing concern lies in the depletion of fossil fuel sources, which calls for an urgent need for alternate energy resources. This leads to the sustainability shift towards low-carbon biofuels, renewable energy, and hydrogen fuel. Moreover, the diminishing fossil fuel also impose heavy pressure on the chemistry industry as petroleum is used to make essential fuels and chemicals.

Globally, 96% of global hydrogen is generated from fossil fuels, and majority of 76% come from steam methane reforming. [11] Only less than 2% is produced from water electrolysis which is a mature technology, capable to produce high purity green hydrogen. [12] The relatively high cost to produce hydrogen from water electrolysis hinders its usage but will gradually improve with declining cost of renewable energy. Among different water splitting systems, alkaline water electrolysis (AWE) is preferred thanks to its excellent scalability as earth abundant, inexpensive non-noble metal electrocatalysts can be utilized. However, water electrolysis produces both hydrogen and oxygen that may mix and trigger a dangerous explosion. In addition, the sluggish kinetic of OER also hinders the rate of hydrogen evolution reaction (HER) and consume more than 90% of the total energy input. [13-15] Therefore, for safety issues, HER-OER decoupling strategies such as the use of electron-coupled-proton buffer [16] ,solid state redox mediators [17] , redox flow battery [18] and bipolar electrodes [19] were explored. Still, the energy consumption issue persists, and the implementation of these methods has further introduced complexity to the water electrolysis infrastructure. Therefore, other thermodynamically more favorable oxidation processes were explored to replace OER that generate low-value oxygen in order to address the aforementioned safety concern and low energy efficiency issue.

The electrolysis of organic molecules consumes less energy, showing promise as a substitute for the OER because of significantly lower thermodynamic potential for the electrooxidation of these compounds compared to water electrolysis. [20] For instance, the generation of hydrogen was demonstrated by coupling to the electrolysis of methanol [21-24] , ethanol [25-29] , and bioethanol [30]. Also, in AWE, electrochemical oxidation of benzyl alcohol had demonstrated lower overpotential than OER. [31] Other organic precursors include furfural, furfuryl alcohol, and 5-hydroxymethylfurfural (5-HMF) also displayed

similar electrochemical improvement. [32, 33] These coupled reactions not only improved the hydrogen generation efficiency, but also generated anodic reaction products that more valuable than oxygen. But some of these alcohols are already valued as essential biofuels. Therefore, it will be impractical to further reform them for cogeneration of hydrogen. In addition, these starting precursors are process-intensive, costly, and not as abundant enough to support hydrogen economy.

Inspired by these innovative findings, it is envisioned that the use of abundant lignocellulosic biomass as a sustainable natural resource could complement the HER process. Moreover, the use of lignocellulosic feedstock is more attractive because it does not compete with either the food supply for the rising global population or essential bio-fuel applications. Therefore, applying the similar principle, direct electrochemical oxidation of abundant lignocelluloses biomass to carboxylic groups was experimented. [34-36] Although, low current density (peak at 0.12 to 0.20 mA cm^{-2}) was recorded, the oxidation reaction occurred before OER. Nevertheless, pretreatment is required before direct usage of lignocellulosic biomass for electrooxidation because of its complex, polymerized composition of mainly cellulose, hemicellulose and lignin. [37] In particular, cellulose (40–50% in plant biomass), is the most abundant natural carbohydrate and much effort was made in recent electroreforming studies. Cellulose and its derivatives were electroreformed to an extensive range of chemical products with different catalyst materials and designs. These recent studies were reviewed and benchmarked for future references and improvements.

1.2 Raw fast-growing plant biomass reforming to value-added products

A possible solution to mitigate climate change could be through rapid carbon sequestering. For example, fast-growing plants that exhibits efficient photosynthesis mechanisms in nature. [38-40] However, their fast growth also associates with shorter lifespan, releasing carbon in the form of methane (a potent greenhouse gas) back to the atmosphere when left to rot under anaerobic conditions. This also present as an opportunity for carbon storage which involves biomass of the fast-growing plant species to be chosen as the subject of study. Specifically, sugarcane bagasse (food waste) and Paulownia (non-food waste) – two typical fast-growing plant species – were chosen as subjects of study in this thesis due to their high abundance in Asia.

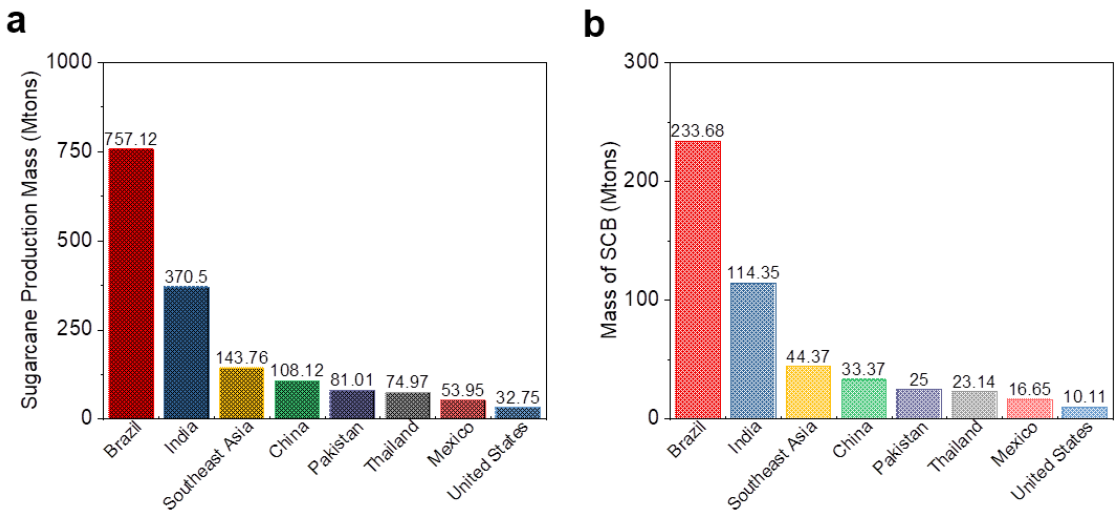

Figure 1 *Global sugarcane and sugarcane bagasse production in 2020. Top 7 countries and Southeast Asia with their – (a) sugarcane production and (b) estimated sugarcane humid bagasse waste generated.*

The first work involved sugarcane, a C_4 plant that is efficient in biomass accumulation. In 2020, the global sugarcane production, as represented in Fig. 1a, illustrates the substantial scale of sugarcane cultivation across the top 7 countries and Southeast Asia. [41] This immense production, as highlighted, contributes significantly to the generation

of sugarcane bagasse waste. Generally, 280 kg of humid bagasse is generated from 1 ton of sugarcane [42], a calculation applied to estimate the data represented in Fig. 1b. Sugarcane is widely used in the bioethanol and food industry because of its readily fermentable, high amount of sucrose, but it also results in the generation of sugarcane bagasse (SCB) waste amounting to millions of metric tons (MMT) annually. [43]

SCB is rich in lignocellulosic components but due to its natural complexity which renders low processability. Hence, SCB is often burned as fuel to generate electricity or steam at bioethanol plants after energy-intensive drying. [44] To better utilize SCB waste, second-generation of bioethanol was initiated by combination of pretreatments and biological processes. Despite having minimal environment impact, biological methods face challenges such as long processing time, strict reaction conditions control and high cost of enzyme. [45] Hence, it is crucial to find less time-consuming and more sustainable alternatives for SCB waste valorization. Electrochemical method is promising with the merits of green, energy-efficient and benign work conditions. [46, 47] Very recently, the electroforming of raw shrimp shell biomass to valuable acetate with cogeneration of green hydrogen pioneered in the author's group, had opened the trend of raw biomass electroreforming. [48]

With the promising results from the above study, the pretreatment-electrochemical upcycling process of SCB waste to cogenerate green hydrogen and green chemicals was demonstrated. Specifically, in pretreatment step, carbon captured in SCB waste in the forms of cellulose and hemicellulose by photosynthesis was firstly depolymerized into mono- and oligosaccharides with very diluted sulfuric acid without prior separation/purification steps. [49] Subsequently, the hydrolysates were electroreformed into small organic acid salts,

dominantly formate, with simultaneous green hydrogen generation. The electrochemical transformation of major mono- and disaccharides detected in SCB, and their intermediates are also studied in detail to unveil the mechanism. Furthermore, the feasibility of driving the electroreforming process with solar panels directly were demonstrated, thanks to the suppression of oxygen evolution reaction (OER). It is also worth noting that potassium formate has been recognized as a hydrogen carrier with the formate-bicarbonate loop. [50] This potentially offers an alternative mild and noncorrosive hydrogen carrier scheme compared to formic acid and contributes towards a sustainable hydrogen economy. Lastly, life cycle assessment (LCA) was performed to verify the environmental benefits of the developed process.

Moving from agricultural crop to woody tree, Paulownia is well-known for fast growth and could be due to its unique genetic trait as well as its crassulacean acid metabolism that enhance photosynthesis. [51] Fig. 2 delineates the global distribution of Paulownia trees (highlighted in orange), including introduced, native, and invasive populations. [52] Notably, Paulownia's geographical presence spans regions across Alaska, USA, South America, Europe, South Africa, India, and Australia, with native species originating from China and Japan. The wood of Paulownia, characterized by high porosity leading to its lightweight nature, has gained widespread popularity for various commercial products. [53, 54] Additionally, Paulownia is also well suited for short-rotation energy crop and in agroforestry agriculture. Under optimal circumstances, a dense plantation with 2000 trees per hectare has the potential to produce 150–300 tons of wood annually, achieved within just 5–7 years after the initial planting. [54] The extensive utilization contributes to a high annual biomass production of up to 50 t/ha (tonnes per hectare) [55] This heightened production level inevitably results in the generation of substantial wood

waste. The estimated timber waste, encompassing both waste from tree harvesting and product residuals, ranges from ~35% to 50%. [56-59]

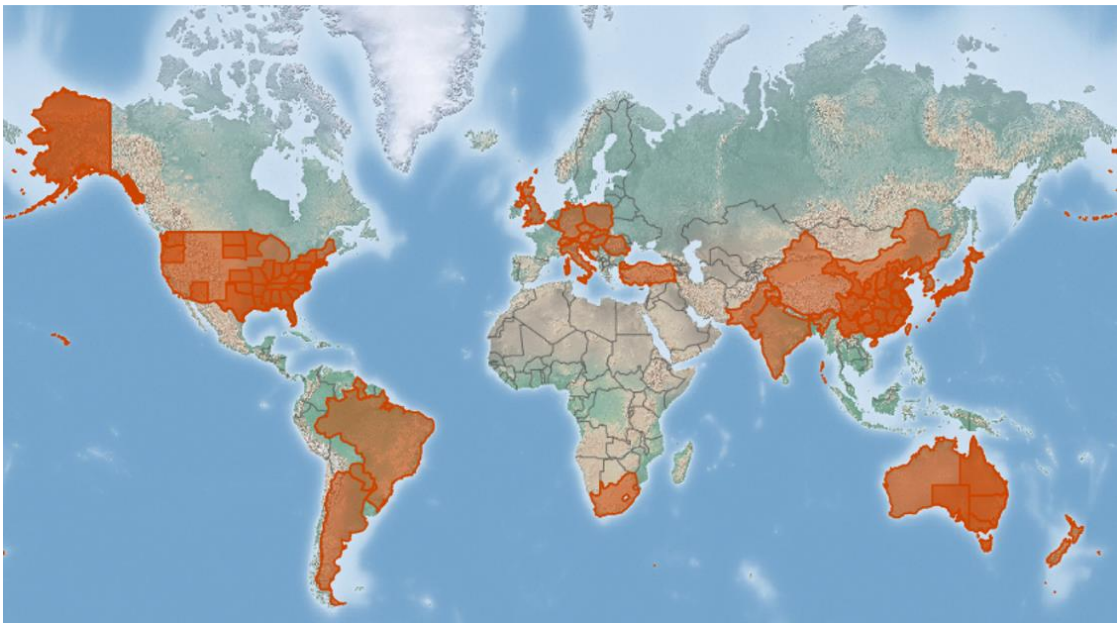

Figure 2 *Global Distribution of Paulownia Trees. (Highlighted regions in orange).* Credit: figure adapted from CABI database. [52]

Wood wastes are often treated as fuel for heating [60] in many industrials and domestic applications or for generating steam [61] as well as electricity [62]. However, the use of lignocellulose biomass feedstocks in producing green chemicals or biofuels will be more appealing as it reduces reliance on fossil fuel. Like SCB waste, biochemical processes were the most common greener method to process Paulownia wood waste to produce bioethanol but faced the same challenges as mentioned earlier.

To date, there was no report on direct Paulownia wood saccharification (glucose and xylose). An extreme low acid (0.2 wt% H_2SO_4) microwave-assisted hydrothermal technique to process milled paulownia wood by depolymerizing cellulose and hemicellulose to monosaccharides was performed. The highest sugar (glucose and xylose) yield was attained through detailed parameters (acid concentration, wood particle size, temperature, heating mode and duration) optimization. Then, this sugar

mixture was further converted to value-added green chemicals by two conversion paths: A) Microwave-assisted thermo-alkaline treatment to lactate; and B) Electro-reform to formate at the anode with coupled generation of green hydrogen at the cathode. Practical application to use renewable solar energy was also conducted to simultaneously convert pretreated paulownia wood derivatives and store excessive, intermittent photovoltaic energy in the form of both formate and hydrogen gas. Latic acid, is highly valued as platform molecules for producing wide range of useful chemicals. [63] On the other hand, formate is less corrosive than its acid form, can be used in clean energy, hydrogen storage. [50, 64] To promote circular economy by minimizing waste, further MHT could upcycle the cellulose-rich residue to glucose with 78% selectivity, and 90% recovery with additional consecutive cycles.

Overall, the novel pretreatment-electrochemical processes for both SCB waste and Paulownia wood reforming were demonstrated for cogeneration of green chemicals and green hydrogen, which is more sustainable and environment-benign compared to conventional biowaste management methods.

1.3 Motivation and objectives of thesis

The usage of fossil fuels leads to two major issues. First, the urgent need to find alternate energy sources to reduce carbon emission and second, new raw materials to synthesize into essential chemicals to meet the rising demands for industries. A suitable material such as abundant plant biomass that is renewable and sustainable can couple with hydrogen generation in the AWE system. This hybrid electrolyzer not only produces green hydrogen to address the energy issue, but also reforms abundant plant biomass into platform chemicals in a green process.

The objectives for this research are to:

1) investigate a sustainable approach for abundant biomass upgrading.

2) develop an efficient raw biomass pretreatment that couples with a high yield electrochemical refinery process of biomass to platform chemicals at ambient temperature and pressure.

3) understand the mechanism of electroreform of biomass with electrooxidation as the main approach for transformation of lignocellulosic biomass into value-added chemicals.

4) develop a PV-driven "hybrid electrolyzer" to simultaneously upgrade biomass and produce hydrogen fuel.

1.4 Organization of Thesis

In this Thesis, the primary focus was on investigating the lignocellulosic biomass reform process, with specific attention given to the transformation of plant biomass into valuable green chemicals. In Chapter Two, the literature review is divided into the several sections which introduces the photosynthesis mechanisms of different plant species, lignocellulosic chemical components of sugarcane and Paulownia, existing plant biomass pretreatments, water electrolysis systems and fundamental, and concept of hybrid electroreforming covering small organics molecules as well as lignocellulosic biomass. The recent studies on electroreforming cellulose, its derivatives, and other biomass derivatives to produce value-added products are also included.

Subsequently, Chapter Three highlights the electroreforming of raw sugarcane bagasse waste, demonstrating its conversion into formic acid cogenerated with green hydrogen. In Chapter Four, the valorization of Paulownia wood to valuable green chemicals is presented.

Finally, chapter five concludes the thesis with an overall outlook and discussion on future works.

Chapter 2: Literature review

2.1 Photosynthetic pathways of plants

To mitigate climate change and substitute fossil fuels, carbon fixation and utilization could be a promising solution that captures inorganic carbon from the atmosphere into growing organisms, converting into organic compounds, and then further processed into value-added chemicals. The fundamental mechanism behind nature's carbon sink is photosynthesis, which occurs biologically in plants, absorbing CO_2 and changing it to organic compounds. Plants exhibit three distinct photosynthetic pathways: C_3, C_4, and crassulacean acid metabolism (CAM). [65] In general, "Photo"/light reaction is initiated by sunlight which enables the formation of adenosine 5′-triphosphate (ATP) and nicotinamide adenine dinucleotide phosphate hydrogen (NADPH) as feedstocks for later "Synthesis" stage. [66]

C_3 or Calvin-Benson Cycle consists of 3 stages which starts with an enzyme, Ribulose bisphosphate carboxylase/oxygenase (RuBisCO), that catalyses the carboxylation of Ribulose 1,5-bisphosphate (RuBP) to form 3-Phosphoglyceric acid (PGA). Second, the reduction of 2 ATP and 2 NADPH per cycle to form carbohydrate or glucose for further plant metabolism. And third, the regeneration of RuBP for the cycle to continue, and 1 ATP is consumed for phosphorylation. However, a wasteful process (photorespiration), coexists in which oxygen is combined with RuBP to produce one PGA and phosphoglycolate. [67] Further conversion of phosphoglycolate resulted in CO_2 that reduces the net efficiency of photosynthesis. The lack of ability to overcome photorespiration is observed in most C_3 plants, making up of 85% of plants which includes soybeans, wheat and trees.

To suppress photorespiration, C_4 plants, can concentrate CO_2 by ten-fold at the site of RuBisCo with the help of a biochemical CO_2 pump. [68] This effectively raises the CO_2/O_2 ratio, and photorespiration is effectively eliminated. The unique leaf structure of C_4 plants consists of two cell compartments, mesophyll and bundle-sheath cells which facilitate the two-step CO_2 fixation process. Specifically in mesophyll cells, contain an enzyme called phosphoenolpyruvate (PEP) carboxylase that catalyzes the reaction involving atmospheric CO_2 to produce oxaloacetate (C_4 acid). The C_4 acid then diffuse to the next compartment (bundle-sheath cell) which decarboxylated to CO_2 in the chloroplasts and readily refixed by RuBisCo. Hence, C_4 plants exhibit enhanced photosynthesis rates under strong light intensities and temperatures. [69] At such, C_4 plants surpass C_3 plants in productivity, making them highly productive crops while also being considered problematic weeds. Some C_4 crops include maize, sugarcane, sorghum, and amaranth, whereas nutgrass, crabgrass, and barnyard grass represent some of the most troublesome C_4 weeds.

Like C_4 plants, Crassulacean acid metabolism (CAM) plants have similar strategy to minimize photorespiration and save water. However, instead of spatial separation, CAM plants separate these steps temporally, distinguishing between night and day. Specifically at night, the stomata of these plants open to allow CO_2 into their leaves. Again, PEP carboxylase is used for carbon fixation into oxaloacetate and later converted to C_4 acid. Interestingly, the C_4 acid stored inside vacuoles are only utilized for photosynthesis the next day. [66] Under sunlight, these plants can still photosynthesis even though their stomata are closed thanks to the stored C_4 acid from vacuoles. The C_4 acid are transported outside and decarboxylated to CO_2 for the Calvin cycle. This not only allows high concentration of CO_2 to be around RubisCo to reduce the unwanted

photorespiration process [70], but also conserve water. Other than pineapples, CAM plants such as cacti and other succulents strive in dry environment such as deserts.

Fast-growing plant has high relative growth rate that correlates with high gross photosynthesis CO_2 intake per unit mass over the initial growth stage. [71, 72] Ever-increasing carbon dioxide levels leads to "CO_2 fertilization" and photosynthesis-respiration enhancement of plant growth. [73] As the terrestrial carbon sink increases, it also offset CO_2 emissions, causing a momentary stop in growth rate of atmospheric CO_2 between 2002 and 2014. [74] However, the fast growth rate of trees also leads to short lifespan. [75, 76] This growth-lifespan tradeoff release carbon in the form of methane (a potent greenhouse gas) back to the atmosphere when left to rot under anaerobic conditions. [75, 76] Moreover, a recent study has associated a warmer climate with shorter tree lifespans, particularly in tropical lowland forests, which are home to the world's most important rainforest carbon sink. [77] The shorter lifespan of trees presents the need for carbon storage [78] and as a potential feedstock for utilization in the shift from fossil fuels to biofuels and green chemicals.

2.1.1 Sugarcane and its chemical composition

Sugarcane, with its C_4 carbon metabolism, exhibits highly efficient biomass accumulation. [79] It is one of the main biomass feedstocks for first-generation bioethanol that has shown great promise for energy supply. [80] Sugarcane with global production of 1.9 Gts in 2018 is one of the top four most productive agricultural commodity (cotton, oil palm, cocoa and sugarcane). [81] A ton of sugarcane generates 130–170 kg of sucrose that can be readily fermented to ethanol while the remaining ~85 wt% sugarcane waste are mostly underutilized. Unlike other crops, the residual sucrose-rich from the sugarcane bagasse (SCB) could also be utilized without prior separation or washing step. Although first-generation bioethanol is widely acknowledged as a clean,

renewable, and environmentally friendly replacement for fossil fuels, its use of food crop feedstocks such as sugarcane and corn compete with the food supply. Moreover, a substantial amount of biomass waste, SCB is generated as a result.

SCB is the major waste in sugarcane industry with an annual generation of 279 MMT globally, posing serious waste problems. [82, 83] Besides the substantial amount of sugar residue, SCB is abundant with lignocellulosic components that are mainly consist of cellulose, hemicellulose and lignin. Indeed, as reported, the chemical composition of matured sugarcane (S. officinarum) consists of 50% soluble sugar, 20% cellulose, 10% hemicellulose, 2% pectin, and 16% lignin. [84] The main hemicellulose of grass species (sugarcane) is xylan [85], leading to high amount of xylose (50%) among monosaccharides. Other monosaccharides consist of 48% glucose with less than 5% for mannose and arabinose. A high percentage of O-acetyl substituent groups on xylan may result in a reduced association between xylan and cellulose, which, in turn, could enhance the yield of saccharification in sugarcane. [86, 87] However, the released acetate from pretreatment is considered as a major fermentation inhibitor. [88] Cellulose is the crystalline form of repeating glucose molecules joined by β-1-4 glycosidic bonds. [89] Hemicellulose is amorphous because of the presence of side branches, such as glucan and acetyl groups, which are linked to xylan. [90] These polysaccharides are surrounded by lignin which provides strong rigid structure to plant. Lignin is a highly branched 3D polymer of phenolic macromolecules linked by C-O or C-C bonds. [91] This complex structure renders SCB low processability, leading to the underutilization of SCB. Conventionally, SCB is burned as fuel for steam or electricity generation at bioethanol plants after energy-intensive drying. [44, 92]

To make full usage of the latent heat value of SCB, second-generation bioethanol from SCB was reported. [93-96] However, the process is complex and costly. Acid,

ionic liquid and hot water pretreatments are generally used to disrupt the plant matrix to enhance enzyme accessibility. [97-99] Moreover, microbial suppressants (e.g. furan derivatives, carboxylic acids and phenolic compounds) are always generated during acid pretreatment, which would hamper/ toxify the fermentation process. [100, 101] Although, these biological processes have shown reduced impact to the environment (compared to combustion), the major disadvantage is the long processing time (over hundreds of hours). [97] Additionally, strict reaction condition control (temperature, pH, oxygen levels, etc.) and high cost of enzyme incur economic concerns. [45] Hence, it is crucial to find less time-consuming and more sustainable alternatives for SCB waste valorization.

2.1.2 Paulownia and its chemical composition

Paulownia, a C_3 plant, exhibits exceptional photosynthesis efficiency, probably due to its unique genetic traits and utilization of the crassulacean acid metabolism pathway. [51, 102, 103] These features enable high carbon fixation, leading to the rapid biomass accumulation within a short timeframe [80, 104] Moreover, the leaves of the Paulownia tomentosa, with an approximate diameter of ~70 cm, absorb an average of ~4 to 22 kg of CO_2 per year (first-year forests absorb 9.04 ± 1.06 t of CO_2 per year) and release approximately ~6 to 54 kg of O_2 due to their expansive surface area. [105] It is worth noting that Paulownia exhibit high productivity and high environmental adaptability and is well-known as an invasive species. [106] Because of these trails, Paulownia cultivation for biomass utilisation has been studied across many research projects. [105, 107-112]

Consequently, it is well-suited for short-rotation energy-crop forestry. [113] Fast-growing Paulownia is also widely utilized in agroforestry systems [114]. Unlike other wood species,

Paulownia wood possess unique large pore size [115, 116, 117], , which leads to a weaker lignocellulosic structure, making it lightweight and also easily processable. Such a material is widely used for production of utensils, surfboards, furniture, building components, and musical instruments. [53, 54] This extensive utilization contributes to a high annual biomass production of up to 50t/ha [55] producing more biomass within a single year than other species, including poplar, switchgrass, miscanthus, or willow. [118] Inevitably, it also contributes to the huge amount of wood waste.

Wood wastes are often treated as fuel for heating [60], producing steam [61] as well as electricity [62] in many domestic applications and industrials. However, the use of lignocellulose biomass feedstocks in producing green chemicals or biofuels will be more appealing as it reduces reliance on fossil fuel.

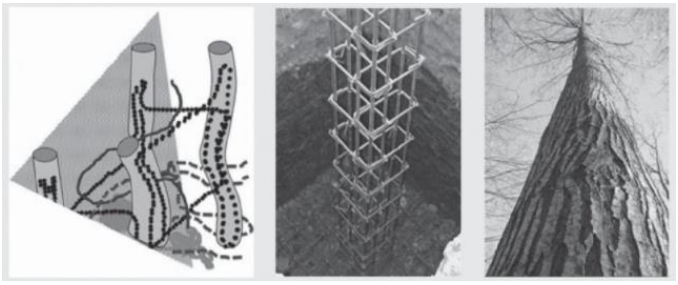

Figure 3 *Comparison between plant and man-made pillar structures.* Credit: all figures adapted from Li et al. [37]

In particular, hardwood Paulownia species are carbon-rich, consisting of (44.0 ± 6.6)% cellulose, (23.4 ± 9.8)% hemicellulose and (21.9 ± 0.5)% lignin. [119, 120] In general, cellulose is constructed into crystalline microfibers to create the main frame of cell walls assisted by hydrogen bonding and van der Waals forces. The remaining gaps are then filled up by amorphous hemicellulose and lignin with hydrogen bonding and covalent linkages to cellulose. [121] This combination forms the lignin-carbohydrate complexes, that can be visualized in Fig. 3 (left). The man-made scaffold structure (center) can be used as an analogue of the plant structure (left and right). The vertical solid bars

represent the cellulosic microfibrils while the cross-sectional reinforced linkage bars correspond to hemicellulose. The cement can be imagined as lignin, the main adhesive agent in plants.

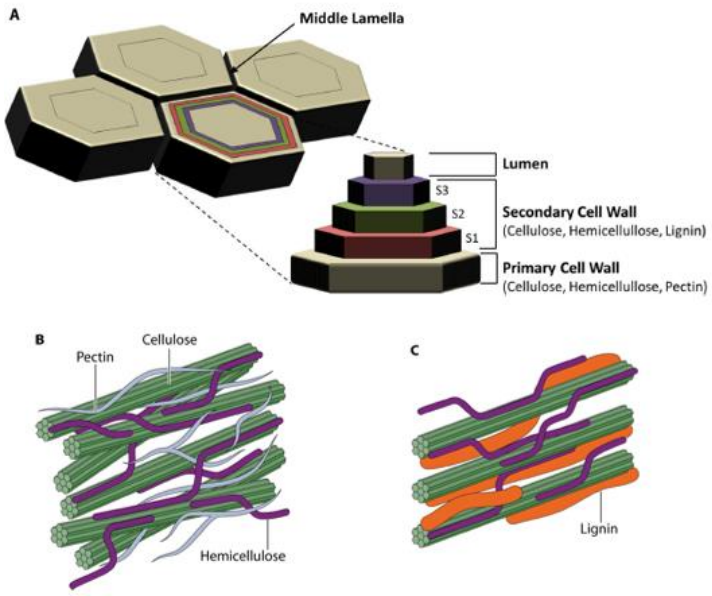

Figure 4 *Simplified diagram of plant cell wall structure. (a) Middle lamella, primary and secondary wall (b) Primary wall layer, (c) Secondary wall layer. Credit: all figures adapted from Kim et al.* [122] *and Rytioja et al.* [123]

Other than the aforementioned components, a mixture of polysaccharides-pectin (5% of primary wall) and soluble protein (0.2%) can be located in the middle lamella as well as in the primary plant cell wall. The crisscross mesh network of cellulose microfibril and hemicellulose chains that embeds in pectin matrix forms the major polysaccharides structural of the primary cell wall. [123] Pectin helps to bind adjacent cells together with its gel ability, providing rigid mechanical and structural support for the primary cell wall. [124] Towards the center, the secondary cell wall, has three layers (S_1, S_2 and S_3) that surrounds the lumen (Fig. 4a). The multiple wall layers constitute the essential ability to hold trees vertical against gravity. Comparing the simplified models in Fig. 4b & 4c, the matrix for primary and secondary wall is pectin and lignin, respectively.

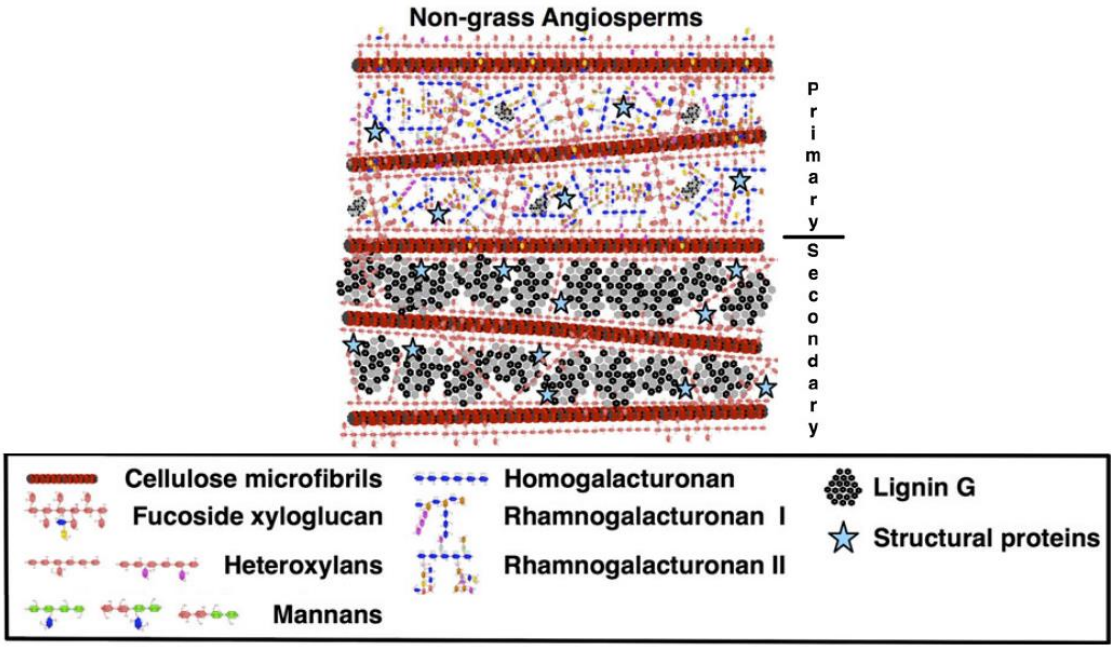

Figure 5 *Simplified 2D representation of cell wall composition of Non-grass Angiosperms. Note: diagram is not drawn to scale.* Credit: figure adapted from Brett et al. [125]

A deeper understanding of the primary and secondary layers of non-grass angiosperms (Hardwood) is analyzed in the illustration (Fig. 5). [125] Cellulose microfibrils are bundled with hemicelluloses that includes fucoside xyloglucan, xylans and some mannans. On the top primary wall layer, 3 types of pectin (Homogalacturonan, Rhamnogalacturonan I and Rhamnogalacturonan II) are present. Their detailed chemical structures are revealed elsewhere. [37] On the bottom secondary wall layer, large amounts of lignin with guaicyl (G) and syringyl (S) units can be observed. [125] Other minor components consist of tannins, quinones, essential oils, fats, terpenes, flavonoids, resins, carbohydrates, glycosides and alkaloids as well as inorganic components. [126, 127]

Such a recalcitrance and complex nature of lignocellulosic barrier necessitates various pretreatments to extract essential chemical intermediates for further processing. So far, Paulownia wood pretreatments include the use of acid, hot water, alkaline, or organosolv methods, either individually or in combination, involving sequential, multiple steps to either extract xylan [128-134] or lignin [135, 136]. Importantly, these treatments disrupted the

lignocellulosic matrix for enzymes accessibility to hydrolyze cellulose to glucose for subsequent second-generation bioethanol production. While biological processes have demonstrated a lower environmental impact compared to thermochemical methods, their prolonged processing time (at least 48 h) remains a significant limitation. [129, 132] Additionally, the need for strict control over reaction parameters (inhibitors, temperature, pH, oxygen levels) and the high cost of enzymes raise economic concerns. [45]

Alternatively, heavy oil product from hydrothermal liquidifcation of Paulownia wood at 300 °C with iron and sodium carbonate catalysts was achieved. [137] However, separation of the complex oil mixture (phenol derivatives, benzene derivatives, ketones, carboxylic acid, long-chain alkanes, and aldehydes) to useful chemicals with high purity can be costly and involves multi-step techniques. [138] Therefore, it is essential to explore sustainable alternatives that are energy-efficient, time-saving, and efficient for the valorization of paulownia waste.

2.1.3 Cellulose

Cellulose is a long chain polymer, linked by β-1,4 glycosidic bonds with D-glucose repeating monomers. Its basic building block consists of repetitive linked of cellobiose dimers by a β (1 → 4) bond (Fig. 6a), where number of cellobiose, n = DP/2 - 2. For cotton, DP of 10k to 15k in secondary cell wall and DP of 2.5k to 4k and 250 to 500 for primary cell wall, while hardwood has around 3k to 5.5k. [139] The cellulose microfibrils which are 10 to 50 nm in diameter and several microns long with disordered amorphous and crystalline regions. [140, 141] The rigid and crystalline characteristic of cellulose is caused by the interchain and intrachain hydrogen bonding between hydroxyl groups. (Fig. 6b) Cellulose nanofibrils, smaller fragments with diameter of 5 to 30 nm and 1 µm long can be separated through various pretreatments methods. [142] Cellulose nanocrystals

of smaller size (diameter of 2 to 20 nm and length of 100 to 600 nm) can be further extracted through strong acid hydrolysis. Undiluted sulfuric acid or hydrochloric acid is utilized to cleave the accessible glycosidic connections of cellulose microfibrils. [143]

Moreover, cellulose can also exist in different formations resulted from different H-bonding position. For instance, in nature form, cellulose exists as cellulose-Iα and Iβ while in a more stable state, the regenerated fibers are called cellulose II. After chemical treatments, other structures such as cellulose III and IV can be obtained. [37]

Utilization of abundant cellulose in applications such as fiber regeneration for textiles, homogeneous chemical reaction for green chemicals and composite materials are faced with challenges. One difficulty is its dissolubility in polar solvent such as water and could be due to its long chain and high degree of polymerization (DP), that reduces solubility with decreased entropic gain. For dissolution, negative free energy change requires to be fulfilled. It is the summation of positive enthalpy that is dependent on intermolecular interaction and entropy.

As the molecular weight of the polymer increases, the quantity of molecules decreases, resulting in a reduction in entropy. As a result, the entropic driving force becomes weak which also make the free energy change positive, unfavorable for dissolution. This is supported by comparing with glucose, cellobiose or oligomer with DP less than 10 that are soluble in water. [144]

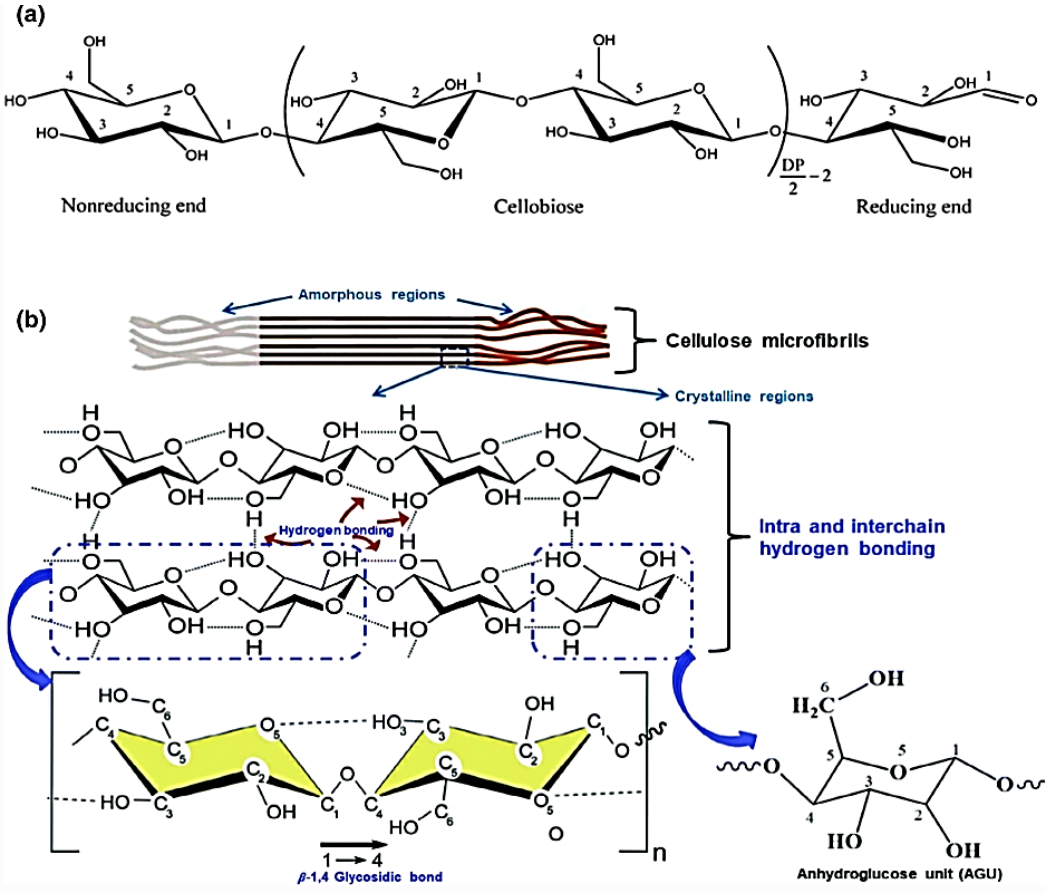

Figure 6 *(a) Chemical structure of cellulose consists of cellobiose with reducing and nonreducing ends (b) crystalline and amorphous regions in cellulose microfibrils. Intrachain & interchain hydrogen bonding (black dotted line), and carbons numbering in AGU*. Credit: all figures adapted from Islam et al. [140]

In some research, it was proposed that the strong hydrogen intra and inter-bonding among hydroxyl groups leads to the stiff 3D extended crystalline structure. [145] Dissolution is much favorable for flexible polymers (e.g. α-linked glucopyranose residues in amylose) than in stiff cellulosic polymers such as β-linked glucopyranose residues. The conformational freedom of stiff crystalline cellulose in water is limited and thus attributes to the low solubility. However, hydrogen bonding mechanism alone is not enough for the cellulose dissolubility. For instance, dextran, a complex branched glucan has similar hydrogen bonding capacity as cellulose yet is hydrophilic. Other complex mechanisms such as van der Waals and hydrophobic interactions could be involved.

Moreover, amphiphilic (both hydrophobic and hydrophilic) nature of cellulose was examined to be the important mechanism to its insolubility. [146] This significant effect from hydrophobic interactions (for e.g., chains of glucose rings, cyclodextrins and helix amylose), both have hydrophobic interior and hydrophilic exterior. In water, the hydrophobic sides of cellulose will tend to merge with each other, resulting in poor solubility. To further demonstrate this, solvents such as ionic liquids and N-methylmorpholine N-oxide (NMMO) that are amphiphilic could dissolve cellulose. [147, 148] Cosolutes such as polyethylene glycol/NaOH and urea/LiOH that weaken cellulose's hydrophobic effect are used together to dissolve cellulose. [149, 150]

Ionization of cellulose is helpful with its solubility due to the increase in entropy by small counterions. [151] Adjusting pH to extreme low and high by using phosphoric acid [152] and NaOH [153]/LiOH, respectively. Acid protonation or alkaline deprotonation of hydroxyls, inevitably, could causes the cleaving of glycosidic bonds of the anhydroglucose polymer.

However, the use of the discussed solvents has limitations. For instance, the usage of ionic liquids (ILs) will incur high cost, reactivity and toxicity and pose recyclability challenges. Like ILs, NMMO also faced problems from high cost in order to recycle. In addition, it can only operate at specific temperature at 90 °C because of its thermal instability. [148] The use of concentrated acid or alkaline will require neutralization to ensure a less hazardous towards man and environment and leads to a higher post-treatment cost.

2.1.4 Hemicellulose

Unlike cellulose, hemicellulose, is rather amorphous owning to its highly branched structure of 5 to 6 carbon sugar. Hemicelluloses have lower molecular mass with DP of 100 to 200. [154] Since the molecular chains are shorter and less regular than those of cellulose, they do not pack so tightly together in regular parallel bundles. As a result, the hemicelluloses do not possess marked fiber-forming properties but are of a more gelatinous nature. Furthermore, they are less chemically resistant than cellulose, making them readily hydrolyzed by acids into their constituent sugars [127], and a large proportion of the hemicelluloses in wood may be extracted by means of alkalis. The chemistry of the hemicelluloses is extremely complex, and their separation and isolation present very considerable practical difficulties. [126]

In hardwood specifically, glucuronoxylan is the main hemicelluloses, that contains β-D-xylopyranose(xylose) 5-carbon sugars in the backbone, connected by (1→4)-linkages. [127] In hardwood, the mass of glucuronoxylan is estimated to be 20 to 30% of the dry wood mass. The hydroxyl groups at the C_2 and C_3 of xylan chains are partially replaced by acetyl groups and can be simply dissociated using alkalis to convert to acetate. (Fig. 7). In addition, some xylose units in the xylan backbone are branched to 4-O-methyl-glucuronic acid residues. The bonds between the glucuronic (uronic) acid groups and xylose units are resistant to acid. [155] Moreover, the uneven distribution of uronic acid in the xylan backbone is estimated to have an average uronic acid to xylose ratio of 1:10. [127, 154]

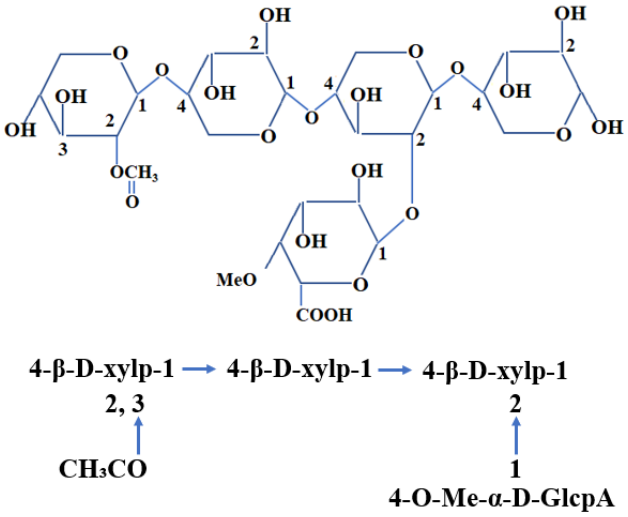

Figure 7 *Chemical structure of glucuronoxylan.* Credit: figure adapted from Bertaud et al. [156]

2.1.5 Lignin

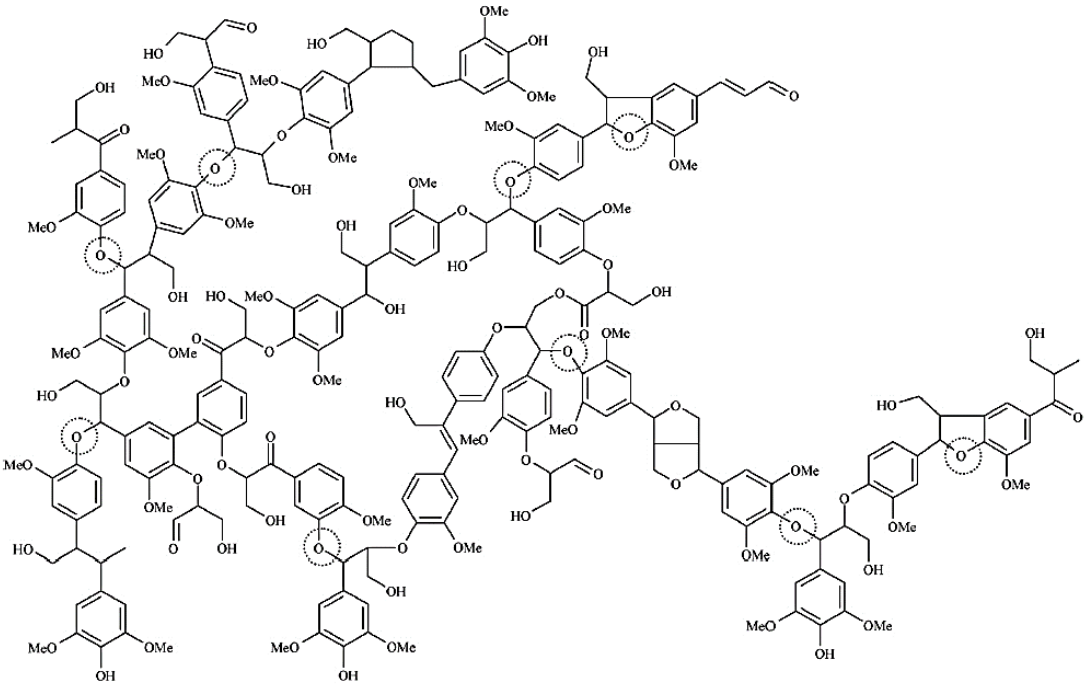

Figure 8 *Chemical structure of lignin from Beech. proposed by Nimtz with dotted circled identified to be the weak α-aryl ether bond.* Credit: figure adapted from Nimtz. [157]

As a cementing material to bond cells together, lignin differs much from cellulose with different chemical properties and structure. Lignin is a complex phenolic polymer with no repeating units and contains large number of aromatic rings. [126] In terms of abundancy, lignin is just behind cellulose in cell wall among vascular plants. Huge amount of lignin waste product from biorefineries and kraft-pulping process is dumped into the environment or incinerated to create heat. For instance, the 80-year old Tomlinson recovery process is used to retrieve inorganics chemicals from the lignin-containing black liquor (effluent after kraft-pulp process). [158] However, it is not environmental-friendly with poor efficiency as it involves excessive heat energy to incinerate waste with high moisture and emits toxic nitrogen and sulphur oxides (NO_x, SO_x). [159] The valorization of lignin biowaste can be achieved by leveraging its intriguing aromatic-rich composition for the production of various phenolic industrial products, such as resins, adhesives, epoxies, binders, polyurethane copolymers, polyolefins, and admixtures for concretes. [160]

Lignin in nature has a complex structure, which can covalently connect to carbohydrate by α-ether, α-ester, and phenyl glycosidic linkages [161, 162] and extraction of the full lignin structure is impossible for analysis. Hence, the partial chemical representation of lignin macromolecule is proposed (Fig. 8). The exceptional stability of lignin is because of the network connection of hydrolysis-resistant ether (α-O-4; β-O-4) linkages, alkyl–aryl carbon-carbon (C-C) bonds between an aliphatic and aromatic carbon and biphenyl carbon-carbon bonds between aromatic carbons. However, the α-aryl ether (α-O-4) bonds (circled in Fig. 8) are known to be the weakest linkage and are hydrolysable. Due to the stable bonds, lignin is very tough against degradation and extreme treatment conditions are therefore required if the more stable, ether bonds are to be hydrolyzed. Three monolignols (p-coumaryl, coniferyl, and sinapyl) and their acylated forms are the

precursors of lignin to form phenylpropanoids — p-hydroxyphenyl (H), guaiacyl(G), and syrnigyl (S) respectively in the lignin polymer. (Fig. 9).

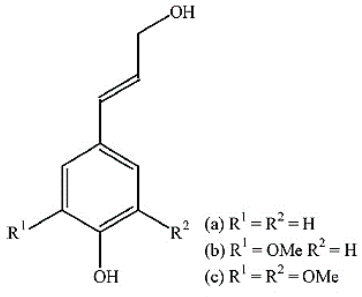

Figure 9 *Primary precursors of lignin – (a) p-coumaryl alcohol, (b) coniferyl alcohol, and (c) sinapyl alcohol.* Credit: figure adapted from Collinson et al. [163]

2.2 Plant Biomass Pretreatment methods

As discussed previously, in plant, cellulose together with hemicellulose are embedded in pectin and lignin matrix of the cell wall, thus hinder accessibility for further processing. Refining, upgrading or conversion of lignocellulosic biomass require the accessibility to the abundant cellulose raw material. The rigid, tough structure and poor permeability of plant cell walls form another barrier and, the particle size, surface area, as well as cellulose's crystallinity and DP further increase accessibility difficulty. To address these challenges, many different pretreatments have been established, each with their advantages and disadvantages. The pretreatment methods or their combinations are also viewed as the most critical step to effectively valorize lignocellulosic biomass. [122] For instance, by removing hemicellulose and/or lignin; modify lignin structure to reduce its inhibition effect, thus increasing efficiency of the refining process (enzymes hydrolysis). [37]

Primarily, lignin is usually removed via extreme dissolution methods involving pyrolytic and solvothermal processes. These harsh methods permanently downgrade its chemical value and result in a waste fraction of biomass. [164, 165] But nowadays, lignin valorization has received attention due to its abundancy and rich aromatic compounds. Thus, greener, and milder pretreatment methods to selectively depolymerize lignocellulosic biomass are explored with interest.

Among the different pretreatments for biomass that had been studied extensively [166-171], the most essential methods are selected for discussion in this section. They are categorized into physical, biological, combinational methods (mechanochemistry, thermochemical and microwave-assisted hydrothermal), and other solvents/methods, are presented in Table 1. This section reviews these pretreatment techniques pertaining to plant biomass.

Table 1 Summary of Pretreatment methods of lignocellulosic biomass.

Category	Pretreament method	Driving force	Major focus/effects	Limitations
Physical	Grinding (Hammer or knife mill)	Mechanical impact, attrition, shear and compression	Size, DP and crystallinity reduction, Surface area development	Energy intensive, non selective, incapability to remove the lignin
	Milling (Ball mill or Disk mill)			
	Ultrasound	High pressure from frequency sound waves	Rupture of cell wall	Energy intensive and costly
	Microwave-enhanced	Vibration from mircowave radiation	Disrupt the crystal structure of cellulose	Energy intensive and costly
Biological	Micobial (fungal)	Enzymatic reaction from fungi	Modify or degrade hemicellulose and lignin	Low hydrolysis rate and costly enzymes
	Organosolv	Breaking of ether bonds	Delignification (lignin removal)	Solvent separation must be performed as they may inhibit the next downstream processes
	Sulfite pretreament (SPORL)	Dissolution of lignin to form lignosulfonate	Delignification (lignin removal) 20–40%, Hemicellulose removal,	Recovery of sulfite is complicated and expensive

Other solvents /methods			Cellulose partially dissolved	
	Ionic liquid	Amphiphilic properties	Dissolution of cellulose	Requires huge amounts of water, recycling systems, corrosion and toxicity may inhibit the next downstream processes
	Concentrated phosphoric acid	Disrupt hydrogen linkages of cellulose	Complete dissolution of cellulose	Recovery of the acid, high cost post-separation of cellulose, hemicellulose and lignin
	Wet oxidation	Free radicals (oxygen species)	Hemicellulose and lignin removal	Requires pressurised system
	Supercritical fluid CO_2	Low viscosites and surface tension allows easy penetration into microporous matrix	Delignification (lignin removal)	Energy intensive
Combinational – Catalytic Mechanochemical	Mechanocatalytic Depolymerization	Mechanical impact, attrition, shear and compression Initmate contact of catalyst to reactant	Versatile interaction with lignocellulose biomass, depends on catalyst/solvent used	Energy intensive and chemical-resistance equipment
Combinational – Thermochemical	Dilute acid hydrothermal	Protonation of hydroxyls groups	Hemicellulose removal, Cellulose partially depolymerize, Effective against hardwood	Acid-resistance equipment, acid neutralization, Handling of waste (e.g. gypsum), Could lead to undesireable degradation of sugar, High pressure may be required
Combinational – Thermochemical	Alkaline hydrothermal	Saponification and cleavage of lignin-carbohydrate linkages	Delignification (lignin removal), Structural swelling, Increases porosity and internal surface area, Decreases DP and crystallinity	Formation of phenolic compounds, High costs due to pH neutralization
Combinational – Microwave-assisted hydrothermal	Microwave-assisted dilute acid hydrothermal	Protonation of hydroxyls groups Vibration from mircowave radiation	Hemicellulose removal, Cellulose partially depolymerize	Acid-resistance equipment, acid neutralization, Handling of waste (e.g. gypsum), Could lead to undesireable degradation of sugar

2.2.1 Physical

Under mechanical methods, different mills such as hammer, knife, ball, and disk mill are usually employed for biomass size reduction to fine particles. Their mechanisms include impact (collision of one object with another); attrition (rubbing motion of materials against two hard surfaces); shear (compresses and cuts particles between two hard edges) and compression (pressing biomass within two solid surfaces). Sometimes, one or combinations of the mechanisms are performed together. [37] The objectives of the mechanical method are to reduce particle size and crystallinity which lead to higher active specific surface area and decrease in DP.(Fig. 10) These reductions amplify the hydrolysis yield of the lignocellulose in general around 5 to 25% that depends on biomass type, milling mechanics, and milling duration, but also increase in hydrolysis rate by 23 to 59%. [172, 173] The milled biomass size must be decreased to one to two mm to permit hydrolysis but particle size below 400 microns has insignificant impact on the hydrolysis rate and yield. [164, 174] On the other hand, size reduction through mechanical option is a costly and energy demanding process that uses up roughly a third of the total electricity consumption within the entire process. Some energy-saving solutions includes chemical or steam-explosion pretreatment of wood chips before further size reduction. [175, 176] Other limitation of mechanical size reduction is its incapability to eliminate lignin, an inhibitor for the microbes or enzymes to access to cellulose. [164]

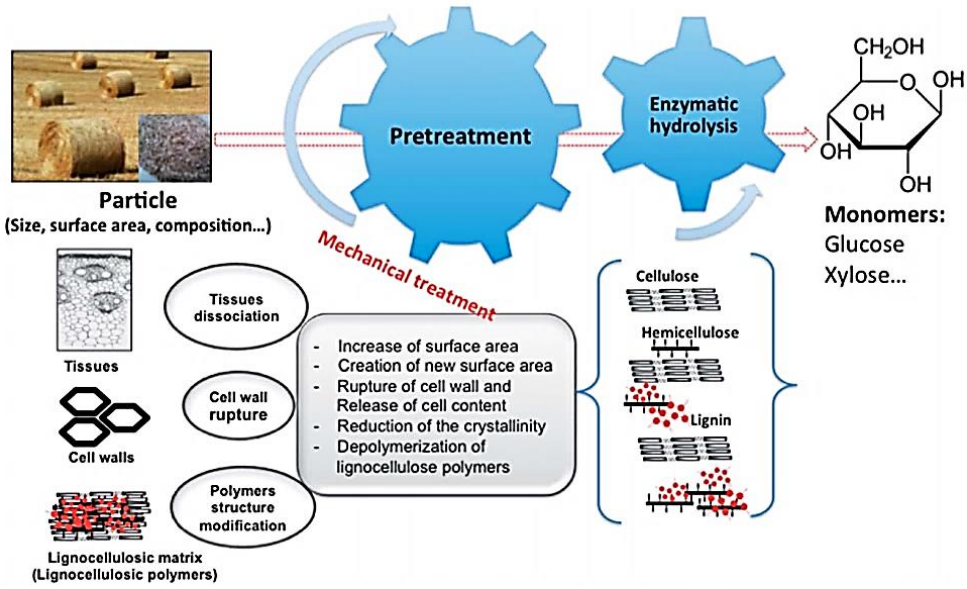

Figure 10 *Role of mechanical treatment for lignocellulosic polymers.* Credit: figure adapted from Barakat et al. [177]

Under the same category, ultrasonic with high frequency sound waves of more than 20k Hz is used to pretreat biomass. The pressure created in a medium of liquid could enhance physical and chemical effect when used with biomass. Though microjet erosion, the plant cell wall collapses and causes mass transfer augmentation which improve delignification by breakage of lignin macromolecules and connections between hemicellulose and lignin. [178] Less than half the time was required for dissolution of holocellulose with combination of ultrasound and IL pretreatments. [179] Despite time-saving, intensive energy is required, thus making it economical unsustainable for industrial applications.

Unlike ultrasonic, microwaves pretreatment employed electromagnetic waves with range from 300MHz to 300GHz. Microwaves can induce fast internal heating and enhance chemical reaction of pretreatment solvents and chemicals when applied to biomass. The “hot spots” created in the polar components of biomass disrupt its structure. In addition, the microwave radiation produces a changing magnetic field which vibrates

the polar bonds and rapidly destroy the crystal structure. [180] However, it also has the same challenges as ultrasonic pretreatment.

2.2.2 Biological

In the past, fungal from nature can be used for processing of lignocellulosic feedstock for paper manufacturing. This renewed environmentally friendly approach has been employed as the biological pretreatment process to enhance the enzymatic saccharification of woody biomass. These fungal can modify or degrade hemicellulose and lignin except cellulose which is more stubborn against these microorganisms. For biogas production, the initial treatment of woody biomass uses soft–, brown–, and white–rot fungi. In particular, white–rot fungi consists of Pleurotus ostreaus ,Cyathus stercolerus, Ceriporiopsis subvermispora, Phanerochaete chrysosporium ,Pycnoporus cinnarbarinus, and Ceriporia lacerate. [181] One study found that Ceriporiopsis subvermispora out of the four fungi used to treat cedar wood chips from Japan and produced four times the methane yield than untreated sample. [182] Generally, biological pretreatments have advantages that includes low startup cost, less energy-intense, no use of chemicals, and can operate in mild conditions. However, unlike physical and chemical processes, biological protocols usually have low hydrolysis rate, incurring to long processing time.

2.2.3 Other solvent(s)/methods

Organosolv pretreatment involves lignocellulosic materials treatment with one or combination of organic solvents or acids at 100 to 250 °C. The chemical process targets the large lignin molecules by cleaving their ether bonds and subsequently solubilzed. [183] The solvents usually employed include methanol, ethanol, acetic and formic acid, acetone [184] and higher boiling alcohols. Elmwood (hardwood) was pretreated with

ethanol at 150 °C and 180 °C for 0.5 h and 1 h, respectively, followed by 55 days of anaerobic digestion, yielded 79.5 mL methane/gVS. Furthermore, methane post-production increased by 73% and showed that organosolv pretreatment is effective for wood with high lignin composition. [185] In other studies, organosolv mixtures include acid catalysts such as H_2SO_4, hydrogen chloride acid, oxalic acid or salicylic acid with purpose of cleaving hemicellulose bonds. [164] Operational costs are reduced when recovery of the solvents is made possible with techniques such as evaporation and condensation. In addition, solvent separation must be performed as they may inhibit the subsequent treatments such as fermentation and enzymatic hydrolysis. [186] Nevertheless, separation is not required if ethanol is used as a solvent because it can be electrooxidized to acetate in the subsequent alkaline water electrolysis process. [187]

Next, sulfite pretreatment to overcome recalcitrance of lignocellulose (SPORL), from its name focus on dissolution of lignin to form lignosulfonate, a valuable lignin product. It is an effective technique that uses aqueous sulfite or bisulfite solution with small amount of acid to maintain pH at 2 that remove lignin (20–40%) of total lignin from the biomass substrate. The operating conditions consists of soaking in 2 to 6% H_2SO_4, and 2 to 10% sulfite (based on dry biomass), at 150 to 180 °C for 10 to 30 mins, accordingly to biomass type. [188] Under this acidic condition, most hemicellulose can be dissolved with cellulose, partially dissolved as well. The buffer function of sulfite slightly raises the pH which reduces the degradation of sugars that could inhibit the final fermentation process. As a result, the recovery of total sugar is higher than the corresponding dilute acid pretreatment with similar amount of acid used. The advantage of SPORL is that feedstock can be treated directly without size reduction, leading to cost savings pertaining to the total energy consumption. However, the recovery of sulfite is challenging and expensive.

Another relatively new solvent-based pretreatment uses ILs which made up of high thermally stable and high polarity organic salts with various melting points with measurable vapor pressure. They are considered as efficient and sustainable because solvation of large amount of cellulose can be accomplished under benign conditions with less power input. Moreover, full recovery of IL is possible with minimal amount of residues for the repeated cycle. [189] Researches were conducted with various ILs, including, 1-n-butyl-3 methylimidazolium chloride and benzyldimethyl (tetradecyl) ammonium chloride to prepare woody biomass for enzymatic digestibility. [164] However, some ILs such as chloride-bearing imidazolium cations are toxic and corrosive. Some other limitations of ILs consists of higher operating costs and the inhibitory impact on the downstream enzymatic process. Moreover, the total recovery of ILs after pretreatment needs huge volume of water and recycling systems, incurring operation costs. [190]

Another solvent used is the phosphoric acid of high concentration (85%) at room temperature that can disrupt hydrogen linkages of crystal structure of cellulose and support complete dissolution. By dilution of adding water to the cellulose dissolution, amorphous cellulose can be regenerated. However, the recovery of the acid, cost, and post-separation of products are the main challenges of this method. [37]

Free radicals from wet oxidation pretreatment using oxygen, ozone, and hydrogen peroxide as the oxidizing agents to catalyze can be applied to lignocellulosic biomass. They are usually performed at elevated temperature of 125–300 °C and pressurized at 0.5–20 MPa. Cellulose is partially degraded with hemicellulose extensively cleaved into monomeric sugars and oxidized into organic acids while lignin was cleaved and oxidized. As a result, wet oxidation prepares the accessibility of cellulose for the next downstream

process through removal of hemicellulose and lignin. For instance, methane yield was enhanced by 50 to 120% with hydrogen peroxide treatment. A milder option is ozonolysis that operates at room temperature and pressure, thus will avoid generation of aromatic compounds from oxidized lignin and furfural, and other inhibitors. Nevertheless, most wet oxidation process usually has high undesirable loss of hemicellulose. [191]

Finally, supercritical fluid extraction involves CO_2 with its supercritical state (SC-CO_2) at ambient temperature and high-pressure of 1071 psi. Its non-toxic, non-corrosive, non-flammable and inexpensive nature makes it appealing for the process when compared to toxic ammonia. However, using it alone is inadequate to pretreat lignocellulosic materials as their interaction are non-reactive. Therefore, the combination of CO_2 with SO_2 at 130 °C for 4 h was tested on aspen wood chips and removed 61% of lignin while keeping 83% of total carbohydrate intact. [192] In addition, other researchers also performed SC-CO_2 on aspen hardwood at higher temperature of 112–165 °C and pressure of 3100 and 4000 psi. [193] After pretreatment, the final sugar produced from enzymatic hydrolysis had high yield of 84.7 ± 2.6% (w/w) of theoretical maximum for aspen. It is concluded that the interaction of moisture and SC-CO_2 was crucial for higher sugar yield.

2.2.4 Combinational methods

2.2.4.1 Catalytic Mechanochemical

The mechanical-assisted grinding of raw materials in ball mills with minimum or no solvent is valued to be a green synthesis process and known as Mechano-chemistry. [194] The mechanical force is essential to overcome the diffusion barrier required in solid-solid catalytic reactions. Whereas, in general catalytic depolymerization, a solvent is

usually used to overcome the diffusion barrier. [195] Unlike other pretreatment methods that use large amount of solvents, mechanochemistry is more cost-effective, environmentally friendly and without additional external heat source. Furthermore, the use of fossil-derived solvents is unsustainable and energy-intensive to produce, purify and recycle (only about 50–80%). [196] Different magnitudes of size reduction can be achieved through varying the intensity of the mechanical operations. [177] The smaller the particles, the greater the surface area, which enhances the mill's ability to "push" the catalyst towards the reactive portions of the woody particles, e.g., the β-1,4-glycosidic bond for both xylan and cellulose. Consequently, this will permit an intimate contact between catalyst and the wood particles which can be attained in the mechanochemical system.

The usage of catalyst, acid, alkaline and oxidizing agents in ball mills to process cellulose and lignin had been studied extensively. First, in a catalytic mechanochemical study [195], various catalysts — bentonite, talc, alumina, kaolinite were tested to dissolve cellulose. Kaolinite, an acidic solid catalyst, was highlighted to have effective cleaving impact on the glycosidic bond of cellulose after mechanochemical hydrolysis for 3 hours in a shaker mill. Under the same conditions, chemically treated delaminated kaolinite further improved the water solubilization of cellulose and Aspen wood to 86% and 60%, respectively. In another study [197], catalyst(K26)-assisted ball milling with cellulose at 60 rpm for two days could produce 70% of oligomers necessarily for high yield of glucose (88%) in mild HCl (0.012%) hydrolysis. The preparation of catalyst, K26 involved coke powder treated in nitrogen gas at 973 K, followed by pH neutralization and drying. The appealing reusability of K26 was demonstrated when both unreacted K26 and cellulose residue after hydrolysis were reused 4 times sequentially with new batch of cellulose. The substantial glucose yield was ascribed to the presence of the

mildly acidic functional group in K26 and the imitate contact of solid catalyst with the substrate during ball milling.

Unlike solid catalysts, gaseous acid (HCl) was introduced as part of solvent-free ball mill study of cellulose. This pretreatment of acid impregnation composes of cellulose (6 g) exposed to HCl vapors for 15 min at ambient temperature and pressure, then evacuated for 1 h under vacuum to achieve concentration of 1.03 mmol HCl per gram of cellulose. After ball mill of one gram of acid-impregnated cellulose at 800 rpm in a stainless-steel vial (internal temperature not above 42 °C), all cellulose was successfully converted to water-soluble oligosaccharides within two hours. When the substrate and acid were switched to beech wood and H_2SO_4, respectively, similar performance was also replicated. [198] Possible use of nanofiltration or ion-exchange resins could be employed to purify water-soluble sugars (glucose and xylose) and separate lignin fragments to prepare for biorefinery processes. [199] In another study, ball milling of barley straw with oxalic acid dihydrate, followed by the 130 °C hydrolysis improved total reducing sugar yield by 30% when compared to samples without mechanically processed. [200]

In contrast, alkaline-assisted ball milling process were conducted using 0.1 g of sodium hydroxide and 2.5 g of sodium sulfate as grinding auxiliary in a planetary ball mill. 100 mg of organosolv lignin was extracted by ethanol/water from beech wood. [201] Experiment on varying parameters (grinding bowl topology, number of balls, and grinding speed) were also carried out and optimized. Sodium sulfate was evidenced to be the best grinding auxiliary to prevent agglutination of molten reactants. 55% of the β-O-4 bonds were discovered to be cleaved into fractioned phenol products. In addition,

cellulose and hemicellulose degradation were also detected by nuclear magnetic resonance (NMR) spectroscopy.

The combination of oxone (potassium peroxymonosulfate) as the oxidizing agent and catalysts, 4-hydroxy-TEMPO and KBr, was targeted for oxidative conversion of lignin β-O-4 chemical structures in the mixer mill. The substrate used was organosolv beechwood lignin and milled at either 25 or 30 Hz for 60 to 180 min. When milled for 180 min, the molecular weight decreased to 40% with the degree of oxidation increased to 84%. This corresponds to the oxidation of β-O-4′ aryl ether linkages and phenylcoumaran substructures, syringyl and guaiacyl units, implying to benzylic alcohol oxidation and cleavage of terminal phenolic groups. The scaling up of the experiment by 100-fold had shown positive results by using a bigger disc mill. Essentially, the energy consumption would decrease with upscaling of reaction especially for mechanochemistry, making it a more economical option for biomass valorization. In other study, industrial lignin was structurally modified by ball milling with IL (1-ethyl-3-methylimidazolium acetate). This modification led to a reduction of the methoxy group content in the lignin by 45%. The use of ionic liquid prevented degradation to the phenolic hydroxyl as well as the carboxyl groups. [200]

Another type of equipment known for its high continuous throughput is the single/twin screw extruders. Extrusion with additives (acid, alkali, hot-compressed water and other solvents) were also used mainly to pretreat agricultural crops and grass. [202-208] Notably, extrusion of pine sawdust with concentrated 5 wt% H_2SO_4 was performed with acid-resistant, twin screw extruder equipment made from a stainless-steel alloy (AL6XN). It was coupled to acid hydrolysis at 130 °C and achieve 50 % glucose yield. [209] Another twin-screw extrusion of Populus tremuloides with NaOH (0.02 g/g biomass) had

extracted 90% of hemicellulose. [210] The importance of energy consumption as a focus for obtaining satisfactory sugar recovery highlights the need to optimize settings during both the biomass preparation and the extrusion process.

Although mechanochemistry shown great potential in biomass valorization, the bottleneck of its scalability lies in its high energy consumption. The combination with other complementary technologies such as enzymatic hydrolysis may decrease energy consumption and further increase the efficiency to enable a broader implementation for sustainable biomass valorization. [211]

2.2.4.2 Thermochemical

Next, thermochemical methods use one or combinations of chemicals with heat to remove or reduce the recalcitrance of biomass. After this pretreatment, hemicellulose can be removed by dissolution or hydrolysis; delignification will be through depolymerization and dissolution; and cellulose will be de-crystallize or depolymerize by pre-hydrolysis. However, unwanted side reactions such as degradation of sugars may lead to reduced sugar and act as inhibitors for fermentation refinery. Moreover, condensation of lignin could delay lignin removal and induce undesirable adsorption of enzymes on lignin during subsequent enzymatic process.

Alkaline pretreatment offers a better way at removing lignin yet less ineffective against hemicellulose. Bases such as potassium hydroxide, lime, sodium carbonate, liquid ammonia and sodium hydroxide are commonly used. The mechanism behind this pretreatment involves and breaking of carbohydrate lignin bonds (ether, ester and glycosidic) and saponification. [37, 212] As a result, this promotes structural swelling and increases porosity, internal surface area and concurrently, decreases DP and crystallinity.

Basically, sodium hydroxide at low concentration is used to specifically on hemicellulose and lignin removal at increased temperature and pressure, without recycling of the alkali. In contrast, cellulose dissolves at higher NaOH concentration under normal pressure and without heating. Several limitations of this process include the likelihood of phenolic compounds formation with increasing cost from post-processing of pH neutralization. [164]

With the use of acid such as H_2SO_4, HCl and H_3PO_4 at temperature (80–220 °C), the hydrolyzed hemicellulose can dissolve into liquid hydrolysate. This creates pores on the cell wall and improve accessibility to cellulose which may be partially depolymerized into glucose during this pretreatment. With dilute acid such as sulfuric acid of 0.5 to 2% in concentration at elevated temperature of 140 to 180 °C for duration of 10 to 40 min, up to 90% of hemicellulose can be dissolved and even degraded into furans. This treatment is effective for hardwood but faces issues such as degradation of sugar (to furans and organic acids) that leads to lower sugar yield. However, the acquiring of acid-resistance equipment, post acid neutralization and handling of gypsum waste are the main challenges of this treatment. The acetyl group in hardwood (3–5%) that linked to hemi-cellulose can be easily hydrolyzed into acetic acid with heating. Acetic acid will serve as a reactive acid during pretreatments that involves steam and hot water. For example, steam explosion is used to process biomass with saturated steam. [169] Inside the reactor, the biomass experiences high pressure and temperature of 0.7 to 3.4 MPa and 160 to 240 °C respectively for short durations (few seconds to minutes). Then, the sudden depressurization causes the biomass to expand and “explode”, and then reduce in size. As mentioned, the acetic acid released further speeds up hydrolysis of hemicellulose and cellulose. Both acid and heat degrade the sugar and produce furans

while lignin condense, relocate, and redistribute. While this method is effective for hardwood, it requires a significant amount of energy and scaling up is challenging. [37]

When performed at moderate temperature (80–240 °C), hydrothermal treatment or hydrolysis of biomass can occur. [171] The bioproducts obtained can potentially serve as chemical building blocks or platform chemicals, and further upgraded to high quality biochemicals and biofuels. Wet woody biomass can directly undergo the hydrothermal process which avoids the energy-intensive drying step. [213, 214] This is a major advantage when handling high moisture biomass such as sugar cane bagasse. [215]

The hydrolysis of lignocellulosic biomass is commonly performed with H_2SO_4 because of its advantages of being cost-effective, efficient, and less toxic and corrosive compared to other acids. [216] To minimize environment impact, dilute H_2SO_4 is used as catalyst in hydrothermal pretreatment which work efficiently to extract sugars from plant biomass for further processing. In addition, heterogeneous acids, heteropoly acids and ionic liquid combined acids had also been employed as shown in Table 2. Despite being more environmentally benign with good recyclability, the cost [217] and stability [218] of heteropoly acids require further improvement for valorization of lignocellulose. On the other hand, solid acids may be easier to recover but lacks efficiency in hydrolysis. [219]

As it is challenging to calculate compare energy-intensive value for various pretreatment methods because of different working parameters, Kazi et al. proposed the comparison of profitability for the short-term economic assessment. [220] The simulated study was based on the product, ethanol from corn stover with the pretreatments consisted of dilute acid, 2-stage dilute acid, ammonia fiber explosion (AFEX), as well as hot water pretreatment. The most effective method was dilute acid pretreatment because of the lowest product value ($1.36 of gasoline equivalent).

Table 2 Dilute acid hydrothermal conversion of different feedstock to sugar.

Catalyst	Feedstock	Temperature (°C)	Time (h)	Solvent	Loading (g/ml)	Xylose Yield (%) [a]	Glucose Yield (%) [b]	Total sugar (g/100 g dry mass) [c]	Reference
H_2SO_4 (0.25–1.0 wt%)	Aspen	160, 175, and 190	0.53	H_2O	0.05	85	12	18.70	[221]
H_2SO_4 (0.25–1.0 wt%)	Balsam fir	160, 175, and 190	0.53	H_2O	0.05	70	10	9.07	[221]
H_2SO_4 (0.25–1.0 wt%)	Basswood	160, 175, and 190	0.53	H_2O	0.05	80	12	17.53	[221]
H_2SO_4 (0.25–1.0 wt%)	Red maple	160, 175, and 190	0.53	H_2O	0.05	82	13	20.12	[221]
H_2SO_4 (0.25–1.0 wt%)	Switchgrass	160, 175, and 190	0.53	H_2O	0.05	94	10	22.69	[221]
H_2SO_4 (1.5 wt%)	Paulownia	Two-step: 1) 210 H_2O 2) 115 H_2SO_4	1.25	H_2O	0.17	81	4.3	26.80	[134]
H_2SO_4 (1.0 wt%)	Oil palm empty fruit bunches	190	0.05 *Ramp	H_2O	0.1	77.5	17.3	20.30	[222]
H_2SO_4 (1.5 wt%)	Corncob	125	1.5	H_2O	0.1	83.4	7.8	31.76	[223]
LiBr (61 wt%) With H_2SO_4 (3 wt%)	Poplar	120	1	H_2O	0.1	72	91	52.28 [d]	[224]
C4mmCl (4 g) with HCl (0.04 g)	Corn stalk	100	0.5	Ionic liquid /H_2O	0.05	66 [e]		13.2	[225]
C4mmCl (4 g) with HCl (0.04 g)	Sugarcane bagasse	100	1	Ionic liquid /H_2O	0.05	66[e]		16.2	[225]

Catalyst	Feedstock	Temperature (°C)	Time (h)	Solvent	Loading (g/ml)	Xylose Yield (%) [a]	Glucose Yield (%) [b]	Total sugar (g/100 g dry mass) [c]	Reference
[EMIM]Cl (0.5 g) with HCl (10 wt%)	Corn stover	105	6 + 3.5	Ionic liquid /H_2O	0.1	74	19	25.2	[226]
phosphomolybdic acid ($H_3PMo_{12}O_{40}$) (H^+ = 18 mol%, $PW_{12}O_{40}^{3-}$ = 6 mol%)	Japanese cedar wood	150	24	H_2O	0.03		32[e]	6.4	[227]
$H_5BW_{12}O_{40}$ solution (0.7 M)	Oil Palm empty fruit brunch	25 then 60	24 + 48	H_2O	0.05	25	43	Not mentioned	[228]
$H_5BW_{12}O_{40}$ solution (0.7 M)	Japanese cedar wood	25 then 60	24 + 48	H_2O	0.05	8	53	Not mentioned	[228]
$H_3PW_{12}O_{40}$ (88% w/w)	Sugarcane bagasse	90	3	H_2O	0.02	3.94	27.8	11.0 [d]	[229]
Weak acid Carbon (0.1 g)	Japanese cedar wood	210	1	H_2O	0.007	34.7	25.3	5.1	[230]
Biochar (0.2 g)	Corn stover	100	6	H_2O	0.05	34.0	9.3	30 [d]	[231]
Biochar (0.2 g)	Prairie Cord grass	100	6	H_2O	0.05	48.1	10.6	30 [d]	[231]
Biochar (0.2 g)	Switch grass	100	6	H_2O	0.05	28.2	11.2	27 [d]	[231]
Partial carbonized cellulose C-SO_3H (0.3 g)	Eucalyptus flakes	100	3	H_2O	0.04	100	6.1	9.3	[232]

Catalyst	Feedstock	Temperature (°C)	Time (h)	Solvent	Loading (g/ml)	Xylose Yield (%) [a]	Glucose Yield (%) [b]	Total sugar (g/100 g dry mass) [c]	Reference
Fe_3O_4-SBA-SO_3H (1.5 g)	Corn cob	150	3	H_2O	0.1	45 [e]		Not mentioned	[233]

a) Yield% calculation was based on total mass of xylose measured to total mass of hemicellulose, b) Yield% calculation based on total mass of glucose measured to total mass of cellulose, c) g/100 g dry mass calculated from total mass of glucose and xylose measured per 100 g of dry biomass, d) g/100 g dry mass calculated from total mass of glucose, xylose, galactose, arabinose and mannose measured per 100 g of dry biomass, e) Total reducing sugar yield%.

2.2.4.3 Microwave-assisted dilute acid hydrothermal

The hydrothermal valorization of biomass with microwave heating instead of conventional heating had showed significant advantages such as cost-effectiveness, rapid conversion rate, uniform volumetric heating performance and increased energy efficiency. [171, 234-236] Furthermore, microwave heating can be controlled to reduce reaction time with high selectivity and yield of products when side-products are minimized. This was demonstrated in Paulownia wood fractionation study with 1.6-fold higher solubility rate of xylan in microwave compared to conventional heating. [237] Furthermore, in a sugarcane bagasse study, the sugar removal was 4 times higher in microwave heating than conventional heating. [238]

Fig. 11a compares the heating profiles of conventional and microwave heating. In conventional heating, heat is transferred from the outer surface to the interior of the biomass through mechanisms such as heat conduction or convection. [239] As a result, this heat flow direction also influences the chemical transformation of rigid biomass from outer region towards the inner region. [240, 241] In contrast, in microwave heating, the heating is opposite of conventional heating and starts from the inside of biomass to the outside. This is due to the direct coupling effect of electromagnetic waves with the dipoles in the reaction medium. The electromagnetic energy is directly converted to localized heat at molecular level is then uniformly dissipated through the biomass material. [169] However, it is difficult for pure water to heat up from 100 to 300 °C as super critical water is transparent to microwave radiation. Hence, additives such as dilute acid or inorganic salts can be added to promote effective heating. Lignocellulosic biomass naturally contains low amounts of inorganic salts, which can increase microwave absorption and facilitate effective heating of water in the reaction medium. [242] The other

important microwave hydrothermal parameters which may affect product yield and selectivity includes microwave power intensity, biomass loading, solvent amount, particle size and distribution, reaction temperature and time, and catalyst amount. [171, 243, 244]

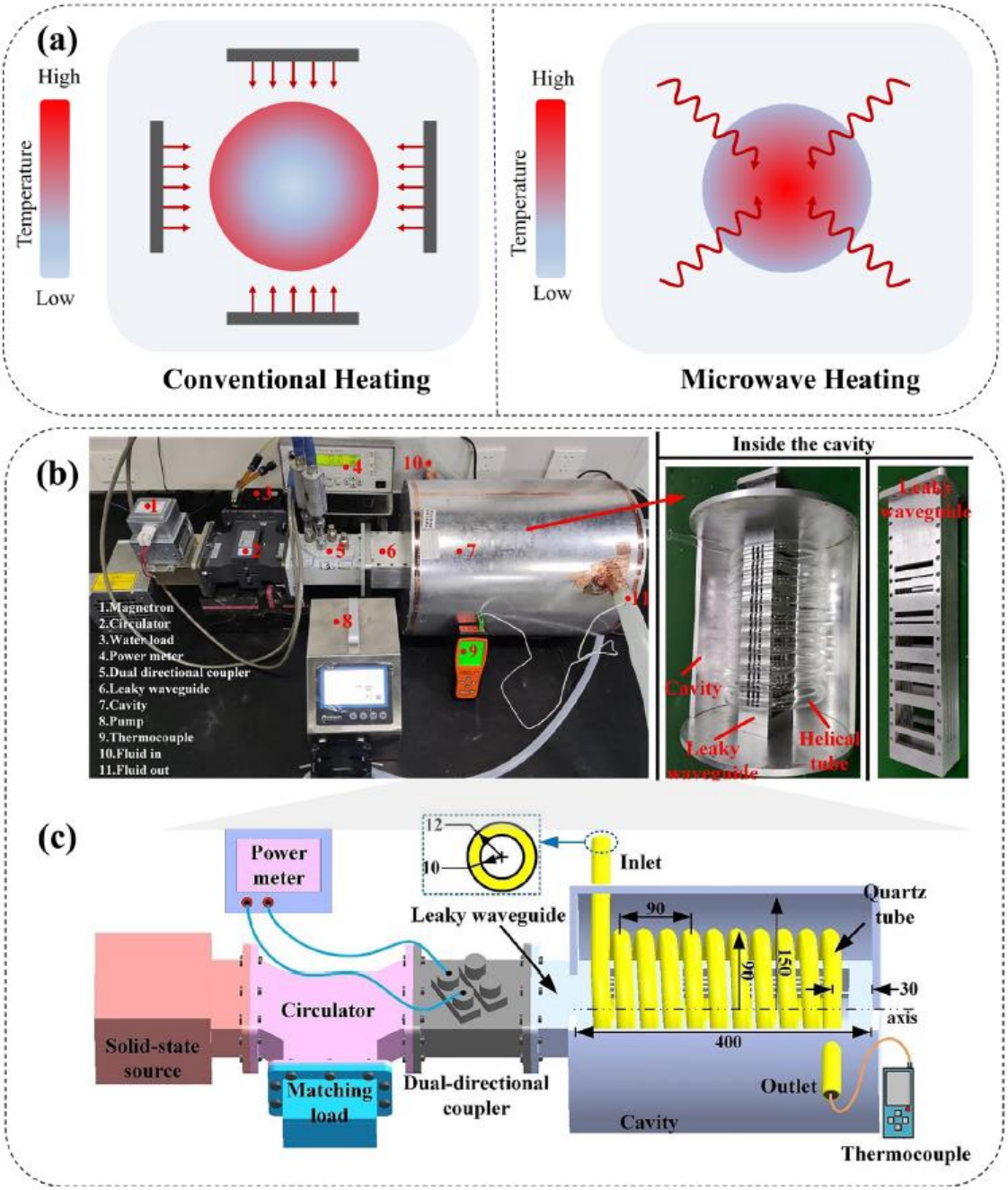

Figure 11 *(a) Heating profiles in conventional and microwave heating. Microwave-assisted continuous-flow reactor – (b) experimental setup, and (c) schematic illustration.* Credit: figures adapted from Zhang et al. [245]

The microwave pretreatment was experimented on plant fiber material and hydrolysis could only be observed at temperature above 160 °C and almost no effect at 100 °C or below. [246] At low temperature of 90 °C, the addition of sulphuric acid (0.24 M) helped with the extraction of xylooligosaccharides (29% yield) from sugarcane bagasse hemicelluloses. [247]

Binod et al. investigated the pretreatment method using microwave with acid, alkali and alkali-acid on sugarcane bagasse. The microwave with alkali-acid made significantly higher sugar yields for downstream enzymatic saccharification. This is due to the alkali effect for lignin removal. [248] Zhu et al. also studied microwave pretreatment on sugarcane bagasse with NaOH and H_2SO_4 and observed that H_2SO_4 exhibited high hydrolysis yield (86%) of total sugars (glucose and xylose) than NaOH at 170 °C. [238] Shao et al. performed microwave-assisted hydrothermal liquefication of bagasse in acidified seawater. [249] The highest yield of HMF (8.1 wt%) was achieved at a reaction temperature of 149 °C, held for 4 min, and with a liquid-to-solid ratio of 12:1. Other microwave hydrothermal studies with H_2SO_4 (0.1 to 0.4 M) on cotton waste [250], bode (Styrax tonkinensis) wood [251], and eucalyptus wood [252] demonstrated better enzymatic hydrolysis to glucose for bioethanol production.

For scalability, the leaky-waveguide reactor for continuous microwave-assisted production was recently developed (Fig. 11b, c). [253] This creates a system for the continuous production of bioproducts, that could be integrated into a biorefinery. [253] As shown in Fig. 11b, magnetron, circulator, water load, power meter, and coupler (items 1 - 5) were used as power and measurement units. [253] The design of the cavity is optimized based on the leaky waveguide to achieve the uniform distribution of

microwave energy. So far, the system has not tested for operational readiness at various temperature and pressure, to be comparable to the existing isolated microwave systems.

2.3 Water Electrolysis

Water electrolysis was first industrialized in 1888 by Dmitry Lachinov, laying the foundation for large MW size electrolysis plants after 1920s but halted by cheaper way to produce hydrogen from fossil fuels. [254] It was only in 1970s when oil crisis hit the global energy sustainability that brought back water electrolysis to produce hydrogen. [255] Intermittent energy issues faced by renewable energy sources can be solved when surplus renewable electricity drive water electrolysis to generate green hydrogen and store for later use. The stored hydrogen can be operated in hydrogen fuel cells, leading to a zero emission in the "Hydrogen economy". [256] Unlike steam reforming of fossil fuels that generates H_2 mixed with CO & CO_2 [20], water electrolysis can produce extremely pure hydrogen (99.9%) but only occupy 2% of global hydrogen market due to its production cost. [257]

Primarily, there are three types of water electrolysis systems (Fig. 12) – proton exchange membrane (PEM), solid oxide and alkaline water electrolysis (AWE). PEM electrolysis consists of acid electrolyte which allows H^+ to pass through the membrane. From the reduction-oxidation (redox) reactions, H_2 and O_2 are produced at the cathode and anode, respectively. The main challenges of PEM electrolysis are high operational cost of materials arising from the membrane (Nafion) [193] and acid-stable, precious metals electrocatalyst (e.g. platinum group metals). Next, solid oxide electrolysis involves the solid electrolyte at high temperature (700 to 1000 °C). Yttria-stabilized zirconia (YSZ)

solid electrolyte is used to only permit oxygen, O^{2-} ion to pass through. Despite having the highest energy efficiency among the electrolysis systems, it comes with high hydrogen cost. AWE uses porous diaphragm that only allows the OH^- anions to flow through for OER to occur at anode. Water is reduced to H_2 at cathode (HER). AWE faces some challenges. [12] First, the possibility of O_2 diffusion towards the cathode will reduce the electrolyzer efficiency and the O_2-H_2 mixture leads to safety-related shutdowns. Second, the maximum current density is limited by ohmic losses from the poor OH^-

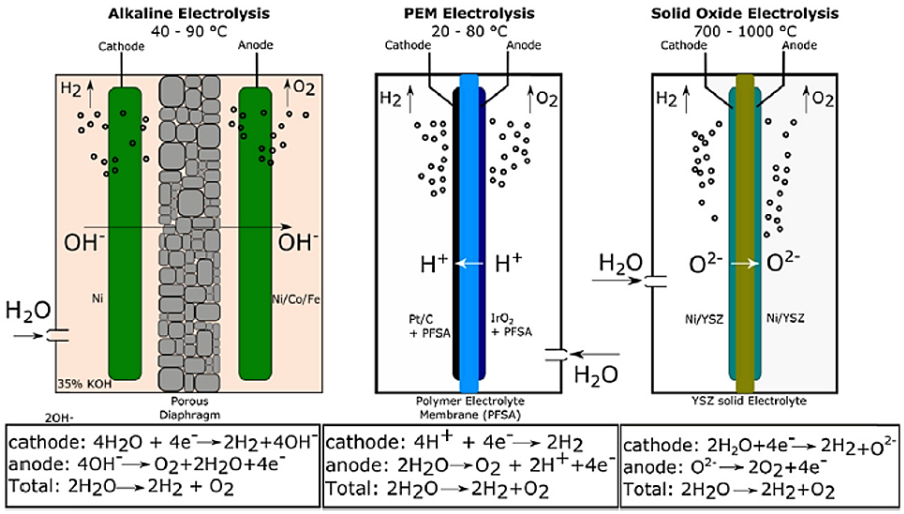

Figure 12 *Three types of water electrolysis systems and their operating principles.* Credit: figures adapted from Carmo et al. [12]

conductivity of ZrO_2 particles and polymer mesh used in the diaphragm, reducing the cell potential efficiency. Lastly, the low operating pressure caused by high porosity of diaphragm material but can be solved with a fixed minimal gap to prevent mixture of generated gas. However, this gap also enables the formation of vertical streams of gas bubbles that increase the Ohmic overpotential. Despite the drawbacks, the main advantage is that non-noble abundant metals can be used to fabricate electrocatalysts for alkaline electrolyzer, thus lowering its entire operating cost and capability to scale up.

The required potential (V_{cell}) for water electrolysis is consisted of theoretical equilibrium cell voltage (E^0), activation energy barrier (η_{act}) and ohmic overpotential (η_{ohm}). (i.e. $V_{cell} = E^0 + \eta_{act} + \eta_{ohm}$). [258] η_{ohm} sums up all cell resistances that influences the electron flow, such as external circuit, membrane, electrodes, and electrolyte and can be minimized through good electrochemical engineering practice. [259] η_{act} can be reduced through better electrocatalyst design and material selection for (OER and HER). For instance, volcano plots from theoretical studies were established with interest to replace costly platinum catalysts with non-noble metal catalysts. [260-262] E^0 is calculated as 1.23 V at 25 °C from Gibbs free energy, ΔG_0 (+237.2 kJ mol^{-1}) for the minimum amount of electrical energy to produce oxygen and hydrogen. [12] The high E^0 is an intrinsic characteristic of OER rather than from HER due to its mechanism.(Fig. 13) In alkaline electrolyte (Fig. 13A), HER consists of two steps: (1) Volmer reaction, followed by either (2) Tafel reaction (consecutively adsorption of another hydrogen atom) or (2) Heyrovsky reaction (combination with a water molecule) to evolve hydrogen. In contrast, OER (Fig. 13B) follows the 4-steps adsorbate evolution mechanism as proposed by Antipin and Risch. [186] The interaction of OH^- with the metal site leads to sequential transformations from: M-OH to M=O (a1), M-OOH (a2), M-OO (a3), and finally M-OH, releasing O_2 (a4). Notably, this involves 4 electron transfer steps which results in its sluggish kinetics nature as well as high energy consumption. [263]

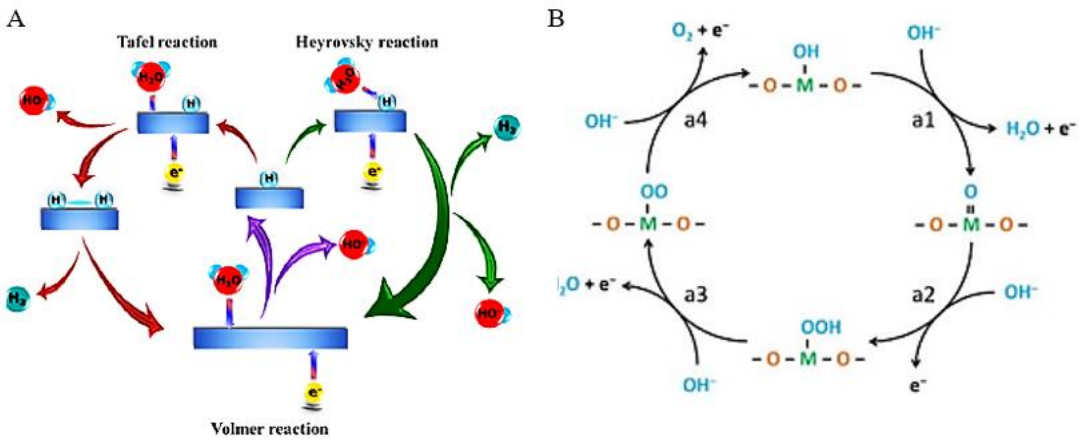

Figure 13 *(a) Mechanism of HER and, (b) OER electrocatalysis in alkaline media*. Credit: figures adapted from A) Yu et al. [264] and B) Antipin et. al. [265]

2.4 Hybrid electrolysis

As water electrolysis is limited by high energy requirement and hazardous oxygen-hydrogen mixture issue, strategies such as hybrid electrolysis emerged. This technology substitutes OER with much more readily oxidizable reactants and significantly decreases the energy needed for hydrogen production. The total reduced energy consumption (30–70%) was shown in electro-reforming of alcohols such as methanol and ethanol and were intensively studied in PEM electrolyser. [23] When methanol is anodised in water, low value carbon dioxide is produced, and protons travelled through the Nafion membrane to the cathode for reduction to hydrogen. In methanol-water electrolysis, the limiting factors involve the concentration of methanol, undesirable crossover of methanol vapor and use of precious metals such as Pt and Ru for electrocatalyst and high toxicity issues. [21, 22]

On the other hand, ethanol aqueous solution is much preferred in electrochemical reforming because of ease in transportation and storage, non-toxicity and can be directly produced from abundant starch or cellulose. [25] In most studies, the electrochemical oxidation of ethanol was carried out at elevated temperature of 80 °C for enhanced kinetics reaction. [24, 27, 28] Addition of 0.01 M sulfuric acid can exclusively contribute to an enhancement of the anodic charge transfer reaction kinetics that reduced energy requirement at 50 °C. [29] In alkaline electrolyte membrane electrochemical reforming of 2 M ethanol with 2 M NaOH, 0.69 V cell potential was applied with corresponding current density of 1 A cm^{-2} and acetate was produced in conjugation with H_2. It is worth noting that only a low energy consumption of 18.49 kWh kg^{-1} was observed when

compared to commercial alkaline water electrolyser of 48.20–64.30 kWh kg^{-1}. [24] Due to the incapability to break the C-C bond of ethanol, incomplete oxidation to CO_2 resulted in CO intermediates that passivated the Pt anode catalyst surface, thus a higher potential (> 0.9 V cell potential) was required to further oxidize the adsorbed intermediates. [25] In all alcohol electro-reforming, due to the non-polar characteristic of alcohol, high concentration may lead to swelling of the separator or poisoning of the anode and will severely affect the catalytic performance. [27]

You et al. developed the bifunctional catalyst (Ni_3S_2/NF) for electrooxidation of various selected organics as well as for H_2 evolution. [32] In their study, the AEM was used with perquisite requirements following: 1) organic precursors used must be soluble, 2) value of oxidized product should be more than precursors compound, 3) organic precursors should have oxidation potential lower than OER (so that Faradaic efficiency of new substituted oxidised reaction will be high), and 4) precursors and product do not interfere and compete with HER. The Linear Sweep Voltammetry (LSV) plots of Fig. 14 demonstrate earlier shift of onset potential from 1.55 to ~1.35 V vs RHE when biomass-derived substrates were added to the electrolyte. It is worth noting that at 1.40 V vs RHE, fast current density increase indicates a more favourable oxidation of organic precursors than OER. Moreover, all five organic precursors were almost fully anodised to value-added products at constant voltage of 1.423 V vs RHE with Faradic efficiency close to 100 %. Likewise, for HER, the measured quantity of H_2 with GC was in line with calculated H_2 quantity at 100 % Faradic efficiency.

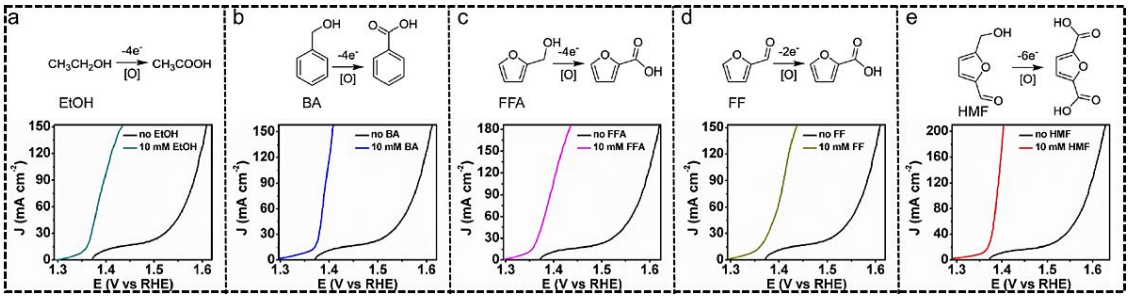

Figure 14 *Anodic reaction of specific organics to value-added chemicals with their LSV plots of Ni_2S_2/NF at scan rate of 2 mV s^{-1} in 1 M KOH with/without 10 mM organic species a) Ethanol (EtOH), b) Benzyl alcohol (BA), c) Furfural alcohol (FFA), d) Furfural (FF), and e) hydroxymethylfurfural (HMF).* Credit: figures adapted from You et. al. [32]

Although hybrid electrolysis of small organic molecules has overcome issues faced by water electrolysis, the production of these molecules is energy intensive and costly. And some are already classified under important biofuels (e.g., ethanol). Instead, abundant raw biomass, e.g., lignocellulose, should be used to match the scale of hydrogen production.

2.5 Electroforming of lignocellulosic biomass

Numerous techniques to upcycle lignocellulosic biomass into value-added chemicals had already existed, for example, saccharification or fermentation of cellulose to ethanol. [266] These methods require specialized equipment and external energy supply for entire operation and infrastructure. On the other hand, lignin valorization involves conversion methods such as pyrolysis, gasification and similar pretreatment techniques discussed earlier. [46] Although each conversion method has their own advantages, an environmental-friendly alternative would always be more esteemed. One possible method is based on electrochemistry that operates at benign conditions (ambient temperature and atmospheric pressure). In addition, green chemistry can also be achieved by the following: 1) its integrability with renewable energy and automated synthesis by flow chemistry; 2) kinetic barriers are overcome by applied electrical

potential instead of thermal source, hence more energy efficient; 3) the produced H_2 or O_2 from water electrolysis can act as reagents; 4) product selectivity and reaction rate can be controlled by tuning the applied voltage or current instead of altering the solvent or catalyst, thus fit well into automated synthesis [267]; 5) the established architecture of water electrolysis makes both reduction and oxidation of reactant possible simultaneously. The existing membrane or diaphragm can act as separator to prevent migration of byproducts; and 6) decentralized processing of biomass where off-the-grid renewable energy can be used to convert biomass, thus reduce transportation energy, and eventually decrease the total carbon footprint.

At the anode, the lignocellulosic biomass could be oxidized by three modes of electron transfer. (Fig. 15) The direct electron transfer is the basic mode of transfer of electron from the reactant (biomass) to the anode's surface. When the reactant loses electron, it becomes oxidized and form the final product. Next, the reactant in the electrocatalytic cascade reaction involves the initial direct electron transfer step and changes into intermediates. Subsequently, the intermediates form final product by self-rearrangement or dimerization coupling. The third mode is through mediated electron transfer, that includes a mediator in the electrolyte. The mediator gets excited at the electrode surface and then oxidizes the reactant by indirect transfer of electron. This method benefits reactions with large molecules that are difficult to adsorb at electrode surface.

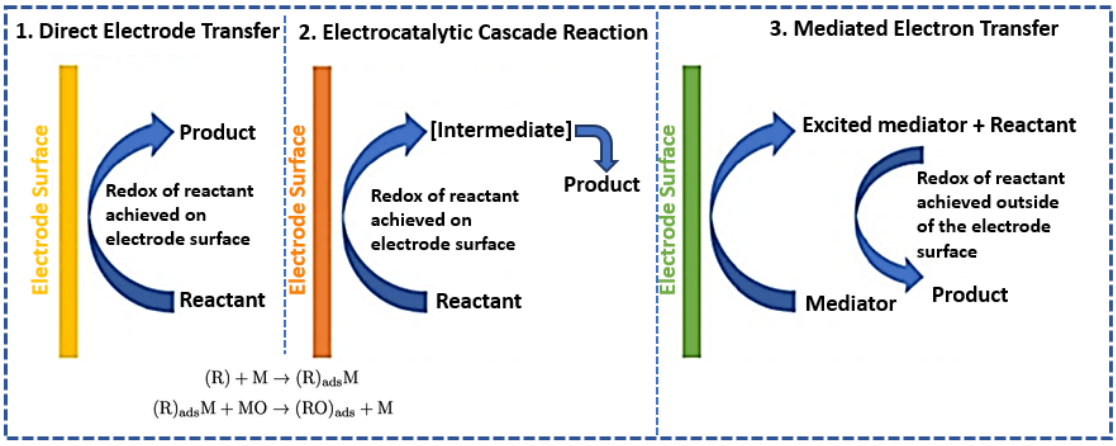

Figure 15 *General mechanism of electron transfer for organic transformation and substrate oxidation equations.* Credit: figures adapted from Garedew et. al. [46]

An important aspect of the performance of electrocatalysis can be determined by Faradaic efficiency, which can be expressed as fraction of charge transferred to form the desired products. One possible interference could be OER that is competing with organic oxidation of biomass. [46] Several influencing factors encompass bond strength of oxygen species on the catalyst surface, overpotential for the OER on a particular electrode material, and current density.

Direct conversion of biomass is rare and so far, there was only one study on crushed barley straw powder and others focused on fractionated cellulose, hemicellulose and lignin from real lignocellulosic biomass. Most of the studies had low current density, with either no specific product or generate CO_2. The anodic oxidation of lignin and hemicellulose is summarized in Table 3.

As mentioned previously, cellulose is the most abundant type of biomass among renewable resources, drawing significant attention of ongoing research. Especially so, the electrochemical reforming of biomass holds great potential due to its controllability over valorization processes and benign requirements. Furthermore, it can be driven by renewable electricity, thus making the process green and sustainable. Consequently, the

integration of green hydrogen production with anodic biomass electroforming has gained growing interest. Cellulose electroreforming requires catalysts, which can be homogeneous (dispersed in solution) or heterogeneous (often anchored on electrode). In most cases, the electrolyte is generated by dissolving cellulose in sodium hydroxide via the freeze–thaw method first reported in 1998. [268] Dissolution allows for greater access to active sites on β-1,4-glycosidic linkages. [269] When these linkages are fully broken, cellulose can be de-polymerized into its monomer, glucose. Glucose is a simple monosaccharide with molecular formula $C_6H_{12}O_6$ and is the main source of energy for most life forms on earth. Apart from cellulose, glucose can also be stored in other polymeric forms, such as starch in plants or glycogen in animals. Glucose can be electrochemically converted to gluconic, glucaric and levulinic acids, as well as 5-HMF. These products can be further valorized into other valuable compounds through electrochemical oxidation (anodic reaction) or hydrogenation (cathodic reaction). Some common glucose transformations are shown in Fig. 16.

Table 3 Anodic oxidation of lignocellulosic biomass - lignin and hemicellulose.

Lignocellulosic biomass	Electrode	Current density	Product selectivity	Hydrogen quantification	Remarks	Reference
Black liquor	Pt, Ni, AISI 304 Stainless steel	< 10 mA cm^{-2}	No product analysis	No	Precious metal used	159
Kraft lignin	Pt, Au, Ni, Cu, DSA-O_2 and PbO_2	< 3 mA cm^{-2}	<17% selectivity to Vanillin	No	Filter press cell used high voltage (12–13 V) to overcome anode passivation	270
Hemicellulose	Gold	< 1 mA cm^{-2}	No product analysis	No	Precious bulk metal used	36
Lignin	Ni/C, Co/C, NiCo/C	< 5 mA cm^{-2}	No product analysis	No	Use of Binder for the nanoparticle electrocatalyst	267
Lignin derivatives	PtFe/C	208 mA cm^{-2}	90% CO_2	15 µmol min^{-1} at 100 mA cm^{-2}	Precious metal used, Concentrated acid used for pretreatment, High temperature 150–170 °C electrolysis	271
Lignin	Pt-Ru catalyst	< 4 mA cm^{-2}	No product analysis	Assumed 0.45 µmol s^{-1}	Precious metal and membrane used, PEM flow mode at 90 °C in alkaline	20
Lignin and its model compounds	Glassy carbon (GC)	25–80 mA	No specific product	No	TEMPO-mediated electrochemical oxidation in mild alkaline electrolyte	272
Crushed barley straw	Nickel foam	< 3mA cm^{-2}	No specific product	No	Methyl viologen-mediated electrochemical oxidation in 5 M NaOH	273

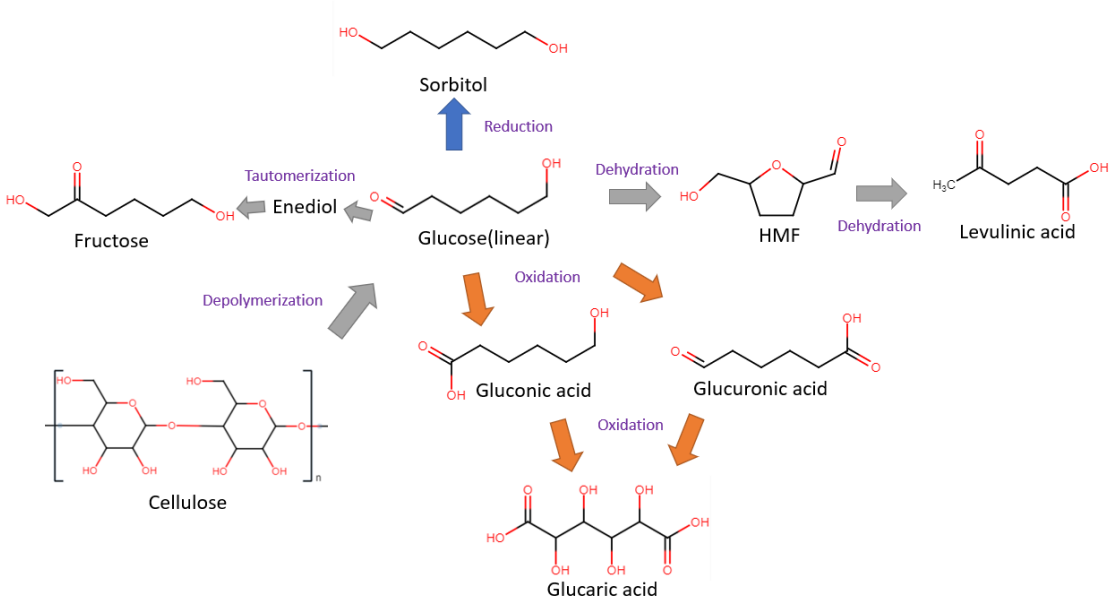

Figure 16 *Cellulose, glucose and its derivatives.*

This next section includes recent developments related to electroreforming cellulose and its derivatives (glucose, 5-HMF, levulinic acid). The electroreforming of biomass can be achieved on the anode of an electrochemical cell through electrooxidation, as well as on the cathode through electroreduction. Recent advances in the anodic electroreforming of cellulose and cellulose-derived glucose and other biomass derivatives are first summarized. Then, the cathodic electroreforming of cellulose and cellulose-derived 5-HMF and levulinic acid are discussed. Subsequently, the emerging research focusing on coupling hydrogen evolution with anodic biomass reforming for the cogeneration of green hydrogen fuel and value-added chemicals is reviewed.

2.5.1 Electroreforming at the anode

2.5.1.1 Cellulose

The earliest study passing electricity through cellulose was reported in 1947. O'Sullivan investigated passing current through regenerated cellulose with varying salt and moisture contents to understand the conductance properties of cellulose. In 1963, Murphy performed the first electrolysis of cellulose and observed that hydrogen gas was produced at the anode. However, studies of cellulose electrolysis remained relatively scarce and sporadic until the 21st century, when ever-increasing demand for green and sustainable chemistry appeared.

In 2010, Sugano et al. performed electrooxidation of cellulose at a polycrystalline gold electrode at a pH of 14 to understand its mechanism. [266] Cellulose powder was first dissolved in NaOH using the freeze–thaw technique, after which the cellulose's structure was no longer crystalline, suggesting the breakage of intra- and intermolecular hydrogen bonding, which is verified by both microscopic images and X-ray diffraction (XRD) spectroscopy, as presented in Fig. 17a, b, respectively. Cyclic voltammetry (CV) revealed two oxidation peaks for dissolved cellulose but not for undissolved cellulose. To explore the effects of particle sizes, ball mill crushing was used to generate cellulose particles of two size ranges, 500 and 100 nm, (Fig 17c, d). Smaller particles led to 13% higher peak current at similar applied potentials, indicating that ball mill pretreatment was efficient in promoting the dissolution of cellulose. Fourier transform infrared imaging (FTIR) scans (Fig 17e) suggested the formation of carboxyl groups, confirming the oxidation of cellulose. To produce direct electricity from oxidation of cellulose nanoparticles, the fuel cell was created and could attain maximum power density of 44 mW m^{-2}.

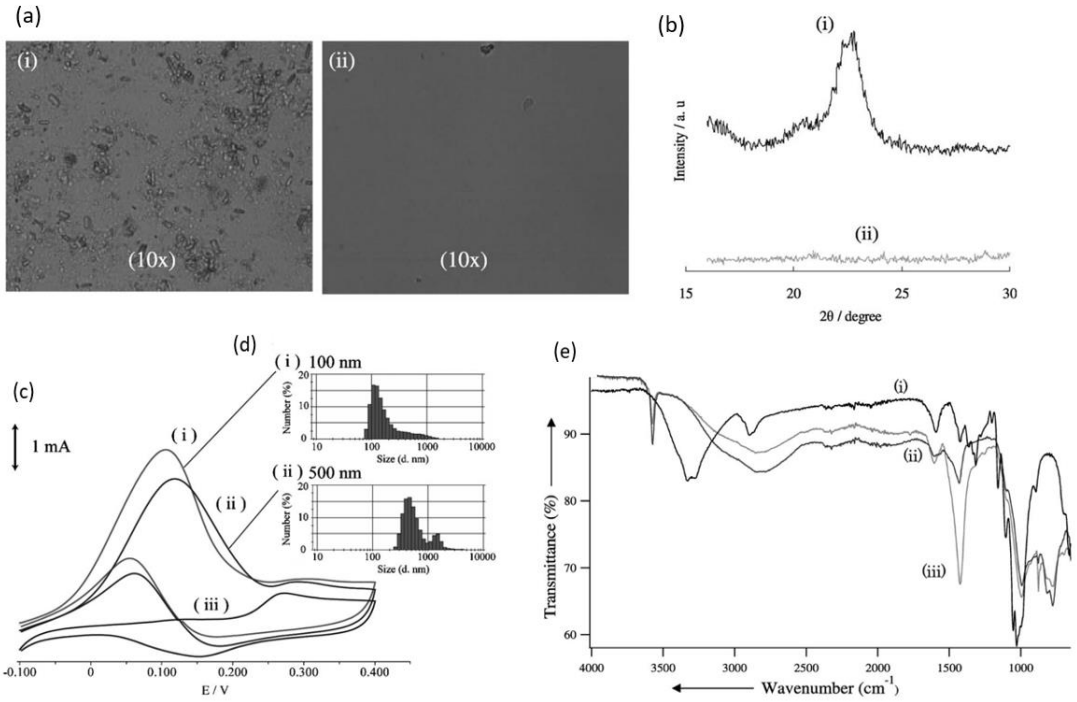

Figure 17*(a) Microscopic images before (i) and after (ii) dissolution. (b) X-ray diffraction of cellulose before (i) and after (ii) dissolution. (c) cyclic voltammogram (vs. Ag/AgCl) of cellulose ball milled to average particle size of 100 nm (i), 500 nm (ii) (e) FTIR scans of cellulose before dissolution (i), after dissolution (ii) and after oxidation (iii).* Credit: figures adapted from Sugano et. al. [266]

Later, their team studied the electroreforming mechanism in a similar alkaline medium. [35] CV scans suggested that cellulose electrooxidation is irreversible and diffusion controlled. FTIR was conducted during CV to understand interactions between cellulose and the Au electrode, which suggests that the adsorbed cellulose displaces OH^- ions near the electrode surface; and during oxidation, the strength of intermolecular H bonds decreases while that of intramolecular bonds increases. The authors proposed the reaction pathway, as illustrated in Fig. 18. Firstly, OH^- ions adsorb onto the surface of gold electrodes to form OH–Au sites. These active sites then allow cellulose to adhere electrochemically with Au electrode surface. Cellulose is oxidized and remains adsorbed until reversed potential is applied. The authors hypothesized that the adsorption and desorption of OH^- ions play an important catalytic role in cellulose electrooxidation.

NMR spectra and scanning electron microscope (SEM) imaging suggested the differences in the structure of cellulose after electroreforming; however, the exact products were not identified.

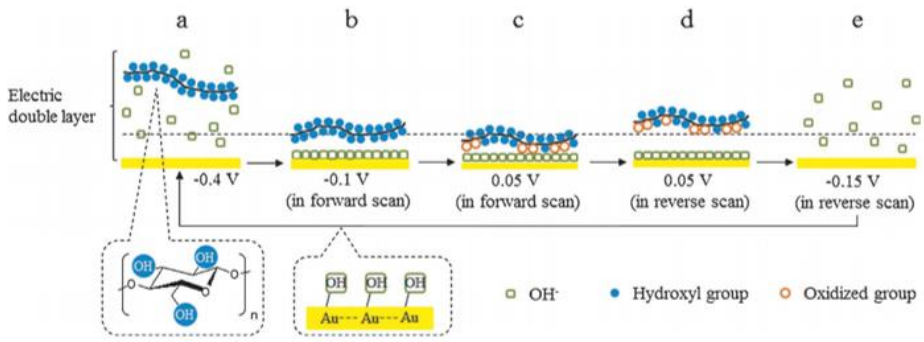

Figure 18 *Proposed cellulose oxidation mechanism on electrode surface in alkali media in CV cycle.(a) initial state, with cellulose dissolved in alkali solution. (b) in forward scan region: adsorption of OH^- ions to surface of electrode, cellulose molecule approaches OH–Au active sites. (c) oxidation of cellulose at electrode. (d) in reverse scan region: desorption of oxidation product and further oxidation of cellulose at revealed electrode surface. (e) desorption of OH^- ions from electrode surface.* Credit: figure adapted from Sugano et. al. [35]

A notable investigation was conducted in 2016, when Xiao and coworkers reported the use of gold nanoparticles (AuNP) for cellulose electroreforming. [274] Motivated by similar works on cellobiose [275, 276], the authors explored the use of HNO_3–pretreated carbon aerogel with AuNP as an anode, as shown in Fig. 19. Carbon aerogel was fabricated as per a previous report [277], before acid pretreatment. A mixture containing Au precipitates was prepared by reacting $HAuCl_4$ and NaB_4. [278] Deposition of AuNP onto carbon aerogel was performed by repeatedly dipping aerogel into the mixture and drying it. The anode was used to oxidize cellulose in 0.125 M NaOH (pH of 13.1) with insufflated air. Introduction of oxygen was proposed to speed up the formation of active oxygen species to accelerate oxidation. The authors compared three anodes to study the activities of AuNP with different sizes: 50 nm gold particles on graphite, 50 nm gold particles on carbon aerogel, and 10 nm gold particles on carbon aerogel, as shown in Fig. 19a-c. AuNP sizes were calculated from XRD data (Fig. 19d) and supported by SEM measurements. Cellulose oxidation was controlled at 10 mA cm^{-2} and products

were evaluated with high-performance liquid chromatography (HPLC), as presented in Fig. 19e.

Comparing anodes consisting of 10 and 50 nm AuNP on the same supporting substrate (CA), one can see that the 50 nm NP anode also obtained high cellulose conversion, but selectivity towards gluconate was significantly lower, suggesting that the size of AuNP influences the selectivity of oxidation products. Reducing aeration did not change oxidation products but decreased the rate of reaction. Ten-nanometer gold particles on acid-pretreated carbon aerogel produced gluconic acid at a 67.8% yield with a conversion yield of at least 88.9%.

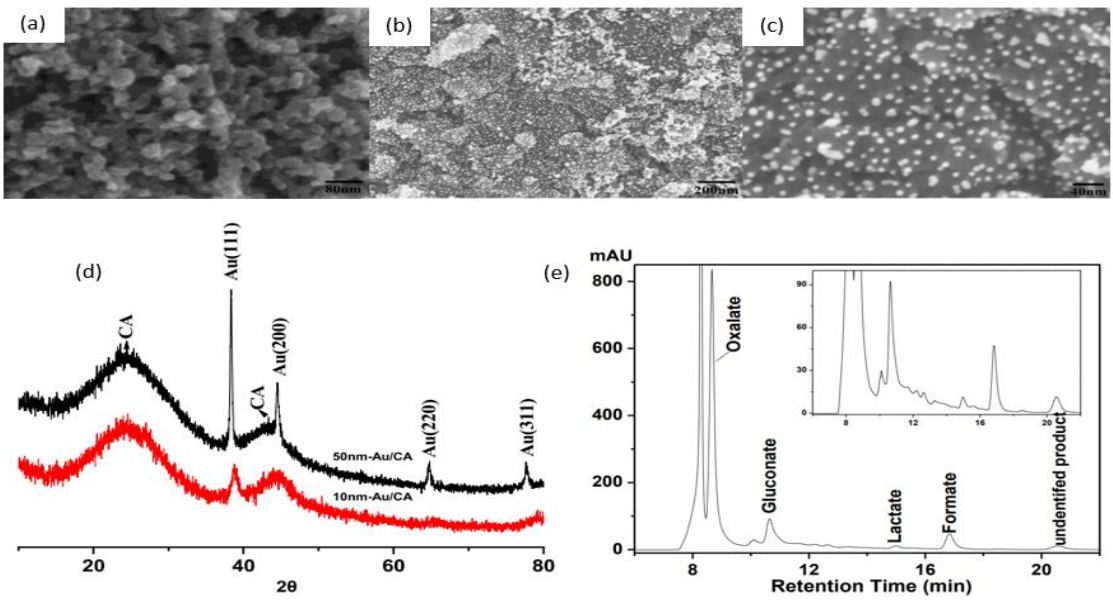

Figure 19 *(a) SEM image of pretreated CA. (b) SEM of 10 nm Au/CA. (c) Magnified SEM of 10 nm Au/CA. (d) XRD results of 10 nm Au/CA and 50 nm Au/CA electrodes. (e) High performance liquid chromatography results of products using 10 nm Au/CA electrodes.*Credit: figures adapted from Xiao et. al. [274]

When comparing anodes with the same 10 nm gold particles on different supporting substrates, the pretreated carbon aerogel supports resulted in better cellulose conversion than that of graphite support. The authors hypothesized that acid pretreatment of CA led to a higher surface area and oxidized surface carbon, favoring the adsorption of cellulose molecules.

Sugano et al. also attempted to understand cellulose electroreforming mechanism using AuNPs, again in alkaline (pH of 14) conditions. [279] Carbon paper supports were loaded with AuNPs through the chemical precipitation-deposition method. The electrodes were then calcinated at different temperatures (40, 250, and 350 °C). The author observed that calcination at 40 °C led to the formation of Au^{+} (52.5%) and Au^{3+} (30%), while calcinations at higher temperature led to completely metallic AuNPs. Moreover, calcination at 250 °C produced AuNPs with sizes ranging in a narrow band (10–25 nm), whereas a further increased temperature of 350 °C resulted in larger clusters (20–30 nm). CVs were conducted with 1.3 M NaOH against the Ag/AgCl reference, with and without (1 wt%) cellulose present. Anode calcinated at 40 °C displayed no electrocatalytic activity. Moreover, the anode calcinated at 350 °C shows lower electrocatalytic activity than the anode calcinated at 250 °C, indicating that small AuNPs (<25 nm) have higher activity.

Meng et al. electrolyzed cellulose powder in 0.5 M sulfuric acid (pH of 0.3), rather than in alkali solution, using lead/lead dioxide (Pb/PbO_2) electrodes [280], as depicted in Fig. 20a. Under ambient conditions, with a controlled current density of 30 mA cm^{-2} for 8 h, the average DP decreased from 1100 to 367. Conversely, the sample that was exposed only to acid had a final DP of 840, as displayed in Fig. 20b, c. XRD measurement showed a reduced degree of crystallinity, while FTIR showed lower intensities associated with H and C-O-C bonds without the formation of new groups. A maximum soluble sugar content yield of 2.5% and the highest 5-HMF yield of 1.8% were obtained.

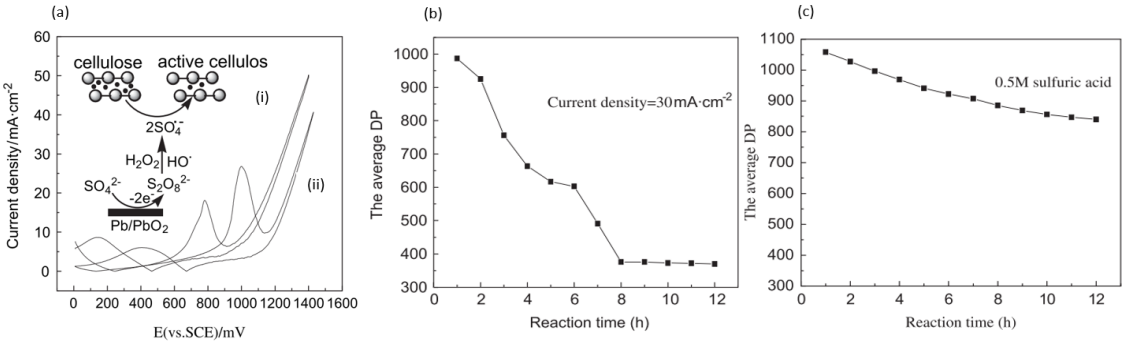

Figure 20 *(a) CVs (vs. SCE) of 0.5 M sulfuric acid (i) and 0.5 M sulfuric acid with 10 g L^{-1} cellulose (ii). (b) Decrease in DP over time at 30 mA cm^{-2}. (c) Decrease in DP over time without applied current.* Credit: figures adapted from Meng et. al. [280]

Meng and coworkers proposed an electrocatalytic depolymerization process, as presented in Fig. 21. Firstly, water molecules lose electrons at the anode to form hydroxyl radicals (OH^-). Next, the OH^- attacks the C-H bond and removes the hydrogen atom from carbon-4 of the glucose unit, leaving a carbon radical (C^-) in cellulose. C^- is then oxidized to become a superoxide radical (O_2^-). Finally, the glycosidic bond is cleaved through the removal of the superoxide radical.

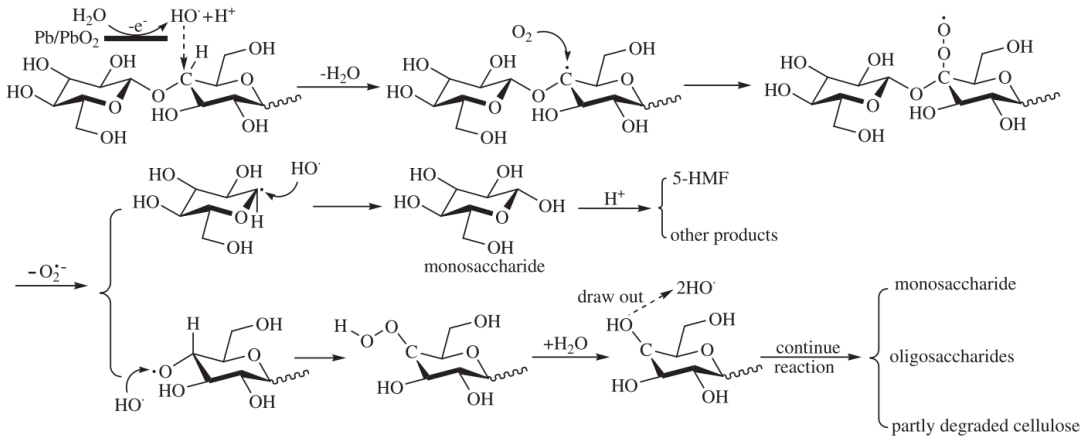

Figure 21 *Proposed cellulose depolymerization mechanism in acidic media.* Credit: figures adapted from Meng et. al. [280]

2.5.1.2 Glucose

Glucose is the most prevalent monosaccharide on across the planet. [281] Electrolysis of glucose was reported as early as 1866 to produce acetaldehyde; early reports also

speculated on the possible formation of alcohol and many other substances. [282] Indeed, studies have revealed a variety of useful products from glucose electroreforming, including 5-HMF, gluconic acid, glucaric acid, gluconolactone and levulinic acid, among others. The synthesis of glucaric acid in particular has been widely acknowledged for its high value. With applications in many industries, glucaric acid has being listed as one of the most value-added chemicals by the US Department of Energy. [283-285] However, conventional methods for glucaric acid production often require intense pressures, temperatures and harsh chemicals. [286] Gluconic acid is an intermediate towards the production of glucaric acid, and by itself has other commercial applications. [287, 288] Levulinic acid and 5-HMF are platform compounds for producing other useful chemicals. [289-291]

In 2014, Bin et al. optimized conversion of glucose to glucaric and gluconic acids with nano-manganese dioxide (MnO_2) loaded tubular porous titanium (Ti) electrodes in a flow-through electrolytic cell, as shown in Fig. 22a,b. [292] Interestingly, unlike most other studies, pH was concluded to be less significant in this case – increasing pH from 2 to 10 only changed glucose conversion slightly, from 90% to 93%. Selectivity to gluconic acid (GLA) and glucaric acid (GA) rose from 87% at a pH of 2 to a maximum of 94% at a pH of 7, before decreasing to 78% at pH of 10. The flow-through cell (Fig. 22b) was believed to limit the expansion of the electrochemical diffusion layer and promote glucose access to anode surface by convection. The effects of current density on glucose conversion to product selectivity were also studied (Fig. 22c). With MnO_2 loading of 4.98%, glucose concentration of 50.5 mM, temperature of 30 °C, pH of 7, residence time of 19 min, and current density of 4 mA cm^{-2}, 98% glucose conversion was achieved with selectivity towards gluconic acid and glucaric acid of 43% and 55%, respectively.

Increasing current density to 6 mA cm^{-2} further led to 99% glucose conversion, with gluconic and glucaric selectivity of 15% and 84%, respectively.

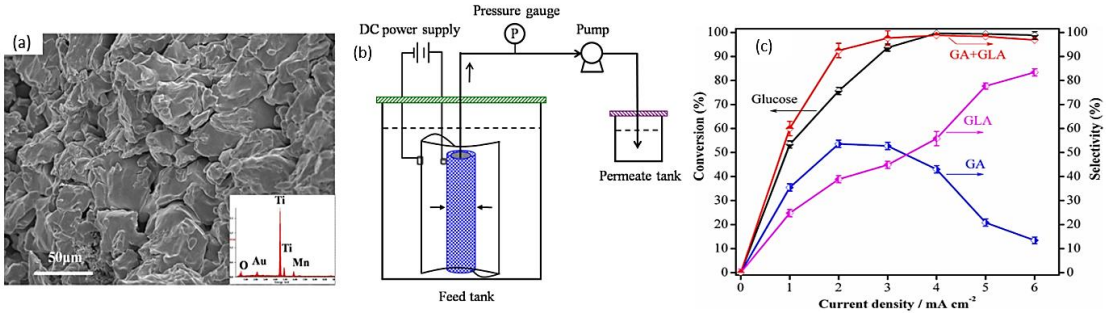

Figure 22 *Nano MnO_2/Ti electrocatalysts in flow-through cells for glucaric acid (GA) and gluconic acid (GLA) production from glucose. (a) SEM image of 5% MnO_2/Ti electrode. (b) Schematic diagram of electrocatalytic flow reactor system. (**c**) Products at different current densities (under 5% MnO_2 loading, glucose concentration of 50.5 mmol/L, pH of 7, 30 °C, 19 min).* Credit: figures adapted from Bin et. al. [292]

In 2017, Solmi et al. investigated the effects of varying ratios of different reactants (glucose to NaOH, glucose to metal catalyst, and glucose concentration levels), temperature and pressure, on glucose conversion to glucaric acid. [293] Under optimal conditions using AuNPs on activated carbon support, the highest yields of glucaric acid, gluconic acid and other by-products attained were 31%, 18% and 40%, respectively. The authors concluded that the optimal glucose concentration was 5% and that the molar ratio of glucose to metal should be 500:1 for obtaining glucaric acid.

Moggia et al. compared electrooxidative performance of bare copper (Cu), platinum (Pt) and Au at varying potentials for different functional groups. [294] The researchers first compared CVs of 0.04 M glucose added to 0.1 M NaOH with Cu, Pt and Au electrodes, and concluded that glucose oxidation is strongly correlated with metal catalysts. Next, gluconic acid, glucuronic acid and glucaric acid were used to identify if different functional groups are oxidized by metal catalysts. Cu was found to selectively oxidize glucose aldehyde group at 0.8–1.2 V, but not the hydroxymethyl group. Pt oxidized hydroxymethyl groups at lower potentials and aldehyde groups at higher potentials,

while Au oxidized hydroxymethyl at higher potentials and aldehydes at lower ones. Finally, to minimize competing side reactions (glucose isomerization and sugar degradation [295]) the authors performed glucose electroreforming at 5 °C at pH 13 for all three metal catalysts. Although good selectivity to glucaric acid was observed at lower potential (38.4% at 0.86 V), current densities with Cu were too low. Increasing potentials resulted in formic acid as the major product. Pt and Au exhibited similar catalytic action: at low potentials (0.55–0.70 V), both showed high selectivity to gluconic acid (78.4–86.8%). Increasing potential to 1.34 V for Pt and prolonged electrolysis at 0.70 V for Au produced glucaric acid selectivities of 13.5% and 12.6%, respectively.

Moggia and co-workers then went on to optimize conditions for each of the two oxidation steps at Au anodes: (1) glucose to gluconic acid, and (2) gluconic acid to glucaric acid. [296] For the first step, pH, glucose concentration, and temperature were all found to influence conversion. Optimal parameters of pH of 11.3, glucose concentration of 0.04 M, temperature of 5 °C and potential of 0.6 V resulted in the highest gluconic acid selectivity of 97.6%, with glucose conversion of 25% across a 6 h reaction. Increasing conversion by elevating pH or temperature produced lower selectivity. Increasing glucose concentration likely affected mass transfer to Au active sites, which also reduced selectivity. On the other hand, none of the above parameters were significant for oxidizing gluconic acid to glucaric acid. Instead, applied potential considerably influenced the product distribution. As illustrated, the maximum selectivity of 89.5% was attained at 1.1 V vs. RHE. Unfortunately, gluconic acid conversion was low (4.6%). Nevertheless, the highest possible glucaric acid concentration obtained was 1.2 mM. Furthermore, the drastic drop in current density was observed after a few hours, likely due to the adsorption of glucaric acids at Au active sites, as reported previously. [297]

Liu et al. used both nanostructured bimetallic nickel-iron oxide ($NiFeO_x$) and nitride ($NiFeN_x$) electrodes for gluconic and glucaric acid production. [298] $NiFeO_x$ nickel foam (anode) was used in 0.5 M glucose and 1.0 M potassium hydroxide, while $NiFeN_x$ nickel foam was used as the cathode in 1.0 M KOH. At a constant applied voltage of 1.4 V, glucose conversion of 21.3% was attained, and glucaric acid and gluconic acid yields were 11.6% and 4.7%, respectively. The Faradaic efficiencies for both glucaric and gluconic acids were 87%. The current density at 1.4 V decreased from 101.2 to 97.8 mA cm^{-2} over a 24 h run. The authors' technoeconomic analysis suggests that this method produces glucaric acid at 54% lower cost compared to conventional production methods. In 2021, Neha et al. created platinum-bismuth alloy (Pt_9-Bi_1) electrocatalyst on glassy carbon electrode for glucose conversion to gluconic acid, accompanied by methyl-glucoside conversion to methyl-glucuronate. [299] In an electrolyte consisting of 0.1 M NaOH (0.1 M glucose added), linear sweep voltammetry (LSV) scans showed the onset voltage to be less than 0.06 V and a broad peak at 4.58 mA cm^{-2} around 0.6 to 0.8 V. Chronoamperometric measurement at a fixed potential of 0.3 V was conducted with Pt_9-Bi_1/C anode and Pt/C cathode for 6 h, in a filter press cell. After about 90 min, the current halved (~0.020 to 0.010 A) and plateaued at around 0.005 A. These readings suggest that some poisoning occurred. The product after a 6 h reaction was confirmed to be gluconate with 100% selectivity using HPLC and NMR, with 40% glucose conversion. Poisoning of electrodes is a significant challenge in scaling up glucose electroreforming, suspected to be caused by the action of reaction intermediates. [300] In 2005, Tominaga et al. compared glucose electrooxidation between pure Au plate and AuNPs (2 nm in diameter) on carbon electrode [297], as shown in Fig. 23a. While CV scans suggested a similar voltametric response, gold nanoparticle catalysts exhibited significantly smaller decreases in current over time, displaying better resistance to poisoning, as displayed in

Fig. 23b. The reduction in current density was mitigated by increasing pH. Additionally, Tominaga et al. identified that high selectivity towards gluconate can be obtained at a high pH of 13.7, while electroreforming at neutral conditions (pH of 7) produced a mixture of gluconate and oxalate. Similarly, applied potential can be another factor to influence products, as seen in Fig. 23c. Most later studies have therefore focused on employing nanoparticle electrocatalysts in alkali media.

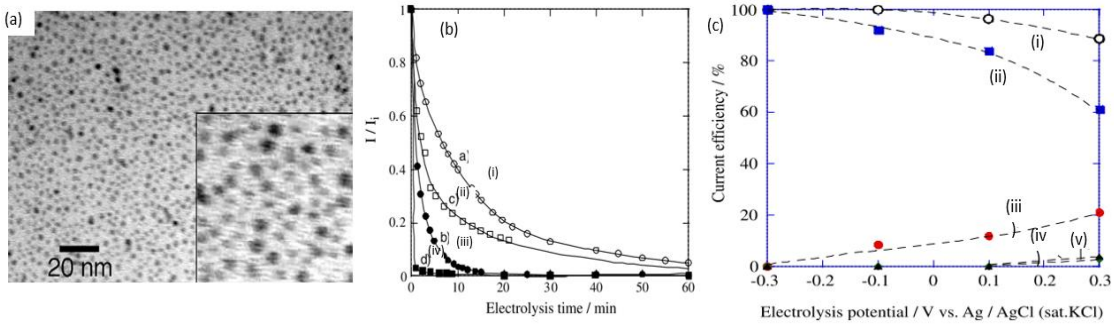

Figure 23 *(a) TEM image of AuNP capped with decanethiolate monolayer shell (for deposition on electrode). (b) Change in current ratios across time with gold nanoparticles in alkali medium (i), bulk gold in alkali medium (ii), gold nanoparticles in neutral medium (iv). (c) Plots of electrolysis products with 2 nm AuNP in 0.1 M NaOH, 0.01 M glucose, at different potentials (vs. Ag/AgCl); total current efficiency of all products (i), gluconolactone (ii), oxalate (iii), glyconate (iv), formate (v).* Credit: figures adapted from Tominaga et. al. [297]

2.5.1.3 Other Biomass Derivatives

5-hydroxylmethylfurfural (5-HMF) was included in the US Department of Energy's list in 2010 for the most valuable chemicals due to its versatility in forming an extensive range of useful chemicals. Among the products, 2,5-furandicarboxylic acid (FDCA) is widely known for its potential to substitute polyethylene terephthalate (PET) in plastic production with comparable mechanical strength and superior cost savings. [301-303] The formation of FDCA from HMF through a series of oxidation first forms the intermediates – 2,5-diformylfuran (DFF) or 5-hydroxymethyl-2-furancarboxylic acid (HMFCA).[304] Both intermediates further oxidize to 5-formyl-2-furancarboxylic acid (FFCA) and lastly into FDCA. Recently, electrooxidation studies of 5-HMF to FDCA with high yield were conducted with various non-noble metals electrocatalysts. [305-314]

The anodic electroreforming of cellulose-derived compound, levulinic acid to 3 products viz. three different routes was investigated by Dos Santos et al. [315] When Pt anode in aqueous KOH solution with methanol at pH of 5.5 was used, main product was 2,7-octanedione. Interestingly, with carbon anode and performed in 0.2 M and 0.1 M NaOH, the product switched to 4-hydroxy-2-butanone and 3-buten-2-one, respectively. Notably, the high surplus biodiesel waste, glycerol leads to extensive research into glycerol electroreforming. [316-318] To avoid using expensive precious metals, Liu et al. successfully used CuO to electroreform glycerol to 1,3-dihydroxyacetone (DHA), a commercially valuable chemical with applications in cosmetics and polymer industries. [319, 320] Vo et al. utilized abundant CoOx catalysts for anodic glycerol valorization with DHA selectivity of 60%. [321] Furthermore, the biomass-derived polyol, sorbitol was electrochemically oxidized by Kwon et al. to glucose, gulose, fructose and sorbose on a Sb-modified Pt anode in a Bi-saturated solution. [322] They emphasized the importance of potential control towards product selectivity. One of the oldest biomass-derived chemicals, furfural can also undergo electrochemical hydrogenation to form 5-HMF. [323, 324] For example, Kubota and Choi used PbO_2 electrodes in acidic media to electrooxidize furfural to 2-furanol and finally to maleic acid. [325] Roman et al. also reported anodic re-forming of furfural to furoic acid, a chemical to produce 2,5-furandicarboxylic acid. [326]

Studies on electroreforming of cellulose and its derivatives as well as other biomass derivatives at the anode are summarized in Table 4 with the key technical information.

Table 4 Studies investigating electroreforming of cellulose and its derivatives at the anode.

Year	Electrocatalyst	Feedstock	Desired Products	Electrolyte	Electrolytic Tests and Conditions (Potentials Respect to RHE)	Yield/Output	Faradaic Efficiency	Reference
2010	polycrystalline Au	NaOH dissolved ball milled cellulose	Carboxyl groups	1.33 M NaOH	CV characterization (0.90 V to 1.40 V)	-	-	[266]
2015	Au nanoparticles/carbon aerogel	NaOH dissolved cellulose	Gluconate	0.125 M NaOH	10 mA cm^{-2} at 18 h	67.8%	-	[274]
2016	Au nanoparticles/carbon paper	NaOH dissolved cellulose	-	1.33 M NaOH	CV characterization (0.60 V to 1.40 V)	-	-	[279]
2011	Pb/PbO_2	Cotton cellulose	Soluble sugars, 5-HMF	0.5 M H_2SO_4	30 mA cm^{-2} at 12 h	Soluble sugar: 2.5%, 5-HMF: 1.8%	-	[280]
2014	MnO_2/Ti	Glucose	Glucaric and gluconic acids	0.07 M Na_2SO_4 (pH 7)	1.41 V at 19 min	99% (both glucaric and gluconic acids) selectivities up to 86.8% for gluconic acid, 13.5% for glucaric acid	37.0%	[292]
2020	Polycrystalline Cu, Au, Pt	Glucose	Glucaric and gluconic acids	0.1 M NaOH	0.70 V at 65 h	11.6% (glucaric acid), 4.7% (gluconic acid)	87% (both)	[294]
2020	NiFeOx/NF, NiFeNx/NF, NiFe(OH)x/NF, NF, RuO_2/NF, Pt-C/NF	Glucose	Glucaric and gluconic acids	1.0 M KOH	1.40 V at 18 h	40.0% yield	~100.0%	[298]
2021	Pt_9-Bi1/C, Pt/C	Glucose	Gluconic acid	0.1 M NaOH	0.30 V at 6 h	98.0%	98.6%	[299]
2018	NiFe, NiAl, NiGa, NI(OH)2	5-HMF	2,5-furandicarboxylic acid (FDCA)	1.0 M KOH	1.33 V at 10 h	94.0%	98.0%	[305]
2018	CoP, CoB, CoTe, Co_2Si, CoAs on Ni foam	5-HMF	FDCA	1.0 M KOH	1.45 V at 70 min	96.4%	95.3%	[306]
2018	electrodeposited Cu/Cu foam	5-HMF	FDCA	0.1 M KOH	1.62 V at 8 h	96.0%	96.0%	[307]
2019	NiOOH, CoOOH, FeOOH/flouride doped tin oxide (FTO) glass	5-HMF	FDCA	0.1 M KOH	1.47 V at 4.7 h			[308]

Year	Electrocatalyst	Feedstock	Desired Products	Electrolyte	Electrolytic Tests and Conditions (Potentials Respect to RHE)	Yield/Output	Faradaic Efficiency	Reference
2019	$NiCo_2O_4$, Co_3O_4/Ni foam	5-HMF	FDCA	1.0 M KOH	1.50 V at 53 min	90.4%	87.5%	309
2020	TpBpy-Ni@FTO	5-HMF	FDCA	0.1 M $LiClO_4$	1.55 V at 40 min	58.0%	-	310
2020	CoO-$CoSe_2$	5-HMF	FDCA	1.0 M KOH	1.43 V at 1 h	99.0%	97.9%	311
2021	WO3 on Ni foam	5-HMF	FDCA	1.0 M KOH	1.57 V at 351 min	81.5%	79.5%	312
2021	Ni3S2/NF, NiS, NiO, NiC, NF	5-HMF	FDCA	1.0 M KOH	1.50 V at 2 h	98.3%	93.50%	313
2018	MnOx/FTO glass	5-HMF	FDCA and maleic acid	0.05 H_2SO_4	1.60 V (duration not reported)	53.8% FDCA, 21.9% maleic acid	33.8% (FDCA)	314
2015	Pt, C	Levulinic acid	2,7-octanedione, 4-hydroxy-2-butanone and 3-buten-2-one	Methanol / KOH pH 5.5 (Pt for 2,7-octanedione), 0.2 M NaOH (C for 4-hydroxy-2-butanone and 0.1m NaOH (C f0r 3-buten-2-one)	5.00 V (2,7-octanedione) at 7 h, 6.00 V (4-hydroxy-2-butanone) at 5 h, 1-3 V (3-buten-2-one) at 5 h.	2,7-octanedione with selectivity 47%, 4-hydroxy-2-butanone with selectivity of 20% and 3-buten-2-one with selectivity of 45%	86.2% for 2,7-octanedione, 5.0% for 4-hydroxy-2-butanone and 24% for 3-buten-2-one	315
2020	CuO	Glycerol	1,3-dihydroxyacetone	0.1 M $Na_2B_4O_7$	3 mA cm^{-2} at 3 h	selectivity of 60.0%	-	319
2021	CoOx	Glycerol	1,3-dihydroxyacetone	0.1 M $Na_2B_4O_7$	1.50 V at 3 h	selectivity of 60.0%	49.4%	321
2015	Bi-Pt/C, Sb-Pt/C	Sorbitol	Varied	0.5 M H_2SO_4	CV characterization (0 to 1.60 V)	-	-	322
2018	PbO_2, MnO_2, Pt	Furfural	Maleic acid	H_2SO_4 (pH of 1)	2.00 V (duration not reported)	65.1%	-	325
2020	Au/Carbon cloth	Furfural	Furoic acid	0.25 M $HClO_4$	CV characterization (0 to 1.50 V)	-	-	326

2.5.2 Electroreforming at cathode

In addition to oxidation at the anode, hydrogenation or reduction can also be conducted at the cathode of electrolytic cells. In hydrogenation, H^+ ions in the solution are reduced to surface-bound atomic hydrogen. Oxygenated organic molecules can react with adsorbed hydrogen to form valuable products. Electrochemical hydrogenation represents an attractive alternative to produce these chemicals without requiring harsh conditions in conventional methods. For instance, the electroreduction of cellulose (oligosaccharides) into glucose (72.4% yield) in acidic media was investigated with a 5% MnO_2/graphite/PTFE cathode. [327] Yang et al. hypothesized that oligosaccharides would first adsorb onto the cathode surface and then depolymerize by MnOOH coordination with the oxygen in the glycosidic bond. Likewise, 5-HMF can also undergo hydrogenation to form potential gasoline alternatives such as 2,5-dimethylfuran (DMF) [305, 324, 328-331]. Other hydrogenated products such as 2,5-dihydroxymethylfuran (DHMF) [328, 329] and 2,5-bis(hydroxymethyl)furan (BHMF) [332, 333] are chemicals for polyester and polyurethane foam production. [334] Lastly, levulinic acid was reformed to biofuel (octane) through a two-steps process: the Kolbe reaction and electrocatalytic hydrogenation (ECH). ECH of levulinic acid to valeric acid and g-valerolactone had been demonstrated in several studies [315, 335, 336] ,and with additional Kolbe reaction step to form octane. [337]

2.5.3 Evolution of Hydrogen Coupled with Biomass Electroreforming

Owing to the ever-increasing demand for green hydrogen, the decoupling of HER and OER by replacing OER with biomass oxidation has attracted intensive attention recently. Thus, the generation of byproducts of biomass electrooxidation, i.e., green hydrogen, has been intentionally optimized in addition to the enhancement of biomass electrooxidation.

2.5.3.1 Glucose Electrooxidation Coupled with Green Hydrogen Generation

Using glucose electrooxidation instead of OER to generate green hydrogen for the first time, Du et al. presented the results of their research in 2017. [338] In their work, iron phosphide films were prepared in situ on stainless steel mesh and used as anodes. The anodic potentials (vs. RHE) to operate at the current density of 10 mA cm^{-2} without and with glucose (of 0.5 M concentration) were 1.52 and 1.22 V, respectively, as compared in Fig. 24a. No effervescence was observed at the anode, suggesting glucose oxidation completely replaced OER. At a fixed potential of 1.9 V, the hydrogen production rate that coupled to glucose oxidation was higher than that for regular water electrolysis where hydrogen production was coupled to OER, as seen in Fig. 24b.

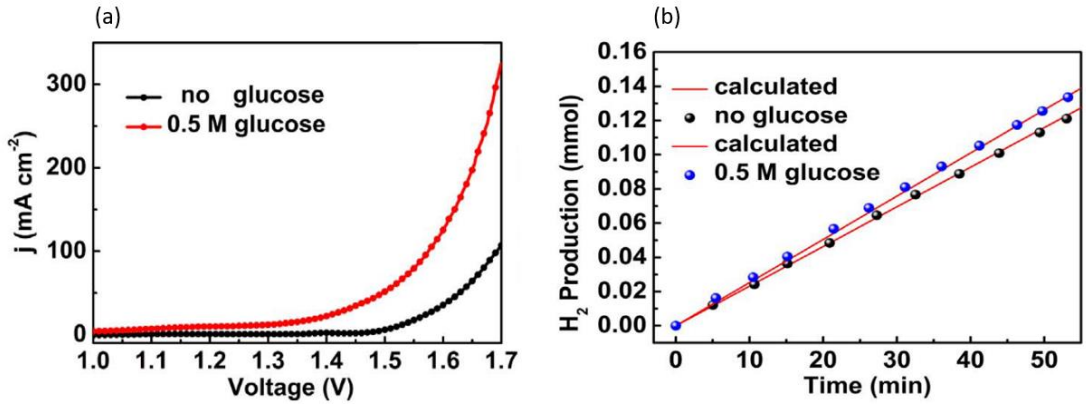

Figure 24 *(a) LSV scan in 2-electrode cell without and with 0.5 M glucose in 10 M KOH, iron phosphide anode. (b) Amount of hydrogen theoretically calculated and collected at 1.9 V, 10 M KOH with and without 0.5 M glucose.* Credit: figures adapted from Du et. al. [338]

In 2019, Rafaïdeen et al. designed Pd–Au nanoparticles on carbon for glucose and xylose oxidation [339] (Fig. 25a). The optimal ratio of Pd to Au composition was found to be 3:7. In 0.1 M NaOH (pH of 13) and 0.1 M glucose, CV revealed the potential required for 1 mA cm^{-2} was 0.2 V, with peak current density (4 mA cm^{-2}) at 0.5 V. Notably, the conversion of glucose was 67%, and the selectivity to gluconic acid was 87%. Hydrogen production was observed at Pt/C cathode without further characterization.

Moreover, the effects of glucose concentration and potentials on the reaction were investigated.[340] Increasing glucose concentration beyond 0.1 M was found to result in lower Faradaic efficiency and chemical yields, suggesting surface poisoning. Unsurprisingly, rate of gluconic acid production was higher with higher voltage, although Faradaic efficiency decreased. The production of hydrogen was estimated by calculating charge transfer to form the measured gluconic acid. It was proposed that, theoretically, 1 ton of 0.1 M glucose could produce 18.47 kg of hydrogen at 0.6 V with the setup, consuming 297 kWh electricity. However, it should be noted that this assumes no degradation of electrodes.

In 2020, Lin et al. explored the application of Co-Ni alloy electrocatalysts on carbon cloth [341] (Fig. 25b). SEM imaging showed significant macropore distribution, and X-ray photoelectron spectroscopy characterizations suggested that the partial oxidation of alloy occurred. Additional LSV determined the potential for 10 mA cm^{-2} on Co-Ni alloy electrode to be 1.096 V in 1 M KOH with 0.1 M glucose, which was less than those on the bulk Co (1.143 V) or Ni (1.138 V) electrodes. Further electrochemical impedance spectroscopy (EIS) measurement and Tafel slope comparisons among Co, Ni and Co-Ni alloy electrodes showed the superior conductivity and kinetics of the alloy electrode. In a two-electrode cell with Co-Ni alloy, both electrodes achieved 10 mA cm^{-2} at a voltage of only 1.39 V in 1.0 M KOH with 0.1 M glucose.

Lin and coworkers also used a customized cobalt nickel hydroxide nanosheet ($Co_{0.5}$ $Ni_{0.5}(OH)_2$ NS) on carbon cloth as the anode and replaced OER with glucose oxidation [342] (Fig. 25c). $Co_{0.5}$ $Ni_{0.5}(OH)_2$ NS electrode measured potential of 1.17 V at current density of 10 mA cm^{-2}. After a 12 h reaction at constant current density, the potential increased slightly to 1.20 V, indicating superior electrode stability. In a two-electrode cell with Pt cathode, the required potentials for 10 and 100 mA cm^{-2} in 1.0 M KOH only

were 1.47 and 1.75 V, respectively. With the addition of 0.1 M glucose, the corresponding potentials decreased to 1.22 V and 1.56 V, respectively.

Similarly, Liu et al. fabricated nickel-molybdenum disulfide (Ni-MoS_2) for both anode and cathode [343] (Fig. 25d). LSV showed the potentials needed for 10 mA cm^{-2} in 1.0 M KOH without and with 0.3 M glucose were 1.64 and 1.46 V, respectively. Additional Tafel slopes, EIS spectra, and double layer capacitance characterizations revealed preferable kinetics and catalytic activity of Ni-MoS_2 compared to MoS_2 and Pt/C, as well as good stability through 12 h chronoamperometric tests. Subsequently, a two-electrode cell was con-structed with Ni-MoS_2 on carbon paper as both the anode and cathode, and 1.67 V was required to reach 10 mA cm^{-2}. No bubbles were observed at the anode, suggesting complete suppression of OER.

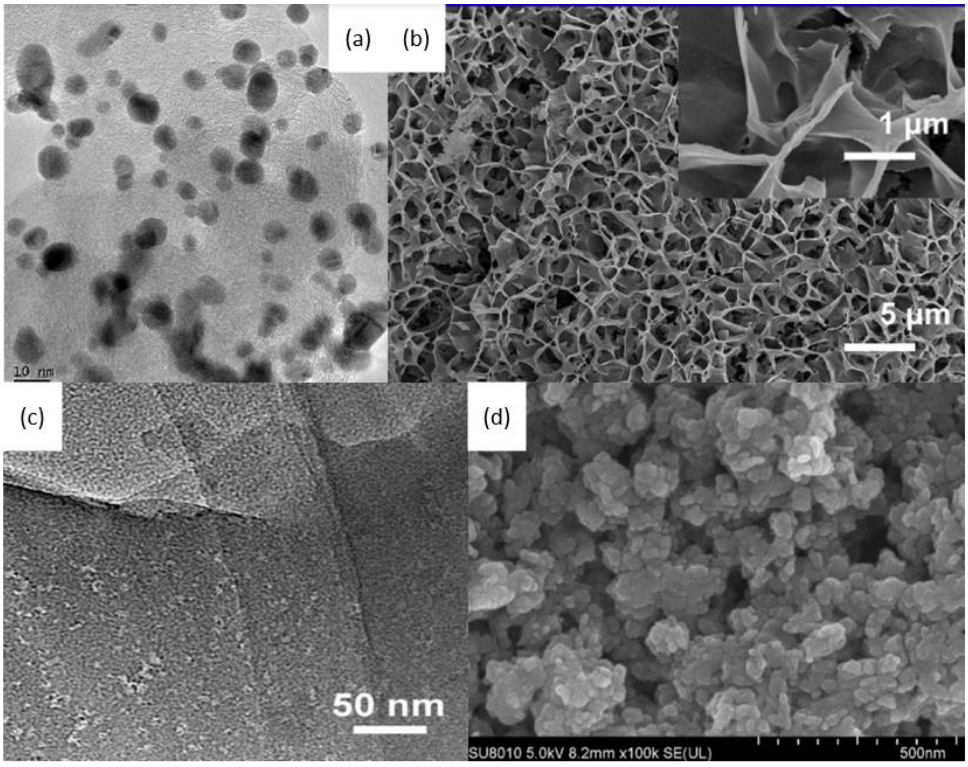

Figure 25 *(a) TEM of Pd_3Au_7/C (b) SEM of Co-Ni alloy. (c) SEM of $Co_{0.5}$ $Ni_{0.5}(OH)_2$. (d) SEM of Ni-MoS_2.* Credit: figures adapted from (a) Rafaïdeen et. al. [339] (b, c) Lin et. al. [341] (d) Liu et. al. [343]

Zheng et al. used iron-doped cobalt diselenide nanowires on conductive carbon cloth ($Fe_{0.1}$-$CoSe_2$/CC) as an alkaline anode and acidic cathode to produce gluconate (salt of gluconic acid) and hydrogen, respectively [344] (Fig. 26a). For a glucose oxidation reaction in 1 M KOH, LSV scans reveal that a $Fe_{0.1}$-$CoSe_2$/CC electrode with and without 0.5 M glucose necessitated voltages of 1.65 V and 1.12 V, respectively, as shown in Fig. 26b. With glucose, no bubbles were observed at the anode, suggesting complete suppression of OER. Moreover, the chronopotentiometric scans showed stable potential responses, signifying stable mass transport properties. The stability of the electrode was confirmed by XRD and morphological scans taken before and after 8 h of electrolysis at 1.15 V, showing no sign of differences.

The authors also analyzed cathodic hydrogen evolution using $Fe_{0.1}$-$CoSe_2$/CC in 0.5 M H_2SO_4 and found that overpotential of 270 mV was required to reach a current density of 100 mA cm^{-2} (Fig. 26c). Similar tests were conducted to confirm catalytic activity and electrode stability. A two-electrode cell was constructed with a bipolar membrane separating 1.0 M KOH anolyte and 0.5 M H_2SO_4 catholyte. To reach 10 mA cm^{-2}, the cell potential in the absence of glucose was applied at 1.34 V, which decreased to 0.72 V with the addition of 0.5 M glucose. For generating green hydrogen, the cell was maintained at 10 mA cm^{-2}, with 1.0 M KOH, 0.5 M glucose at the anode and 0.5 M H_2SO_4 at the cathode. Performing chronopotentiometric electrolysis for 100 min yielded 0.15 mmol of H_2 with 99% Faradaic efficiency.

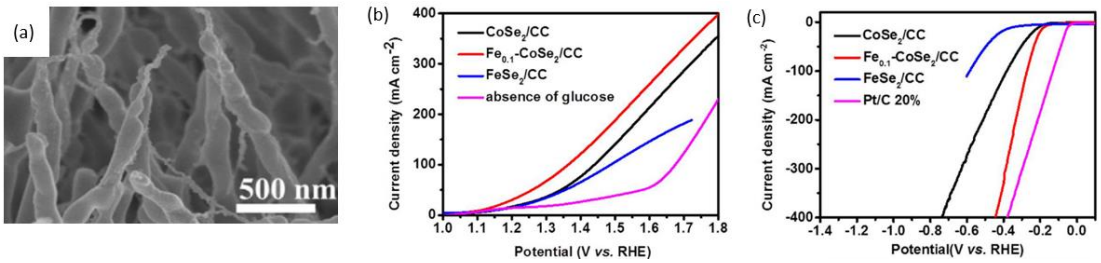

Figure 26 *(a) SEM image of $Fe_{0.1}CoSe_2$/CC. (b) LSV for anodic glucose oxidation, 1 M KOH, 0.5 M glucose with different electrodes. (c) LSV for cathodic hydrogen evolution, 0.5 M H_2SO_4.* Credit: figures adapted from Zheng et. al. [344]

Ding et al. further proposed that in order for hydrogen electrolysis to be truly green, electrodes should be part of a closed material cycle. [345] Interestingly, they developed carbon electrodes from biowaste to replace OER with carbon oxidation, intending for the carbon anode to be consumed in the process. Rather than electrolyzing glucose in solution, the authors fabricated carbon pellets (Fig. 27a) by means of hydrothermal treatment of glucose, which were deposited onto glassy carbon electrodes. The two-electrode cell potential was fixed at 2.4 V, and the sacrificial carbon anode and Pt cathode were deployed. This anode was maintained at a pH of 13, and the carbon anode was oxidized to carbonate, allowing continuous hydrogen formation at the cathode. The test cell was left to run for 10 days, and the products were quantified (Fig. 27b). Doping carbon pellets with nitrogen resulted in better anode stability without influencing electrode conductivity or hydrogen production, as seen in the higher H_2 evolution after 10 days in Fig. 27c compared to that without nitrogen doping in Fig. 27b.

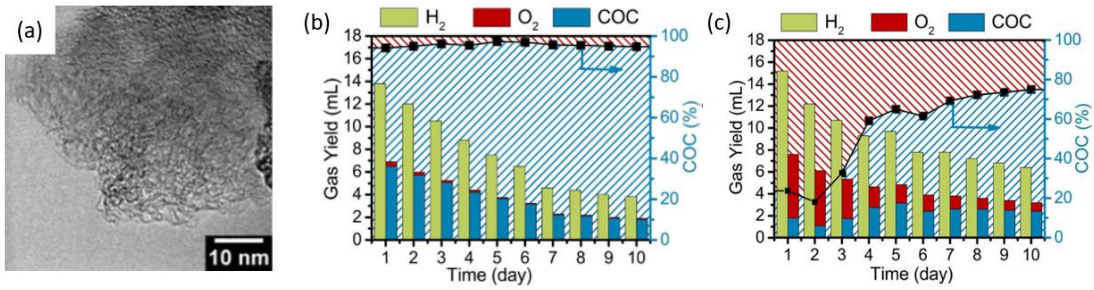

Figure 27 *(a) SEM image of carbon pellet. (b) Hydrogen production over days, from carbon oxidation contribution (COC) or oxygen evolution, with a carbon electrode. (c) Hydrogen*

production under similar conditions with a nitrogen-doped carbon electrode. Credit: figures adapted from Ding et. al. [345]

2.5.3.2 5-HMF Electrooxidation Coupled with Green Hydrogen Generation

5-HMF electrooxidation was demonstrated to replace OER in AWE and oxidized to valuable FDCA with co-generation of green H_2 in several studies. Yang et al. explored the use of bi-functional Mo-doped nickel selenides on Ni foam at an anodic potential of 1.4 V with complete 5-HMF conversion. At the cathode, hydrogen (3.8 mmol) was produced with a Faradaic efficiency close to 100%. [346] Next, Jiang et al. used Co-P/Cu foam electrodes [347] at anodic potential of 1.42V with 100% 5-HMF conversion, while 8 mmol of hydrogen gas was produced with 100% Faradaic efficiency at the cathode. Lastly, Liang et al. fabricated a bi-functional nickel nitride-vanadium trioxide (Ni_3N-$V2O_3$) catalyst with enhanced HER activity that was on par with Pt/C. [348, 349] Experiments were performed using a two-electrode cell at a fixed current of 10 mA cm^{-2} with corresponding overall potential of about 1.4 V. FDCA yield of 96.1% and selectivity of 98.7%, and hydrogen Faradaic efficiency of over 90% were reported.

Studies on evolution of hydrogen coupled with biomass electroreforming are summarized in Table 5 with the key technical information.

Table 5 Studies investigating evolution of hydrogen coupled with biomass electroreforming.

Year	Electrocatalyst	Feedstock	Desired Product(s)	Electrolyte (Catholyte)	Electrolytic Conditions	Coupled Product Yield (If Any)	OER Potential	Reactant Oxidation Potential	Reference
2017	Fe_2P/Stainless steel mesh	0.5 M glucose	Hydrogen	10 M KOH	CV characterization	-	1.52 V for 10 mA cm^{-2}	1.22 V for 10 mA cm^{-2}	338
2019	Pd-Au/C	0.1 M glucose	Hydrogen, gluconic acid	0.1 M NaOH	CV characterization, applied 0.40 V at 6 h	Gluconate yield 58.3%	-	0.2 V for 1 mA cm^{-2}, 0.5 V for max 4 mA cm^{-2}	339
2020	Co, Ni, Co-Ni/Carbon cloth	0.1 M glucose	Hydrogen	1.0 M KOH	CV characterization	-	1.39 V for 10 mA cm^{-2}	1.096 V for 10 mA cm^{-2}	341
2020	$Co_{0.5}$ $Ni_{0.5}(OH)_2$ Nanosheet	0.1 M glucose	Hydrogen	1.0 M KOH	CV characterization	-	1.47 V for 10 mA cm^{-2}	1.22 V for 10 mA cm^{-2}	342
2020	Ni-MoS_2/carbon paper	0.3 M glucose	Hydrogen	1.0 M KOH	CV characterization	-	1.64 V for 10 mA cm^{-2}	1.46 V for 10 mA cm^{-2}	343

Year	Electrocatalyst	Feedstock	Desired Product(s)	Electrolyte (Catholyte)	Electrolytic Conditions	Coupled Product Yield (If Any)	OER Potential	Reactant Oxidation Potential	Reference
2020	$Fe_{0.1}$-$CoSe_2$/Carbon cloth	0.5 M glucose	Hydrogen, gluconic acid	0.5 M H_2SO_4	CV characterization	-	1.34 V for 10 mA cm^{-2}	0.72 V for 10 mA cm^{-2}	344
2020	glucose derived carbon/glassy carbon	sacrificial carbon at cathode	Hydrogen	0.1 M KOH	CV characterization	-	OER onset 1.52 V	Carbon oxidation onset 1.02 V	345
2021	Mo-Ni0.85Se/NF	10 mM 5-HMF	Hydrogen, FDCA	1.0 M KOH	1.40 V at 2 h	FDCA yield 95.0%, FE 95.0%	Overall 1.68 V for 50 mA cm^{-2}	Overall 1.5 V for 50 mA cm^{-2}	346
2016	Co-P/Cu foam	50 mM 5-HMF	Hydrogen, FDCA	1.0 M KOH	1.42 V at 6 h	FDCA yield 90.0%	Anodic 1.53 V, overall 1.59 V for 20 mA cm^{-2}	anodic 1.38 V, overall 1.44 V for 20 mA cm^{-2}	347
2021	Ni_3N-V_2O_3	10 mM 5-HMF	Hydrogen, FDCA	1.0 M KOH	10 mA cm^{-2} at 112 min	FDCA yield 96.1%	-	1.4 V for 10 mA cm^{-2}	349

2.6 Perspectives and research gaps

The electroreforming of biomass compounds represents a promising green and sustainable route for synthesizing value-added chemicals with minimum damage to the environment. Compared to thermochemical routes, the operating conditions of electroreforming route are usually milder, and product controllability is better through tuning electrolytic cell parameters such as pH and potential. When compared to the biochemical routes, electroreforming processes can be conducted in more compact devices and in much shorter durations. For electroreforming of cellulose derivatives (glucose, 5-HMF, levulinic acid), exciting progress has been made by using various metal electrocatalysts to improve products and yields. In particular, recent studies have demonstrated the usage of non-noble metals or bimetallic alloys as electrocatalysts for both oxidation and hydrogenation processes. These developments shift reliance away from expensive noble metals, potentially increasing the economic viability of electroreforming techniques. Studies of flow reactor cells [292, 306, 333, 350], showcased the possible continual production they provide, and therefore their industrial scalability. Notably, a great advantage of the electrochemical route is the cogeneration of green hydrogen, which plays an indispensable role in decarbonization. From an energy saving prospective, both holes and electrons from electricity are utilized in such hybrid electrolysis, coupling biomass electrooxidation and water reduction, leading to valuable anodic and cathodic products. Despite these promising advantages of biomass electroreforming over the state-of-the-art biomass valorization, there are challenges to tackle before large-scale implementation.

Investigations into direct electroreforming of cellulose remains under-represented mainly due to the large polymer that could not be readily hydrolyzed in electrolyte. In order to make every stage in electroreforming pipeline green and sustainable, glucose

and the other derivatives should be obtained from cellulose, so as not to compete with edible plant sources. At the time of writing, several studies have been published to uncover electrooxidation and depolymerization mechanisms of cellulose. A few studies have analyzed useful products from cellulose electrolysis. [274] Thus, more investigations into energy-efficient and cost-effective pre-treatment methods are needed for converting raw bio-mass polymers to smaller molecules that can be readily reformed by electrochemical process. To this end, the rational combination of mechanochemical and biological processes could hold great promise.

High-value products would offset the overall production cost, increasing the economic viability of the electroreforming route. Raw biomass consists of large polymers and selectively converting them to high-value products is challenging.

Studies were also mostly focused on exploring the feasibility of different advanced catalysts and electrodes. It is noted that most reported catalysts show superior activity but inferior stability, which is very crucial for practical use. Many lessons can be learnt from the development of water electrolysis across the full pH range. Alkaline water electrolysis is by far the cheapest and most scalable technique for green hydrogen generation. Despite the recent drastic reduction in its cost, PEM water electrolysis still suffers from poor scalability mainly due to its Pt-group catalysts, particularly its anodic catalyst based on iridium and ruthenium. Similar challenge faces biomass electroreforming in acidic media. To this end, strategies for stabilizing non-precious catalyst and decreasing load of precious catalysts for PEM water electrolysis can be implemented for acidic biomass electroreforming. Nevertheless, biomass electroreforming in alkaline media is still relatively more cost-effective and scalable. More importantly, many reforming products are more stable in alkaline media than that in acidic media.

Electroreforming of biomass represents a greener route of electrosynthesis of chemicals. Despite its advantage of better sustainability, it is challenging to control the reaction pathways. Advanced catalyst design, e.g., tandem catalysts, could enrich the toolbox of pathways for biomass electroreforming. The above benchmarking will greatly facilitate the development of catalysts and electrodes.

Coupling HER to biomass oxidation in a 'hybrid electrolysis' will address the two challenges (green hydrogen generation and biomass refinery) in one device, greatly benefiting the cost reduction because both electrons and holes are fully utilized in this redox couple. Nevertheless, there are a few technical issues to address before such a hybrid electrolysis become useful practically. Firstly, abundant raw biomass, e.g., lignocellulose, should be used to match the scale of hydrogen production. However, previous studies on electrooxidation of cellulose, hemicellulose and lignin show very low current density (< 10 mA cm^{-2}) at room temperature; too long to be useful practically. The most critical issue is the solubility of lignocellulosic biomass in the electrolyte. Thus, a pre-treatment method to significantly increase the solubility of the lignocellulosic biomass in the electrolyte of hybrid electrolysis is desired. Secondly, the issue of crossover of oxygen and hydrogen in the mentioned electrooxidation studies were also not covered substantially and thus, could not guarantee the safety of the operation. In order to minimize the oxygen production, a well-defined potential window where biomass oxidation dominates the anodic reaction is needed. Thirdly, the possibility of electrooxidation of the mixed components from lignocellulosic biomass to any specific valuable chemical is significant but had yet to be answered. With the low yield of product, costly separation will be needed; and thus, increase the overall cost. Thus, highly selective biomass electrooxidation is highly desirable. Fourthly, the use of a better electrocatalyst (e.g., 3D porous catalyst) for the process might address the low

current density issue. Last but not least, existing methods that process lignocellulosic biomass usually are limited by prolonged processing time, low efficiency and adverse environmental impact, and these issues should be addressed.

Chapter 3: Raw biomass electroreforming to formic acid

As introduced in Chapter 2, sugarcane is highly effective in biomass accumulation due to its C_4 carbon metabolism. Sugarcane bagasse, the second most abundant biomass waste in Southeast Asia, had approximately 45 million tons generated in 2020. It contains residual sucrose, a characteristic attributed to the inherently high sucrose levels in sugarcane. Recognizing the potential of this sucrose-lignocellulosic rich biomass waste, an efficient method, which will be elaborated later, was introduced to valorise this resource.

The use of sugarcane in bioethanol and sugarcane industrials resulted in 279 Mts of waste globally and often burned as fuel for steam or electricity generation. Instead, SCB waste could be used for second-generation bioethanol from SCB was reported.[93-96] However, current biological processes require strict reaction condition control, costly enzyme and long processing time. [45, 97] Hence, it is crucial to find less time-consuming and more sustainable alternatives for SCB waste valorization.

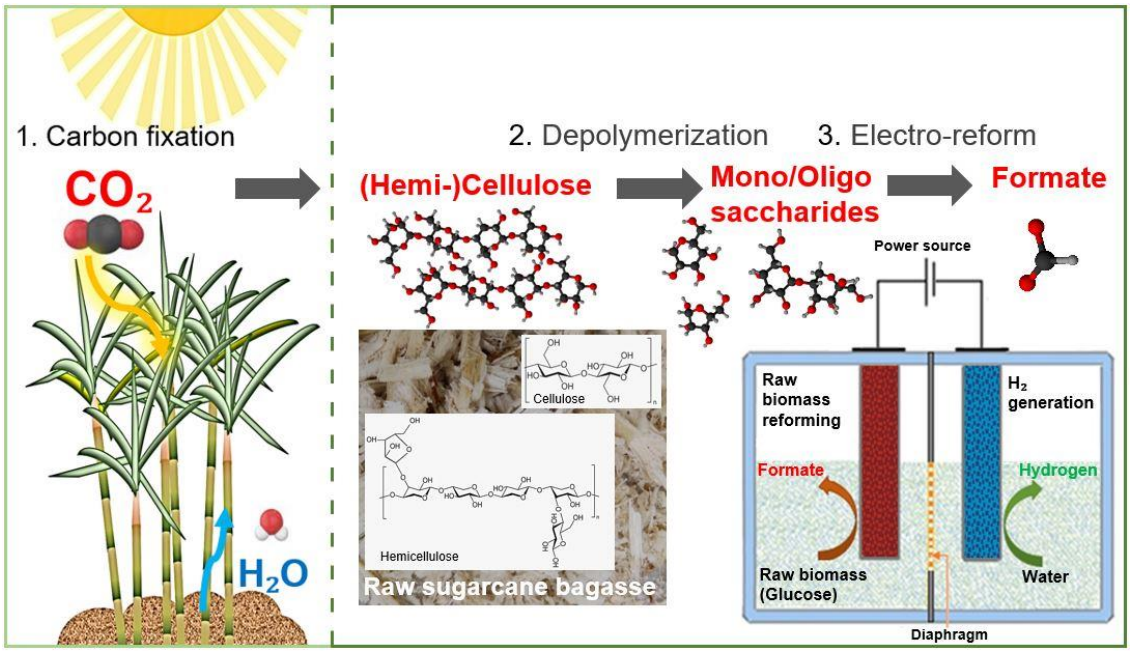

Figure 28 *Schematic diagram of coupled formate and green hydrogen generation from raw sugarcane bagasse.*

One such alternative is the pretreatment-electrochemical upcycling process that was developed in this work for SCB waste to cogenerate green hydrogen and green chemicals efficiently. (Fig. 28) Specifically, in pretreatment step, carbon captured in SCB waste in the forms of cellulose and hemicellulose by photosynthesis was firstly depolymerized into mono- and oligosaccharides with very diluted sulfuric acid. [49] Subsequently, the hydrolysates were electroreformed into small organic acid salts, dominantly formate, with simultaneous green hydrogen generation. The electrochemical transformation of major mono/disaccharides detected in SCB, and their intermediates are also studied in detail to unveil the mechanism. Furthermore, the feasibility of driving the electroreforming process with PV panels directly were demonstrated, thanks to the suppression of oxygen evolution reaction (OER). It is also worth noting that potassium formate has been recognized as a hydrogen carrier with the formate-bicarbonate loop. [50] This potentially offers an alternative mild and noncorrosive

hydrogen carrier scheme compared to formic acid and contributes towards a sustainable hydrogen economy. Lastly, life cycle assessment (LCA) was performed to verify the environmental benefits of the developed process. Overall, this novel electrochemical process for SCB waste upcycling for cogeneration of green chemicals and green hydrogen, was demonstrated to be more sustainable and environment-benign compared with conventional biowaste management methods.

.

3.1 Experimental section

3.1.1 Materials

Sugarcane (Saccharum officinarum) was crushed with the juice roller in a local hawker centre to obtain sugarcane bagasse (SCB). Hydrochloric acid (37%) was purchased from VWR while acetone and ethanol were from Aik Moh. Ammonium chloride, nickel sulfate hexahydrate, , D-(+)-Glucose, D-(+)-xylose, L-(+)-Arabinose, sucrose, D-(+)-Cellobiose, maleic acid, glycolic acid, lactic acid, D-(-)-Fructose, oxalic acid, D-(-)-Gluconic acid, D-(-)-Saccharic acid potassium salt(glucaric acid salt), D-(-)-Tartaric acid and potassium hydroxide were bought from Sigma Aldrich. Formic acid standard was procured from LGC Standards Ltd. No further purification was done before use. Deionized water with resistivity of 18 MΩ cm was used.

3.1.2 Synthesis of electrocatalysts

The anode of 3D hierarchical porous *(hp)* Ni on Ni foam (Ni-F) was prepared by cathodic electrodeposition to provide the dynamic hydrogen bubble template for porous

Ni microsphere formation on the Ni-F (1×1 cm^2). [31] To remove any grease and oxide layer from the nickel foam, it was sonicated for 5 min sequentially in: 0.1 M HCl aqueous solution, acetone, ethanol, and washed with deionized water. The electrodeposition was conducted in a conventional two-electrode arrangement at ambient condition at fixed current density of -2A cm^{-2} for 500 s. Pt wire was used as the auxiliary electrode and the electrodeposition electrolyte consisted of 4.0 M NH_4Cl and 0.2 M $NiSO_4$. The as-fabricated *hp*-Ni was rinsed with DI water to wash off excess deposition solution and dried before storing in an evacuated desiccator for later use.

The cathode was constructed by phosphidation of the prepared *hp*-Ni electrode in a chemical vapor deposition system according to literature with minor changes. [351]

3.1.3 Pretreatment of sugarcane bagasse waste

The as-received raw SCB was cut into 25 mm × 10 mm and dried in oven at 60 °C overnight. After drying, it was ball-milled and sieved (40-mesh). Dilute sulphuric acid hydrothermal treatment was performed on the sugarcane bagasse powder according to a report. [49] A hydrothermal treatment was conducted in an autoclave (Parr Instruments Company) of 45 mL internal volume. 30 mL of 0.14 V/V% sulphuric acid with 1:20 SCB powder: liquid loading was loaded into the Teflon liner. Two-step hydrothermal at 210 °C was performed with first duration of 10 min followed by a second duration of 40 min. After each step, the autoclave was cooled immediately with running tap water to stop the reaction. The supernatant from each step was separated by centrifuge and combined to be used as hydrolysate of SCB (HSCB) for further electrochemical tests. Meanwhile, the HSCB solid residue was stirred in 1.0 M KOH solution for 2 h at room temperature for lignin recovery.

3.1.4 Electrochemical reforming of HSCB and sugars/organic acids

Electrochemical reforming was performed in a standard three-electrode configuration with *hp*-Ni, Pt wire and Ag/AgCl/ Sat. KCl (in 1.0 M KOH unless specified) as the working, counter, and reference electrodes, respectively. Electrochemical reforming was conducted at room temperature with magnetic stirring. HSCB was adjusted to pH of 13.8 with KOH before test. The newly fabricated *hp*-Ni was activated in 1.0 M KOH at a constant current of 50 mA cm^{-2}. After stabilization, cyclic voltammetry (CV) and linear sweep voltammetry (LSV) were scanned from 0–0.8 V (vs. Ag/AgCl) at 10 and 2 mV s^{-1}, respectively.

For electrochemical surface area (ECSA) calculation, CV at potential ± 0.05V of non-faradaic potential window of the selected electrocatalyst were scanned in 1.0 M KOH solution at varying scan rates from 5 to 100 mV s^{-1}. The double layer capacitance, C_{dl} (mF cm^{-2}) can be calculated using the following Eq. 1A:

$$C_{dl} = \frac{Q}{U} = \frac{\int_{t1}^{t2} I\, dt}{U} \quad (1A)$$

$$C_{dl} = \frac{I\,\Delta t}{U} = \frac{I}{v} \quad (1B)$$

$$C_s = \frac{C_{dl}}{S_{geo}} \quad (1C)$$

$$R_f = \frac{C_s}{C_{s\,flat}} \quad (1D)$$

$$ECSA = R_f \times S_{geo} = \frac{C_{dl}}{C_{s\,flat}} = \frac{I}{v \cdot C_{s\,flat}} \quad (1E)$$

, whereby C_s (mF cm^{-2}), $C_{s\,flat}$ (mF cm^{-2}), I (mA), Δt (s), S_{geo} (cm^2), ν and U represent the specific capacitance of the electrode, specific capacitance of a flat surface, discharge or charge current, discharge or charge time, geometric surface area of the electrode, scan rate and potential window, respectively.

In the non-faradaic potential region, an ideally near-rectangular cyclic voltammetry (CV) curve is always obtained. This allows one to transform the above Eq. (1A) into the format of Eq. (1B). By considering the geometric surface area, the specific capacitance can be determined using Eq. (1C). Additionally, for a flat surface, the specific capacitance typically falls within the range of 20–60 μF cm^{-2} for metal surfaces, and an average specific capacitance of 40 μF $cm^{-2}{}_{geo}$ is commonly selected to estimate the surface roughness using Eq. (1D). Finally, the electrochemical surface area (ECSA) can be calculated by substituting all the computed variables into Eq. (1E).

Tafel slope 35 mL of 16.4 g L^{-1} HSCB or 0.1 M sugars/organic acids in 35 mL of electrolyte was used in the electrochemical tests. Tafel slope was calculated according to Tafel equation: $E = a + b\ log(j)$, performed during the LSV test, E represents the applied potential, a stands for a constant, b represents the Tafel slope, and j indicates the current density.

All electrode potentials have been converted to potential of reversible hydrogen electrode (RHE) according to the equation: $E_{RHE} = E_{Ag/AgCl} + 0.197\ V + 0.0591\ pH$.

Electrochemical impedance spectroscopy (EIS) was conducted with 0.1 M glucose/xylose in 1.0 M KOH at (0.55 V vs Ag/AgCl) at frequency range of 0.01–1000 Hz at 100 mV_{rms}. Long-term electrooxidation of 0.1 M glucose/xylose, 16.4 g L^{-1} HSCB or mixture of various saccharides (carbon mole ratio of 35% glucose, 10% cellobiose, 35% xylose and 20% sucrose) was performed at specific constant voltages. At the intervals, sample of 3 mL was collected for product analysis.

HER measurement of the prepared Ni_2P/Ni-F cathode: LSV was scanned from 0 to -2 V (vs Ag/AgCl) at 2 mV s^{-1} with Ni_2P/Ni-F and graphite rod as the working and counter electrode, respectively, comparing with and without glucose in electrolyte.

Gas sample was collected after 5 h of electrooxidation of 0.1 M glucose at constant 1.48 and 1.58 V vs RHE, with current density of 140 and 200 mA cm^{-2}, respectively. For comparison, gas from alkaline water electrolysis at 1.80 V vs RHE with current density of 200 mA cm^{-2} was also collected.

3.1.5 Solar-driven Electrooxidation of HSCB

HSCB was loaded to a single-compartment air-seal electrochemical cell and connected to 1 L gas sampling bag with an airflow meter. Argon gas was used for purging for 20 min. The liquid products were extracted at intervals by needle syringe. A solar panel of 15 × 20 cm^2 was used to supply solar electricity to the system and the electricity signal was recorded with a voltage-current meter. Real-time data acquisition of airflow and voltage-current was collected on a laptop. The solar experiment was conducted at Nanyang Technological University, School of Mechanical and Aerospace Engineering (Latitude: 1.347159, Longitude: 103.681756) on a partial cloudy day on 8th January 2023 from 11.00 am to 4.00 pm.

3.1.6 SCB and electrocatalyst characterization

For chemical composition analysis of SCB, extractives were first removed from SCB by neutral detergent according to the reported methods. [352-354] Then, ash and quantitative acid hydrolysis (NREL/TP-510-42618) were performed in duplicates to determine the lignocellulosic component. [355] The chemical composition of SCB consists of 37.2 ± 2.4% extractives, 30.1 ± 1.5% cellulose, 19.4 ± 0.9% hemi-cellulose, 29.3 ± 0.3% lignin and

0.8 ± 0.2% ash. Notably, much higher extractives of 57.9%, consisting of mainly soluble sugars, was reported previously, likely due to their incomplete juice extraction. [356]

Scanning electron microscopy (SEM), element mapping and energy dispersive spectroscopy (EDS) were conducted with the FESEM 700F, providing details such as surface, topographical, morphological, and compositional information of the electrocatalysts. Shimadzu XRD-6000 was used to capture X-ray diffraction (XRD) patterns to study the crystallinity and structure change in synthesized *hp*-Ni electrocatalyst and reference against Ni: face-centered cubic (FCC) Crystallographic Structures (JCPDS card no. 04-0850). [357]

X-ray photoelectron spectroscopy (XPS) analyses were conducted using a Kratos Axis Supra Spectrophotometer. The monochromatic Al Kα source (1486.7 eV) was used with a spot size of 300 × 700 μm^2. Samples were charge neutralized, and sputter cleaned with 1 keV Ar^+ ions. CASA XPS software was utilized to fit the data with the Shirley background and Gaussian-Lorentzian function, referencing the C 1s peak (284.8 eV).

The size and structure of the nanoparticles were verified using transmission electron microscopy (TEM), which was performed with a JEOL JEM-2100F microscope. The *hp*-Ni catalysts were suspended in an ethanol solvent by sonicating for 3 hours. Subsequently, a small solution drop was placed onto commercial copper-coated carbon TEM grids. The instrument was operated at an ultra-high-resolution voltage of 200 kV.

3.1.7 Product analysis

Liquid samples were adjusted to pH of 6–7 and passed through 0.45 µm syringe filters before analyzing in the Agilent 1260 HPLC. The column used was Agilent Hi-Plex H, 7.7 × 300 mm, 8 µm. The injection volume was 20 µL with a run time of 30 min. UV

and Refractive Index detectors (RID) are used. For organic acids quantification, the flowrate was 0.6 mL min^{-1} with mobile phase of 0.01 M H_2SO_4 at column temperature of 50 °C. Carbohydrate concentrations were also determined with the same column and mobile phase with RID at flowrate of 0.4 mL min^{-1} at column temperature was 65 °C.
358

Total organic carbon (TOC) in solid and liquid phase was analysed by using TOC analyser (Shimadzu TOC 5000A). The product yield% and sugar remaining % can be calculated based on the equations (2) and (3):

$$\text{Product yield } \% = \frac{\text{Moles of carbon in measured product}}{\text{Moles of carbon in initial reactant}} \times 100\% \quad (2)$$

where reactant is glucose/xylose or HSCB

$$\text{Sugar remaining } \% = \frac{\text{Sugar concentration at specific reaction times}}{\text{Initial sugar concentration}} \times 100\% \quad (3)$$

where sugar is glucose/xylose

For NMR analysis, samples were freeze-dried before the addition of a specific amount of D_2O, and 0.7 mL were transferred into NMR tube for analyzing. For product quantification, maleic acid of known concentration was added as internal standard. ^1H NMR spectra were recorded with JEOL ECA400 NMR spectrometers operating at 400 MHz at room temperature.

The gas samples of 1 mL were delivered into a GC-TCD/TCD system (Agilent 7890A, 10-ft molecular sieve 13× column) with argon as the carrier gas and at 400 °C for quantification.

The Faradaic efficiency of H_2 generation is calculated using equation (4):

$$H_2 \text{ Faradaic efficiency } = \frac{nH_2}{Q/2F} \times 100\% \quad (4)$$

where Q(C) is the total amount of charge passed through the cell, nH_2(mol) is the total amount of hydrogen produced and F is the Faraday constant.

3.1.8 Life cycle assessment

Life cycle assessment of the SCB processing systems was carried out following ISO 14040 and 14044: ISO 14040: 2006 – Principles and framework [359], as well as ISO 14044: 2006 – Requirements and guidelines [360]. LCA model was implemented using GaBi software, with a cradle-to-gate system boundary. Raw materials and energy process flows were extracted from Sphera 2022.1 and Ecoinvent 3.8 databases, as detailed in Table 6. ReCiPe 2016 v1.1 (H) was selected as the impact assessment method, considering only the impacts of global warming potential (GWP). All process data use global average values. SCB composition by weight consists of 46% cellulose, 27% hemicellulose, 23% lignin and 4% ash [361] , and ash composition values was taken from reference [362].

Table 6 Utilities used, and their corresponding global warming potential assumed in LCA.

Utility	Electricity from natural gas [363]	Electricity from photovoltaic [363]	Process steam from natural gas [363]	Process steam from biomass [363]	Heat from municipal waste incineration [364]	Cooling water via cooling tower [365]
Global warming potential (kg CO_2-eq/kWh)	0.469	0.0322	0.253	0.014	0.000779	0.00264

The environmental impacts of the sugarcane bagasse upcycling process were compared against conventional sugarcane bagasse waste management methods, viz. closed landfill and incineration. Landfill is a common waste disposal practice in many countries. Specifically, closed landfill was selected to utilize landfill gas in electricity generation which reduced the environmental impacts from methane emissions. For the incineration process, the heat of SCB is recovered by electrical generation, using processes described in the literature. [366] The amount of carbon dioxide and methane generated by conventional sugarcane bagasse treatment methods are estimated according to reference [367].

In the comparative LCA, the functional unit used was defined as "management of one tonne of waste sugarcane bagasse". The inventory associated with transportation of materials within the processing system was omitted, assuming the waste management facilities, whether upcycling, incineration or landfill, is located near the sugarcane plant. The overall inventory data of the upcycling process are shown in Table 7. To fully realize the carbon-saving potential of the electroreforming process, the modeling was done using sodium hydroxide because the production of potassium hydroxide is carbon intensive (4080 kg CO_2-eq/tonne SCB). Notably, sodium hydroxide offers identical functionality in the electrolyte.

Although the product collected by the lab-based study is predominantly potassium formate, the system boundary of LCA was designed to produce formic acid and other organic acids, because formic acid is a platform molecule with a larger market size (in monetary terms) than formate salts (e.g., potassium formate). Accordingly, the potassium formate produced by the electroreforming process is

transformed into formic acid through an additional acid neutralisation and subsequent product separation by distillation.

Table 7 Flow inventory of the SCB upcycling process, as modelled in LCA. LCA data source [363] and [364] refer to Sphera database and Ecoinvent 3.8 database, respectively.

Flows	Amount	LCA data source
Input		
Cane bagasse	1000 kg	[364]
Sulphuric acid	94 kg	[363]
Process water	162 kg	[363]
Sodium hydroxide	2006 kg	[363]
Hydrochloric acid	1479 kg	[363]
Sulfolane	138 kg	[363]
Electricity	6925 kWh	[363]
Heating	8190 kWh	[363]
Cooling	8144 kWh	[365]
Output		
Hydrogen, H_2	39 kg	[363]
Formic Acid (>99%)	366 kg	[363]
Acetic Acid (>99%)	86 kg	[363]
Sodium chloride	2371 kg	[363]
Carbon dioxide	34 kg	[363]
Wastewater	1983 kg	[364]

3.2 Results and discussion

3.2.1 Preparation of the anode and cathode

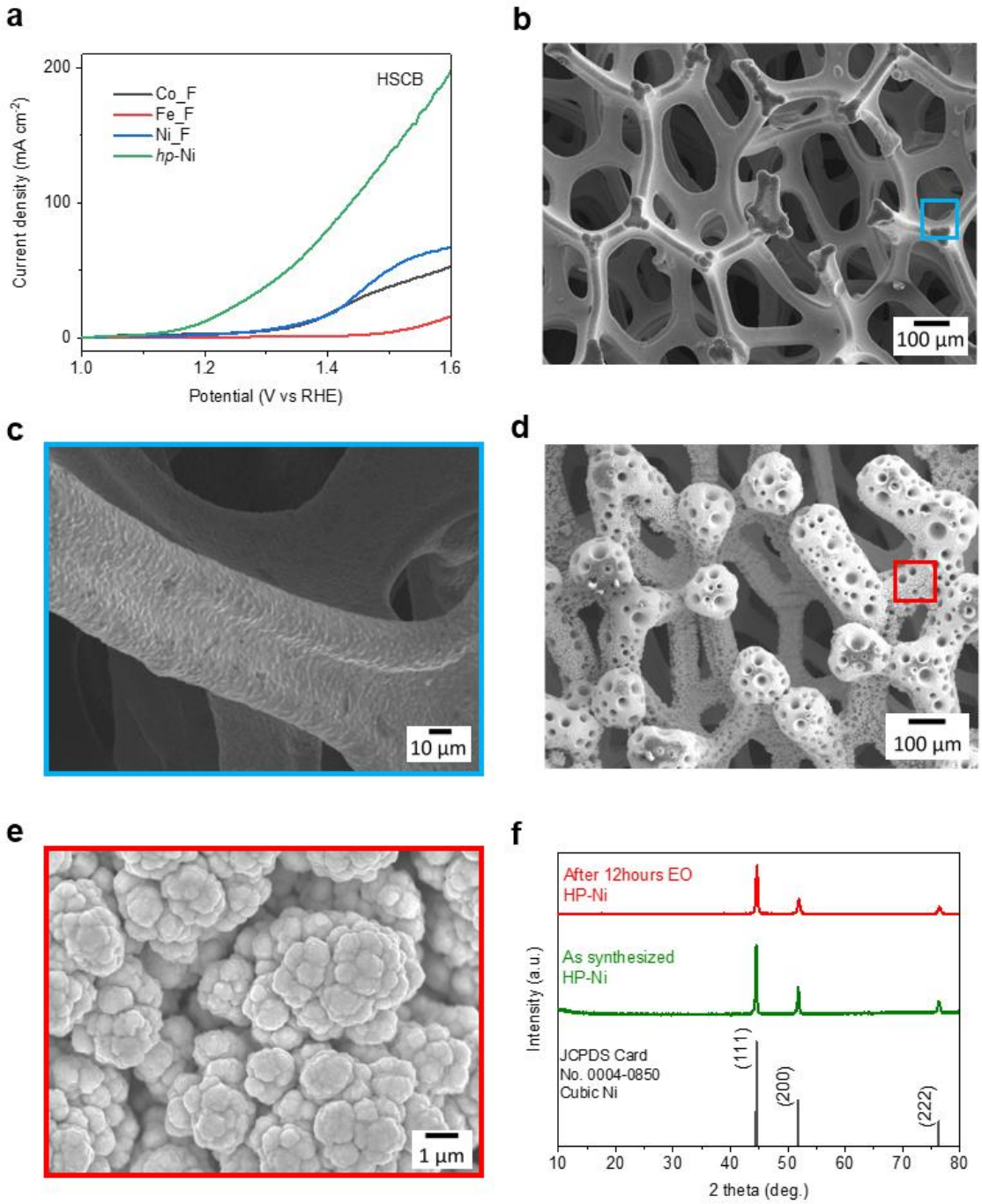

Figure 29 *(a) LSV of nickel foam (Ni-F), cobalt foam (Co-F), iron foam (Fe-F) and hp-Ni in HSCB. Bare Ni Foam (b) SEM image, (c) zoom-in SEM image of region in image (b). hp-Ni (d) SEM image, (e) zoom-in SEM image of region in image (d). (f) XRD of hp-Ni After 12 hours. glucose electrooxidation (red), as synthesized (green) and cubic Ni standard from JCPDS card No. 0004-0850 (black).*

Nickel was selected for both anode and cathode due to its low cost, earth abundance and great alkaline electrochemical stability. Nickel also exhibits the most enhanced activity for SCB electroreforming among other catalysts such as Fe and Co (Fig. 29a). To promote mass transport, gas diffusion and electron transfer, hierarchical porous nickel anodes are fabricated with large-current density cathodic electrodeposition. Vigorous hydrogen bubbles serve as the template for the porous structure generation. [368] The SEM images of the electrode before (Fig. 29b, c) and after electrodeposition (Fig. 29d) show the change in morphological structure of the starting Ni-F support. The smooth Ni-F skeleton (Fig. 29e) is decorated with porous 100 to 200 μm microspheres. The Ni-F framework (Fig. 29b) contains a variety of pores diameter sizes approximately 63 to 471 μm, while the porous microspheres are of sizes from 1.6 to 7.0 μm in Fig. 29e. The deposited layer is made up of "popcorn-shaped" Ni nanoparticles segregated by nanoscale gaps ranging from 0.5 to 5.0 nm. Hence, this hierarchical electrode structure exposes abundant active sites and facilitates mass transport to enhance the electrochemical performance.

In Fig. 29f, the XRD pattern (as-synthesized *hp*-Ni) distinguishes that the presence of crystalline cubic Ni in the *hp*-Ni electrode. Such a monolithic structure in the *hp*-Ni electrode can contribute to its great stability and outstanding electrical conductivity. This cubic Ni phase still existed even over 12 hours of glucose electrooxidation, suggesting the robust structure was still intact.

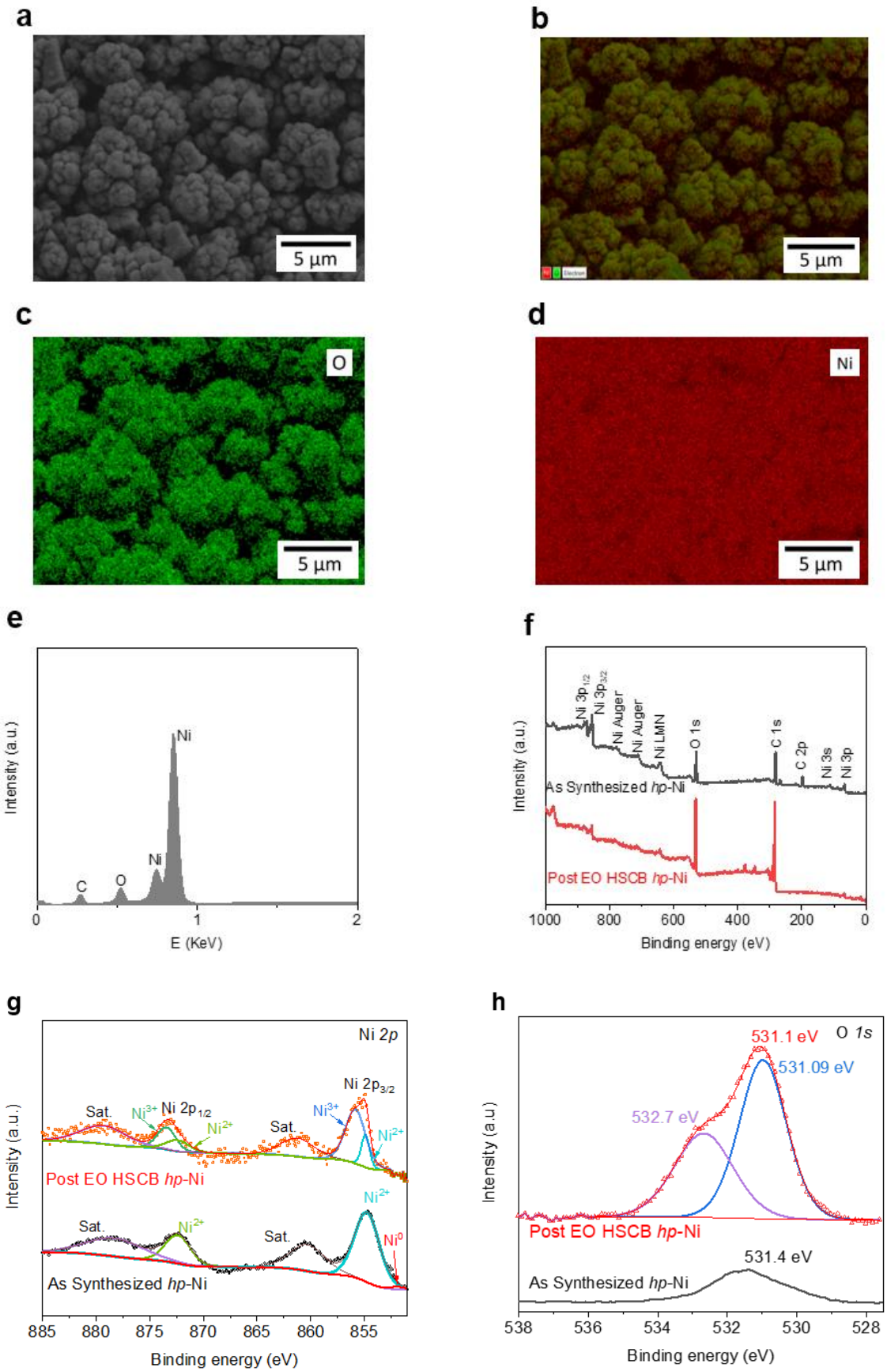

Figure 30 *hp-Ni – (a) SEM image used for EDS analysis; hp-Ni EDS – (b) combined layered image of the detected elements, (c) oxygen element mapping image, (d) nickel element mapping*

image, (e) EDS spectrum of area in image (a). XPS spectra of (f) full survey spectra, (g) Ni 2p states, and (h) O 1s states of As synthesized hp-Ni electrode after activation (black spectra) and Post EO HSCB for 4 h at 1.58 V vs RHE. (red spectra).

The elemental mappings (Fig. 30a-d) show that the elemental composition of the anode surface is uniform. Fig. 30e shows the EDS spectra of *hp*-Ni which reveals the presence of oxygen, which can be attributed to the surface oxide or hydroxide layers developed during ambient oxidation and, or activation process.

The structure of the *hp*-Ni electrocatalysts were characterized using XPS (Fig. 30f-h). As shown in Fig. 30g, after activation in 1.0 M KOH, almost complete oxidation of the as synthesized *hp*-Ni electrode can be observed with the XPS peak at 855 eV which can be ascribed to be Ni^{2+} of nickel hydroxide. [369] After EO of HSCB, a slight increase in the peak (856.1 eV) corresponds to Ni^{3+} in the form of nickel oxyhydroxide [370] and could also be a mixture of $Ni(OH)_2$/ NiOOH, similar to those observed in previous works. [48, 371] The increase in O *1s* XPS spectrum of post-EO HSCB anode shows that electrooxidation of HSCB could have caused deeper oxidation to the nickel surface (Fig. 28h). The peaks at 531.1 eV and 532.7 eV correspond to bonds of Ni-oxygen and Ni-hydroxide in NiOOH and $Ni(OH)_2$, respectively. [372] The full survey XPS spectra showed the similar spectrum pattern for Ni associated peaks with increase in intensity of O *1s* and C *1s* peaks. (Fig. 28f) It is likely the formation of NiOOH species from oxidation of $NiO/Ni(OH)_2$ electrode surface ($NiO/Ni(OH)_2 + OH^- \rightarrow NiOOH + e^-$) was responsible for the catalytic activity of glucose electrooxidation, according to previous studies. [298, 373, 374]

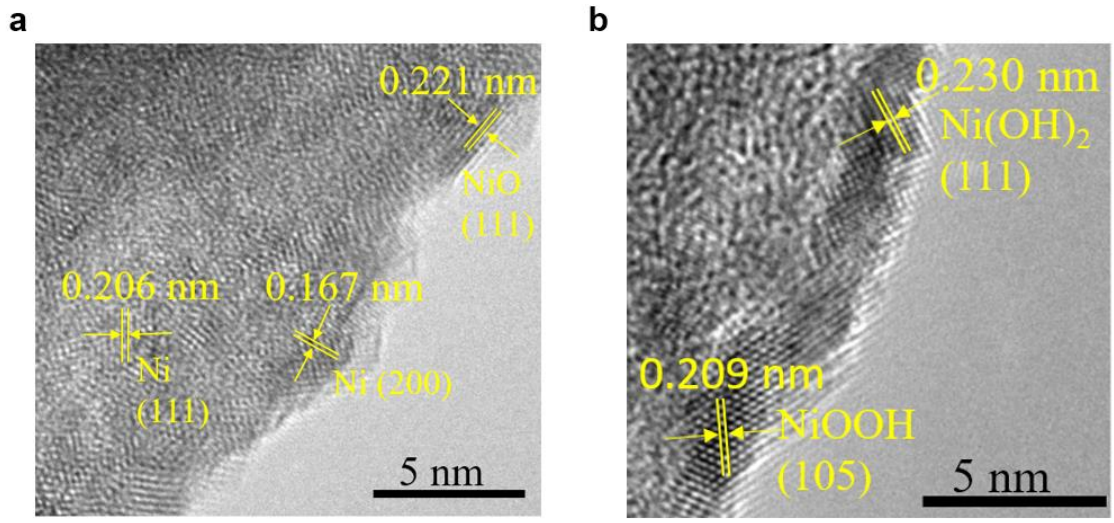

Figure 31 *HR-TEM images of nanoparticles from (a) As synthesized hp-Ni, showing the d-spacing of 0.206 and 0.167 nm of fcc Ni (111) and (200) planes, respectively. The d-spacing of 0.221 nm corresponds to NiO (111) plane; (b) Post EO HSCB hp-Ni, showing the d-spacing of 0.209 and 0.230 nm of NiOOH (105) and $Ni(OH)_2$ (111) planes, respectively.*

The HR-TEM image as shown in Fig. 31a confirms the presence of cubic phase structure of nickel nanoparticles and nickel oxidation in the form of NiO on *hp*-Ni. After EO of HSCB, NiOOH and $Ni(OH)_2$ can be identified clearly in Fig. 31b and is consistent with the XPS results.

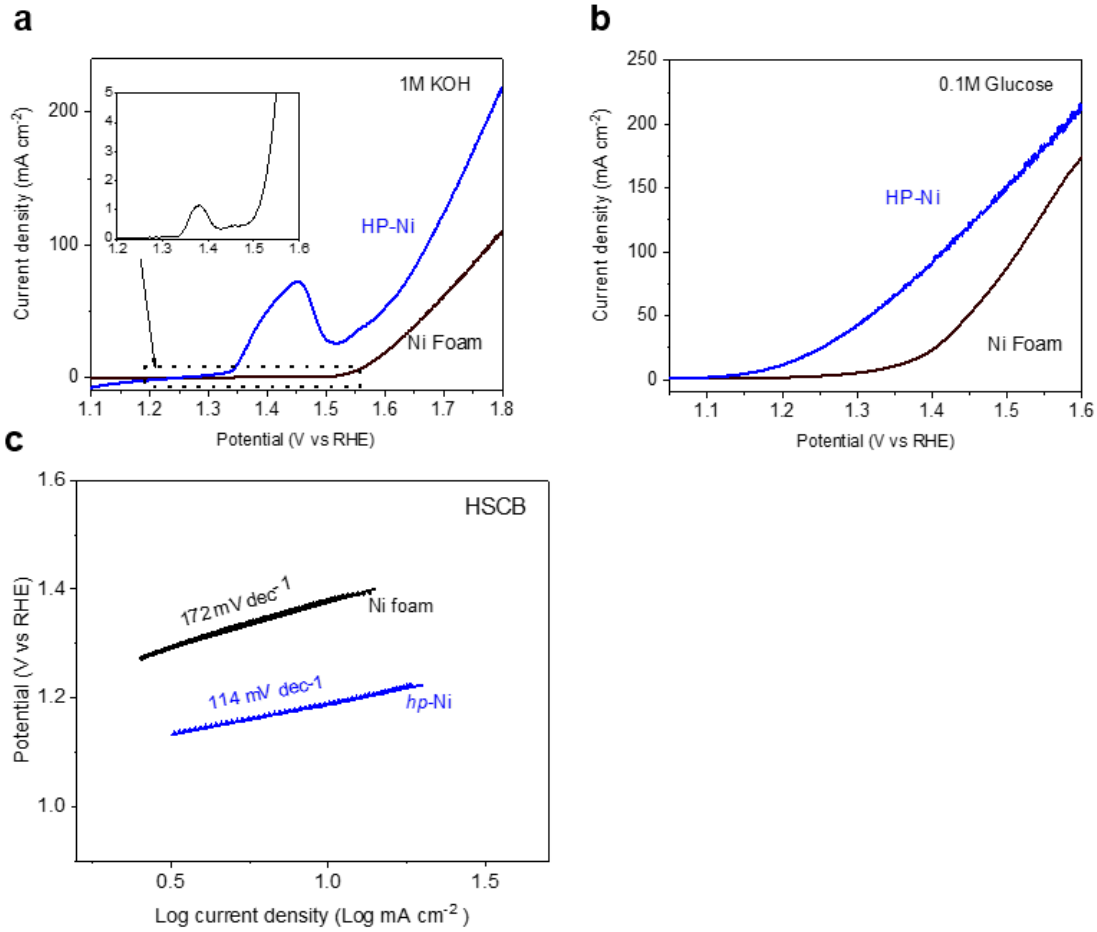

Figure 32 *LSV of Bare NF (black curve) vs hp-Ni (blue curve) – (a) in 1 M KOH (b) with addition of 0.1 M Glucose; and (c) their corresponding Tafel slopes in HSCB.*

The electrode activity was also compared with its pristine Ni foam counterpart, showing that *hp*-Ni significantly increases the current density in both OER and glucose electrooxidation. (Fig. 32a, b) This comparison confirms that the deposited porous Ni microspheres on *hp*-Ni offers a higher catalytic activity due to the increased active sites and mass transfer. The accelerated kinetics could also be corroborated by the reduced Tafel slope in Fig. 32c.

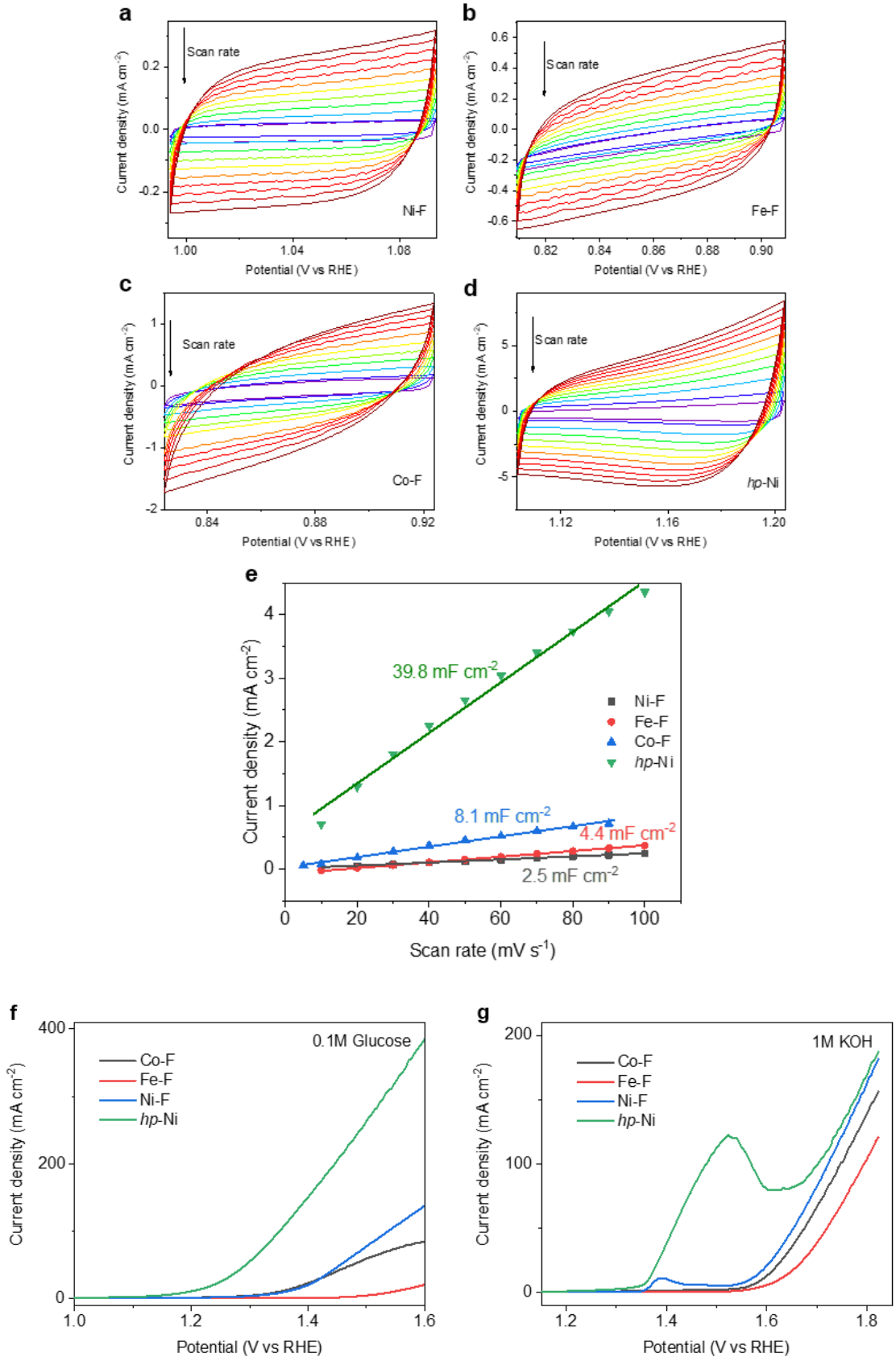

Figure 33 *Electrochemical active surface area measurements. CV curves of – (a) Ni-F, (b) Fe-F, (c) Co-F, and (d) hp-Ni collected in 1.0 M KOH solution at the non-Faradaic region with different scan rates. (e) Linear-fitted scan rate dependence of the current density difference at*

the open circuit potential; LSV of Co-F, Fe-F and Ni-F and hp-Ni as working anode in – (f) 1.0 M KOH solution, (g) 0.1 M Glucose in 1.0 M KOH solution.

ECSA of nickel foam (Ni-F), iron foam (Fe-F), cobalt foam (Co-F) and *hp*-Ni were also measured (Fig. 33a-d) and compared in Fig. 33e. As expected, *hp*-Ni exhibits much increased ECSA (~39.8 mF cm^{-2} vs 2.5 mF cm^{-2} for Ni-F), which is ascribed to the large number of stacked nanoparticles on the porous 3D skeletons. Overall, the metallic nature of the prepared *hp*-Ni endows its inherent electrical conductivity, while the hierarchically porous structure ensure it has sufficient exposure of active sites and efficient mass transfer, which is especially critical for such complex biomass system with a range of molecular weight. The ECSA results are in consistent with the LSV measurements (Fig. 32a, 33f-g). Among the catalysts, *hp*-Ni exhibits the highest activity for OER, glucose and HSCB electrooxidation.

For excellent HER activity, the prepared *hp*-Ni was further phosphidated to form Ni_2P cathode, which shows the appearance of well-distributed thin nanosheet array (Fig. 34a). The surface appeared to be coated with rough and porous geometry which contributes to the large active sites for promoting HER activities. [375] Moreover, additional elemental mappings revealed the full coverage of both nickel and phosphorus on the surface which signifies good uniformity of phosphidation. (Fig. 34b-d) The main elements for Ni, and P were identified in the EDS spectrum of Ni_2P/NF in Fig. 34e.

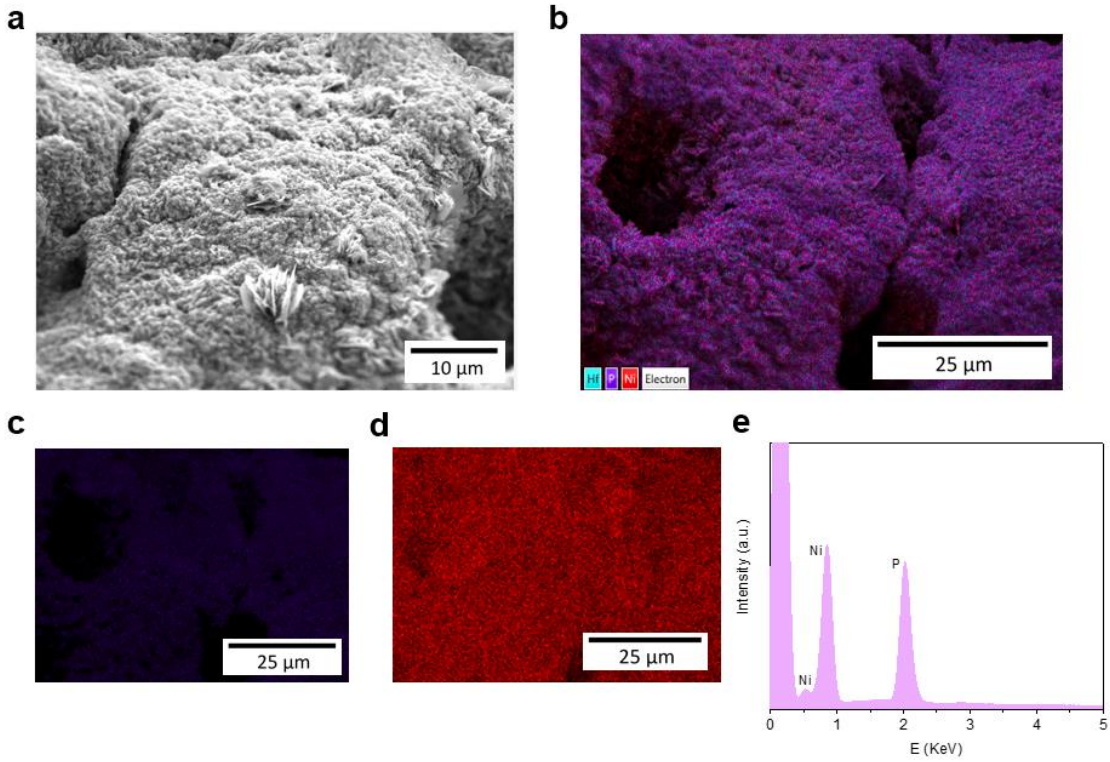

Figure 34 *Ni_2P cathode – (a) SEM image; Ni_2P EDS – (b) combined layered image of the detected elements, (c) phosphorus element mapping image, (d) nickel element mapping image, (e) EDS spectrum of area in image (a).*

3.2.2 Pretreatment and electrooxidation of SCB

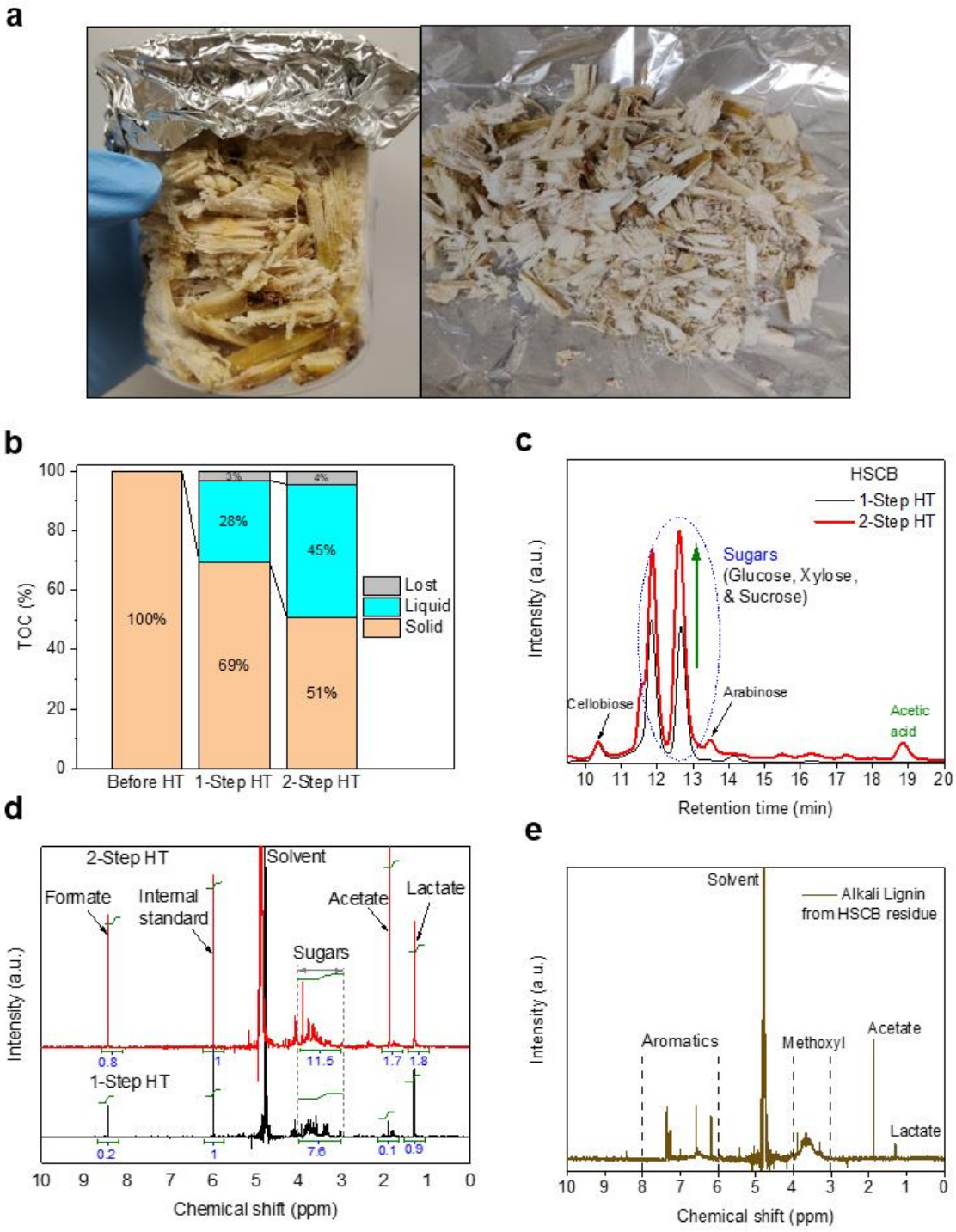

Figure 35 *Pretreatment of SCB. (a) RSCB rough cut to smaller pieces (Left: Before drying, Right: after overnight drying); (b)Total TOC% comprising of solid, liquid, and lost components of SCB before HT (Hydrothermal), 1-step HT and 2-Step HT; (c) HPLC chromatograms and (d) ^{1}H NMR spectrums of RSCB after dilute H_2SO_4 hydrothermal process (Black: 1-Step Hydrothermal (HT), Red: 2-Step HT) with maleic acid as internal standard; (e) ^{1}H NMR spectrum of dissolved products from residue of HSCB by mild alkaline treatment.*

Since raw SCB (Fig. 35a) contains rigid polymeric structures and complex components, a 2-step dilute H_2SO_4 hydrothermal pretreatment was adopted for extraction of residual sugars and depolymerization of cellulose and hemicellulose to water-soluble mono/oligosaccharides. After separation, the insoluble lignin residue was recovered with mild alkaline treatment. Subsequent HPLC and NMR analysis of the products from the pretreatments were conducted.

The solubility enhancement of the hydrothermal pretreatment is shown in Fig. 35b. The difference of 1-step and 2-step hydrothermal treatment is significant. Solid TOC residue decreased from 69% to 51% with corresponding liquid TOC increased from 28% to 45%. The negligible amount of TOC loss of 3–4% was probably due to experimental error during handling of samples or volatile carbon products loss during drying.

Fig. 35c shows the HPLC chromatographs of the liquid product analysis of both hydrothermal processes, highlighting that 2-step hydrothermal treatment is essential to extract more sugars. The sugars to be identified as glucose and xylose which are monosaccharides of cellulose and xylan, respectively. Small amount of arabinose that exists in hemicellulose branch was also detected. Cellobiose peak was observed, indicating depolymerization was not 100% complete. Sucrose could also exist as it shares the same peak locations as glucose and xylose. Further comparison can be seen in the NMR spectra in Fig. 35d, revealing a higher area for 2-step hydrothermal corresponding to sugars at region of 3–4 ppm. [376] Other carboxylic acid salts such as acetate, formate and lactate were also identified. Acetic acid was mainly from the hydrolysis of the acetyl group in hemicellulose [100] present in SCB while formate and lactate are the degradation products of the monosaccharides. Other dehydrated products such as 5-HMF, furfural and levulinic acid were not detected, suggesting that the hydrothermal condition was mild and energy-saving. [377]

Lignin recovery from HSCB residue was attempted with mild alkaline treatment. Around 80% of lignin could be dissolved and was further analyzed with ^{1}H NMR. Obvious multiple peaks corresponding to aromatics from lignin can be observed in Fig. 35e. The broad peaks at 3–4 ppm and singlet peak at 1.9 ppm are attributed to methoxy and methyl groups from lignin, respectively. Combinatorial acid and alkali pretreatment of corn stover exhibited similar lignin recovery in another study. [378] Hence, it is possible to recover and utilize lignin with a broad scope of potential applications, such as upcycling into advanced materials and aromatics chemicals. [379]

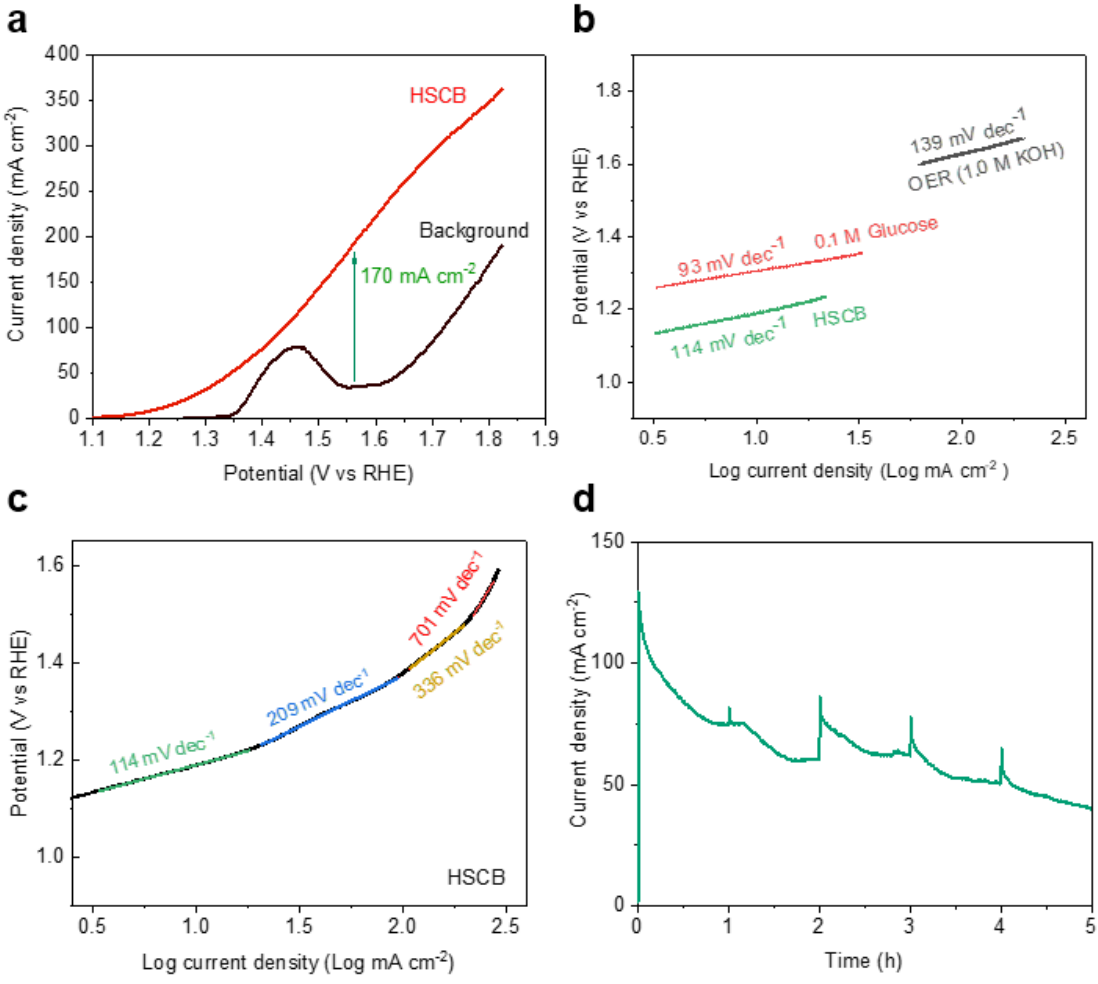

Figure 36 *(a) LSV of hp-Ni working anode (black curve: background 1.0 M KOH, red curve: HSCB adjusted to pH 13.8 (equivalent to pH of 1.0 M KOH); (b) Tafel plots derived from current–potential curves obtained of hp-Ni electrode at scan rate 5 mV s^{-1} in the presence of 1.0 M KOH (black), 0.1 M Glucose (red) and HSCB (green). HSCB electrooxidation at 1.58 V vs RHE with (c) Tafel plot derived from a current–potential curve obtained of hp-Ni electrode at scan rate 5 mV s^{-1} of HSCB and (d) Chronoamperometric plot of HSCB electrooxidation in 1.0 M KOH for 5 hours.*

Next, HSCB was subjected to electroreforming to analyze the performance in alkaline condition. The LSV of hydrothermal-treated SCB showed much higher current activity and a much earlier onset potential (1.2 V vs RHE) as compared to the background electrolyte. (Fig. 36a) Specifically, at 1.58 V vs RHE, the current density was increased by 170 mA cm^{-2}. This enhanced activity implies that favorable organic oxidation than water oxidation. It is also worth noting that at lower potentials, e.g., below 1.58 V vs RHE, HSCB oxidation could completely replace OER. This also reduces the overall energy requirement for green H_2 production compared to pure water electrolysis by 12% at current density of 200 mA cm^{-2}, leading to ~10% higher energy efficiency. The energy efficiency calculation [380] is based on the heating value of produced hydrogen gas with respect to required energy consumed by the system as follows equation: $\eta_{eff} = \frac{HHV_{H2\ produced}}{Electricity\ consumed}\ X\ 100\%$, where $HHV_{H2\ produced}$ is the higher heating value of the produced 1 kg of hydrogen (142 MJ), and *Electricity consumed* is the input energy for the water electrolysis or the electroreforming process. At a current density of 200 mA cm^{-2}, the potential of AWE and HSCB electroreforming is 1.80 V vs RHE and 1.58 V vs RHE, respectively, suggesting a 12% higher efficiency. Table 8 compares the energy efficiency of the HSCB electroreforming process and AWE.

Table 8 Energy efficiency comparison of AWE and HSCB electroreforming.

Parameters	AWE	HSCB electroreforming
Electricity consumed	203 MJ	178 MJ
Energy of H_2 generated	142 MJ	142 MJ
Energy efficiency	~70%	~80%

Based on 1.0 kg H_2 produced, which requires 33.8 kg of SCB. HHV for the combustion of hydrogen is 285.8 kJ $mole^{-1}$. [380]

Similar electrochemical behaviors were also observed in other studies with glucose as well as alcohols. [31, 298, 381] Active species on *hp*-Ni, Ni^{3+} is crucial for the cleavage of C-C bond [382], while Ni^{2+} can catalyse the oxidation of nucleophile groups, such as alcohol groups. [383, 384] Moreoever, The corresponding LSV curve (red curve of Fig. 36a) shows earlier onset before the formation of Ni^{3+} which indicates Ni^{2+} was also involved in biomass electroreforming. Specifically, the LSV with 1.0 M KOH (black curve of Fig. 36a) shows the distinctive anodic peak from (1.4 to ~1.6 V vs RHE) that attributed to Ni(II) oxidation to NiOOH, ($NiO/Ni(OH)_2 + OH^- \rightarrow NiOOH + e^-$) [385, 386]. In contrast, for OER, Ni^{3+} is identified as the active site. This becomes evident after the formation of Ni^{3+} at ~1.6V vs RHE, coinciding with an apparent increase in current density during OER. It also further reaffirms that the diluted acid hydrothermal pretreatment of the RSCB was effective, mainly by depolymerization of cellulose (β-1,4 glycosidic bond cleavage) and hemicellulose to mono- and oligosaccharides by acid-catalyzed hydrolysis. [387]

Tafel slopes were plotted from I-V curves to study the kinetics for electroreforming of derived mono- and disaccharides from SCB. Fig. 36b shows accelerated kinetics of glucose oxidation (93 mV dec^{-1}) and HSCB oxidation (114 mV dec^{-1}) over OER (139 mV dec^{-1}) in 1.0 M KOH. The poorer kinetics of HSCB oxidation compared to glucose oxidation was likely due to the presence of complex extractives and soluble lignin which may slow down mass transport and then hinder the kinetics during HSCB oxidation. Nevertheless, the electrocatalyst shows much better kinetics (109 mV dec^{-1}) than the NiO modified GC/MWNT electrode for oxidizing 0.01 M glucose with a Tafel slope of 167.5 mV dec^{-1}.[388] In HSCB (Fig. 36c), four different kinetic regions were observed (114 mV dec^{-1} between 1.13 V to 1.20 V, 209 mV dec^{-1} between 1.23 V to 1.37 V, 336 mV dec^{-1} between 1.39 V to 1.48 V, and 701 mV dec^{-1} between 1.50 V to 1.57 V),

revealing a multistep electrochemical process of HSCB oxidation. The first and fastest kinetic region occurred below 1.22 V vs. RHE (before the formation of Ni^{3+}), corresponding to the electrooxidation of much smaller molecules in HSCB by Ni^{2+}. At the 2nd and 3rd slower kinetic regions at 1.23 V to 1.48 V, the formation of Ni^{3+} species from Ni^{2+} species starts. Meanwhile, these Ni^{3+} species are reduced back to Ni^{2+} by the reducing sugars in HSCB. The reducing sugars also undergoes electrooxidation to become intermediates/products. This process is rather slow due to the rate limiting Ni^{2+} via the redox chemistry. Finally, the slowest kinetic region occurred after 1.50 V, where the larger (more stable) molecules got oxidized. The slow mass transport of these large molecule could limit the reaction kinetics. Moreover, the competing effect of OER together with electrooxidation of the HSCB complex to intermediates/products could also have an effect. This is consistent with past study, which shows that the rate-determining step of glucose (>10 mM) oxidation reaction is the oxidative removal of the adsorbed intermediates from Ni^{3+} at higher potential (above 0.545 V vs Ag/AgCl). [389]

HSCB electrooxidation was carried out at 1.58 V vs RHE over 5 h. Each interval run of 1 hour were plotted together (Fig. 36d) and noticed a spike at the start of each new run. The sudden spike in current was due to the instantaneous potential increase from open circuit potential to the applied constant potential. This caused the reactant species within the proximity of the *hp*-Ni electrode to be immediately oxidized and resulted in current increase. As the concentration of the species decreased, the current decayed and stabilized within 40 s into the diffusion-controlled regime, as shown in all intervals. This typical behaviour was also observed in other chronoamperometric studies. [159] Overall, the decay in current density from 135 mA cm^{-2} to 40 mA cm^{-2} is attributed to the consumption of mono/oligosaccharides to form oxidation products. [339]

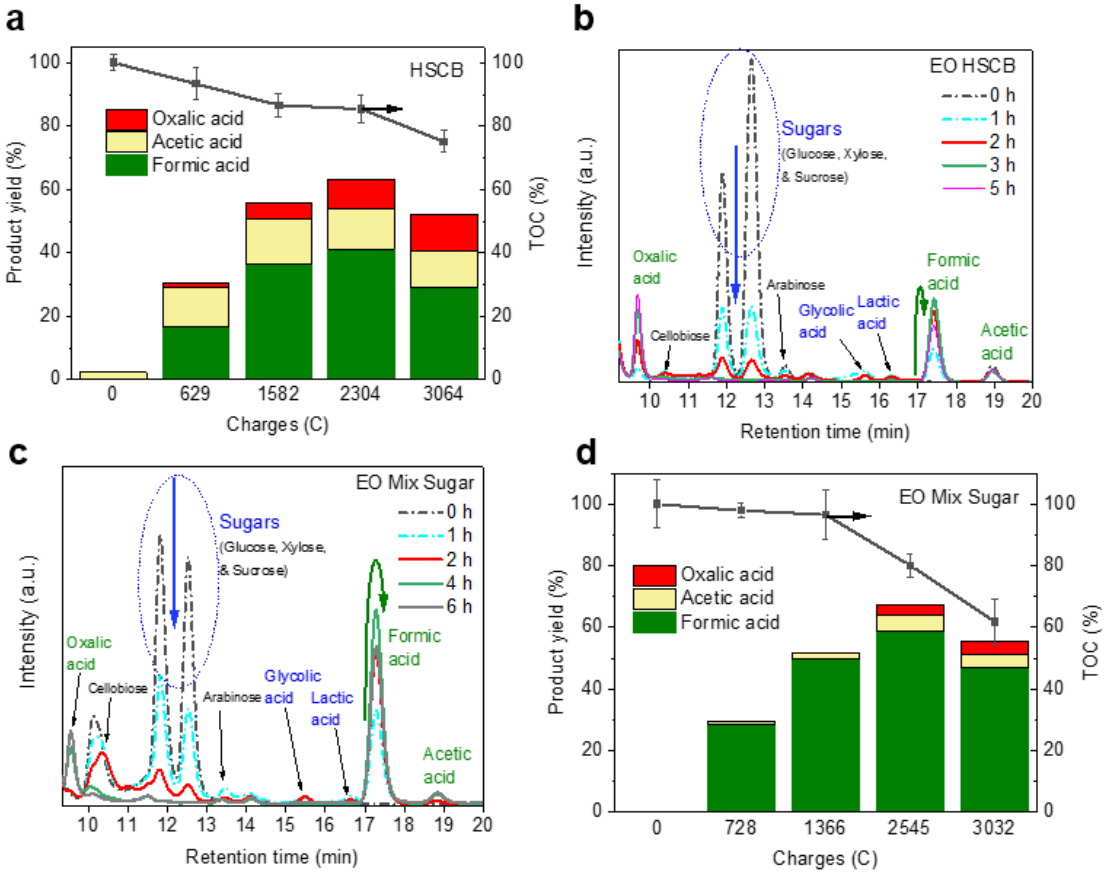

Figure 37 *HSCB electrooxidation at 1.58 V vs RHE with (a) Effect of applied charges on products yield% (oxalic acid, acetic acid and formic acid) and TOC %; (b) HPLC chromatograms of products at different electrooxidation intervals; Electrooxidation of mixture of various saccharides with (c) HPLC chromatograms at different intervals at 1.58 V vs RHE and (d) Effect of charges on product yield.*

Fig. 37a shows the charge transfer against the yield of three main organic acid products and change in TOC during the electrooxidation of HSCB at constant 1.58 V vs RHE. A sharp increase in both formic acid and acetic acid at the beginning at 629 C was noticed, accompanied by the production of a slight amount of oxalic acid. As the accumulated charges increased, acetic acid remained stable (11–14%) while oxalic acid continued to increase to a maximum of 11.5%. Within 5 h, the highest yield of formic acid was 41% with total carboxylic acids yield of 63% at applied charges of 2304 C. With further electrooxidation, formic acid yield dropped to 29%. The decreasing trend of TOC% is

ascribed to the overoxidation of formic acid to inorganic carbon that could have happened concurrently.

HPLC analysis of products in Fig. 37b reveals overall transformation of various identified compounds with electrooxidation time progression. The consumption of sugars progressed with time and finished at 3 h. This trend was also observed for other saccharides like cellobiose and arabinose. Several peaks from intermediates such as lactic acid and glycolic acid appeared from 1 to 2 h and vanished over time. Peak of acetic acid remained constant while oxalic acid continued to increase during the test. On the other hand, formic acid started to increase but decreased after 5 h. In addition, the electrooxidation of mixture of various saccharides with a carbon mole ratio of 35% glucose, 10% cellobiose, 35% xylose and 20% sucrose based on the composition analysis and previous literatures [84, 356] was conducted. The HPLC characterizations in Fig. 37c demonstrate similar intermediates and products when compared to the EO of HSCB. As expected, formic acid is the dominant electroformed product among the identified carboxylic acids. (Fig. 37d) This suggests that the effectiveness of the developed process remains despite the different chemical structure of various sugar oligomers.

It is worth noting that this process displayed significantly high performance in terms of activity, product selectivity and stability as compared to previously reported anodic oxidation studies of lignocellulosic biomass. (Table 9)

Table 9 Anodic oxidation of lignocellulosic biomass.

Anodic oxidation (Lignocellulosic biomass)	Electrode	Current density	Product selectivity	Stability	Ref.
Black liquor	Pt, Ni and AISI 304 Stainless steel	< 10 mA cm^{-2}	No product analysis	N. D	[159]
Kraft lignin	Pt, Au, Ni, Cu, DSA-O_2 and PbO_2	< 3 mA cm^{-2}	<17% selectivity to Vanillin	N. D	[270]
Cellulose	Glassy carbon plates	0.2 to 0.4 mA	No specific product	N. D	[390]
Cellulose & Cellobiose	Gold	< 2 mA cm^{-2}	No product analysis	N. D	[266]
Cellulose, Oligosaccharides	MnO_2/graphite/PTFE	< 5 mA cm^{-2}	High selectivity to glucose	N. D (24 h)	[327]
Cellulose	Gold	< 1 mA cm^{-2}	No product analysis	N. D	[35]
Hemicellulose	Gold	< 1 mA cm^{-2}	No product analysis	N. D	[36]
Lignin	Ni/C, Co/C, NiCo/C	< 5 mA cm^{-2}	No specific product	N. D (2 h)	[267]
Cellulose	AuNPs/C	< 1 mA cm^{-2}	No product analysis	N. D	[279]
Cellulose	Au/carbon aerogel	10 mA at 2.75 V_{cell}	67.8% Gluconate	N. D (24 h)	[274]
Lignin derivatives	PtFe/C	208 mA cm^{-2}	90% CO_2	N. D (1.1 h)	[271]
Lignin	Pt-Ru catalyst	< 4 mA cm^{-2}	No product analysis	10 CV cycles (0 to 1.1 V_{cell})	[20]
Lignocellulose mono- and Disaccharide derivatives	PtFe/C	0.15 – 0.20 mA cm^{-2}	Near 100% selectivity to CO_2	N. D (1.1 h)	[391]
Lignin and its model compounds	Glassy carbon (GC)	25 – 80 mA	No specific product	N. D (24 h)	[272]
Crushed barley straw	Nickel foam	< 3 mA cm^{-2}	No specific product	80 h	[273]
Glucose	Nickel	3.9 mA cm^{-2}	22% Formate, 12% Oxalate, 7% Glycolate and 8% carbonates	N. D (6 h)	[392]
Xylose	Nickel	3.9 mA cm^{-2}	42% Formate, 5% Oxalate, 16% Glycolate and 7% carbonates	N. D (6 h)	[392]
Sugarcane bagasse	*hp*-Ni	Average 100 mA cm^{-2}	41% Formate, 9% Oxalate, 13% Acetate	3 CA runs (5 h each)	This work

Glucose	*hp*-Ni	Average 216 mA cm^{-2}	88% Formate, 0.5% Oxalate, 9% Acetate	3 CA runs (5 h each)	This work
Xylose	*hp*-Ni	Average 170 mA cm^{-2}	68% Formate, 3% Oxalate, 5% Acetate	3 CA runs (5 h each)	This work

N.D denotes no details. CA denotes Chronoamperometry. CV denotes Cyclic Voltammetry.

3.2.3 Electrooxidation of mono/disaccharides and intermediates

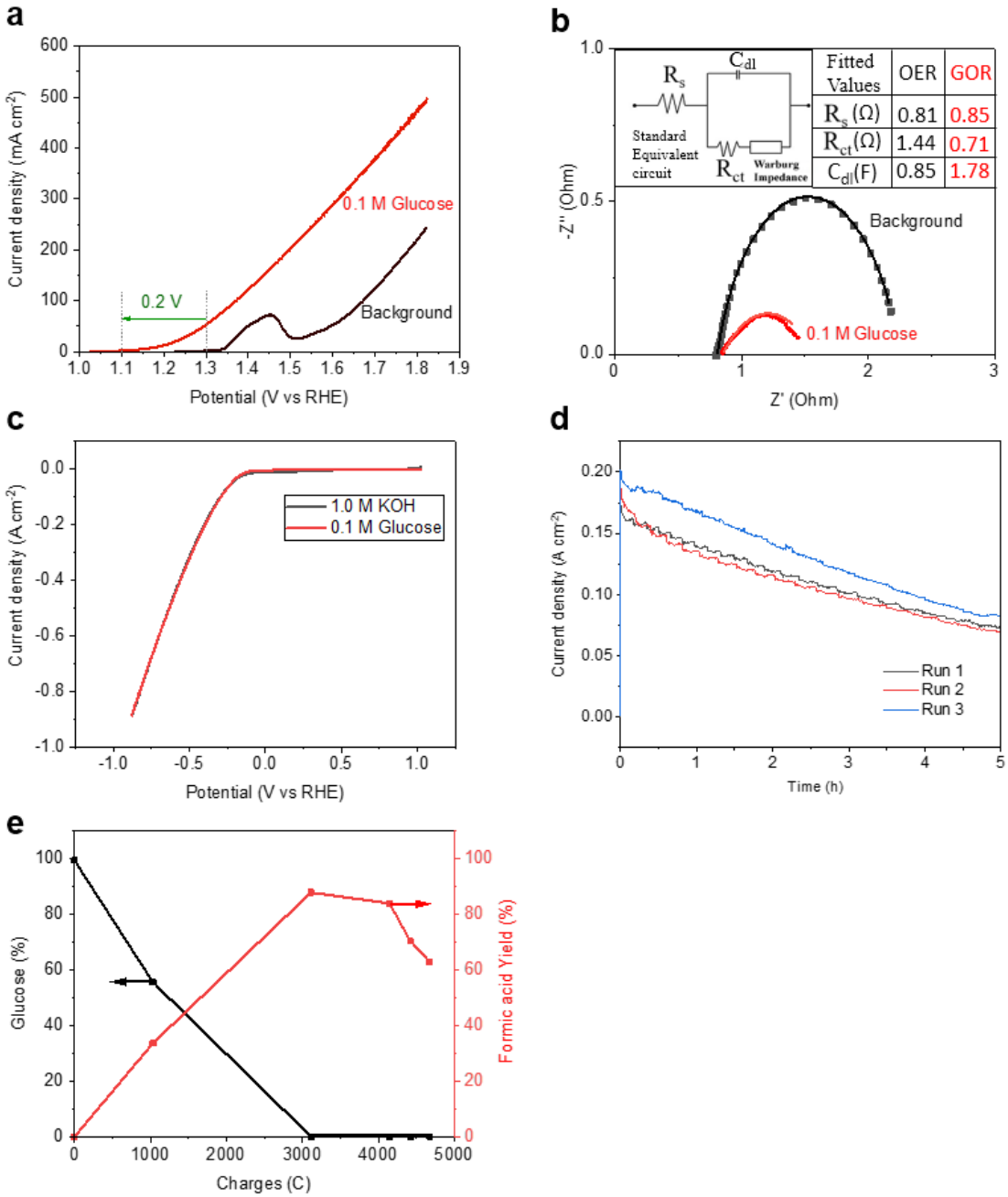

Figure 38 *Glucose electrooxidation tests. (a) LSV of hp-Ni working anode (black curve: background 1 M KOH, red curve: 0.1 M glucose in 1 M KOH), (b) Nyquist plots in 1 M KOH at 1.58 V vs. RHE; (c) LSV of Ni_2P cathode anode (black curve: background 1M KOH, red curve: 0.1 M Glucose in 1 M KOH), (d) 3 consecutive runs with 0.1 M glucose in 1 M KOH at constant potential at 1.58 V vs RHE; (e) Effect of charges on formic acid yield % and glucose conversion % at 1.58 V vs. RHE.*

The reaction mechanism involving the oxidation of the identified sugars and their intermediates from pretreated SCB to formate were further investigated with additional electrochemical tests. First, the LSV in Fig. 38a shows the addition of glucose in the background electrolyte caused the disappearance of the distinctive anodic peak of Ni(II) oxidation to NiOOH (1.3 to 1.5 V vs RHE) of the *hp*-Ni. At higher potential of more than 1.5 V vs RHE, the current density increases dramatically, which could be due to the combination of OER and glucose oxidation. As compared to the LSV of background 1 M KOH, the addition of glucose shows a reduced onset potential at 1.1 V vs RHE. The difference in onset potential of 0.2 V vs RHE implies that glucose oxidation is much thermodynamically favorable than OER. The electrochemical impedance spectroscopy (EIS) in Fig. 38b compares glucose electrooxidation and normal OER at 1.58 V vs RHE. After fitting the EIS curves to the standard equivalent circuit (Randles circuit) [393], the information such as series resistance (R_s), charge-transfer resistance (R_{ct}), double layer capacitance (C_{dl}), Warburg impedance can be obtained. The R_s values for both OER and GOR are similar while R_{ct} for GOR is halved of OER as shown in Fig. 38b. Hence, this shows that the enhanced current density and reduced overpotential of GOR over OER is ascribed to the much thermodynamic and kinetic favorability of glucose molecules. The reduced diameter (semi-circle) of GOR over OER indicates a much easier charge transfer ability and faster kinetics. [394] The larger C_{dl} value of GOR could be due to the inclusion of glucose molecules that interfered with the hydroxide ions at the surface of the electrode which is similar to another study [389]. Furthermore, the lack of the 45° slope in diffusion-controlled region of the Nyquist plots could mean that the Warburg element (electrochemical element of diffusion) [395] is absent in both OER and GOR.

As shown in Fig. 38c, the HER LSV profiles remained unchanged with glucose inclusion, suggesting that no reduction reaction had occurred. Fig. 38d demonstrated the

repeatability and stability of the anode from 3 consecutive runs of glucose electrooxidation at 5 h duration each. The decay in current density from 150 mA cm^{-2} to 100 mA cm^{-2} is ascribed to consumption of glucose to oxidized products. [339]

The highest yield of formic acid (88%) was obtained at 3115 C and glucose was totally converted. (Fig. 38e) Notably, with 12 electrons transfer involved for this reaction [396], the theoretical charge required is calculated to be 3566 C. This difference in charges consumed potentially shows that there could be competing reactions to glucose oxidation that happen simultaneously during the electrooxidation.

Indeed, formic acid could be detected without applying electrical potential with the same setup in 8 to 12 h, as shown in Fig. 39a. Fructose with other organic acids (glycolic acid and lactic acid) were also identified and are believed to participate in the formation of formic acid. It is well known that glucose in strong alkaline environment undergoes isomerization to fructose (i.e., Lobry de Bruyn von Ekenstein transformation). Next, fructose undergoes retro aldol reaction and cleaves the 3-3 bond to form dihydroxyacetone and glyceraldehyde, which isomerize at dynamic equilibrium. [397] The products further dehydrate to pyruvic aldehyde or re-hydrate (Cannizzaro rearrangement) to form lactic acid. [398] Additionally, side reaction of trioses could also produce glycolic and formic acid. [399]

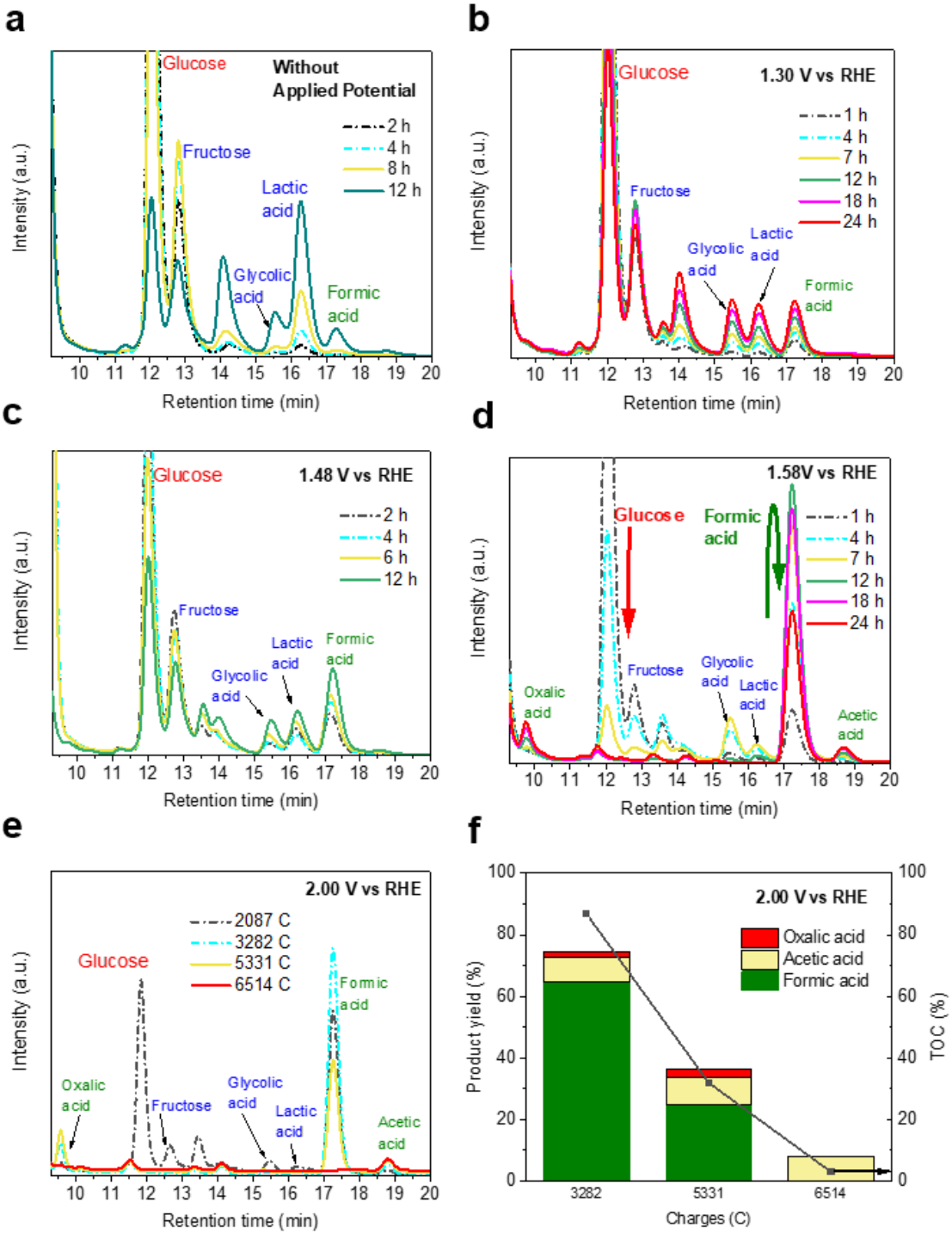

Figure 39 *HPLC chromatograms of Glucose electrooxidation at – (a) 0 V vs RHE, (b)1.30 V vs RHE, (c) 1.48 V vs RHE, (d) 1.58 V vs RHE, (e) 2.00 V vs RHE, and (f) Effect of applied charges on products yield% (oxalic acid, acetic acid and formic acid) and TOC % of (e).*

Glucose electrooxidation at different working potentials (1.30, 1.48, 1.58 and 2.00 V vs RHE) were investigated to study their corresponding products. The HPLC plots revealed

different product ratios over electrooxidation time, as shown in Fig. 39b-e. At 1.58 V vs RHE, both glycolic acid and lactic acid are consumed rapidly unlike at 1.30 and 1.48 V vs RHE. This suggests that higher voltage is essential to increase the electrooxidation reaction rate for glycolic acid and lactic acid conversion. At potentials closer to OER onset potential (i.e., 1.58 V vs RHE), OER could occur and is more of a competing reaction against biomass electroreforming. The main reason that they have similar onset potential could be due to the same active sites shared. For instance, as the voltage is controlled to reduce the evolution of oxygen (i.e., 1.48V vs RHE), glucose conversion consistently occurs, as shown in Fig. 39c.

However, at 2.00 V vs RHE (Fig. 39f), both of formic acid and oxalic acid could be further oxidized into carbonate or CO_2 as illustrated by the complete decrease of the TOC. Indeed, this shows that overoxidation of formic acid and oxalic acid results in inorganic carbon.

Notably, fructose, the tautomerized counterpart of glucose, also electrooxidized similarly like glucose in Fig. 40a. Glycolic acid was electrooxidized to formic acid and oxalic acid (Fig. 40b) while the electrooxidation of lactic acid produced acetic acid, as depicted in Fig. 40c. Further electrooxidation of possible intermediates from glucose oxidation (gluconic acid, glucaric acid salt and tartaric acid) were also evaluated. As shown in Fig. 40d-f, the HPLC chromatographs contain identical products, indicating the same reaction pathway may follow. With the above information, glucose electrooxidation in this study can be represented with the proposed reaction pathway in Fig. 41.

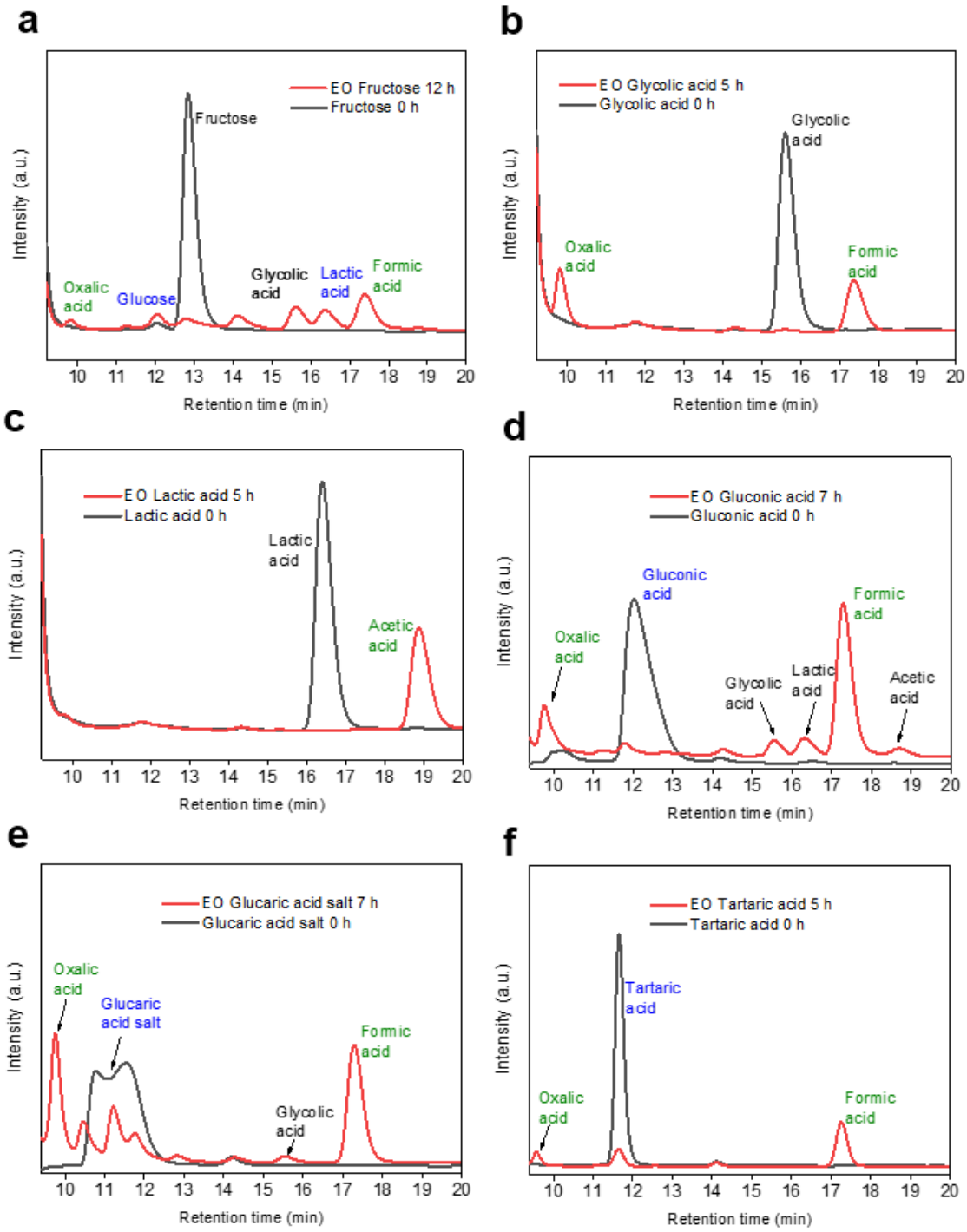

Figure 40 *EO of Intermediates – (a) Fructose; (b) Glycolic acid; (c) Lactic acid; and EO of possible intermediates – (d) Gluconic acid; (e) Glucaric acid salt; (f) Tartaric acid.*

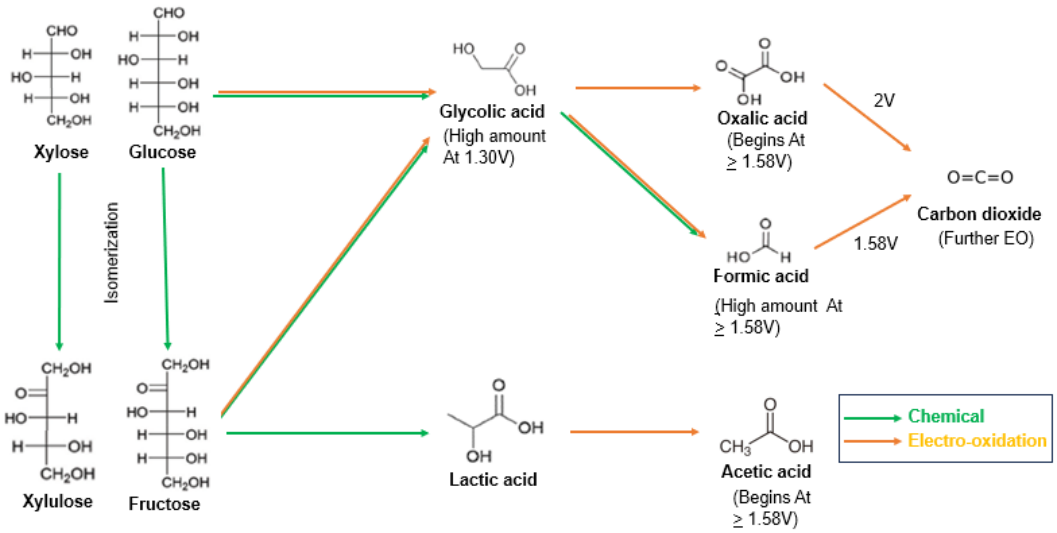

Figure 41 *Proposed reaction pathway of xylose / glucose to formic acid, and other products.*

Fig. 42a details the three main products and TOC with increasing applied charges. Formic acid dominated among the products with small amount of oxalic acid. Acetic acid yield was consistently around 8%, indicating stable operation under the electrooxidation conditions. The highest concentration of formic acid was attained with 8% loss of TOC at applied charges of 3115 C. The loss was due to overoxidation of formic acid to inorganic carbon. This loss of TOC correlates positively with the decrease in formic acid yield and increase in the applied charges.

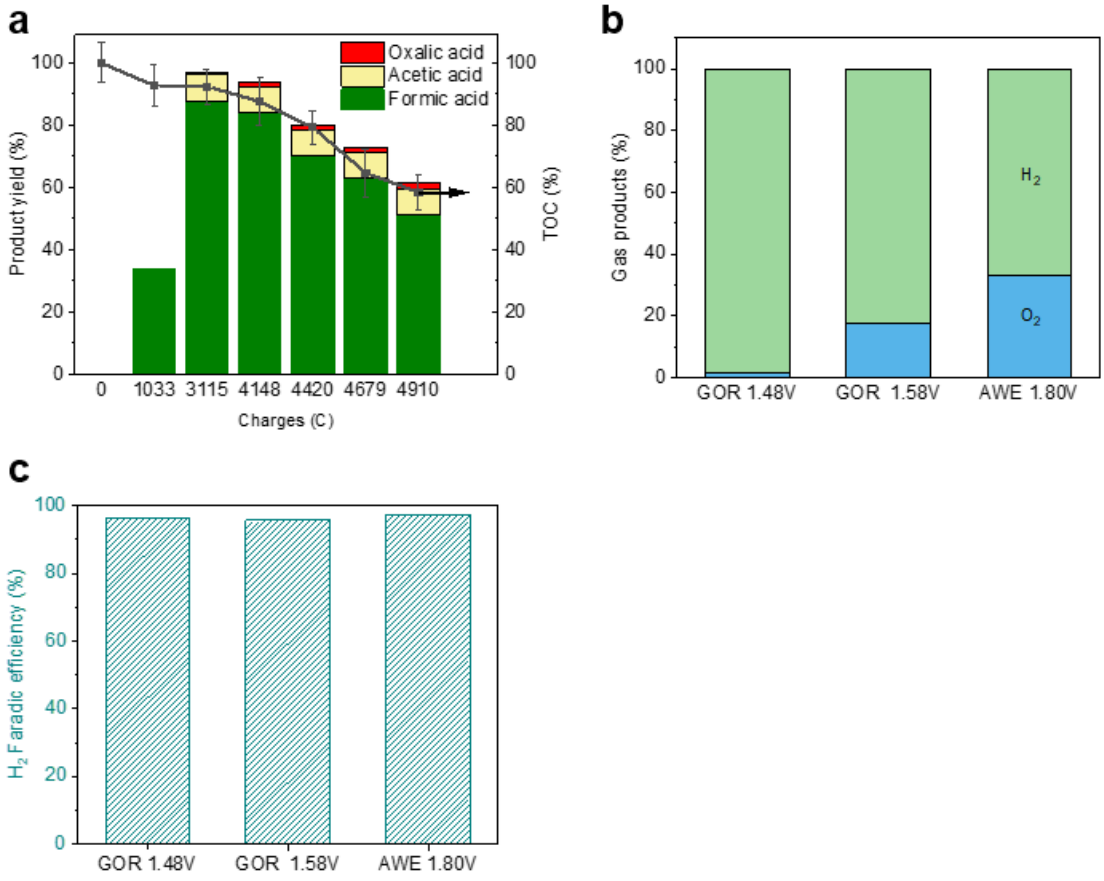

Figure 42 *Glucose electrooxidation tests (a) Effect of charges on product analysis (oxalic acid, acetic acid and formic acid and TOC % at 1.58 V vs RHE; Comparison of glucose oxidation reaction at 1.48 V vs RHE, 1.58 V vs RHE and AWE at 1.80 V vs RHE on: (b) ratio of H_2 to O_2 gas products and (c) H_2 Faradaic efficiency.*

Gas production during GOR in alkaline media is plotted in Fig. 42b to show the ratio of oxygen and hydrogen. Alkaline water electrolysis (AWE) followed well with the molar ratio of 1:2, whereas GOR at 1.48 V vs RHE had only 1.7% of O_2. This indicates that GOR at a lower potential is capable of effectively suppressing the production of oxygen (OER). At 1.58 V vs RHE, 17% O_2 was detected, which implies that GOR and substantial OER had occurred concurrently. The production of some reactive oxygen species / O_2 near the OER potential could be beneficial to achieving high formic acid selectivity, as demonstrated in another study with H_2O_2 as the oxidant. [399] Overall, the H_2 Faradaic efficiencies of the above electrooxidation reactions is well above 95% as illustrated in Fig. 42c.

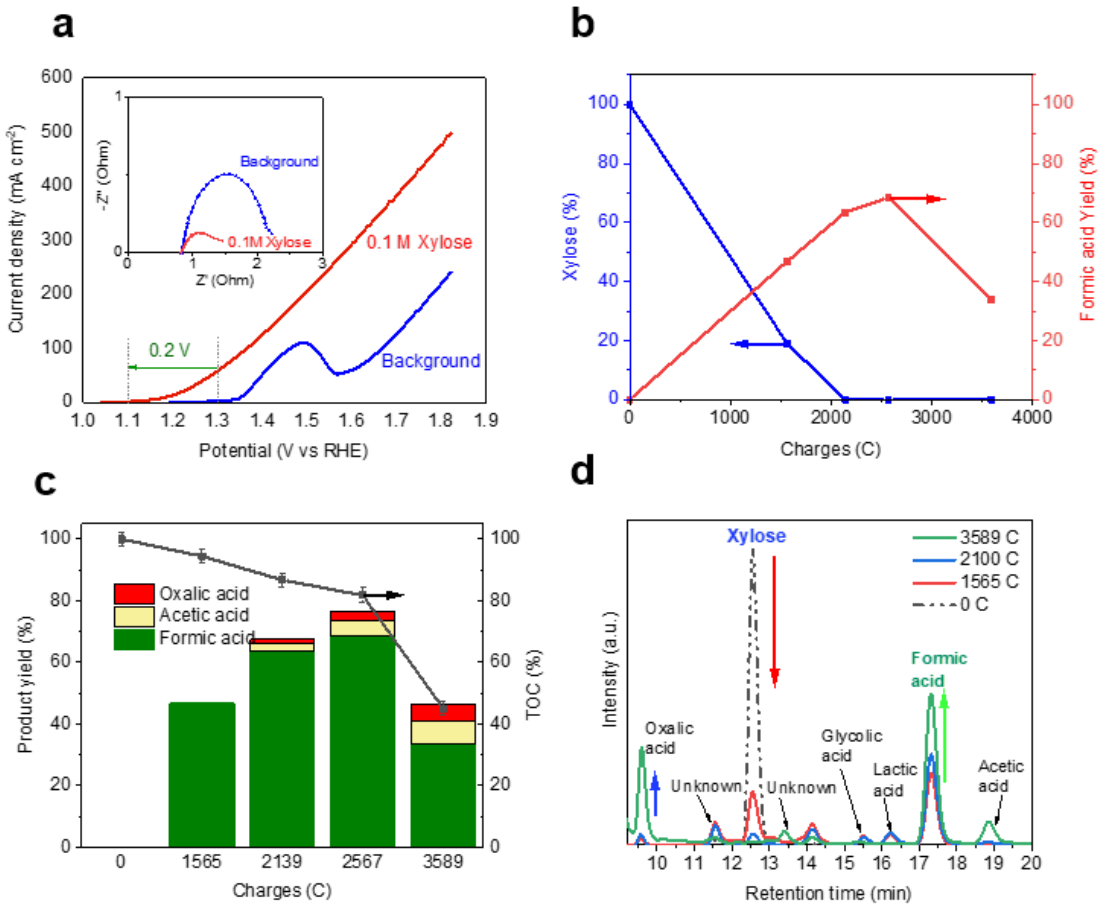

Figure 43 *Xylose electrooxidation tests. (a) LSV of hp-Ni working anode (blue curve: background 1 M KOH, red curve: 0.1 M glucose in 1 M KOH), Inset: Nyquist plots in 1 M KOH at 1.58 V vs. RHE; (b) Effect of charges on formic acid yield % and xylose conversion % at 1.58 V vs. RHE; (c) Effect of charges on product analysis (oxalic acid, acetic acid and formic acid) and TOC % from EO 0.1 M xylose at 1.58 V vs RHE. (d) HPLC chromatograms of xylose electrooxidation at 1.58 V vs RHE.*

Subsequent electrochemical tests were also performed on xylose. The LSV sweep of 0.1 M xylose displays similar electrochemical performance to glucose, as shown in Fig. 43a. Moreover, as shown in the inset, the smaller diameter of Nyquist plot of xylose reaffirms that oxidation of xylose also possesses easier charge transfer and faster kinetics than OER. Xylose electrooxidation to high yield formic acid (70%) at 2139 C with full conversion of xylose. (Fig. 43b) With 10 electron transfer involved for this reaction, the theoretical charge required to achieve the specific amount of formic acid is 2895 C. Just like glucose, there could be similar competing reactions to xylose electrooxidation that

happen simultaneously during the electrooxidation. Fig. 43c illustrates the evolution of the yield of products and TOC with increasing applied charges. Formic acid is the most prominent product, with only a minimal amount of oxalic acid (less than 6%) detected. As the applied charges increase, the concentration of acetic acid rises from 2% to 7%. The highest concentration of formic acid with 13% TOC loss was observed at an applied charge of 2139 C and the loss of TOC is believed to result from the overoxidation of formic acid into inorganic carbon. This increasing TOC loss is correlated with a decrease in formic acid as more applied charges are applied. The products from xylose electrooxidation with cumulative charges were studied, showing similar chemical transformation pattern as that of glucose electrooxidation. (Fig. 43d) Hence, xylose could follow the same oxidation pathway as glucose (Fig. 41) because xylose would also isomerize to xylulose in alkaline media [400, 401]. The lower yield of formic acid from the electrooxidation conversion of xylose compared to glucose could be due to the difference in molecular structure that could cause different alignment orientation and influence the absorption on the electrocatalyst.

Further NMR spectra in Fig. 44a, b reaffirm that the electrooxidation of the abundant monosaccharides (glucose, xylose) resulted in mainly formate and acetate as well as trace amount of lactate. Electrooxidation of the less abundant pentose in SCB, arabinose produced similar products like both hexoses. (Fig. 44c) Noting that disaccharides such as cellobiose or sucrose from extractives also exist after pretreatment, further electrooxidation of them were conducted to analyze their products. As shown in Fig. 44d and e, the HPLC chromatographs reveal the main product are also formic acid and oxalic acid.

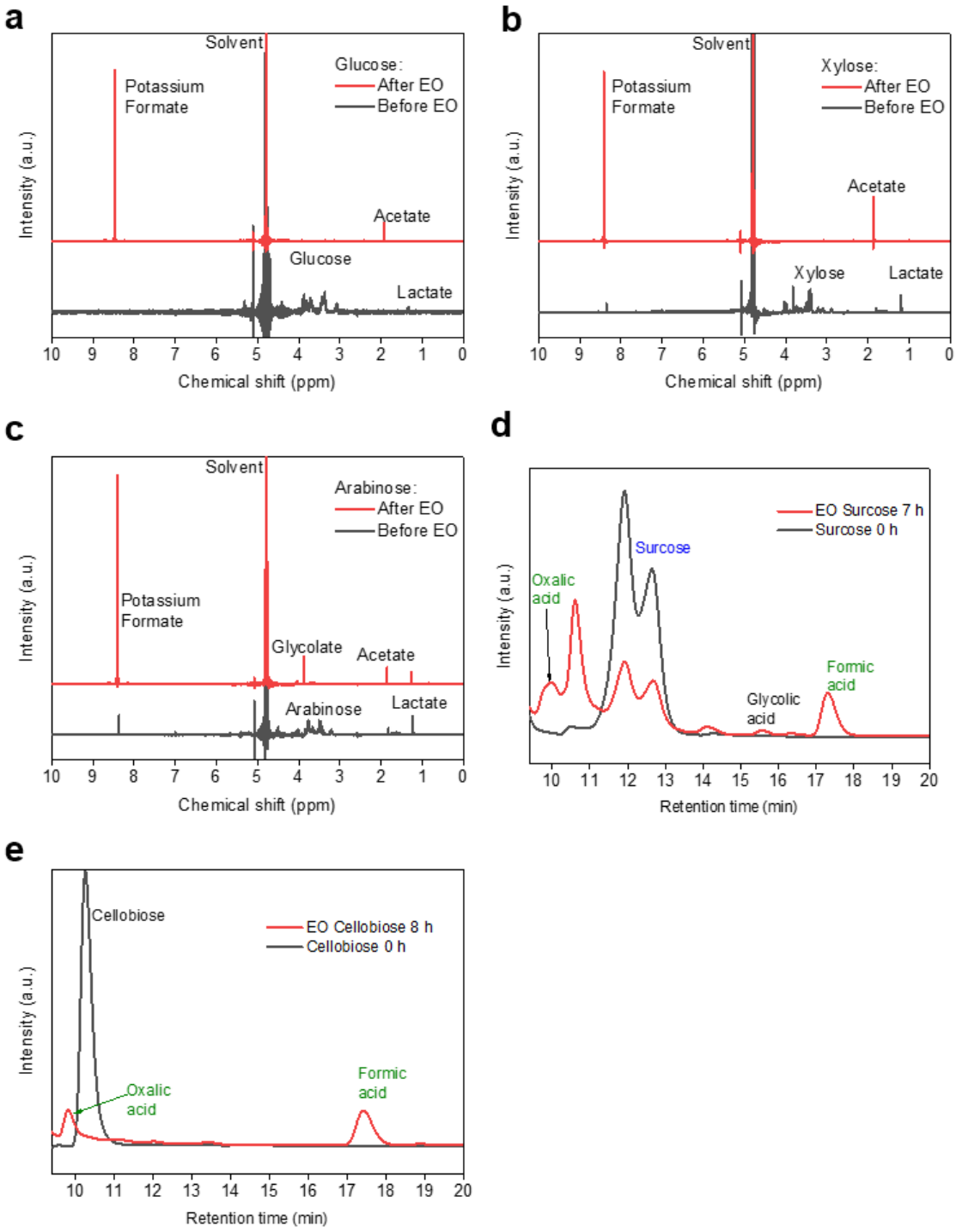

Figure 44 *^{1}H NMR spectrums of Before and After EO of monosaccharaides – (a) glucose; (b) xylose; (c) arabinose (Black curve: Before EO, Red curve: After EO); and HPLC chromatographs of Before and After EO of disaccharides – (d) sucrose; (e) cellobiose.*

3.2.4 Solar-driven electroreforming of HSCB

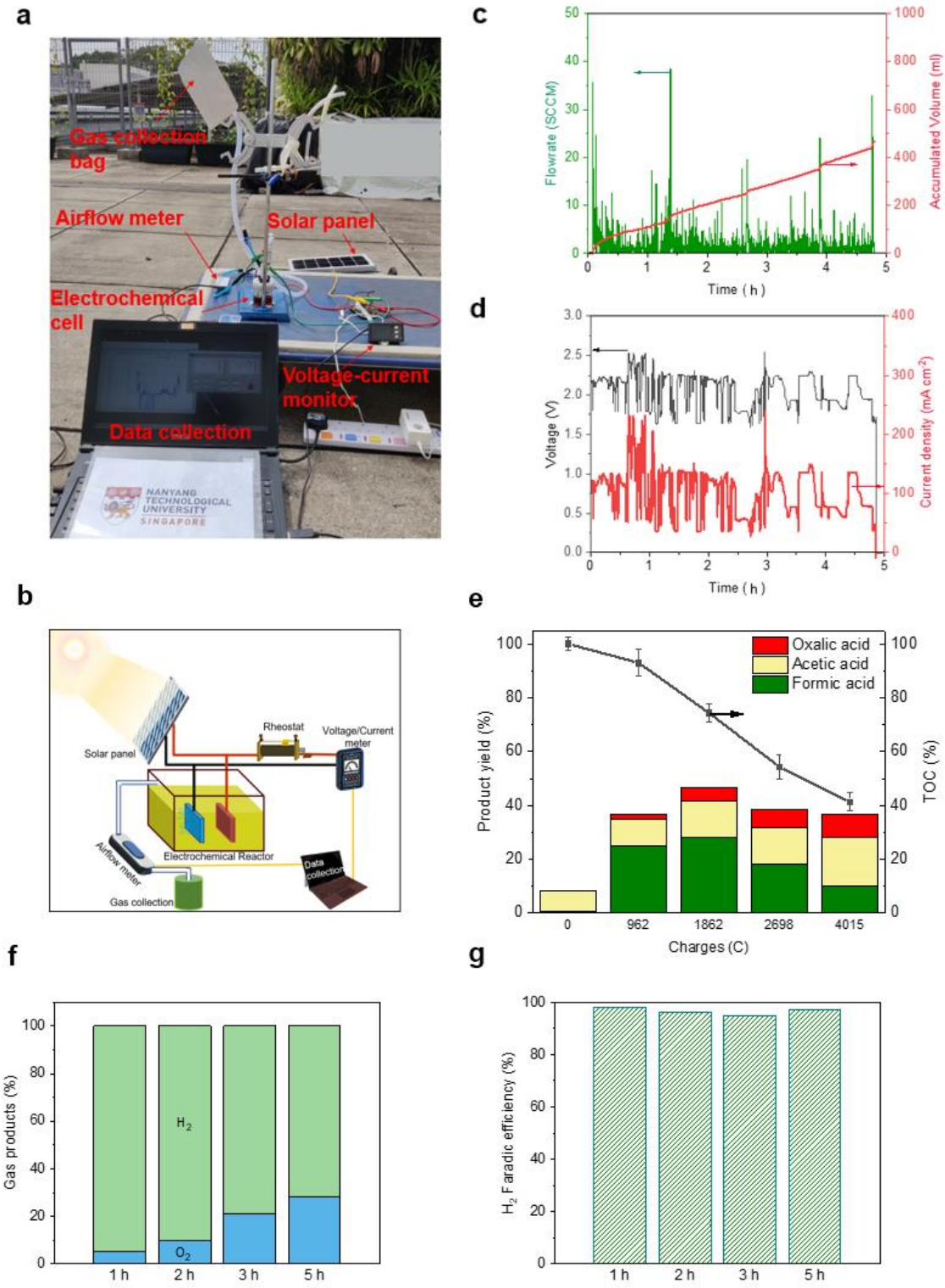

Figure 45 *Solar photovoltaic HSCB-reforming process – (a) Experimental setup; Real-time monitoring of (b) Schematic diagram; (c) Gas flow rate with accumulated volume; (d) Voltage with Current density; (e) Effect of applied charges on products yield% (oxalic acid, acetic acid,*

and formic acid) and TOC% from electrooxidation of HSCB; Effect of Solar electroreforming of HSCB on (f) gas products in ratio of H_2 to O_2 and (g) H_2 Faradaic efficiency.

As a proof-of-concept, the feasibility of electroreforming of HSCB directly powered by PV was demonstrated, as illustrated in Fig. 45a, b. The slide rheostat was used to adjust the resistance load to control the applied DC voltage of < 2.5 V on the system to suppress oxygen evolution. With the voltage/current meter and airflow meter, real-time data was collected with the laptop. The average current density was around 100 mA cm^{-2} with fluctuation caused by cloud movement which randomly interrupted the sun ray to the solar panel. (Fig. 45c) This also interferes with the gas flow which contributes to irregular pikes throughout the airflow plot as shown in Fig. 45d. Liquid product quantification revealed (28% yield) to formic acid at 1862 C with full conversion of glucose and xylose. (Fig. 45e) Oxalic acid and acetic acid were also detected as side products. Formic acid yield could have been higher if sample collection can be done between 1862 – 2698 C with more precise control. Fig. 45f provides the overall gas contents of the sampling collected at different durations. At 1 h, only 5% O_2 was detected which is attributed to the fluctuating potential causing OER together with electrooxidation of HSCB. The O_2 increased to 10% at 2 h, ascribed to the depletion of the monosaccharides to support the suppression of OER. With further electrooxidation of HSCB after 2 h, there is an increase in oxygen content which follows normal AWE process as HSCB was completely converted. Fig. 45g illustrates the H_2 Faradaic efficiency of the solar electrooxidation reactions at different intervals were well above 95%. Notably, the reactor is a single-compartment reactor without a membrane. With a membrane and better control of maximum potential fluctuation, high-purity green H_2 can be obtained.

3.2.5 Life cycle assessment

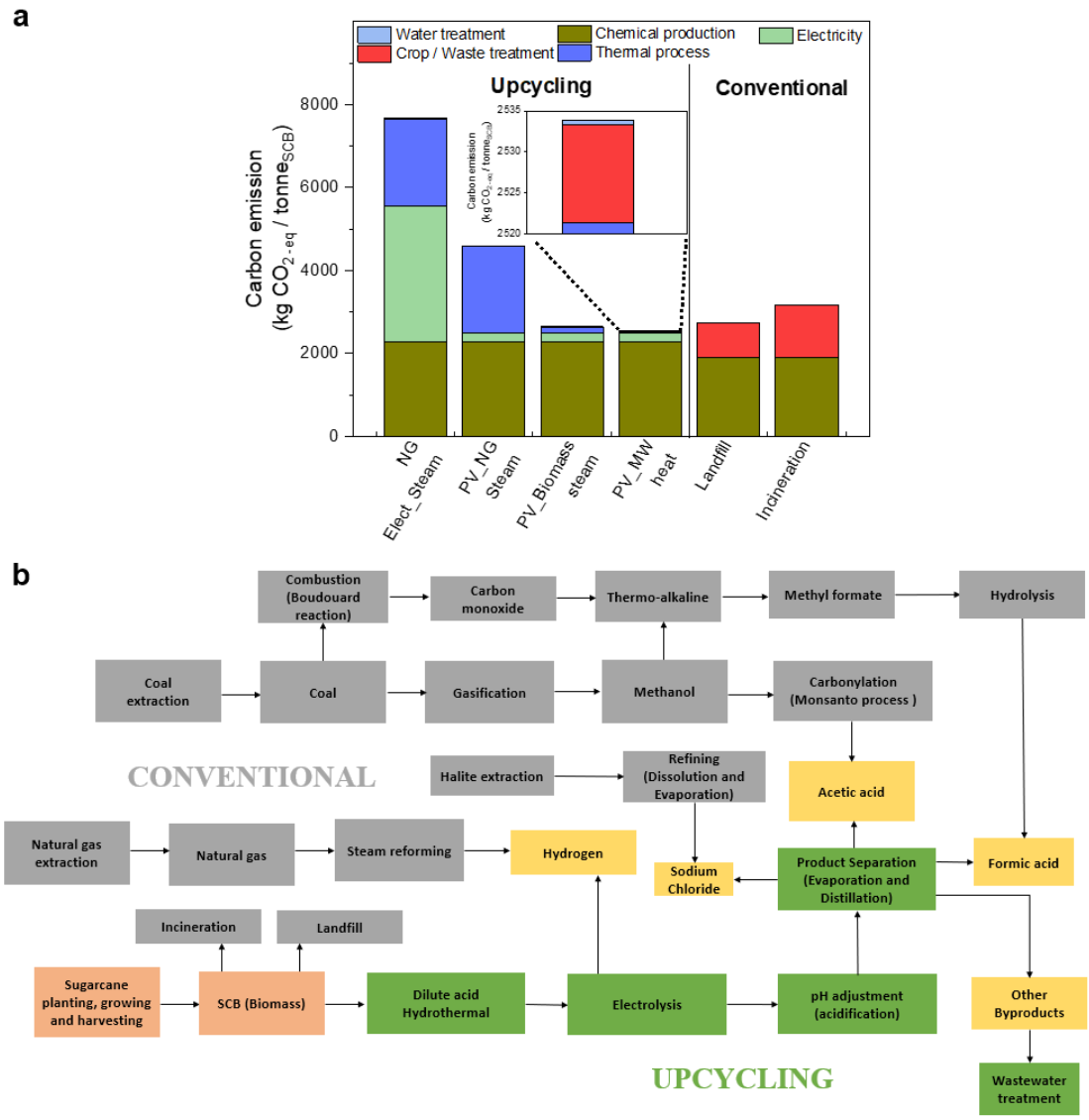

Figure 46 *Life cycle assessment of the SCB Process in terms of carbon emission, showing (a) Carbon emission per tonne of SCB processed by SCB upcycling and conventional SCB management processes. For electro-reforming processes, the sources of electricity and heat are denoted as: NG Elect_Steam: Electricity and steam from natural gas; PV_NG Steam: Electricity from photovoltaics and steam heat from natural gas combustion; PV_Biomass steam: Electricity from photovoltaics and steam from biomass combustion; PV_MW heat: Electricity from photovoltaics and heat from municipal waste incineration ; (b) Cradle-to-gate system boundary for the present work, showing the conventional(grey) and upcycling (green) modeled production routes to products – formic acid, acetic acid, sodium chloride, hydrogen, and other byproducts.*

The life cycle environmental impacts of the various SCB management processes were analyzed by life cycle assessment, with a focus on the life cycle global warming potential (GWP) of the processes in terms of equivalent CO_2 emission. The assessments of the impacts of GWP focus on six different scenarios, including four ways to supply heat and electricity to the SCB upcycling process and two conventional waste management processes. (Fig. 46a, b)

The system boundary, as shown in Fig. 46b, starts from the sugarcane plantation, which also accounts for upstream activities. After retrieval of the by-product of the sugarcane plantation, i.e., sugarcane bagasse from cane sugar production, the processing of sugarcane bagasse includes extraction, electrolysis, and product separation. The resulting products are further purified by multi-evaporators, neutralisation, and distillation.

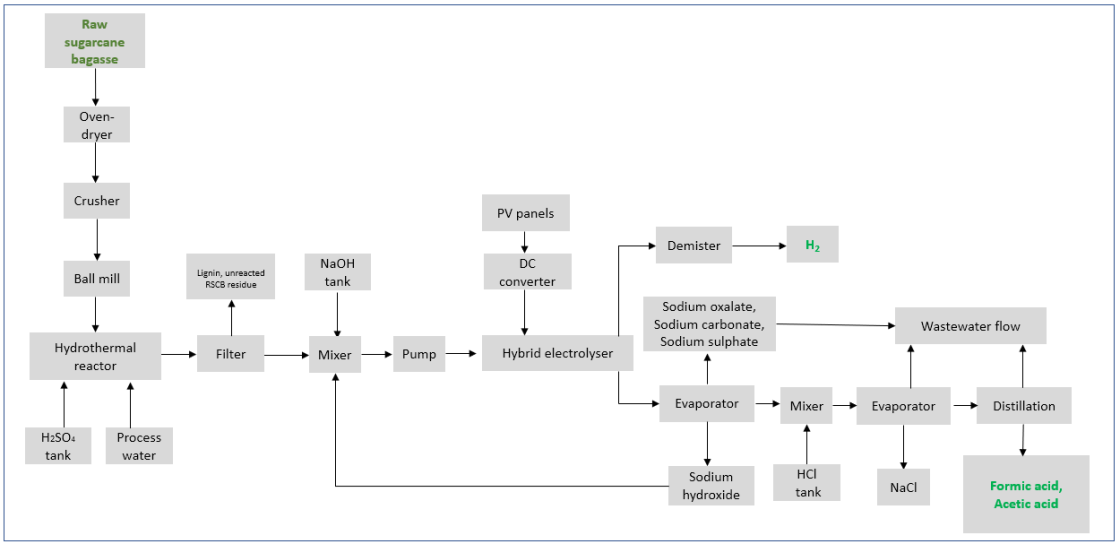

Figure 47 *Flowchart of upcycling process of raw sugarcane bagasse to end products (Main products in green).*

The parameters used to model the separation process in the multi-evaporators is based on the relative molar solubility of the resulting salts, e.g., chlorides, acetate and formate, as shown in the downstream processes in Fig. 47. Here, the temperature and water content of the process streams are moderated to effectively recycle the solvent and

separate formate and acetate salts. By-products such oxalate, sulphate and carbonate salts leave the system in a separate stream, which is sent for wastewater treatment. After this salt separation, hydrochloric acid is introduced to neutralise the remaining base and displace the weak organic acids (e.g. formic and acetic acid) from the salts. The displaced acids are evaporated for further purification e.g., by distillation. The distillation process uses sulfolane entrainer to achieve separation of the water-formic acid-acetic acid azeotropic mixture. [402] Three distillation columns were set up in series to extract water, then formic acid, and acetic acid sequentially.

When SCB is upcycled by electroreforming, the major GWP contributors are chemical production, electricity generation and thermal management (heating and cooling) processes. The GWP arising from electricity generation can be greatly reduced by 90% when the source is switched from natural gas (NG) to renewable solar energy (PV). The GWP associated with thermal management can be further decreased by 90% and 98% when the steam generated by burning natural gas is substituted with waste heat generated from biomass powerplant and municipal waste (MW) incineration plant, respectively. Water supply and waste treatment contributed insignificant amount of greenhouse gas emission, i.e., less than 13 kg $CO_{2\text{-eq/tonne}}$ SCB. In contrast, the conventional management of SCB, viz. landfill or incineration, do not co-produce chemicals such as organic acids. Therefore, the co-production of chemicals by the electroreforming upcycling of SCB could displace the GWP associated with producing these chemicals through conventional methods (i.e., using fossil fuel feedstocks and fossil fuel energies). Overall, it is obvious that the upcycling process, when coupled with renewable energy sources (PV_MW heat), has lower global warming potential than the conventional waste treatment practices.

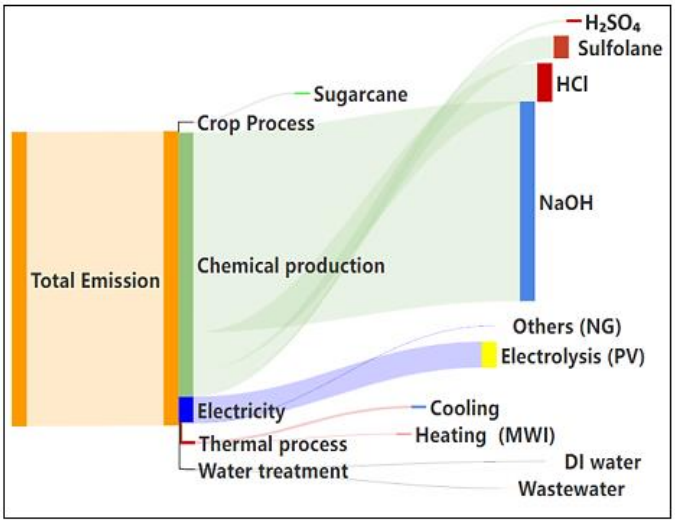

Figure 48 *Sankey diagram showing breakdown of the total carbon emission allocated to individual process component for the upcycling of SCB in the PV_MW heat scenario.*

Fig. 48 shows a breakdown of the life cycle GWP contribution by various process components in the SCB upcycling system when it is powered by photovoltaics and municipal waste heat. It can be seen that the major GWP contributor are the production of NaOH, which was used as the electrolyte of the electro-reforming process. In contrast, electrolysis driven by solar power provides large carbon saving compared to electrolysis using fossil fuel (e.g., natural gas) fired electricity. Other auxiliary processes, such as crop processing, thermal management, and water treatment contribute relatively little to the GWP of the electroreforming. Therefore, this upcycling process can be a means of better resource management to promote circularity and low-carbon production, contrasting the traditional waste management approaches featuring linear economy practices.

3.3 Summary

In this Chapter, an energy-efficient process was developed for the cogeneration of green hydrogen and green chemical from raw sugarcane bagasse waste via electroforming. Cellulose and hemicellulose in waste sugarcane bagasse were depolymerized to

mono/oligosaccharides after a facile hydrothermal pretreatment with dilute acid at low temperature. Earth-abundant and cost-effective nickel-based electrocatalysts were used to electrooxidize the hydrolysate to organic acid salts with 63% total yield of useful chemical products, dominated by formate. With abundant active sites on a hierarchical geometry, the resultant *hp*-Ni catalyst acts as a highly active and robust electrocatalyst for SCB electroreforming. Control experiments on monosaccharides (glucose and xylose), disaccharides (sucrose and cellobiose), and intermediate suggest that a slight high potential voltage could provide reactive oxygen species for high selectivity of formic acid, but too high potential could also lead to unwanted inorganic carbon formation due to overoxidation. Hence, precise control of voltage and charge transferred was essential for high yield of formic acid. LCA confirms that the upcycling process in this work emits 8–20% less greenhouse gases than traditional SCB waste management and chemical production processes using fossil fuels. The cogeneration of green hydrogen and green chemicals from raw biomass electroreforming directly driven by PV panel was also demonstrated, showing great promise for green fuel and chemical manufacturing from abundant biomass waste.

Chapter 4: Valorization of Paulownia wood to valuable green chemicals

Motivated by the earlier SCB electroreforming work, subsequent efforts were directed towards non-food biomass species, represented by Paulownia—a fast-growing wood species abundant in Asia. Fast-growing wood, with its exceptionally high carbon fixation ability, holds significant potential for decarbonization.

Further effort to reduce energy consumption and environmental impact was also focused on the pretreatment process in this Chapter. Promising biomass microwave hydrothermal treatment (MHT) had shown energy consumption reduction and better product yield compared to non-isothermal conventional oven heating. [130, 132, 403] When coupled with the electroreforming, it could promote sustainability because of its environmentally friendly, energy-efficient, and safe working conditions. [46, 47] In recent decades, the electrochemical oxidation of biomass-derived commodity chemicals has been reported to facilitate the generation of green hydrogen, but it often leads to the production of low-value carbonaceous gases like CO_2 and CO. [23, 25] Comparatively, recently, the author's group has demonstrated that it is possible to convert raw shrimp shell biomass into valuable acetate via electroforming, which co-generates green hydrogen, opening up possibilities for the electrolysis of raw biomass.[48] This coupled electroreforming of abundant biomass and green hydrogen generation enables the recovery of fuel and chemicals from biomass waste in an environmentally benign manner.

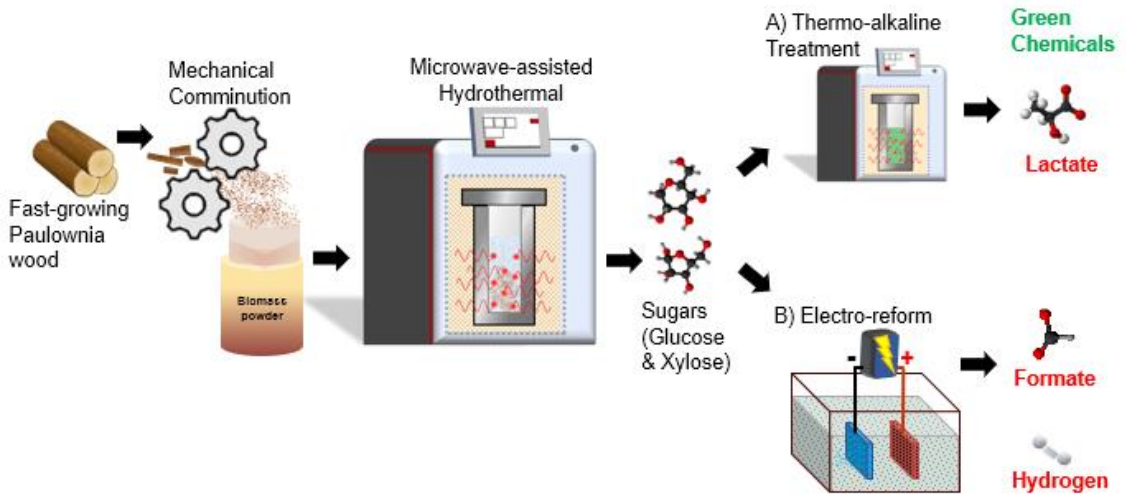

Figure 49 *Schematic diagram of valorization of Paulownia wood to green chemicals – Dilute acid microwave-assisted hydrothermal of Paulownia wood powder to simple sugars followed by: (A) Thermo-alkaline treatment in microwave to lactate; (B) Electro-reforming to formate at anode and hydrogen generated at cathode simultaneously.*

So far, there was no report on direct Paulownia wood saccharification (glucose and xylose). Notably, Paulownia is a low-density, fast-growing and one of the softest hardwood species, which may lead to less rigid structures. As a result, the pretreatment of Paulownia may need less energy, leading to an energy-saving biomass feedstock for green chemical manufacturing. In this work, an extreme low acid (0.2 wt% H_2SO_4) microwave-assisted hydrothermal technique was developed to process milled paulownia wood by depolymerizing cellulose and hemicellulose to monosaccharides. (Fig. 49) The highest sugar (glucose and xylose) yield was attained through detailed parameters (acid concentration, wood particle size, temperature, heating mode and duration) optimization. Then, this sugar mixture was further converted to value-added green chemicals by two conversion paths: A) Microwave-assisted thermo-alkaline treatment to lactate; and B) Electro-reforming to formate at the anode with coupled generation of green hydrogen at the cathode. Practical application to use renewable solar energy was also conducted to simultaneously convert pretreated paulownia wood derivates and store excessive, intermittent photovoltaic energy in the form of both formate and hydrogen gas. The high

value product, lactic acid, is used as platform molecules for producing wide range of useful chemicals. [63] On the other hand, formate is less corrosive than its acid form, can participate in the Formate-Bicarbonate Cycle for hydrogen vehicle and energy storage. [50] To promote circular economy by minimizing waste, further MHT could upcycle the cellulose-rich residue to glucose with 78% selectivity, and 90% recovery with additional consecutive cycles. This chapter demonstrates the potential valorization of Paulownia wood to offer a viable energy-saving approach for green chemicals and hydrogen fuel manufacturing. This work thus contributes to the promising hydrogen economy and as a renewable chemical synthesis replacement for fossil fuels.

4.1 Experimental section

4.1.1 Materials

Commercial natural paulownia wood strips were purchased from Fujian, China supplier from main source paulownia timber processing factory (Longlong.Ptv Ltd). Formic acid standard was purchased from LGC Standards Ltd. Chemicals from Sigma Aldrich included alpha cellulose, xylan, lignin (alkali lignin), sulphuric acid (95%), lactic acid, oxalic acid, glycolic acid, acetic acid, levulinic acid, maleic acid, glucose, xylose, fructose, sodium hydroxide, potassium hydroxide (⩾ 85%), ammonium chloride, furfural, 5-Hydroxymethylfufural, nickel (II) sulfate hexahydrate. Hydrochloric acid (37%) was purchased from VWR while acetone and ethanol were from Aik Moh. The chemicals were used without further purification. The resistivity of deionized water was 18.2 MΩ cm.

4.1.2 Pretreatment of Paulownia wood

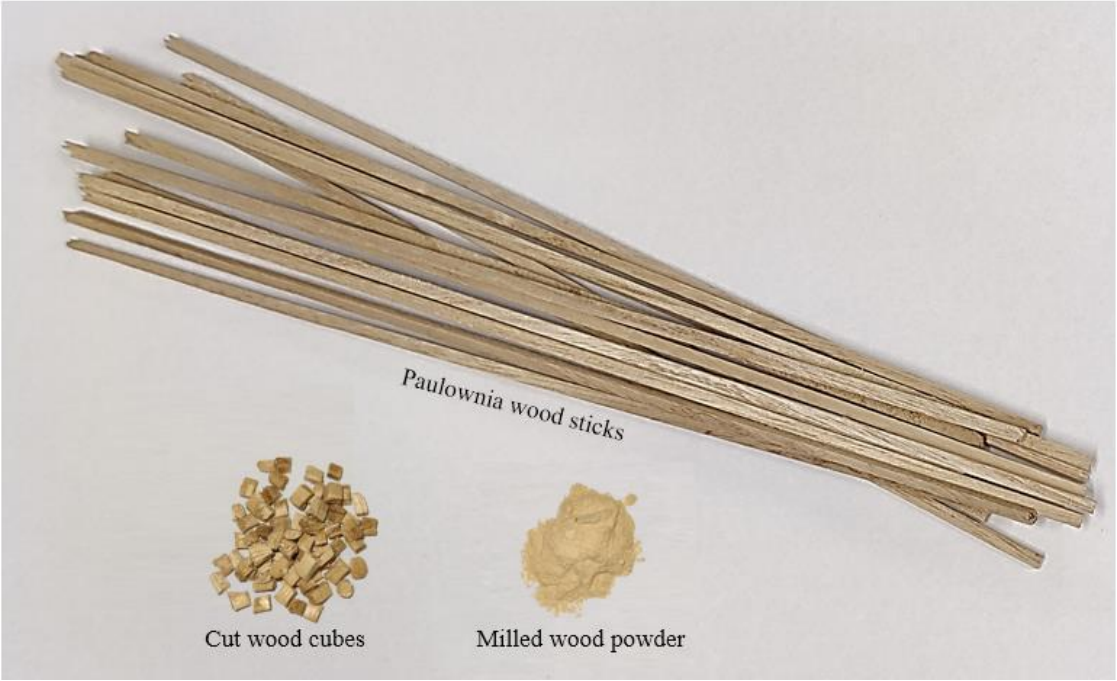

Figure 50 *Paulownia wood sticks in pristine condition and after cutting and milling into cubes and powder, respectively.*

Paulownia wood strips were cut into 3mm cubes and dried in oven at 60 °C overnight (Fig. 50). After drying, the wood cubes were ball milled and passed through specific sieve to obtain 100-, 300- and 400-microns size particles. The processed paulownia wood powder was stored under vacuum desiccator in room temperature for later use. For MHT, dilute sulphuric acid (0.2, 0.4 and 0.8) wt% hydrothermal treatment was performed on the paulownia wood powder without any purification or separation steps. The hydrothermal was conducted in a microwave digestion Oven (Multiwave 5000, Anton Paar GmbH) at different maximum temperature (T_{Max}: 160, 180 and 200 °C) with fixed ramp rate at 0.3 °C s^{-1} and hold time of 15, 30 and 60 min. Ramp mode heating to 200 °C with ramping duration of 10, 20 or 30 min without hold time were also performed. 15 mL of dilute sulphuric acid with 1:20 wood powder: liquid loading was loaded into the 50 mL vessel. After treatment, the vessel was cooled with internal fan to 55 °C before product extraction. The supernatant was extracted by centrifuge for further product

analysis. The hydrolysate of Paulownia wood (HPW) with the optimized highest sugar yield was used for the next step in development of green chemicals (formate and lactate). The remaining residue was dried and used for further MHT with same loading ratio and conditions unless specified. Additional parameters include 1 wt% sulphuric acid, ramp mode heating to 180 °C, 200 °C at duration of (60, 90 and 120 min). MHT was performed for 5 cycles on remaining residue immediately after the supernatant was separated and dilute sulfuric acid was replenished for each cycle. The typical microwave temperature, power to time profiles and energy consumption are displayed in Fig. 51a-c.

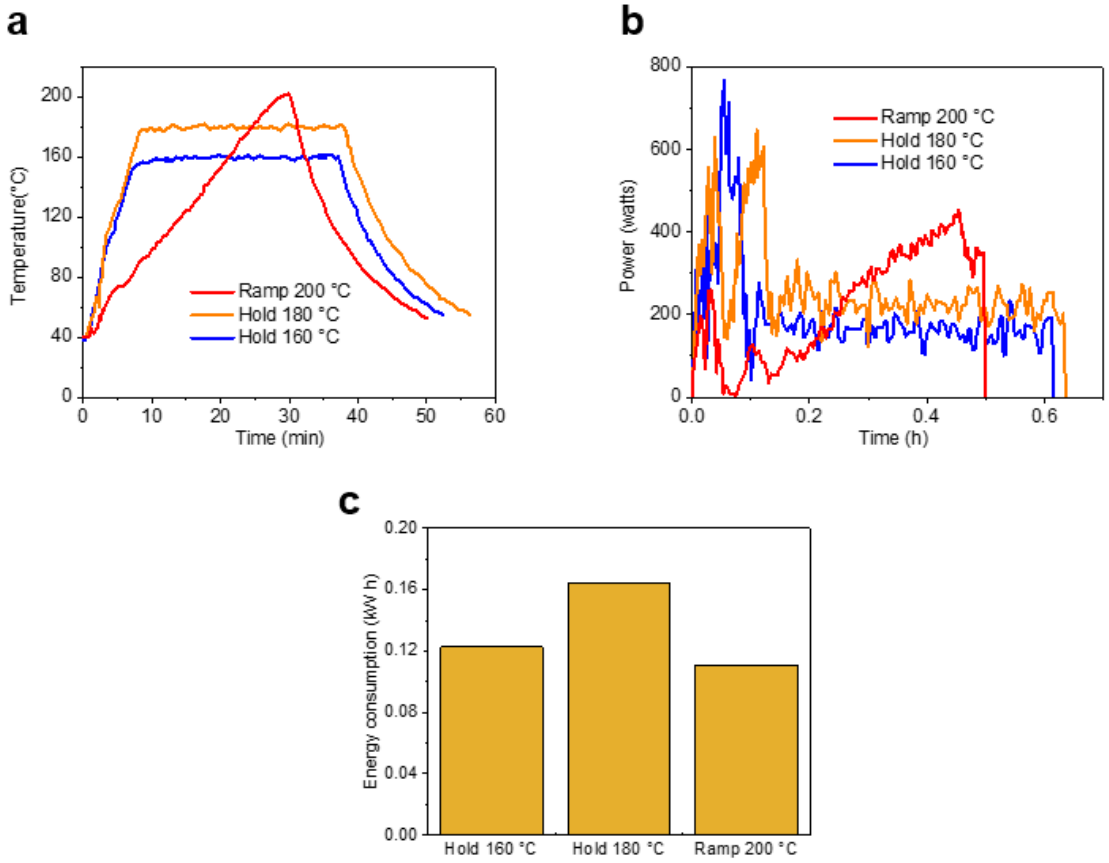

Figure 51 *Microwave heating of 3 settings Ramp 200 °C, Hold 180 °C and 160 °C – (a) Temperature profiles; (b) Power profiles; (c) Energy consumption.*

4.1.3 Thermo-alkaline treatment of HPW and sugars to lactate

HPW preadjusted to pH 14 with NaOH before loading 5 mL of the solution into the vessel. For lactate optimization, different temperatures (T_{Max}: 25, 50, 70 and 100 °C) with fixed ramp rate at 0.3 °C s^{-1} and hold time of 30, 60, 120, and 180 min were tested. The treatment was conducted in the same microwave digestion oven and cooled internally to 55 °C before extraction for product analysis. Preliminary tests of sugars (xylose or glucose) in 1.0 M NaOH were conducted at ambient temperature of 25 °C and in conventional oven at 70 °C.

4.1.4 Electroforming of HPW to formate

Electrochemical tests were performed in a standard three-electrode configuration with working, counter and reference electrodes as 3D hierarchical porous Ni on Ni foam (*hp*-Ni), Pt wire and Ag/AgCl/ Sat. KCl, respectively, in 1.0 M KOH electrolyte unless specified. The synthesis of *hp*-Ni electrode was mentioned earlier in section 3.1.2. Electrochemical tests were conducted at room temperature with magnetic stirring. HPW was adjusted to 13.8 pH with KOH prior to test. First, the newly fabricated *hp*-Ni was activated in 1.0 M KOH via constant current of 50 mA cm^{-2}. After stabilization, the cyclic voltammetry (CV) and positive linear sweep voltammetry (LSV) were scanned from (0 - 0.8 V vs Ag/AgCl) at 10 and 2 mV s^{-1}, respectively. 25 g L^{-1} HPW was used in the electrochemical tests. All electrode potentials have been aligned to potential of reversible hydrogen electrode (RHE) according to the equation: $E_{RHE} = E_{Ag/AgCl} + 0.197$ V + 0.0591 pH.

Electrochemical impedance spectroscopy (EIS) was conducted with and without 25 g L^{-1} HPW at (0.55 V vs Ag/AgCl) at frequency range of 0.01 - 1000 Hz at 100 mVrms.

Electroreforming HPW to formate was performed at specific constant voltage of 1.58 V vs RHE. At intervals, sample of 3 mL was collected for product analysis.

HER LSV was scanned from 0 to -1.5 V vs Ag/AgCl) at 2 mV s^{-1} with Ni_2P and graphite rod as the working and counter electrode, respectively, in 1.0 M KOH with or without 0.1 M glucose or HPW.

4.1.5 Solar-driven Electrooxidation of HPW

HPW was loaded to air-seal electrochemical cell and purged with argon gas for 20 mins and connected to an airflow meter and 1 L gas bag. The liquid products were extracted at intervals with needle syringes. A solar panel of 15 x 20 cm^2 provided electricity for the experiment and connected to a voltage-current monitor. Real-time data acquisition of airflow and voltage-current was collected on a laptop. The solar experiment was conducted at Nanyang Technological University, School of Mechanical and Aerospace Engineering (Latitude: 1.347159, Longitude: 103.681756) on a partial cloudy day at 10.00 am to 1.30 pm on 8 January 2023.

4.1.6 Paulownia wood and electrocatalyst characterization

For chemical composition quantification of paulownia wood, extractives was first removed by neutral detergent according to existing methods. [352-354, 404] Duplicates of ash and quantitative acid hydrolysis (NREL/TP-510-42618) were performed to determine the lignocellulosic component. [355] The average chemical composition of paulownia wood consisted of 37.5 ± 1.9% cellulose, 13.5 ± 0.6% hemi-cellulose and 27.8 ± 2.3% lignin, 18.1 ± 0.7% extractives, and 0.3 ± 0.26% ash. Extractives (20–25%) were also reported in other hardwoods with similar extraction technique. [405] Quantitative acid

hydrolysis was also employed to analyse the chemical composition of residues from optimized MHT runs.

Scanning electron microscopy and element mapping were conducted on a FESEM 700F, providing details such as surface, topographical, morphological, and compositional information of the electrocatalysts, and Paulownia wood before and after MHT reactions. The dried wood powders were sputter-coated with Au/Pd before SEM analysis. XRD patterns were captured on the Shimadzu XRD-6000 to study the structure change and crystallinity in synthesized *hp*-Ni electrocatalyst and reference against Ni: face-centered cubic (FCC) Crystallographic Structures (JCPDS card no. 04-0850). [357] XRD examinations were also performed on reference materials (alpha cellulose, xylan and alkali lignin) and Paulownia wood samples before and after MHT reactions.

XPS measurements were carried out using the Kratos Axis Supra Spectrophotometer. The XPS instrument used a monochromatic Al Kα source and a spot size of 300 × 700 μm². Before analysis, the samples were neutralized to avoid charging effects and sputter cleaned using 1 keV Ar^+ ions. To process the data, CASA XPS software was employed, which involved fitting the spectra with the Shirley background and Gaussian-Lorentzian functions, with reference to the C 1s peak at 284.8 eV.

4.1.7 Product analysis

Liquid product samples were neutralized to pH of 6–8 and passed through 0.45 μm syringe filters before analyzing in the Agilent 1260 HPLC. The column used was Agilent Hi-Plex H, 7.7 × 300 mm, 8 μm with refractive index detectors (RID) with injection volume of 20 μL with mobile phase of 0.01 M H_2SO_4. For 5-HMF and organic acids quantification, the flowrate was 0.6 mL min^{-1} with run time of 45 min at column

temperature of 50 °C. For carbohydrate quantification, flowrate was 0.4 mL min^{-1} with a run time of 30 min at column temperature of 65 °C.

Total organic carbon (TOC) and inorganic carbon (IC) in liquid phase was analyzed with TOC analyzer (Shimadzu TOC 5000A).

The corresponding yield% and sugar remaining % can be calculated based on the equation (1), (2), (3) and (4):

$$\text{Sugar yield (g/100g of dried wood)} = \frac{\text{Mass of xylose product (g)+ Mass of glucose product(g)}}{\text{Mass of dried wood used (g)}} \times 100 \quad (1)$$

$$\text{Product yield \%} = \frac{\text{Moles of carbon in measured product}}{\text{Moles of carbon in initial reactant}} \times 100\% \quad (2)$$

where liquid reactant HPW (mixture of xylose and glucose); or unless specified.

$$\text{Sugar yield \%} = \frac{\text{sugar concentration (g/l)} \times \text{volume of liquid hydrolysate (l)}}{\text{sugar equivalents in raw biomass (g)}} \times 100\% \quad (3)$$

where sugar is glucose or xylose.

$$\text{Sugar remaining \%} = \frac{\text{Sugar concentration at specific reaction times}}{\text{Inital sugar concentration}} \times 100\% \quad (4)$$

where sugar is glucose or xylose.

For nuclear magnetic resonance (NMR) analysis, samples were freeze-dried prior adding D_2O and 0.7 mL were transferred into NMR tube for analysing in the. Maleic acid was added as internal standard for quantification. ^1H NMR spectrums were recorded with JEOL ECA400 NMR spectrometer operating at 400 MHz at room temperature.

Gas sample (1 mL) was injected into GC-TCD/TCD. The equipment used was Agilent 7890A, equipped with TCD detector and 10 Ft molecular sieve 13× column, operated at 400 °C for quantification. Argon was used as the carrier gas.

The Faradaic Efficiency (FE) is calculated using equation (5):

$$\text{Faradaic efficiency} = \frac{\text{n}}{Q/2F} \times 100\% \quad (5)$$

where (Q(C) and n(mol) defines the total amount of charge transferred and total amount of gas (H_2 or O_2) produced, respectively. z is the number of electrons for H_2 or O_2 (i.e., 2 for H_2 and 4 for O_2) and F (C mol^{-1}) represents the Faraday constant (96,485 C mol^{-1})) The Paulownia wood Oxidation Reaction (POR) FE is calculated after subtraction from O_2 Faradaic efficiency with the assumption of no other FE losses.

4.2 Results and discussion

4.2.1 Pretreatment of Paulownia wood to sugar

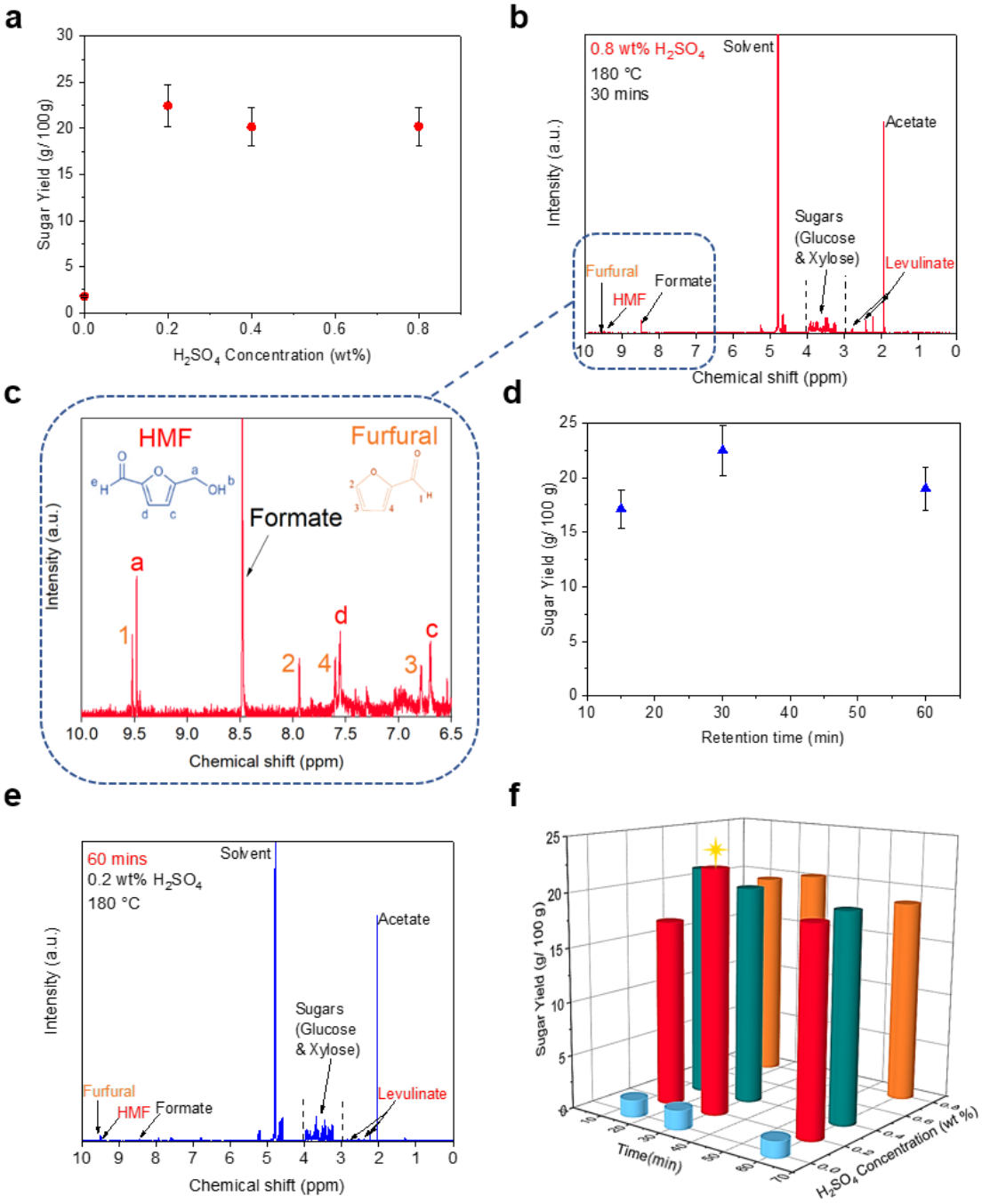

Figure 52 *Optimization of microwave hydrothermal parameters to obtain highest total sugar yields from Paulownia wood – (a) Effect of concentration of H_2SO_4 on sugar yield at 180 °C and 30 min. ^1H NMR spectra of microwave-assisted hydrothermal of Paulownia wood focused on – (b) 0.8 wt% H_2SO_4, (c) Zoom in of NMR spectrum of (c) from 6.5 to 10 ppm with insets of HMF and Furfural compound and their corresponding peak location. (Note: for NMR spectra (d & e), for simplification, HMF is represented only with peak "a" and Furfural is represented only with peak "1". In fact, all peaks a, d, and c of HMF and 1, 2,4 and 3 of Furfural can be represented.) (d) Effect of MHT duration on sugar yield with fixed – 0.2 wt% H_2SO_4 and at*

*180 °C; (e) ^{1}H NMR spectra of MHT at 60 min. (f) 3D plot overall effect of microwave time and concentration of H_2SO_4 on sugar yield. (*Yellow star indicates the optimized condition for highest sugar yield).*

Different acid concentrations were evaluated for the microwave-assisted hydrothermal treatment of the paulownia wood particles to obtain the highest sugar yield. This is essential to maximize the sugar yield while minimize acid consumption for a lower environmental and economic impact. The influence of the acid concentration on the sugar yield at fixed 180 °C and 30 min can be observed in Fig. 52a. It is obvious that the sugar yield drastically increased by an order of magnitude with increase of H_2SO_4 concentration (from 0 to 0.2) wt%. The role of acid is to act as a catalyst in the efficient hydrolysis of cellulose to glucose, i.e., cleavage of the β-1,4 glycosidic bonds. Additionally, acid also catalyzes the hydrolysis of xylan, the primary component of hemicellulose, to produce xylose. [387] Further increasing of acid concentration to (0.4 and 0.8) wt% caused the sugar yield to decline. Higher acid concentration may induce harsh dehydration reaction of the hydrolyzed monosaccharides to form furfural and HMF. [406, 407] Then, HMF rehydrates to produce formic acid (FA) and levulinic acid (LA). [377] Indeed, these side products (Furfural, HMF, formate and levulinic acid) can be identified in the NMR spectrum in Fig. 52b, c. Furthermore, the multiple peaks between 3–4 ppm corresponds to the sugars (glucose and xylose). [376] Acetate at around 2 ppm was also detected as hydrolyzed products of acetyl groups in hemicellulose and are considerably high in hardwoods. [408]

Fig. 52d depicts the retention time of the wood particles in the microwave hydrothermal pretreatment process versus the sugar yield. The maximum sugar yield was recorded at 30 min, extension of the acid exposure time to 60 min would induce the formation of degradation products (such as, Furfural, HMF, FA and LA) as shown in Fig. 52e. Longer duration with higher acid concentration may also increase the possibility of condensation

of these side products with acid-soluble lignin to form large molecular compounds such as pseudo-lignin that may hinder further processing. [408] Further fragmentation and coupling reactions of HMF can lead to the formation of insoluble humins, leading to loss of sugar yield. [409]

The overall effect of different durations at various H_2SO_4 concentration at fixed temperature of 180 °C is plotted in Fig. 52f. The high effectiveness of very low amount of acid additives can be seen by comparing 0% and 0.2 wt% H_2SO_4 concentration. Without catalyst, cellulose is recalcitrant to solubilization and it may take hours to have significant changes. [410] Although biomass normally has poor microwave absorption ability, adding polar materials can improve its microwave absorption properties [411], thus improving the hydrolysis effect. However, increasing H_2SO_4 concentration (0.4 and 0.8 wt%) did not demonstrate any improvement on sugar yield. Longer duration time (60 min) was too severe that further degradation of sugar occurs while short residence time of 15 min appeared to be inefficient for hydrolysis of the polysaccharides.

Next, the effect of temperature on sugar yield was investigated (Fig. 53a). Sugar yield reached 15 g per 100 g of dried wood (DW) at 160 °C, peaked at 180 °C, but decreased to 18 g per 100 g DW at 200 °C. This significant change indicates that the temperature has a substantial influence on the hydrothermal process, especially at 180 °C, where the hydrolysis reaction rate on the polysaccharides is notably higher. The drop in sugar yield at 200 °C can be mainly due to glucose/xylose decomposition to side products (Fig. 53b). Despite the lower sugar yield at 160 °C, it is worth noting that 100% xylose yield (from hemicellulose) was achieved.

The influence of the particle size on the sugar yield was further analyzed. Selecting the correct size may also conserve energy on the mechanical comminution of Paulownia wood.[412] Fig. 53c illustrates that 100-microns wood particles yield less sugar than the

case of 300-microns. Smaller particles possess higher specific surface areas, leading to more particles to collide and faster reaction.

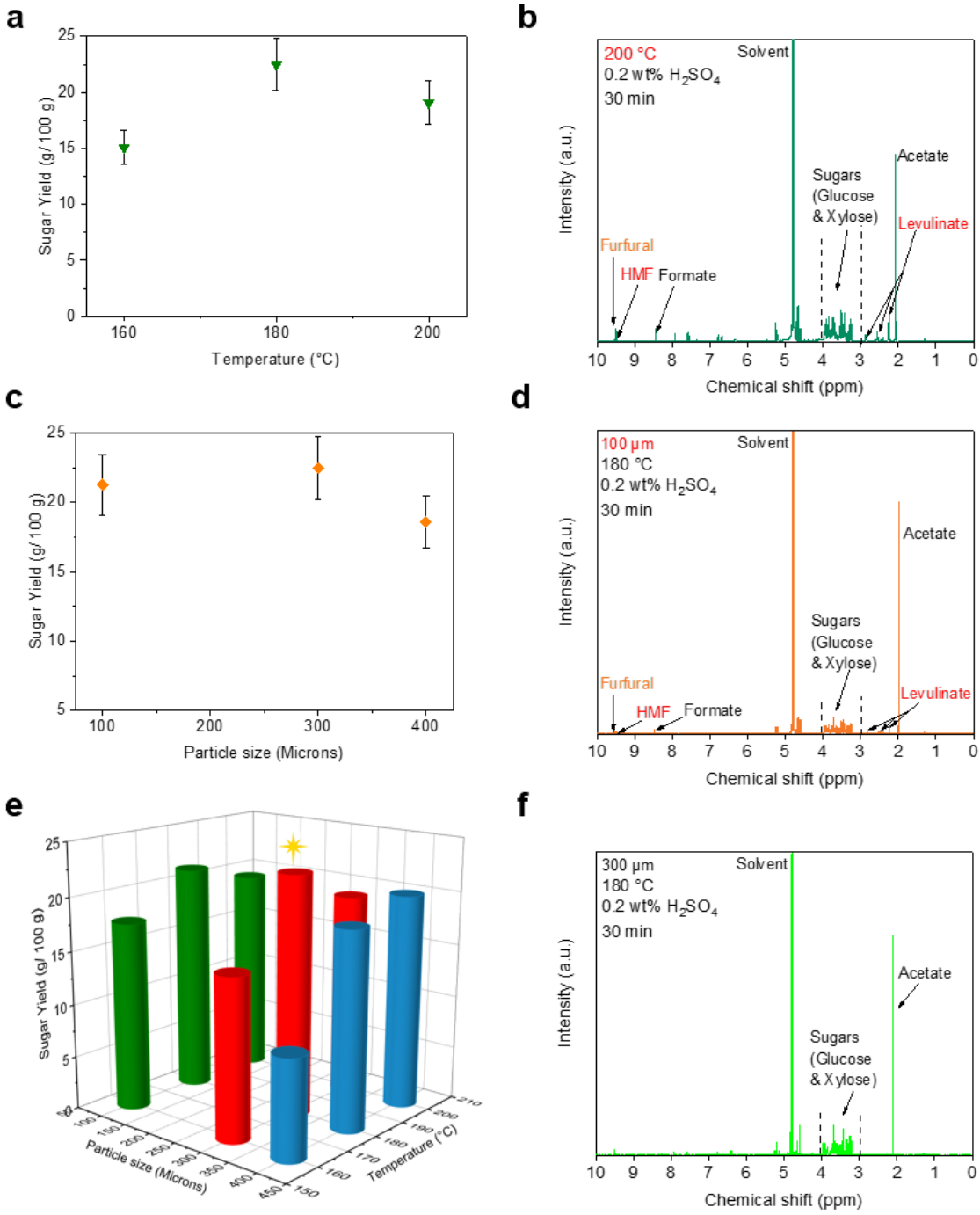

Figure 53 *Optimization of microwave hydrothermal parameters to obtain highest total sugar yields from Paulownia wood – (a) Effect of temperature on sugar yield with 300 micron particle size; (b) ^{1}H NMR spectrum of MHT at 200 °C (c) Effect of particles size on sugar yield at 180 °C; (d) ^{1}H NMR spectrum of MHT with Paulownia wood of 100 micron (e) 3D plot overall effect of particles size and temperature on sugar yield. (*Yellow star indicates the optimized condition for highest sugar yield); (f) optimized parameter.*

(Note: for NMR spectrums (c-e), for simplification, HMF is represented only with peak "a" and Furfural is represented only with peak "1". In fact, all peaks a, d, and c of HMF and 1, 2,4 and 3 of Furfural can be represented).

Hence, smaller particle size would increase the rate of polysaccharides hydrolysis as well as monosaccharides degradation to side products. Fig. 53d highlights similar side products for the 100-microns particles, implying that monosaccharides degradation was present. On the other hand, the larger particle, 400-microns faced lesser sugar yield and is likely because of its lower surface area. Inevitably, this negatively impacts the polysaccharides hydrolysis reaction.

The effect of Particle Size-Temperature towards sugar yield is presented in Fig. 53e. At 160 °C, sugar yield was higher with 100-micron wood particles but decreased as the particle size increased. This suggests that stronger hydrolysis decomposition of polysaccharides is in effect. At 200 °C, the sugar yield was less than 20 g/ 100 g DW for all particle sizes, implying that the competing degradation of monosaccharides dominated over the generation of monosaccharides.

The optimized parameters (180 °C, 30 min with 0.2 wt% H_2SO_4 and 300-micron particle size) achieved the highest sugar yield (23 g/ 100 g DW) with no loss of xylose and partial recovery of glucose (17%). Fig. 53f confirms negligible amount of monosaccharides degradation products (FA, HMF and furfural).

Notably, smaller particles require significantly more energy for mechanical milling. For instance, 100-micron wood particles require approximately 5 times the energy (based on longer milling duration required) needed for 300-micron wood particles. Thus, large particle is preferred if similar product yields are obtained. The overall characteristics and morphology of Paulownia wood before ball milling (PW), after ball milling to 300 µm size (PW300), and 100 µm (PW100) are shown in Fig. 54a, b, and c, respectively. The images reveal a fibrous texture, capturing the natural characteristics of Paulownia

wood despite the size differences. The higher magnification images in Fig. 54d-f further reveal the smooth surfaces of these samples, similar to an earlier study. [413]

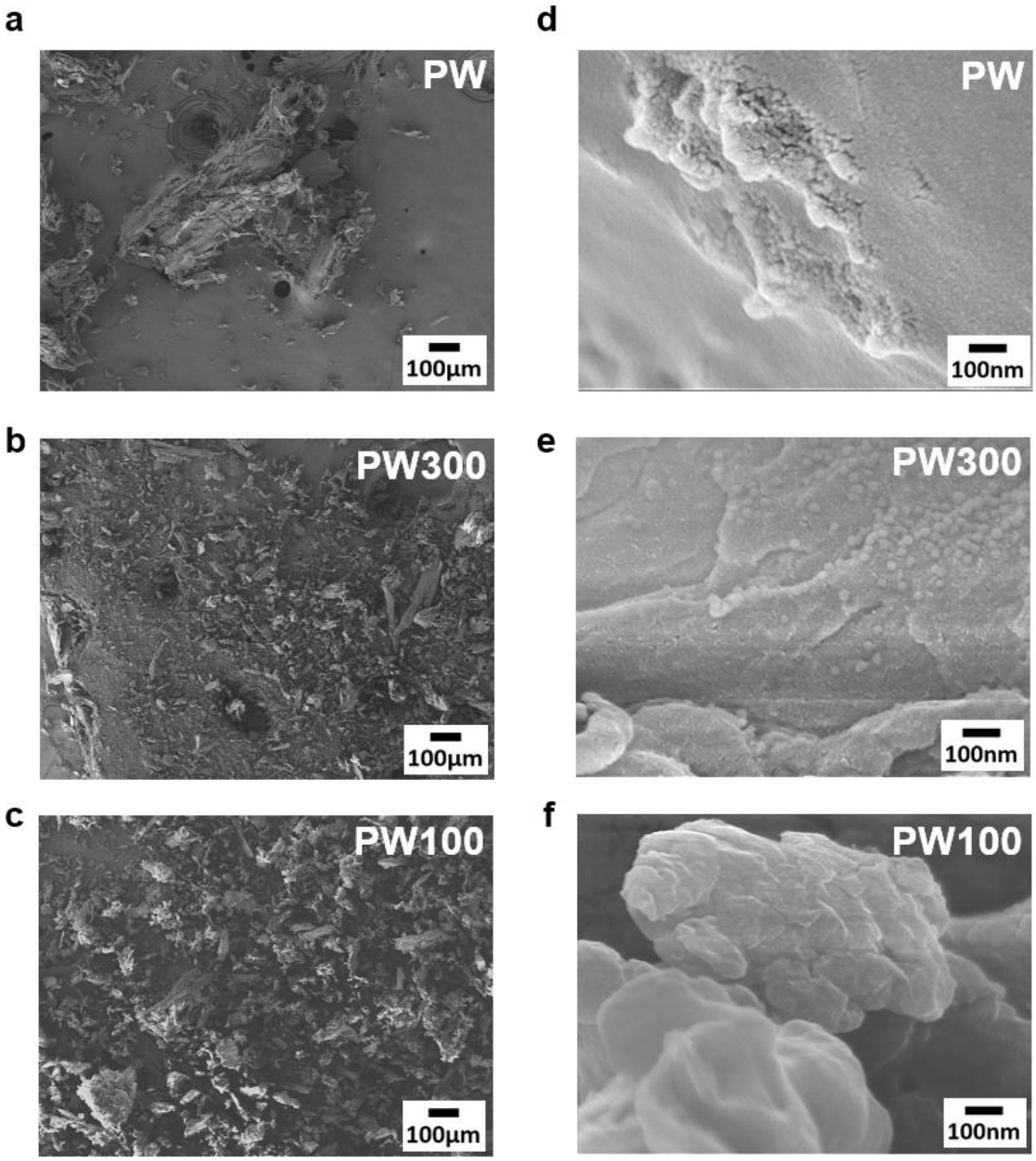

Figure 54 *FE-SEM images of Paulownia wood (PW) before MHT at different magnifications: (a) 80 ×, (d) 100,000 ×; and Paulownia wood of 300 microns (PW300) at different magnifications: (b) 80 ×, (e) 100,000 ×; and Paulownia wood of less than 100 microns (PW100) and Paulownia wood of less than 100 microns (PW100) at different magnifications: (c) 80 ×, (f) 100,000 ×.*

Furthermore, after the extraction of xylose (post X), the overall structure exhibited a porous nature (Fig. 55a), with the presence of sub-micrometer-sized pores on the surface

(Fig. 55b, c). In Fig. 55d-f, the SEM images reveal the remaining of intact cellulose fibers surrounded by lignin fragments, demonstrating the high selectivity of xylose.

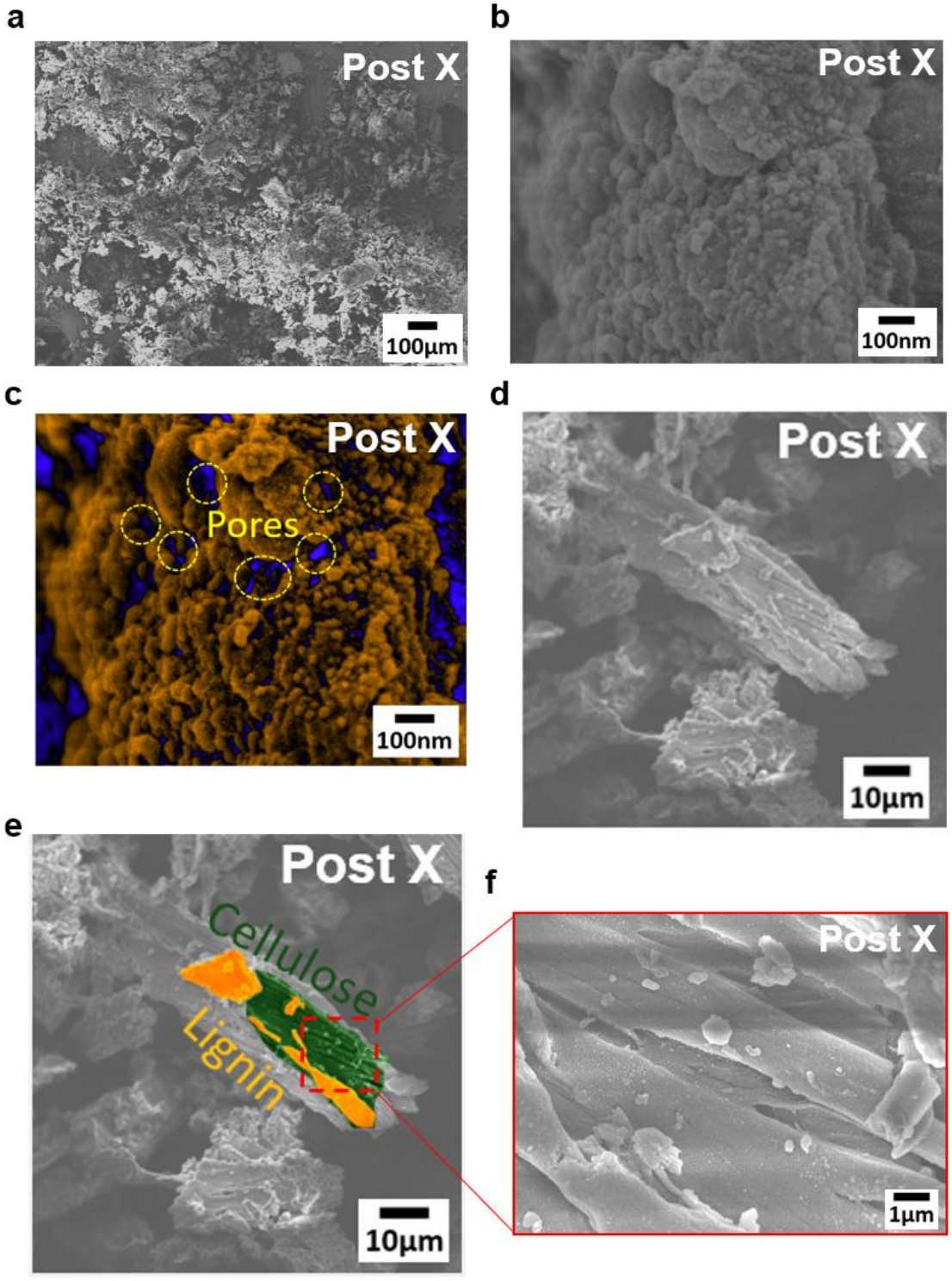

Figure 55 *FE-SEM images of Post xylose extraction (Post X) at different magnifications – (a) 80 ×, (b) 100,000 ×, (c) color-enhanced image of (b) with pores circled in yellow; (d) 1000 ×; (e) color-enhanced image of (d) with lignin highlighted in orange and cellulose in green, and (f) close-up image of (e).*

In Fig. 56, specifically, prior to MHT, the characteristic XRD peaks of cellulose (approximately at 15 °, 23 ° and 35 °) [414] exhibited lower intensity than those after MHT (post xylose extraction). This observation indicates the presence of amorphous cellulose in the wood [415], contributing to a lower crystallinity value of cellulose. As expected, after xylose extraction, amorphous cellulose was also effectively removed by the acid hydrolysis, resulting in narrower cellulose XRD peaks.

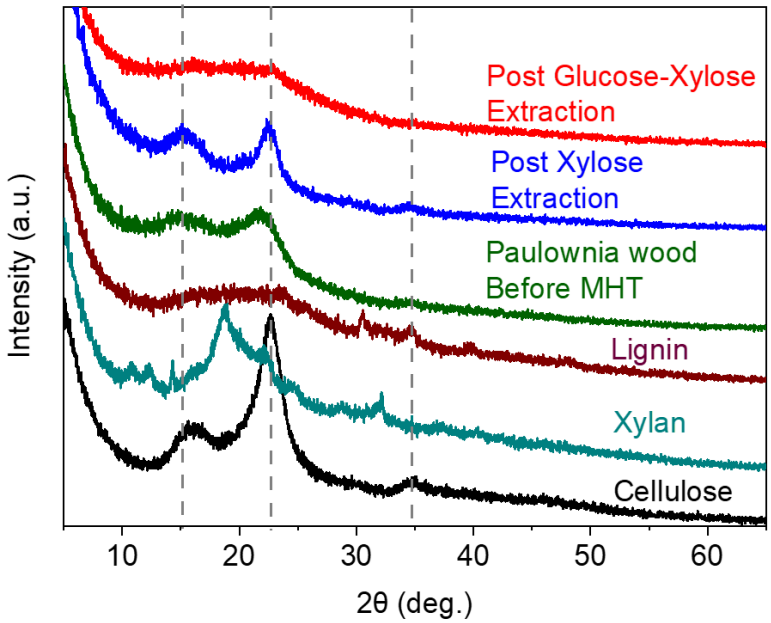

Figure 56 *XRD patterns of reference samples cellulose, hemicellulose (xylan) and lignin in comparison to Paulownia wood samples before and after MHT (Post xylose and glucose-xylose extractions).*

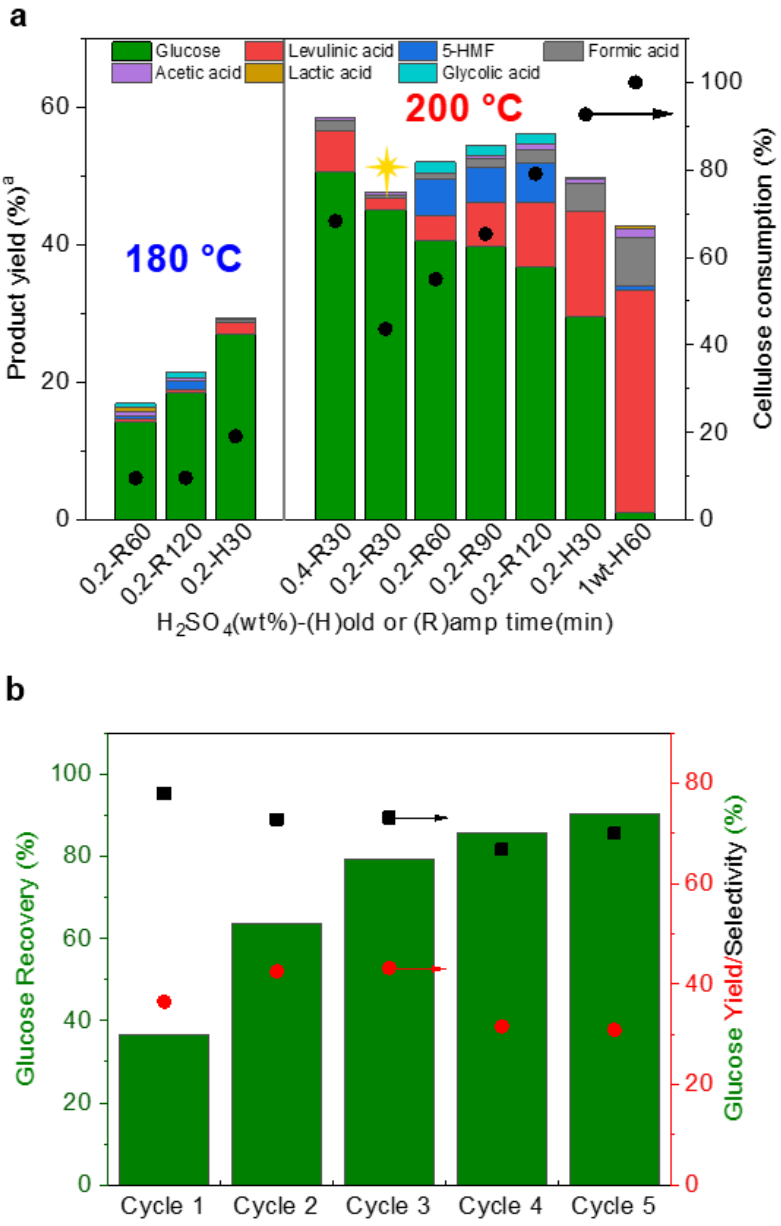

Figure 57 *Study of glucose conversion from cellulose residue after optimized MHT. (a) Effect of acid concentration, heating mode and temperature (a Product yield based on moles of carbon from cellulose residue from after MHT); (b) Consecutive MHT cycles of cellulose residue with glucose recovery and yield based on initial cellulose content in residue, and glucose selectivity was calculated based on measured liquid TOC. (*Yellow star indicates the selected condition for cellulose residue conversion).*

With hemicellulose fully separated, the recovery of the remaining glucose from the cellulose-rich (55%) residue would be meaningful towards the production of essential platform chemicals or biofuels. [416, 417] Indeed, with further studies (Fig. 57a), high glucose yield of 45% with least byproducts was achieved with the parameters (*0.2-R30*,

i.e., 0.2 wt% H_2SO_4 with reaction time of 30 min at 200 °C). With 4 more MHT cycles (Fig. 57b), up to 90% glucose recovery (average selectivity of 70%) was demonstrated with 15% fewer byproducts than a microcrystalline cellulose study. [418]

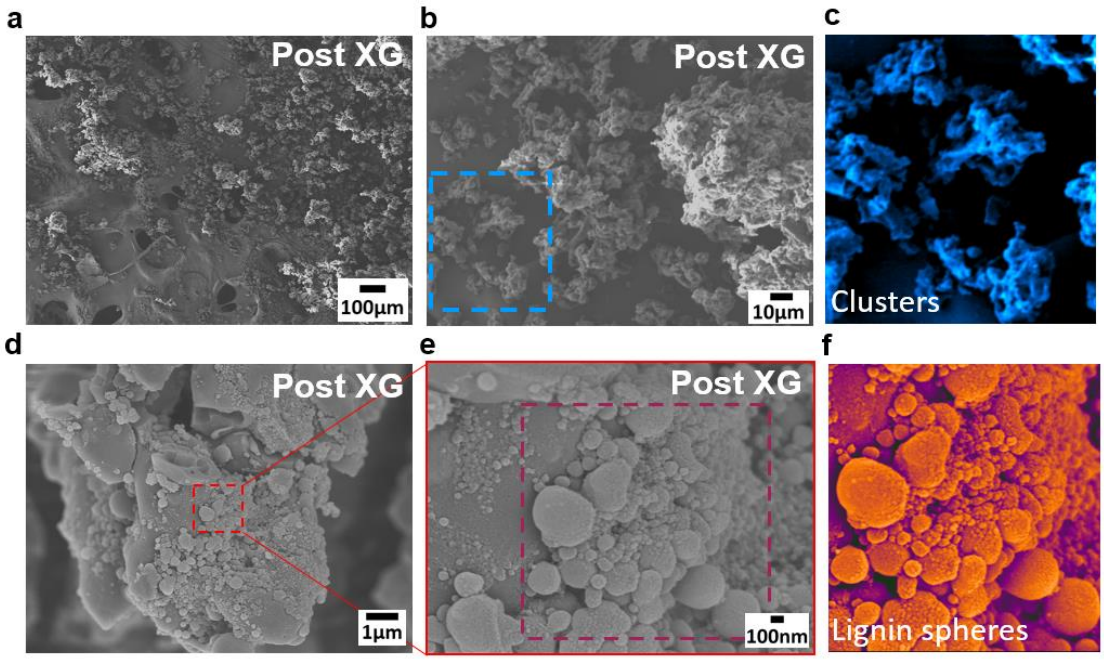

Figure 58 *FE-SEM images of post xylose-glucose extraction (Post XG) at - a) magnification of 80 ×, b) 650 ×. c) color-enhanced image of dotted blue area in image (b) with small, clustered size particles (blue). d) magnification of 10,000 × of surface of cluster and e) close-up image of (d); f) color-enhanced image of dotted purple area in image (e) with lignin nanospheres (orange) with diameters ranging from 5 to 50 nm on lignin agglomeration (purple).*

The SEM images of the residue after glucose extraction (post XG), revealed smaller, clustered-sized particles, as displayed in Fig. 58a-c. In addition to the fiber disappearance, the close-up images in Fig. 58d-f reveal nano-sized lignin spheres on lignin agglomeration, suggesting their potential suitability for dispersion applications [419]. This also demonstrates that the removal of carbohydrates by MHT was complete, similar to the enzymatic hydrolysis of hardwood reported elsewhere [413]. These SEM images are consistent with the XRD results (Fig. 56), where the post glucose xylose extraction (red curve) exhibits a profile similar to lignin (brown curve) without the characteristic cellulose peaks.

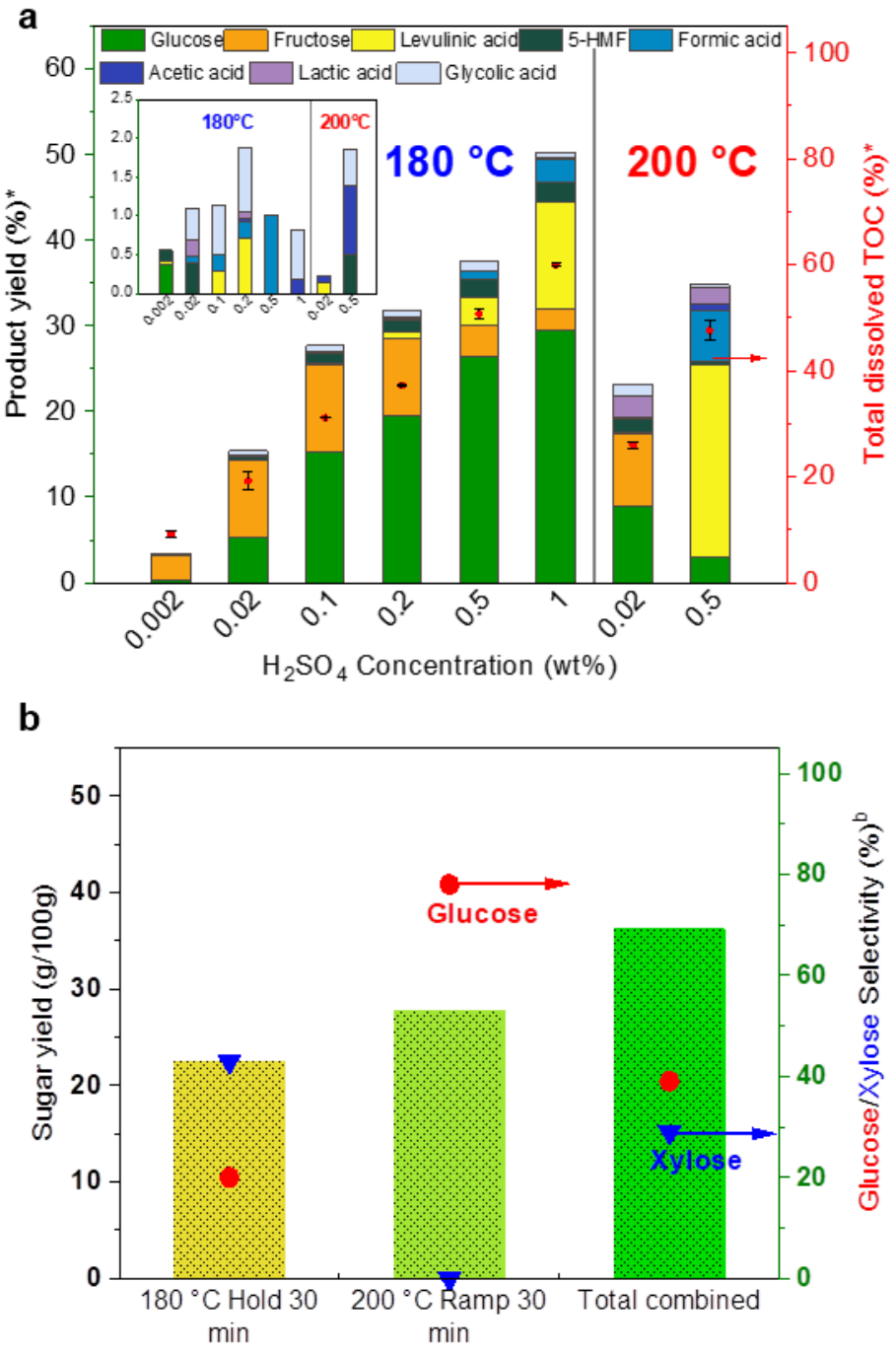

Figure 59 *(a) Cellulose control study - Influence of acid concentrations and microwave set temperatures (180 and 200 °C) on product yield and dissolved TOC, Inset: shows the zoom-in of products of less than 1% *calculated based on moles of carbon of initial cellulose); (b) Comparison of 180 °C hold 30 min (optimized MHT), 200 °C ramp 30 min (cellulose-residue conversion) and their total combined sugar yield for paulownia wood MHT with glucose and xylose selectivity. [a] Product selectivity based on measured liquid TOC).*

The selected glucose recovery MHT condition also aligns with the in-depth study of cellulose conversion to glucose in Fig. 59a, emphasizing two key conditions for high

glucose yield and selectivity: (1) H_2SO_4 concentration, less than 0.5 wt%, (2) residence time, shorter than 30 min at 200 °C. Notably, employing *1wt-H60* (i.e., 1 wt% H_2SO_4 and reaction duration of 60 min) resulted in direct cellulose conversion to LA with a 32% yield.

Fig. 59b summaries the sugar yields from microwave hydrothermal treatments of paulownia wood which show comparatively higher values. These results exceed the sugar yields achieved in similar H_2SO_4 hydrothermal treatments with other biomasses. For example, sugarcane bagasse exhibited yields of 18.0 g/100 g DW (raw) and 36.4 g/100 g DW (separated cellulose) [49] , while hybrid poplar wood yielded 17.7 g/100 g DW [420]. The high sugar yield from Paulownia wood could be due to its unique large pore size [115, 116], leading to weaker lignocellulosic structure and hence, a higher sugar processability.

As demonstrated in Fig. 51c, the energy consumption for the microwave settings were well below 0.17 kWh (227 kWh kg^{-1}) and are consistent with other studies. [421] The comparison of conventional oven and microwave-assisted hydrothermal is illustrated in Table 10. To obtain an equivalent sugar yield from Paulownia wood in conventional oven hydrothermal process, higher temperature, more acid, and longer time are required. This again highlights the advantages (efficiency, environmental friendliness, and up to ~38% energy-saving) of the microwave-assisted process. In fact, a much higher sugar yield was achieved by MHT at milder condition.

Table 10 Comparison of oven and microwave-assisted hydrothermal method on Paulownia wood to yield equivalent sugar yield (glucose and xylose).

Heating method	Acid use (volume)	Temperature (°C)	Duration (mins)	Glucose yield (%)	Xylose yield (%)	Energy consumption (kWh)
Oven	0.34 wt% 30ml	210	40	16%	93%	0.265*
Microwave	0.20 wt% 15ml	180	30	22%	100%	0.165

*Energy consumption estimated from holding power of oven with 13mins ramp time and 40mins hold time.

4.2.2 Thermo-alkaline treatment to lactate

To gain better insight, preliminary studies of lactate synthesis from glucose and xylose were first assessed in 1 M NaOH at 25 °C and 70 °C. After 4 hours of incubation in the oven at 70 °C, glucose was fully converted to lactic acid with traces of formic acid, glycolic acid and acetic acid as shown in Fig. 60a. In contrast, there were no formation of carboxylic acids at 25 °C except for some isomerization of glucose to fructose. This implies that essential heating accelerates the conversion rate and was consistent with another study. [422] The classic theory of alkaline degradation of glucose follows by isomerization of glucose into enediol, which then forms fructose. Fructose is then transformed into dihydroxyacetone and glyceraldehyde by retro aldol reaction. [397] After dehydrating, pyruvaldehyde is formed, which is re-hydrated to form lactic acid. [398] A further side reaction on the trioses could produce glycolic acid and formic acid. [399] Like glucose, xylose is another aldose sugar type, and it can also undergo the same isomerization reaction to form xylulose. [423]

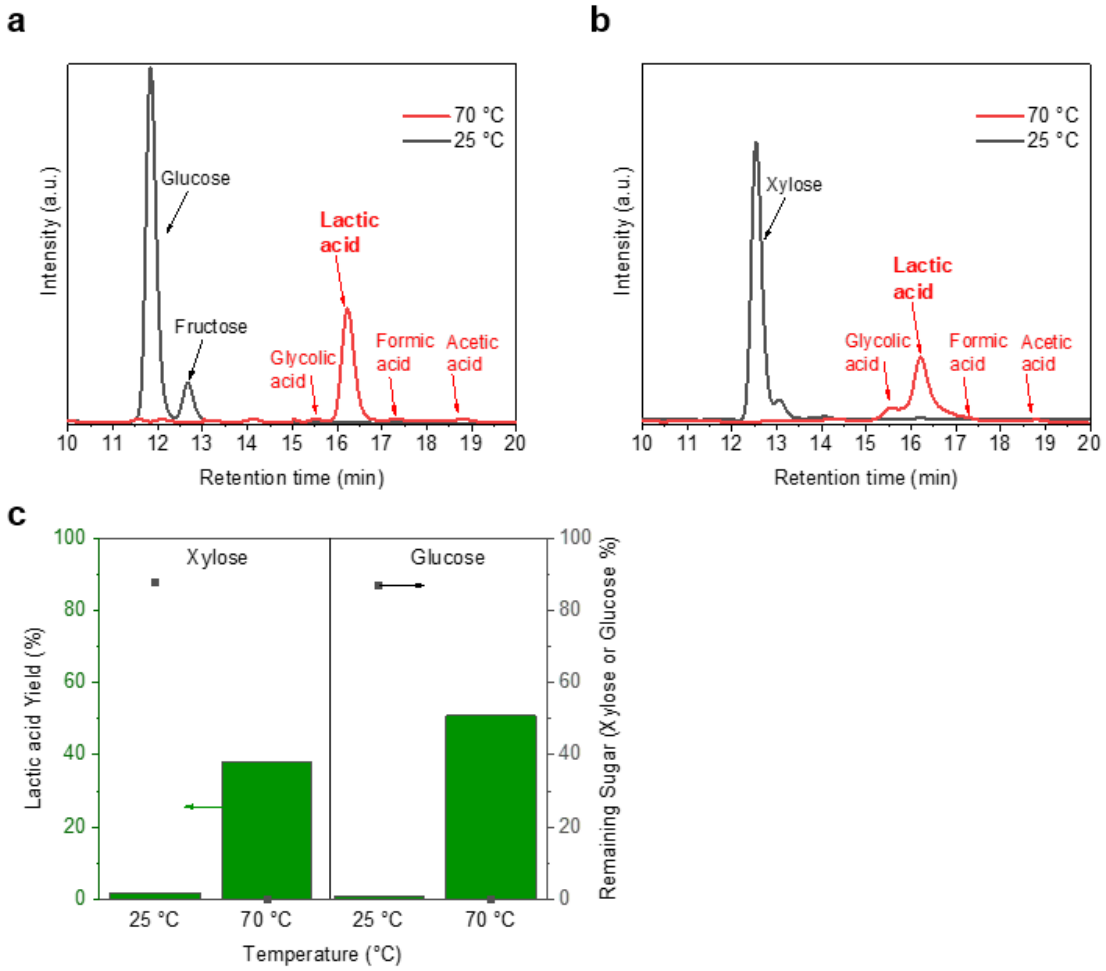

Figure 60 *Monosaccharides conversion to lactic acid in 1 M NaOH at 25 °C and 70 °C (a) HPLC chromatograms of glucose to lactic acid by conventional oven incubation; (b) HPLC chromatograms of xylose to lactic acid by conventional oven incubation; (c) Overall sugar conversion at 4 hours, 0.1 M glucose and 0.1 M xylose with lactic acid yield %.*

The HPLC results of xylose conversion (Fig. 60b) showed similar products like glucose conversion to lactic acid. This suggests that the chemical pathway could be same as glucose. [424] Fig. 60c shows the conversion of xylose and glucose with lactic acid yield, comparing the effect of heating at 70 °C and at ambient. As expected, the heating effect was significant for both monosaccharides. In the case of xylose, the lactic acid yield achieved was 38%, which is below the maximum theoretical yield of 60%. Although the xylose peak in the HPLC chromatogram has disappeared, the less lactic acid yield could be due to incomplete transformation to lactic acid from intermediates or further degradation of lactic acid to C1 and C2 aldehydes or carboxylic acids. The former

probably was the case because of only traces amount of formic acid (C1) and acetic acid (C2) was detected. [425]

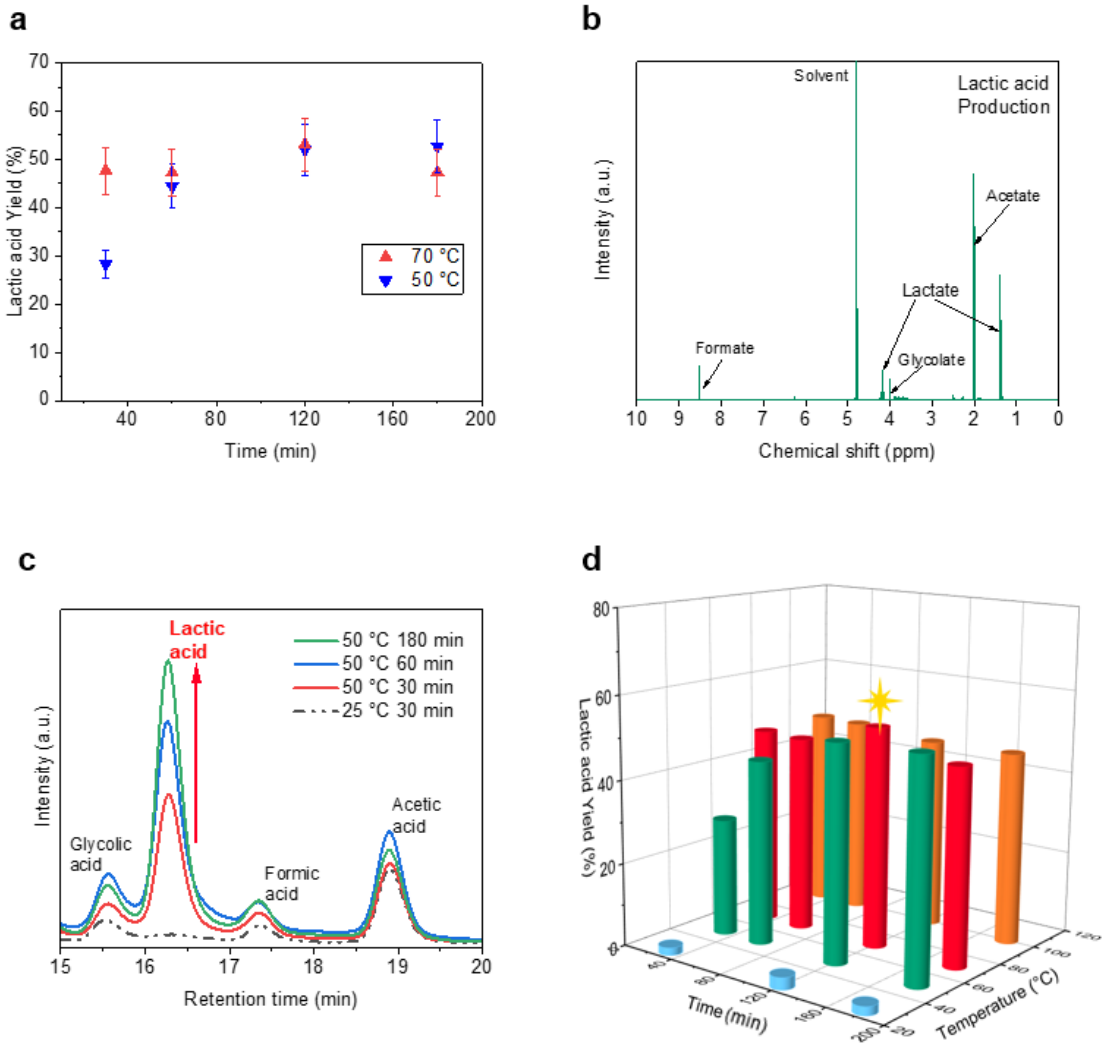

Figure 61 *Lactic acid production from HPW – (a) Effect of lactic acid yield% at 50 and 70 °C at different microwave duration; (b) ^{1}H NMR spectrum of pretreated Paulownia wood to lactic acid at 70 °C, 120 min (c) HPLC chromatograms of product at various durations when microwaved at 50 °C with control sample at 25 °C; (d) 3D plot overall effect of microwave duration and temperature on lactic acid yield. (*Yellow star indicates the optimized condition for highest lactic acid yield).*

Following the successful transformation of single monosaccharides into lactic acid, we continued to optimize the study on the HPW with the combined sugars as the starting precursor. Microwave-assisted HPW with sodium hydroxide at different temperatures were performed with emphasis on lower temperature (50 and 70 °C) as shown in Fig.

61a. Initially at 30 min, lactic yield (47%) for 70 °C was expected to be higher than 50 °C (28%) due to faster reaction rate. At 60 min, drastic increase of lactic acid production rate was observed for 50 °C while 70 °C experimented slow increment until at 120 min. The maximum yields of lactic acid (53%) were observed for 50 °C and 70 °C at 180 and 120 min, respectively. The ^{1}H NMR spectrum (Fig. 61b) revealed the various products (Lactate, acetate, formate and glycolate) after 120 min for the reaction of HPW to lactic acid at 70 °C and is consistent with the HPLC chromatograms. (Fig. 61c)

The typical HPLC chromatograms of the lactic acid production at 25 °C and 50 °C. The major peak of lactic acid increase with time at 50 °C with small increment of formic acid and glycolic acid as well as acetic acid. As seen in the 25 °C at 30 min, some little amounts of acetic, formic, and glycolic acids were already present in HPW at the beginning, but no lactic acid had formed yet.

The overall Temperature-Duration effect of lactic acid production was evaluated and plotted in Fig. 61d. Apparently, very low lactic acid yield was observed at 25 °C, and this trend is aligned to the earlier study on single monosaccharide conversion. The lactic acid yield followed a decreasing behavior (48%, 47.7%, 46.3% and 46.1% at 30, 60, 120 and 180 min, respectively) when the reaction was at 100 °C. The higher temperature could have caused severe reaction to further degrade lactic acid.

4.2.3 Electroreforming to Formate

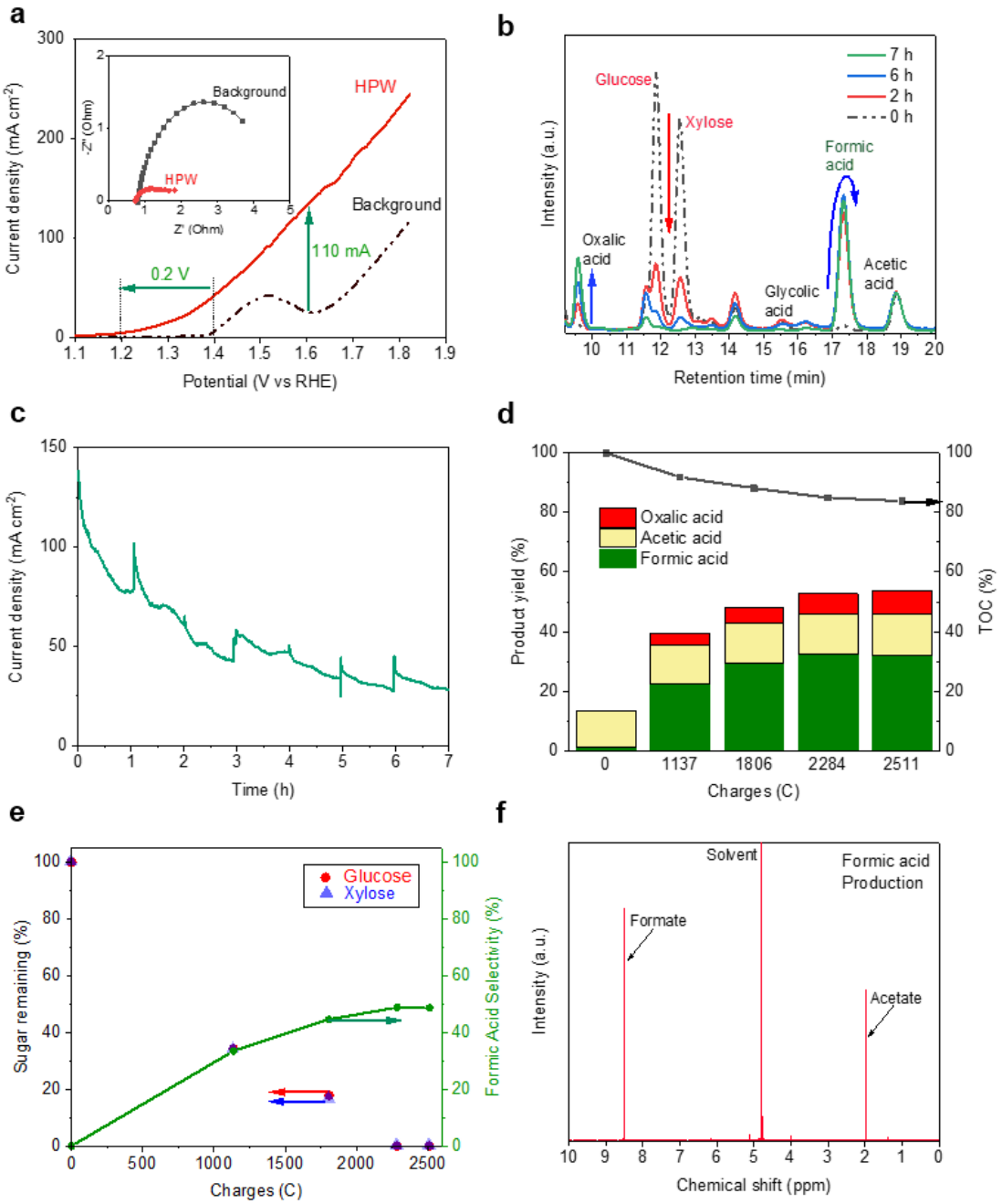

Figure 62 *Formic acid production from HPW – (a) Positive sweep LSV of hp-Ni working anode (black curve: background 1 M KOH, red curve: HPW), Inset: Nyquist plots in 1 M KOH at 1.58 V vs. RHE; (b) HPLC chromatograms of reactants and products; (c) Chronoamperometry at constant potential at 1.58 V vs RHE; (d) Effect of charges on product yield (oxalic acid, acetic acid and formic acid) and TOC % at 1.58 V vs RHE; (e) Effect of charges on formic acid selectively and consumption of sugar (red dot: glucose, blue triangle: xylose) at 1.58 V vs. RHE; (f)* ^{1}*H NMR spectrum of pretreated Paulownia wood to formic acid with applied charges of 2284 C.*

The electrochemical characteristics of *hp*-Ni anode were first investigated in both HPW and background (1.0 M KOH) to determine the potential for the electroreforming process. The background LSV in Fig. 62a shows a distinctive anodic peak from (1.4 to 1.6 V vs RHE) that attributed to Ni(II) oxidation to NiOOH. After 1.6 V vs RHE, oxygen evolution reaction (OER) occurred, causing the increase of current density. In contrast, the LSV of HPW showed higher current activity and an earlier onset potential at 1.2 V vs RHE. The earlier onset potential (0.2 V shift) implies that oxidation of HPW is more thermodynamically favorable (i.e., easier to be oxidized). It could be resulted from its small organic molecule structure which can align and adsorb readily on the electrode surface. This steep current density increase was also observed in other studies with glucose as well as alcohols. [31, 298, 381].

It reaffirms that the Paulownia wood pretreatment was effective for cellulose and hemicellulose depolymerization to monosaccharides. This is consistent with the HPLC chromatograms in Fig. 62b, showing HPW before electrooxidation (0 h) with the identified sugars (glucose and xylose). Specifically, at 1.60 V vs RHE, the current density was increased by 110 mA cm^{-2}. Notably, to achieve a current density of 100 mA cm^{-2}, the required potentials for EO HPW and OER are 1.54 V vs RHE and 1.79 V vs RHE, respectively. This implies an energy saving of 14% when HPW substitutes OER as the anodic reaction in green hydrogen production. The electrochemical impedance spectroscopy in the inset figure shows that HPW has a significantly smaller semicircle compared to background electrolyte. The small diameter of the semicircle represents a low charge-transfer resistance [394] which suggest that HPW has better charge transfer ability and enhanced kinetics.

To minimize the undesirable OER as well as to reduce the energy requirement of the coupled H_2 production from electrolysis, a lower electrooxidation potential (1.58 V vs

RHE) was selected. Fig. 62c demonstrated HPW electrooxidation over 7 h. Each interval of 1 h runs were plotted together and spikes were observed whenever a run was restarted. The current spike was from the sudden switch from open circuit potential to the high constant potential. After 40 s, the current stabilized when the concentration of reactant species decreased after being oxidized at the *hp*-Ni electrode. This identical behavior was also demonstrated in another study.[159] The exponential decay in current density from 145 mA cm^{-2} to 45 mA cm^{-2} was mainly because of the consumption of reactant species (mixture of glucose and xylose).[339] The correlation of decreasing concentration of monosaccharides with increasing of oxidized products was observed in the HPLC chromatograms (Fig. 62b) with electrooxidation time.

Fig. 62d shows the product yields from electrooxidation of HPW with accumulated charges at 1.58 V vs RHE. At the beginning, acetic acid and slight amount of formic acid was present in HPW. After initial electrooxidation (1137–1806 C), formic acid increased at a faster rate than oxalic acid. Throughout the whole electrooxidation, the stable acetic acid remains constant. At 2284 C, the highest concentration of formic acid (49% yield) was recorded and decreased with more applied charges. The decreasing trend of TOC% may implies that further EO of formic acid to inorganic carbon happened simultaneously.

The decrease in pH was observed with the increase in anodic products such as formic acid, oxalic acid and acetic acid with further biomass electroreforming, leading to the formation of organic acid salt (for. eg. potassium formate). This process results in the consumption of hydroxide ions, subsequently causing a slight decrease in electrolyte conductivity and a reduction in current density. Notably, hydroxide ions (OH^-) exhibit a molar ionic conductivity of 0.1986 S m^2 mol^{-1}, whereas potassium ions (K^+) have a lower value of 0.0735 S m^2 mol^{-1}. [426] For example, in a scenario with 0.5 M KOH and 1.0 M

KOH, the specific conductivity is measured at 0.115 S cm^{-1} and 0.215 S cm^{-1}, respectively. [427]

However, it's worth noting that the drop in pH may offer advantages in the continuous separation of products. Additionally, the remaining electrolyte can be recycled by implementing a flow reactor, where it is replenished with new biomass extract and alkaline components to adjust the pH value.

Notably, both monosaccharides (xylose and glucose) decreased rapidly to 35% and 18% with applied charges of 1137 C and 1806 C, respectively. (Fig. 62e). At 2284 C, both sugars were completely consumed. Moreover, the NMR spectrum in Fig. 62f, reaffirms that formate and acetate are the main products without any peaks in the 3–4 ppm region (sugar). Notably, oxalate was not detected in ^{1}H NMR because of its chemical structure. The maximum formate selectivity for HPW electroreforming was close to 49% as there were multiple pathways, which resulted in another byproduct, oxalic acid (~10% yield), while formic acid can also further electro-oxidized to carbon dioxide (over oxidization). Another reason is due to the alkaline catalyzed reaction of glucose/xylose to other compounds [397-399, 423] such as lactic acid and later electrooxidized to acetic acid. Complex mono- / oligosaccharides involves a more diverse electrooxidation pathway. To improve the selectivity, it is possible to control the potential, modify the electrode, reduce side reactions (isomerization of glucose to fructose/mannose and degradation to lactic acid in alkaline condition), increase the selectivity of the pretreatment for monosaccharides and control the pH, etc.

These results were close and identical to the electroreforming of sugarcane bagasse study in Chapter 3. Hence, the previous mechanism study and this study can be

combined to propose the pathway of xylose/glucose to lactic acid (path A), and to formic acid (Path B) in Fig. 59.

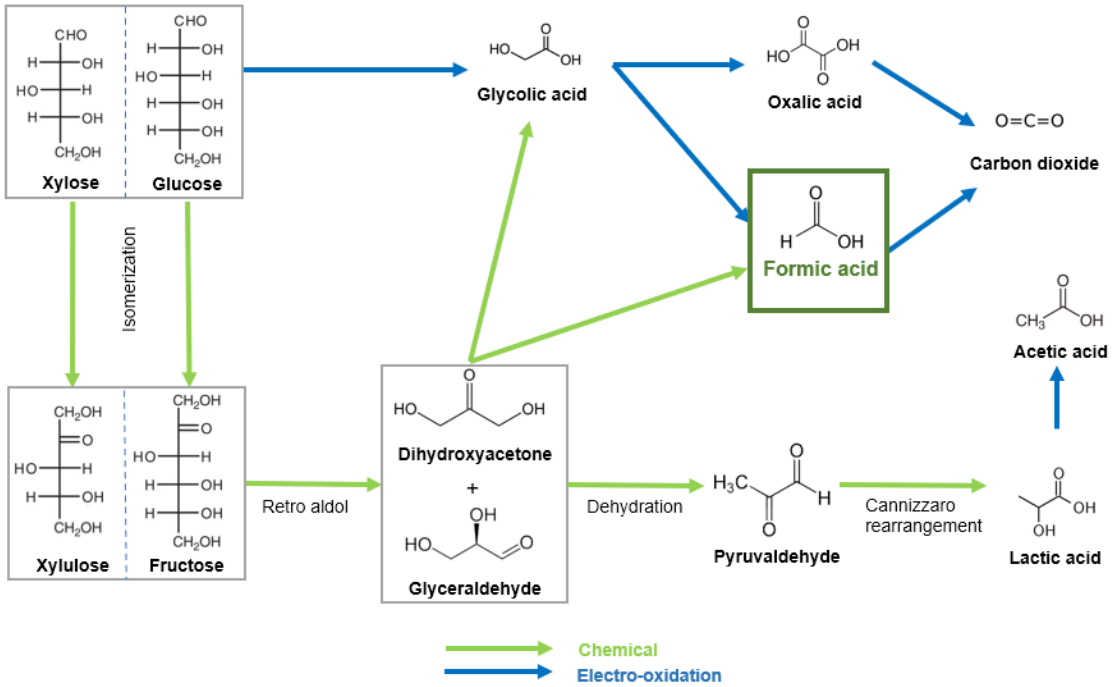

Figure 63 *Proposed reaction pathway of xylose/glucose to lactic acid (path A) and to formic acid (Path B).*

To ensure the integrity of the anode before and after electrooxidation process, XRD and XPS were performed to check the crystal structure, surface composition and chemical states of the *hp*-Ni electrode. The XRD pattern presented in Fig. 64a indicates that *hp*-Ni catalyst consists of crystalline cubic Ni, and this monolithic structure confers the electrode with exceptional electrical conductivity and remarkable stability. After post-electrooxidation of HPW, the *hp*-Ni electrode showed insignificant changes to its crystalline cubic Ni structure, indicating robustness and stability.

The XPS shown in Fig. 64b reveals that after activation in 1 M KOH, almost complete oxidation of the *hp*-Ni electrode can be seen with the XPS peak at 855.3 eV which can be ascribed to be Ni^{2+} of nickel hydroxide. [369] After EO of HPW, a slight increase in the peak (856.5 eV) correspond to Ni^{3+} in the form of nickel oxyhydroxide [370] and could

also be a mixture of $Ni(OH)_2$/ NiOOH, similar to previous work. [48, 371] The peak increase in O *1s* XPS spectrum of post-EO HPW electrode shows that the electrooxidation of HPW could have caused deeper oxidation to the nickel surface (Fig. 64c). The O *1s* peak of Post EO is deconvoluted and further analysed. The peaks at ~531.4 eV and ~532.1 eV correspond to bonds of Ni-oxygen and Ni-hydroxide in NiOOH and $Ni(OH)_2$, respectively. [372] This nickel oxidation is highly advantageous for enhanced electrooxidation activity as the catalytic activity centers in *hp*-Ni anode are primarily composed of high-valent nickel species. [428] Furthermore, the peak at ~533.6 eV is identified to be the ester component that is present in extractives and lignin from wood. [429] It is likely that HPW contains acid-soluble extractives and lignin that was produced during the MHT process.

The full survey XPS spectra showed the similar spectrum pattern for Ni associated peaks with increase in intensity of O *1s* and C *1s* peaks. (Fig. 54d) The new peak that appear at 374 eV is identified to be Ca $2p_{3/2}$ which is possible from the wood sample at the bark/wood interface [430], fibers [429] or as a pectin-complex [431]. Another peak at 399 eV indicates the presence of N *1s* presents the NH_2 functional group in amino acids/proteins which is likely found in wood [429]. Other unidentified peaks could be caused by experimental error.

Overall, the formation of NiOOH species from oxidation of $NiO/Ni(OH)_2$ electrode surface ($NiO/Ni(OH)_2 + OH^- \rightarrow NiOOH + e^-$) was responsible for the catalytic activity of HPW electrooxidation, according to previous glucose studies. [298, 373, 374]

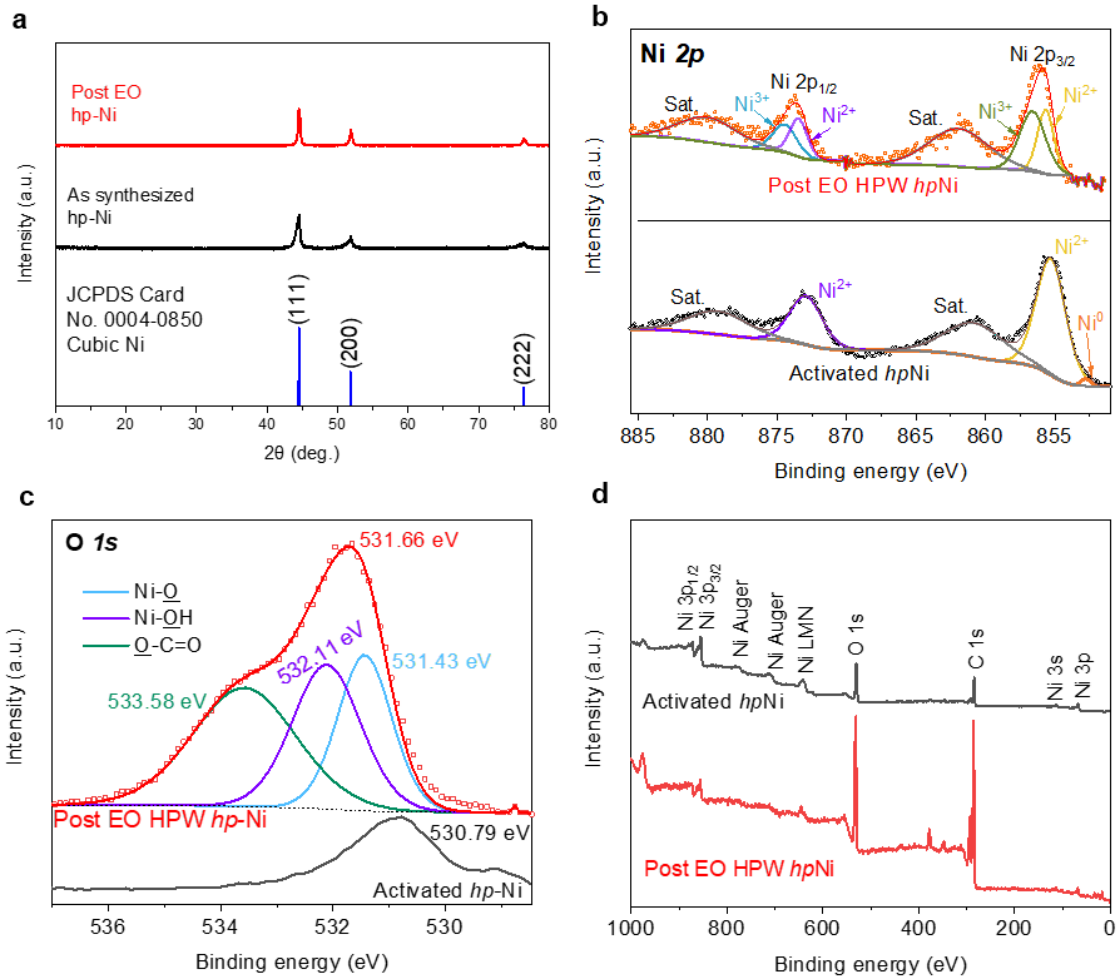

Figure 64 *(a) XRD spectra of hp-Ni – (red) Post electrooxidation (EO) of HPW, (black) As synthesized, and (blue) cubic Ni standard from JCPDS card No. 0004-0850. XPS spectra of (b) Ni 2p states, (c) O 1s state, and (d) full survey spectra of Activated hp-Ni electrode (black) and Post EO HPW for 4 h at 1.58 V vs RHE (red).*

4.2.4 Solar-driven electroreforming of HPW

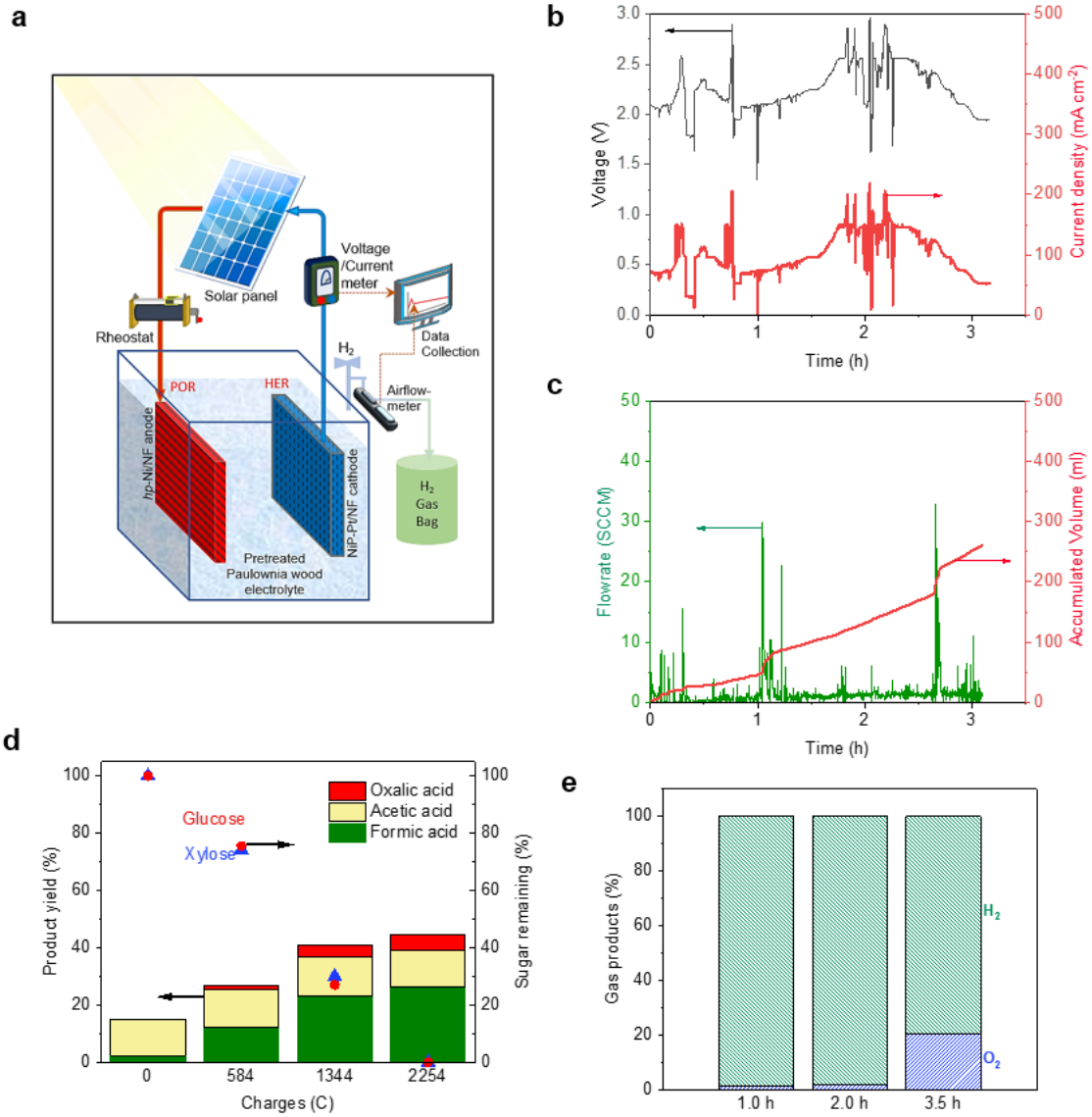

Figure 65 *Solar reforming to formic acid from HPW – (a) Overall schematic diagram, (b) Voltage and current density against time plot, (c) Gas airflow rate and accumulated volume with time plot; (d) Effect of charges to liquid products and conversion of glucose and xylose from HPW; (e) Gas products composition at different solar reforming time intervals.*

For a better green and sustainable application, renewable solar energy was implemented to drive the electroforming process and the schematic diagram is illustrated in Fig. 65a. To suppress oxygen evolution, the resistance load was adjusted to control the applied DC voltage to be less than 2.5 V. The average current density was around 150 mA cm^{-2} with fluctuation resulted from cloud movement which disrupted the sun ray intensity

towards the photovoltaic (PV) system. (Fig. 65b) Inevitably, this also interfered the gas flow which contributed to irregular pikes throughout the airflow plot. (Fig. 65c) Liquid product quantification revealed (26% yield) to formic acid at 2254 C with full conversion of glucose and xylose. (Fig. 65d) Oxalic acid and acetic acid were also detected as side products. Yield of formic acid could have improved if sample collection can be done between 1344–2254 C with more precise control of the applied charges. Fig. 65e shows the gas contents of the collected gas at three intervals. At 1 and 2 h, slight amount of O_2 (1.4–1.7%) was detected which is attributed to the fluctuating potential causing OER together with the electrooxidation of HPW. However, the increased O_2 (20.6%) at 3.5 h, ascribed to the depletion of the monosaccharides to support the suppression of OER as full conversion of HPW was completed.

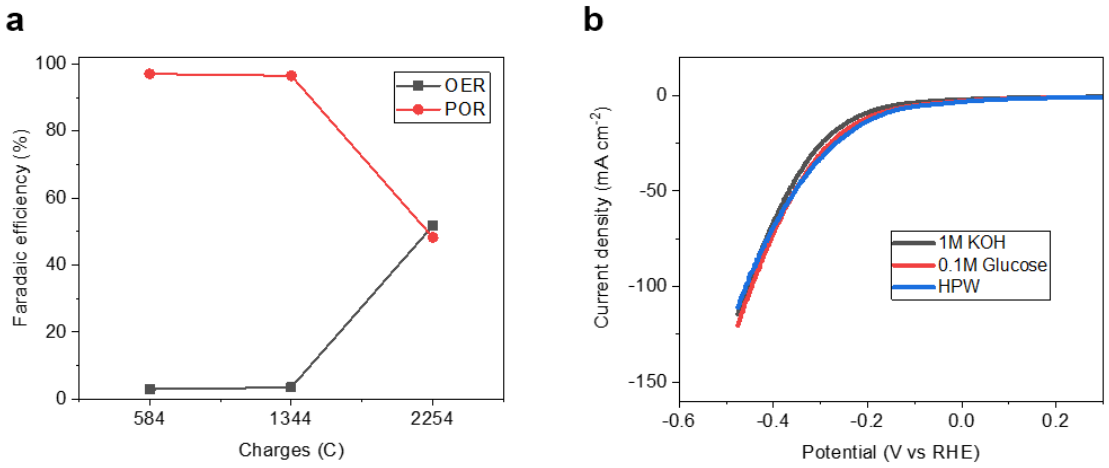

Figure 66 *(a) Faradaic efficiency at the anode (black curve: OER, red curve: POR); (b) LSV of Ni_2P cathode anode. (black curve: background 1 M KOH, red curve: 0.1 M Glucose in 1 M KOH, and blue curve: HPW).*

Fig. 66a compares the Faradaic efficiency at the anode for OER and POR over the applied charges. As expected, POR was initially prioritized over OER because POR is thermodynamically more favorable, but the situation reverses when the sugar is consumed by continuous POR. The oxygen species generated near OER potential could facilitate POR and over oxidation of sugar to CO_2 would occur if OER dominates the reaction.

On the other hand, the H_2 Faradaic efficiencies were above 95%. Our gas measurements errors and loss in gas collection procedures may have led to a hydrogen FE lower than 100%. Additionally, there is a chance that the electrocatalyst surface, which is inevitably oxidized in air by oxygen and moisture, could undergo partial reduction. To address these concerns, we conducted additional LSV scans, confirming that there are no other reduction reactions of organics besides the HER, as illustrated in Fig. 66b.

As a feasibility study, the possibility of using a single-compartment electrochemical cell with *hp*-Ni and Ni_2P as anode and cathode, respectively, for sustainable HPW electroreforming was demonstrated. It is worth noting that high purity H_2 can be collected with a membrane and at a regulated constant potential output.

4.3 Summary

In this work, the extraction of sugar (xylose and glucose) directly from fast-growing Paulownia wood using very low concentration of sulphuric acid, energy-saving, microwave-assisted hydrothermal process was demonstrated. The systematic optimization study on various parameters resulted in the highest sugar yield of 100% xylose and 17% glucose, which were then converted into value-added green chemicals. Through two conversion paths, thermo-alkaline treatment to lactate and electro-reform to formate. Furthermore, the cellulose-rich residue after microwave pre-treatment could also recover high glucose yield (45% in 1 cycle and 90% in 5 cycles of MHT). Significantly, the sugar yield extracted from Paulownia wood is as high as commonly used biomass, thanks to its large pore size, which results in a weaker lignocellulosic structure.

Furthermore, the practical application of coupling renewable energy with biomass electroreforming was also demonstrated, which shows the possibility of simultaneously

upcycling of biomass waste and storing excessive, intermittent photovoltaic energy in the form of formate and green hydrogen. These green chemicals, namely lactate and formate, have various applications, such as being used as platform molecules for producing a wide range of useful chemicals and participating in the Formate-Bicarbonate Cycle for hydrogen vehicle and energy storage. Promisingly, our developed valorization approach of Paulownia wood may provide a potential energy-saving approach for green chemicals and hydrogen fuel manufacturing. This work thus contributes to the renewable chemical synthesis replacement for fossil fuels, as well as to the promising hydrogen economy.

4.4 Effect of CNT on microwave-assisted hydrothermal for cellulose conversion to glucose

Further investigation work was conducted to reduce microwave energy consumption – the introduction of microwave absorbance material, such as carbon nanotubes (CNT), into the MHT process. Apart from having the dielectric loss property for absorbing electromagnetic waves, CNT also possesses other excellent properties – low mass, high specific surface area and excellent chemical stability. [432, 433] Given its acid stability properties and its derivation from abundant plant biomass, this makes CNT a suitable material to support the sustainability and greener route for MHT of lignocellulosic biomass.

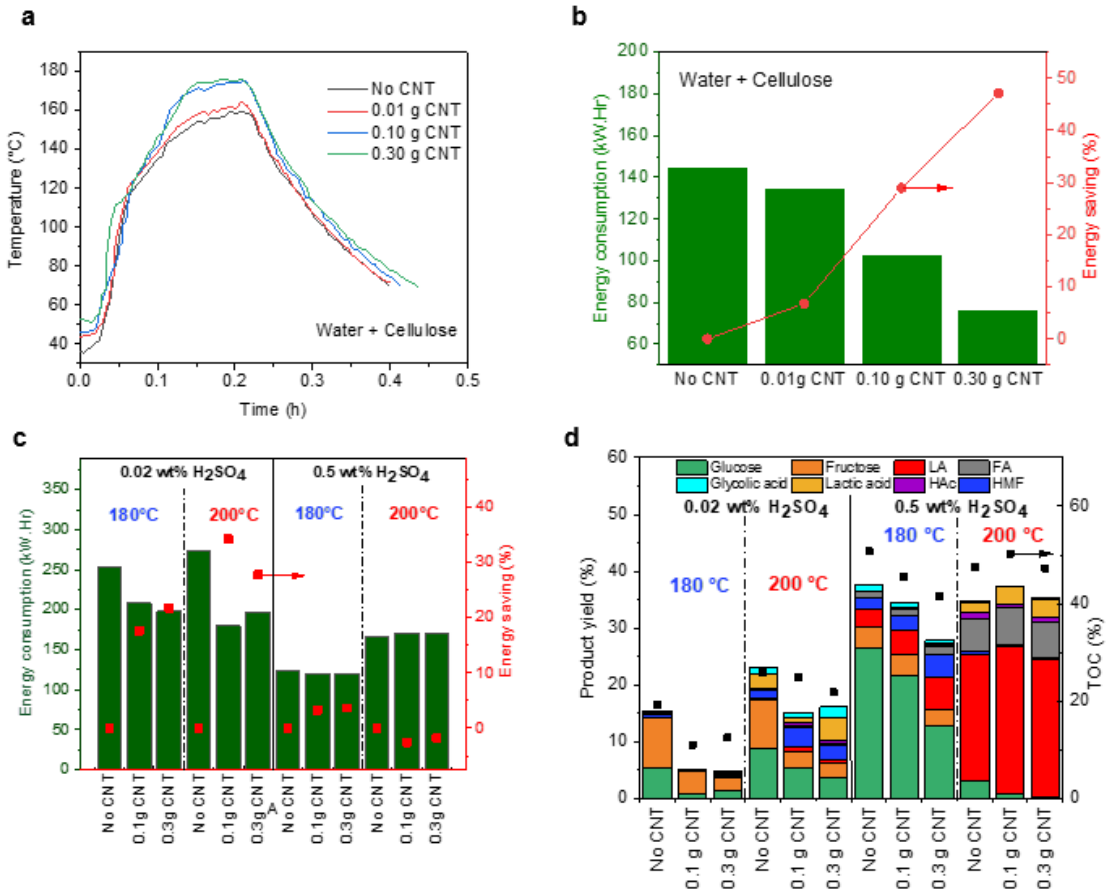

Figure 67 *CNT study of cellulose MHT in water – (a) Temperature profile with different amount of CNT, (b) Energy consumption and energy saving at 180 °C; and in dilute H_2SO_4 - (c) Energy consumption and energy saving at 180 °C and 200 °C, (d) Effect of CNT on liquid products yield % and TOC%. (Product yield % and TOC % calculated based on moles of carbon of initial cellulose).*

First, the impact of CNT on temperature and energy consumption was investigated during MHT of cellulose in water. Fig. 67a illustrates the remarkable effect of CNT on temperature when 0.10 g CNT was added. Notably, in both 0.10 g and 0.30 g CNT additions allowed the temperature to almost reach the set temperature of 180 °C, whereas vessels with 0.01 g of CNT and without CNT could only reach 160 °C. Furthermore, the inclusion of 0.30 g CNT resulted in a significant reduction in energy consumption, leading to nearly 50% energy savings compared to other conditions. (Fig. 67b) These preliminary results showed that CNT has a significant impact on the temperature and energy efficiency of the hydrothermal treatment (MHT) of cellulose in water, making it

a promising additive for progressing towards more effective and energy-efficient MHT process.

As shown earlier, to effectively depolymerize cellulose to glucose, the addition of H_2SO_4 is required. Hence, the inclusion of dilute acid (0.02 wt% and 0.5 wt%) was further studied on the effect of product yield from cellulose MHT with CNT. The energy consumption reduction (35%) was more significant with (0.10 g of CNT and 0.02 wt% H_2SO_4) at 200 °C among other parameters (Fig. 67c). Despite the energy-saving benefit at 180 °C, the addition of CNT did not contribute to significant cellulose to glucose conversion in 0.02 wt% acid solution (Fig. 67d). However, more glucose degradation byproducts (HMF, lactic acid and LA) were observed at 200 °C which could be probably caused by additional localized heating effect with CNT. In contrast, the cellulose conversion in 0.5 wt% acid solution was relatively higher. Overall, the addition of 0.10 g of CNT shown higher cellulose conversion to glucose and levulinic acid (LA) at 180 °C and 200 °C, respectively. These results suggest that CNT could promote levulinc acid production from cellulose MHT with lesser amount of H_2SO_4. The use of functionalized group CNT with further optimization could enhance the LA yield.

Chapter 5: Overall outlook and future work

5.1 Overall outlook

In this thesis, the sustainable and novel approach for abundant biomass upgrading was demonstrated on two fast-growing plant species namely Sugarcane (bagasse waste) and Paulownia (wood). The key objectives were met, and the main contributions are summarized:

1) In Chapter 3, the efficient raw biomass pretreatment was developed successfully using dilute sulphuric acid hydrothermal overcome the natural recalcitrance of SCB and effectively depolymerize the abundant polysaccharides to mono/oligosaccharides with minimal production of degraded sugar byproducts. Our demonstrated process bypasses the need for laborious multi-separation and purification steps, such as fractionation of cellulose, hemicellulose, and lignin. This results in increased energy efficiency and environmental friendliness, with reduced water consumption and carbon emissions.
2) In Chapter 4, further effort was made to reduce the energy consumption and environmental impact of the pretreatment process. Specifically, the energy-saving microwave hydrothermal pre-treatment of paulownia wood was optimized systematically to obtain the highest sugar yield with the mildest conditions (temperature, duration and acid amount). Additionally, glucose from cellulose residue was also successfully recovered by investigating the temperature and acid influence on cellulose in MHT.
3) After pretreatment, the sugar-rich soluble mixture can further be converted into value-added green chemicals by two routes. First, the sugar mixture can undergo

additional thermo-alkaline microwave treatment to yield high value lactate. Second, the same sugar mixture can be coupled with a high yield electrochemical refinery process to produce the platform chemical (formate) at ambient temperature and pressure. This was also showcased in the electroreforming of SCB in Chapter 3 with the synthesized earth abundant, nickel electrocatalyst. In both works, the OER was suppressed by the much favorable biomass electrooxidation reaction, showing reduced energy consumption (12–14%) for a safer green hydrogen production.

4) 4) The mechanism of electroreforming SCB was investigated through electrooxidation studies to understand the transformation of lignocellulosic biomass into value-added chemicals. However, due to the biomass's complexity (mixture of oxygenates with a range of molecules up to thousands of Da), the theoretical calculation is challenging to fully determine the reaction mechanism. Therefore, product identification with HPLC and NMR techniques was performed to determine the possible intermediates. Then, subsequent electrooxidation of the intermediates were performed to determine the possible reaction pathways. In addition, electrocatalyst characterization was conducted using XRD, XPS, SEM and TEM techniques to elucidate the active species responsible for the catalytic reaction.

5) The PV-driven "hybrid electrolyzer" was successfully developed for a better green and sustainable application. The hybrid electrolyzer not only upcycles the abundant lignocellulosic biomass to value-added products, but also produces emission-free green hydrogen, as implemented in both Chapters 3 and 4. Moreover, the life-cycle analysis evaluated that the developed SCB upcycling process emits less greenhouse gases than traditional SCB waste management and chemical production processes using fossil fuels.

Moreover, the innovative pretreatment-electrochemical processes exhibit several key advantages over existing methods. Firstly, the anodic oxidation of various lignocellulosic biomass, such as SCB waste and Paulownia wood, demonstrates enhanced efficiency (12–14% compared to water electrolysis) for cogeneration of green chemicals and green hydrogen. This not only reduces waste but also maximizes the utilization of biomass resources. As discussed earlier, the developed *hp*-Ni anode with abundant nickel active species facilitated high electrochemical kinetics for both biomass extracts (averaging 60–100 mA cm^{-2}), in contrast to other lignocellulosic biomass works, which typically exhibit rates below 10 mA cm^{-2}, as discussed in Chapter 3.The main electrooxidized product, formate, showed higher selectivity (38–41%) than an earlier work on crushed barley straw [273] , which reported 22%.

Moving on to sugar extraction, the time efficiency achieved in sugar extraction of Paulownia using MHT is noteworthy, requiring only 1 hour for xylose and an additional 3 hours for the recovery of 90% glucose. This surpasses the enzymatic hydrolysis approach, which takes 72 hours to achieve an 80–90% yield [136, 434, 435]. This accelerated process not only improves production speed but also enhances economic viability as a more efficient solution for biofuel production. The optimal sugar yield of Paulownia wood (22.5 g / 100 g DW) outperformed benchmarks set by other lignocellulosic biomass species (such as Aspen, Balsam fir, Basswood, Red maple) [221] at a similar acid concentration level, ranging from 9.07–20.12 g / 100 g DW.

Furthermore, this work stands out in terms of environmental impact. The LCA results showcase a notable reduction in carbon emissions (8–20% fewer greenhouse gases) compared to traditional landfill disposal methods. This underscores the environmental-benign nature of our approach, aligning with the global effort to mitigate climate change.

Lastly, the energy comparison for sugar production using microwave technology, as opposed to conventional energy heating consumption, demonstrates a more energy-efficient process with approximately a 38% energy saving. This contributes to the overall sustainability of the production process.

In conclusion, the novel pretreatment-electrochemical processes for both SCB waste and Paulownia wood upcycling presented in this study not only contribute to the cogeneration of green chemicals and green hydrogen but also offer a more sustainable and environmentally friendly alternative to conventional biowaste management methods.

5.2 Recommendations for future work

Raw biomass reforming has demonstrated significant potential for sustainable production of low-carbon biofuels, clean hydrogen fuel, and essential green chemicals, leading to an ever-increasing number of research studies in this field. The findings of this thesis are significant and contributed as an alternative strategy for producing green chemicals without relying on fossil fuels. Additionally, below are some important considerations for ongoing research:

1) Chapters 3 and 4 have demonstrated similar results, indicating potential applicability to other abundant lignocellulosic biomass or in the form of biomass mixtures (such as hardwood species). This suggests that the separation process of different lignocellulosic biomass types could be avoided, leading to efficient waste management.

   However, the product yield and selectivity may vary due to differences in plant structures and chemical compositions, particularly for softwood species which require further studies. For instance, a typical fast-growing hardwood, poplar wood

contains 49% cellulose, 23% hemicellulose and 27% lignin. [436] On the other hand, oil palm empty fruit brunch fiber, an abundant biomass in Southeast Asia consists of 55% cellulose, 30.5% hemicellulose and 16.5% lignin. [437] Unlike hardwood, softwood species contains higher content of glucomannan, lower amounts of xylan [438] and a different lignin species of mainly guaiacyl phenolic monomers [439], requiring additional feasibility studies.

2) Lignin valorization could be explored with greener and sustainable pretreatment method to first separate lignin from polysaccharides [440], and then electrocatalytically degrade it into monolignols [441] or electrooxidize it into products [442-444]. However, irreversible lignin degradation may occur that leads to condensed, unreactive structures, posing challenges for the breakdown into useful chemicals and reducing the maximum monomer yield [445]. Another issue is that the mixture of electrooxidized aromatic products will require further optimization to improve its product selectivity. [441]

   Another strategy involves a one-pot depolymerization of lignocellulosic components into small molecules, which may be possible in an alkaline solution. [268, 379] The subsequent electroreforming of these small molecular fragments can also be upgraded to produce value-added products. However, attention (stabilization strategies) is required to prevent unwanted side reactions such as aldol condensation of small molecules derived from cellulose/hemicellulose and lignin condensation. [446]

3) Modulating the selectivity of electroreforming of lignocellulose to other value-added products. Promising selective electrooxidation of glucose to glucaric acid [298] or to lactic acid [447] had been successfully demonstrated with different electrode materials such as iron and copper.

4) The improvement of solar-driven hybrid electrolyzer could be made with the better control of maximum potential fluctuation to obtain high purity of hydrogen. The fixed dc voltage bus [448] with voltage control [449], or with an extra lithium-ion battery [450] can modulate the electricity fluctuation.

   In addition, the flow cell design [451-453] can be implemented to continuously supply the pre-treated biomass feedstock for electrooxidation, thereby suppressing the OER. This design also facilitates the replenishment of alkaline electrolyte, addressing the decrease in pH resulting from the formation of acid salt as a product.

5) The analysis of potential reaction pathways relied on identified intermediates and existing literature in this study; however, the exact reaction mechanism remains unclear at the current stage due to the biomass's complexity. A more comprehensive understanding of the reaction mechanism is needed and can be achieved through the application of advanced characterization methods and theoretical calculations. A review study [454] highlighted techniques such as isotope-labelling technique [455], in situ solid state NMR [456], synchrotron X-ray powder diffraction (SXPD) [457], X-ray absorption spectroscopy (XAS) [458] and inelastic neutron scattering (INS) [459] could be used to study the reaction mechanism of biomass conversion. Moreover, density function theory (DFT) and molecular dynamics (MD) could be used to create modelling of cellulose and lignin to study their reactions [460]. The kinetics and thermodynamic analyses through DFT could propose the formation pathways such as nitrogenous chemicals products in complex bio-oil [461].

6) The addition of efficient microwave absorbing materials, such as CNT, holds the potential to decrease microwave energy consumption. Recent research had demonstrated promising outcomes, as highlighted in the section 4.4.

7) The incorporation of mechanochemical method to enhance microwave synthesis of sugar – to reduce energy consumption and enhance the efficiency of microwave synthesis for sugar production. For instance, solid acid (oxalic acid, adipic acid, salicylic acid, benzoic acid, malonic acid, trichloroacetic acid, succinic acid, maleic acid, tartaric acid and etc) can be co-milled together with wood. In reference to a previous study [200], solid dicarboxylic acids and cyclic acids were ground with barley straw. Subsequent hydrolysis processes were conducted at different temperatures (room temperature, 100 °C, and 130 °C) for 1 h. Remarkably, oxalic acid demonstrated the highest total reducing sugar yields, reaching 42%.

   This outcome suggests the potential to decrease both the temperature and duration of microwave-assisted sugar extraction by co-milling larger pieces of wood waste with solid acid. The introduction of solid acid not only acts as a grinding auxiliary to reduce milling time but also results in a reduction in the size of the wood particles and facilitates the intimate impregnation of the solid acid into the wood powder or smaller particles.

8) Utilizing acid-containing waste for sustainable acid hydrolysis of wood waste – The utilization of acid-containing waste, specifically grape marc, as a supplement to sulphuric acid for the acid hydrolysis of wood waste represents an innovative approach. This strategy is designed to repurpose waste materials, fostering a more sustainable and environmentally friendly process. Grape marc is notable for its reported pH of 3.6 ± 0.2 [462] and tartrate concentration [463] ranging from 50–75 kg T^{-1}. Additionally, grape skins, a component of this waste stream, contain 20.8% cellulose and 12.5% hemicellulose. [464] In 2012, this waste stream amounted to approximately 70 million tonnes of grapes, with nearly 60% earmarked for "pressed grapes" (primarily wine and grape juice), resulting in a global wine production of

almost 26 billion liters. [465] These details support the potential of employing MHT process to valorize both wine and wood waste into a mixture rich in tartaric acid and sugars. Subsequently, electro-reforming of this mixture would result in formic acid as the primary dominant product, as evidenced in earlier electrooxidation studies in Chapter 3. This integrated approach not only addresses waste management but also holds promise for generating green hydrogen, contributing to a comprehensive and sustainable utilization of agricultural and wood waste streams.

References

[1] C. Le Quéré *et al.*, "The global carbon budget 1959-2011," *Earth System science data,* vol. 5, pp. 165-185, 2013.

[2] T. R. Anderson, E. Hawkins, and P. D. Jones, "CO_2, the greenhouse effect and global warming: from the pioneering work of Arrhenius and Callendar to today's Earth System Models," *Endeavour,* vol. 40, no. 3, pp. 178-187, 2016.

[3] R. Etkins and E. S. Epstein, "The rise of global mean sea level as an indication of climate change," *Science,* vol. 215, no. 4530, pp. 287-289, 1982.

[4] I. P. o. C. Change, *Global warming of 1.5° C: An IPCC special report on the impacts of global warming of 1.5° C above pre-industrial levels and related global greenhouse gas emission pathways, in the context of strengthening the global response to the threat of climate change, sustainable development, and efforts to eradicate poverty*. Intergovernmental Panel on Climate Change, 2018.

[5] C. C. IPCC, "The physical science basis. Contribution of working group I to the fourth assessment report of the Intergovernmental Panel on Climate Change," *Cambridge University Press, Cambridge, United Kingdom and New York, NY, USA,* vol. 996, no. 2007, pp. 113-119, 2007.

[6] S. Jevrejeva, L. Jackson, A. Grinsted, D. Lincke, and B. Marzeion, "Flood damage costs under the sea level rise with warming of 1.5 °C and 2 °C," *Environmental Research Letters,* vol. 13, no. 7, pp. 074014, 2018.

[7] A. Gasparrini *et al.*, "Projections of temperature-related excess mortality under climate change scenarios," *The Lancet Planetary Health,* vol. 1, no. 9, pp. e360-e367, 2017.

[8] D. Deryng, D. Conway, N. Ramankutty, J. Price, and R. Warren, "Global crop yield response to extreme heat stress under multiple climate change futures," *Environmental Research Letters,* vol. 9, no. 3, pp. 034011, 2014.

[9] A. Mehran *et al.*, "Compounding impacts of human-induced water stress and climate change on water availability," *Scientific reports,* vol. 7, no. 1, pp. 6282, 2017.

[10] J. Tollefson, "IPCC says limiting global warming to 1.5 [degrees] C will require drastic action," *Nature,* vol. 562, no. 7726, pp. 172-174, 2018.

[11] C. Zhang, P. Song, Y. Sui, J. Hou, and X. Wang, "Economic competitiveness of compact steam methane reforming technology for on-site hydrogen supply: a Foshan case study," *International Journal of Hydrogen Energy,* vol. 47, no. 76, pp. 32359-32371, 2022.

[12] M. Carmo and D. Stolten, "Energy storage using hydrogen produced from excess renewable electricity: Power to hydrogen," *Science and Engineering of Hydrogen-Based Energy Technologies*, pp. 165-199, 2019.

[13] H. Kasap *et al.*, "Solar-driven reduction of aqueous protons coupled to selective alcohol oxidation with a carbon nitride–molecular Ni catalyst system," *Journal of the American Chemical Society,* vol. 138, no. 29, pp. 9183-9192, 2016.

[14] N. Jiang, X. Liu, J. Dong, B. You, X. Liu, and Y. Sun, "Electrocatalysis of furfural oxidation coupled with H2 evolution via nickel‐based electrocatalysts in water," *ChemNanoMat,* vol. 3, no. 7, pp. 491-495, 2017.

[15] L. Yi *et al.*, "Scalable Synthesis of Tungsten Disulfide Nanosheets for Alkali‐Acid Electrocatalytic Sulfion Recycling and H2 Generation," *Angewandte Chemie International Edition,* vol. 60, no. 39, pp. 21550-21557, 2021.

[16] M. D. Symes and L. Cronin, "Decoupling hydrogen and oxygen evolution during electrolytic water splitting using an electron-coupled-proton buffer," *Nature chemistry,* vol. 5, no. 5, pp. 403-409, 2013.

[17] L. Chen, X. Dong, Y. Wang, and Y. Xia, "Separating hydrogen and oxygen evolution in alkaline water electrolysis using nickel hydroxide," *Nature communications,* vol. 7, no. 1, pp. 11741, 2016.

[18] V. Amstutz *et al.*, "Renewable hydrogen generation from a dual-circuit redox flow battery," *Energy & Environmental Science,* vol. 7, no. 7, pp. 2350-2358, 2014.

[19] S. Goodwin and D. A. Walsh, "Closed bipolar electrodes for spatial separation of H2 and O2 evolution during water electrolysis and the development of high-voltage fuel cells," *ACS applied materials & interfaces,* vol. 9, no. 28, pp. 23654-23661, 2017.

[20] A. Caravaca, W. E. Garcia-Lorefice, S. Gil, A. de Lucas-Consuegra, and P. Vernoux, "Towards a sustainable technology for H2 production: Direct lignin electrolysis in a continuous-flow Polymer Electrolyte Membrane reactor," *Electrochemistry Communications,* vol. 100, pp. 43-47, 2019.

[21] G. Sasikumar, A. Muthumeenal, S. S. Pethaiah, N. Nachiappan, and R. Balaji, "Aqueous methanol eletrolysis using proton conducting membrane for hydrogen production," *international journal of hydrogen energy,* vol. 33, no. 21, pp. 5905-5910, 2008.

[22] B. Hasa, J. Vakros, and A. D. Katsaounis, "Effect of TiO2 on Pt-Ru-based anodes for methanol electroreforming," *Applied Catalysis B: Environmental,* vol. 237, pp. 811-816, 2018.

[23] F. Sapountzi, M. Tsampas, H. Fredriksson, J. Gracia, and J. Niemantsverdriet, "Hydrogen from electrochemical reforming of C1–C3 alcohols using proton conducting membranes," *International Journal of Hydrogen Energy,* vol. 42, no. 16, pp. 10762-10774, 2017.

[24] Y. Chen *et al.*, "Nanotechnology makes biomass electrolysis more energy efficient than water electrolysis," *Nature communications,* vol. 5, no. 1, pp. 1-6, 2014.

[25] A. Caravaca, F. Sapountzi, A. de Lucas-Consuegra, C. Molina-Mora, F. Dorado, and J. Valverde, "Electrochemical reforming of ethanol–water solutions for pure H2 production in a PEM electrolysis cell," *International journal of hydrogen energy,* vol. 37, no. 12, pp. 9504-9513, 2012.

[26] N. Gutierrez-Guerra, M. Jimenez-Vazquez, J. Serrano-Ruiz, J. Valverde, and A. de Lucas-Consuegra, "Electrochemical reforming vs. catalytic reforming of ethanol: a process energy analysis for hydrogen production," *Chemical Engineering and Processing: Process Intensification,* vol. 95, pp. 9-16, 2015.

[27] A. De la Osa, A. Calcerrada, J. Valverde, E. Baranova, and A. de Lucas-Consuegra, "Electrochemical reforming of alcohols on nanostructured platinum-tin catalyst-electrodes," *Applied Catalysis B: Environmental,* vol. 179, pp. 276-284, 2015.

[28] A. B. Calcerrada, R. Ana, H. A. Dole, F. Dorado, E. A. Baranova, and A. de Lucas-Consuegra, "Stability Testing of Pt x Sn 1− x/C Anodic Catalyst for Renewable Hydrogen Production Via Electrochemical Reforming of Ethanol," *Electrocatalysis,* vol. 9, no. 3, pp. 293-301, 2018.

[29] A. B. Calcerrada, R. Ana, J. Llanos, F. Dorado, and A. de Lucas-Consuegra, "Hydrogen from electrochemical reforming of ethanol assisted by sulfuric acid addition," *Applied Catalysis B: Environmental,* vol. 231, pp. 310-316, 2018.

[30] A. Caravaca, A. de Lucas-Consuegra, A. Calcerrada, J. Lobato, J. Valverde, and F. Dorado, "From biomass to pure hydrogen: electrochemical reforming of bio-ethanol in a PEM electrolyser," *Applied Catalysis B: Environmental,* vol. 134, pp. 302-309, 2013.

[31] B. You, X. Liu, X. Liu, and Y. Sun, "Efficient H2 Evolution Coupled with Oxidative Refining of Alcohols via A Hierarchically Porous Nickel Bifunctional Electrocatalyst," *ACS Catalysis,* vol. 7, no. 7, pp. 4564-4570, 2017.

[32] B. You, X. Liu, N. Jiang, and Y. Sun, "A general strategy for decoupled hydrogen production from water splitting by integrating oxidative biomass valorization," *Journal of the American Chemical society,* vol. 138, no. 41, pp. 13639-13646, 2016.

[33] B. You, N. Jiang, X. Liu, and Y. Sun, "Simultaneous H2 Generation and Biomass Upgrading in Water by an Efficient Noble-Metal-Free Bifunctional Electrocatalyst," *Angewandte Chemie,* vol. 128, no. 34, pp. 10067-10071, 2016.
[34] K. R. Vuyyuru and P. Strasser, "Oxidation of biomass derived 5-hydroxymethylfurfural using heterogeneous and electrochemical catalysis," *Catalysis Today,* vol. 195, no. 1, pp. 144-154, 2012.
[35] Y. Sugano, R. M. Latonen, M. Akieh - Pirkanniemi, J. Bobacka, and A. Ivaska, "Electrocatalytic oxidation of cellulose at a gold electrode," *ChemSusChem,* vol. 7, no. 8, pp. 2240-2247, 2014.
[36] Y. Sugano, T. Saloranta, J. Bobacka, and A. Ivaska, "Electro-catalytic oxidation of hemicelluloses at the Au electrode," *Physical Chemistry Chemical Physics,* vol. 17, no. 17, pp. 11609-11614, 2015.
[37] Y. Li and S. K. Khanal, *Bioenergy: principles and applications*. John Wiley & Sons, 2016.
[38] R. C. Dewar and M. G. Cannell, "Carbon sequestration in the trees, products and soils of forest plantations: an analysis using UK examples," *Tree physiology,* vol. 11, no. 1, pp. 49-71, 1992.
[39] G. A. Tuskan and M. E. Walsh, "Short-rotation woody crop systems, atmospheric carbon dioxide and carbon management: A US case study," *The Forestry Chronicle,* vol. 77, no. 2, pp. 259-264, 2001.
[40] J. Weslien *et al.*, "Effects of increased forest productivity and warmer climates on carbon sequestration, run-off water quality and accumulation of dead wood in a boreal landscape: A modelling study," *Scandinavian Journal of Forest Research,* vol. 24, no. 4, pp. 333-347, 2009.
[41] V. Voora, S. Bermúdez, H. Le, C. Larrea, and E. Luna, "Sugar cane prices and sustainability," *IISD.org*, 2023.
[42] C. R. Soccol *et al.*, "Bioethanol from lignocelluloses: status and perspectives in Brazil," *Bioresource technology,* vol. 101, no. 13, pp. 4820-4825, 2010.
[43] E. Ajala, J. Ighalo, M. Ajala, A. Adeniyi, and A. Ayanshola, "Sugarcane bagasse: a biomass sufficiently applied for improving global energy, environment and economic sustainability," *Bioresources and Bioprocessing,* vol. 8, no. 1, pp. 1-25, 2021.
[44] G. M. Aita and M. Kim, "Pretreatment technologies for the conversion of lignocellulosic materials to bioethanol," *Sustainability of the sugar and sugar– ethanol industries*, 2010, pp. 117-145.
[45] N. Srivastava *et al.*, "Recent advances on lignocellulosic bioresources and their valorization in biofuels production: Challenges and viability assessment," *Environmental Technology & Innovation,* pp. 103037, 2023.
[46] M. Garedew *et al.*, "Greener routes to biomass waste valorization: Lignin transformation through electrocatalysis for renewable chemicals and fuels production," *ChemSusChem,* vol. 13, no. 17, pp. 4214-4237, 2020.
[47] Z. I. Lai, L. Q. Lee, and H. Li, "Electroreforming of Biomass for Value-Added Products," *Micromachines,* vol. 12, no. 11, pp. 1405, 2021.
[48] H. Zhao *et al.*, "Raw biomass electroreforming coupled to green hydrogen generation," *Nature communications,* vol. 12, no. 1, pp. 2008, 2021.
[49] L. V. A. Gurgel, K. Marabezi, M. D. Zanbom, and A. A. d. S. Curvelo, "Dilute acid hydrolysis of sugar cane bagasse at high temperatures: a kinetic study of cellulose saccharification and glucose decomposition. Part I: sulfuric acid as the catalyst," *Industrial & Engineering Chemistry Research,* vol. 51, no. 3, pp. 1173-1185, 2012.
[50] A. Bahuguna and Y. Sasson, "Formate-Bicarbonate Cycle as a Vehicle for Hydrogen and Energy Storage," *ChemSusChem,* vol. 14, no. 5, pp. 1258-1283, 2021.
[51] Y. Cao *et al.*, "Genomic insights into the fast growth of paulownias and the formation of Paulownia witches' broom," *Molecular Plant,* vol. 14, no. 10, pp. 1668-1682, 2021.

[52] "Paulownia tomentosa. In: Invasive Species Compendium." CAB International. https://www.cabidigitallibrary.org/doi/10.1079/cabicompendium.39100 (accessed 12-27, 2023).
[53] Z.-H. Zhu, C.-J. Chao, X.-Y. Lu, and Y. G. Xiong, *Paulownia in China: cultivation and utilization*. International Development Research Centre, 1986.
[54] F. López, A. Pérez, M. A. Zamudio, H. E. De Alva, and J. C. García, "Paulownia as raw material for solid biofuel and cellulose pulp," *Biomass and Bioenergy,* vol. 45, pp. 77-86, 2012.
[55] J. C. García *et al.*, "Soda-AQ pulping of Paulownia wood after hydrolysis treatment," *BioResources,* vol. 6, no. 2, pp. 971-986, 2011.
[56] J. Jenkins, "Percentage of waste resulting from the conversion of the tree into lumber in the southeastern coast region of British Columbia," *The Forestry Chronicle,* vol. 9, no. 3, pp. 11-13, 1933.
[57] S. Pandey, "Wood waste utilization and associated product development from under-utilized low-quality wood and its prospects in Nepal," *SN Applied Sciences,* vol. 4, no. 6, pp. 168, 2022.
[58] O. Asamoah *et al.*, "Assessing wood waste by timber industry as a contributing factor to deforestation in Ghana," *Forests*, vol. 11, no.9, pp. 939, 2020.
[59] A. Ogunwusi, "Wood waste generation in the forest industry in Nigeria and prospects for its industrial utilization," *Civil and Environmental Research,* vol. 6, no. 9, pp. 62-69, 2014.
[60] L. W. Beurskens, M. Hekkenberg, and P. Vethman, "Renewable energy projections as published in the national renewable energy action plans of the European member states," *ECN and EEA,* 2011.
[61] J. Koppejan and S. Van Loo, *The handbook of biomass combustion and co-firing*. Routledge, 2012.
[62] D. Gielen, F. Boshell, D. Saygin, M. D. Bazilian, N. Wagner, and R. Gorini, "The role of renewable energy in the global energy transformation," *Energy strategy reviews,* vol. 24, pp. 38-50, 2019.
[63] M. Dusselier, P. Van Wouwe, A. Dewaele, E. Makshina, and B. F. Sels, "Lactic acid as a platform chemical in the biobased economy: the role of chemocatalysis," *Energy & Environmental Science,* vol. 6, no. 5, pp. 1415-1442, 2013.
[64] Y. J. Hwang *et al.*, "Development of an autothermal formate-based hydrogen generator: From optimization of formate dehydrogenation conditions to thermal integration with fuel cells," *ACS Sustainable Chemistry & Engineering,* vol. 8, no. 26, pp. 9846-9856, 2020.
[65] A. S. Bhagwat, "Photosynthetic carbon assimilation of C3, C4, and CAM pathways," *Handbook of photosynthesis,* vol. 2, pp. 367-389, 2005.
[66] J. R. Ehleringer and R. K. Monson, "Evolutionary and ecological aspects of photosynthetic pathway variation," *Annual Review of Ecology and Systematics,* vol. 24, no. 1, pp. 411-439, 1993.
[67] T. D. Sharkey, "Photosynthesis in intact leaves of C 3 plants: physics, physiology and rate limitations," *The Botanical Review,* vol. 51, pp. 53-105, 1985.
[68] R. T. Furbank and W. C. Taylor, "Regulation of photosynthesis in C3 and C4 plants: a molecular approach," *The plant cell,* vol. 7, no. 7, pp. 797, 1995.
[69] M. D. Hatch, "C4 photosynthesis: a unique elend of modified biochemistry, anatomy and ultrastructure," *Biochimica et Biophysica Acta (BBA)-Reviews on Bioenergetics,* vol. 895, no. 2, pp. 81-106, 1987.
[70] P. Raven, G. Johnson, K. Mason, J. Losos, and S. Singer, *EBOOK: Biology*. McGraw Hill, 2013.

[71] B. K. Singh, A. Tomar, F. A. Khan, and K. Beauty, "Growth, biomass and carbon sequestration of fast-growing tree species under high-density plantation in Prayagraj, Uttar Pradesh, India," *CURRENT SCIENCE,* vol. 122, no. 5, pp. 618, 2022.
[72] P. Icka, R. Damo, and E. Icka, "Paulownia tomentosa, a fast growing timber," *Ann. Valahia Univ. Targoviste, Agric,* vol. 10, no. 1, pp. 14-19, 2016.
[73] C. A. Gunderson and S. D. Wullschleger, "Photosynthetic acclimation in trees to rising atmospheric CO 2: a broader perspective," *Photosynthesis research,* vol. 39, pp. 369-388, 1994.
[74] T. F. Keenan *et al.*, "Recent pause in the growth rate of atmospheric CO_2 due to enhanced terrestrial carbon uptake," *Nature communications,* vol. 7, no. 1, pp. 13428, 2016.
[75] R. Aerts and F. S. Chapin III, "The mineral nutrition of wild plants revisited: a re-evaluation of processes and patterns," *Advances in ecological research*, vol. 30: Elsevier, 1999, pp. 1-67.
[76] R. J. Brienen *et al.*, "Forest carbon sink neutralized by pervasive growth-lifespan trade-offs," *Nature communications,* vol. 11, no. 1, pp. 4241, 2020.
[77] G. M. Locosselli *et al.*, "Global tree-ring analysis reveals rapid decrease in tropical tree longevity with temperature," *Proceedings of the National Academy of Sciences,* vol. 117, no. 52, pp. 33358-33364, 2020.
[78] C. Körner, "A matter of tree longevity," *Science,* vol. 355, no. 6321, pp. 130-131, 2017.
[79] S. Pan, H. M. Zabed, Y. Wei, and X. Qi, "Technoeconomic and environmental perspectives of biofuel production from sugarcane bagasse: Current status, challenges and future outlook," *Industrial Crops and Products,* vol. 188, pp. 115684, 2022.
[80] C. Kole, C. P. Joshi, and D. R. Shonnard, *Handbook of bioenergy crop plants*. CRC Press, 2012.
[81] M. A. de Almeida and R. Colombo, "Production chain of first-generation sugarcane bioethanol: characterization and value-added application of wastes," *BioEnergy Research,* pp. 1-16, 2021.
[82] A. K. Chandel, S. S. da Silva, W. Carvalho, and O. V. Singh, "Sugarcane bagasse and leaves: foreseeable biomass of biofuel and bio‐products," *Journal of Chemical Technology & Biotechnology,* vol. 87, no. 1, pp. 11-20, 2012.
[83] J. Smithers, "Review of sugarcane trash recovery systems for energy cogeneration in South Africa," *Renewable and Sustainable Energy Reviews,* vol. 32, pp. 915-925, 2014.
[84] J. P. P. Llerena *et al.*, "Deposition of lignin in four species of Saccharum," *Scientific Reports,* vol. 9, no. 1, pp. 1-19, 2019.
[85] M. Pauly and K. Keegstra, "Cell‐wall carbohydrates and their modification as a resource for biofuels," *The Plant Journal,* vol. 54, no. 4, pp. 559-568, 2008.
[86] H. V. Scheller and P. Ulvskov, "Hemicelluloses," *Annual review of plant biology,* vol. 61, pp. 263-289, 2010.
[87] G. Xiong, K. Cheng, and M. Pauly, "Xylan O-acetylation impacts xylem development and enzymatic recalcitrance as indicated by the Arabidopsis mutant tbl29," *Molecular Plant,* vol. 6, no. 4, pp. 1373-1375, 2013.
[88] S. Helle, D. Cameron, J. Lam, B. White, and S. Duff, "Effect of inhibitory compounds found in biomass hydrolysates on growth and xylose fermentation by a genetically engineered strain of S. cerevisiae," *Enzyme and Microbial Technology,* vol. 33, no. 6, pp. 786-792, 2003.
[89] R. A. Sheldon, "Green and sustainable manufacture of chemicals from biomass: state of the art," *Green Chemistry,* vol. 16, no. 3, pp. 950-963, 2014.
[90] F. M. Gírio, C. Fonseca, F. Carvalheiro, L. C. Duarte, S. Marques, and R. Bogel-Łukasik, "Hemicelluloses for fuel ethanol: a review," *Bioresource technology,* vol. 101, no. 13, pp. 4775-4800, 2010.

[91] J. Ralph, "Hydroxycinnamates in lignification," *Phytochemistry Reviews,* vol. 9, pp. 65-83, 2010.
[92] T. Ramjeawon, "Life cycle assessment of electricity generation from bagasse in Mauritius," *Journal of Cleaner Production,* vol. 16, no. 16, pp. 1727-1734, 2008.
[93] C. Geddes *et al.*, "Optimizing the saccharification of sugar cane bagasse using dilute phosphoric acid followed by fungal cellulases," *Bioresource technology,* vol. 101, no. 6, pp. 1851-1857, 2010.
[94] L. Ingram, X. Lai, M. Moniruzzaman, B. Wood, and S. York, "Fuel ethanol production from lignocellulose using genetically engineered bacteria," ACS Publications, 1997.
[95] J. Zhu, "Physical pretreatment− woody biomass size reduction− for forest biorefinery," *Sustainable production of fuels, chemicals, and fibers from forest biomass*, pp. 89-107, 2011.
[96] J. Hernández-Salas *et al.*, "Comparative hydrolysis and fermentation of sugarcane and agave bagasse," *Bioresource technology,* vol. 100, no. 3, pp. 1238-1245, 2009.
[97] Z. Wang, B. S. Dien, K. D. Rausch, M. Tumbleson, and V. Singh, "Fermentation of undetoxified sugarcane bagasse hydrolyzates using a two stage hydrothermal and mechanical refining pretreatment," *Bioresource technology,* vol. 261, pp. 313-321, 2018.
[98] A. Guilherme, P. Dantas, E. Santos, F. A. Fernandes, and G. R. d. Macedo, "Evaluation of composition, characterization and enzymatic hydrolysis of pretreated sugar cane bagasse," *Brazilian Journal of Chemical Engineering,* vol. 32, pp. 23-33, 2015.
[99] L.-Q. Jiang, Z. Fang, X.-K. Li, J. Luo, and S.-P. Fan, "Combination of dilute acid and ionic liquid pretreatments of sugarcane bagasse for glucose by enzymatic hydrolysis," *Process Biochemistry,* vol. 48, no. 12, pp. 1942-1946, 2013.
[100] N. Sritrakul, S. Nitisinprasert, and S. Keawsompong, "Evaluation of dilute acid pretreatment for bioethanol fermentation from sugarcane bagasse pith," *Agriculture and Natural Resources,* vol. 51, no. 6, pp. 512-519, 2017.
[101] C. Cara, E. Ruiz, J. M. Oliva, F. Sáez, and E. Castro, "Conversion of olive tree biomass into fermentable sugars by dilute acid pretreatment and enzymatic saccharification," *Bioresource technology,* vol. 99, no. 6, pp. 1869-1876, 2008.
[102] J. Wang, H. Wang, T. Deng, Z. Liu, and X. Wang, "Time-coursed transcriptome analysis identifies key expressional regulation in growth cessation and dormancy induced by short days in Paulownia," *Scientific reports,* vol. 9, no. 1, pp. 16602, 2019.
[103] Y. Li *et al.*, "Identification of genes related to the phenotypic variations of a synthesized Paulownia (Paulownia tomentosa× Paulownia fortunei) autotetraploid," *Gene,* vol. 553, no. 2, pp. 75-83, 2014.
[104] K. SUGAWARA, K. OMIYA, H. FUJII, S. KATO, and S. SUZUKI, "Development of carbon fixation technology by afforestation of fast-growing paulownia trees: An example in Fukushima prefecture, Japan," *Journal of Arid Land Studies,* vol. 32, no. S, pp. 7-11, 2022.
[105] L. B. Magar *et al.*, "Total biomass carbon sequestration ability under the changing climatic condition by Paulownia tomentosa Steud," *International Journal of Applied Sciences and Biotechnology,* vol. 6, no. 3, pp. 220-226, 2018.
[106] M. Jakubowski, "Cultivation Potential and Uses of Paulownia Wood: A Review. Forests 13 (5), 668," ed, 2022.
[107] M. Abreu *et al.*, "Evaluation of the Potential of Biomass to Energy in Portugal—Conclusions from the CONVERTE Project," *Energies,* vol. 13, no. 4, pp. 937, 2020.
[108] O. Dubova, O. Voitovych, and O. Boika, "Paulownia tomentosa–new species for the industrial landscaping," *Curr. Trends Nat. Sci,* vol. 8, pp. 19-24, 2019.
[109] J. Berdón Berdón, A. Montero Calvo, L. Royano Barroso, A. Parralejo Alcobendas, and J. González Cortés, "Study of Paulownia's Biomass Production in Mérida (Badajoz), Southwestern Spain," *Environ. Ecol. Res,* vol. 5, pp. 521-527, 2017.

[110] C. Huber *et al.*, "Paulownia (Paulownia elongata SY Hu)–importance for forestry and a general screening of technological and material properties," *Wood Material Science & Engineering,* pp. 1-13, 2023.
[111] M. Beel, S. Davis, J. Murphy, and P. Piper, "Product potential of Paulownia timber," *Australian Forestry,* vol. 68, no. 1, pp. 3-8, 2005.
[112] S. El-Showk and N. El-Showk, "The paulownia tree," *An alternative for sustainable forestry, Crop Development, Morocco,* pp. 1-8, 2003.
[113] N. K. Yadav *et al.*, "A review of Paulownia biotechnology: A short rotation, fast growing multipurpose bioenergy tree," *American Journal of Plant Sciences,* vol. 4, no. 11, pp. 2070, 2013.
[114] Q. Wang and J. F. Shogren, "Characteristics of the crop-Paulownia system in China," *Agriculture, ecosystems & environment,* vol. 39, no. 3-4, pp. 145-152, 1992.
[115] D. Dogu, F. D. Tuncer, D. Bakir, and Z. Candan, "Characterizing microscopic changes of paulownia wood under thermal compression," *BioResources,* vol. 12, no. 3, pp. 5279-5295, 2017.
[116] E.-S. Jang and C.-W. Kang, "Sound absorption characteristics of three species (binuang, balsa and paulownia) of low density hardwood," *Holzforschung,* vol. 75, no. 12, pp. 1115-1124, 2021.
[117] P. Li and J. Oda, "Flame retardancy of paulownia wood and its mechanism," *Journal of materials science,* vol. 42, pp. 8544-8550, 2007.
[118] F. Marsal *et al.*, "Biomass yield assessment of five potential energy crops grown in southern Ontario, Canada," *Agroforestry Systems,* vol. 90, pp. 773-783, 2016.
[119] N. Joshee, "Paulownia: A multipurpose tree for rapid lignocellulosic biomass production," *Handbook of Bioenergy Crop Plants, Taylor & Francis, Boca Raton,* pp. 671-686, 2012.
[120] L. Jiménez, A. Rodríguez, J. Ferrer, A. Pérez, and V. Angulo, "La Paulownia: una planta de rápido crecimiento como materia prima para la fabricación de papel," *Afinidad,* vol. 62, no. 516, pp. 100-105, 2005.
[121] A. Kumar, P. Daw, and D. Milstein, "Homogeneous catalysis for sustainable energy: hydrogen and methanol economies, fuels from biomass, and related topics," *Chemical reviews,* vol. 122, no. 1, pp. 385-441, 2021.
[122] S. M. Kim, B. S. Dien, and V. Singh, "Promise of combined hydrothermal/chemical and mechanical refining for pretreatment of woody and herbaceous biomass," *Biotechnology for biofuels,* vol. 9, pp. 1-15, 2016.
[123] J. Rytioja, K. Hildén, J. Yuzon, A. Hatakka, R. P. De Vries, and M. R. Mäkelä, "Plant-polysaccharide-degrading enzymes from basidiomycetes," *Microbiology and Molecular Biology Reviews,* vol. 78, no. 4, pp. 614-649, 2014.
[124] D. Mohnen, "Pectin structure and biosynthesis," *Current opinion in plant biology,* vol. 11, no. 3, pp. 266-277, 2008.
[125] C. T. Brett and K. W. Waldron, *Physiology and biochemistry of plant cell walls*. Springer Science & Business Media, 1996.
[126] R. H. Farmer, *Chemistry in the Utilization of Wood: Pergamon Series of Monographs on Furniture and Timber*. Elsevier, 2013.
[127] E. Sjostrom, *Wood chemistry: fundamentals and applications*. Gulf professional publishing, 1993.
[128] J. Yan, N. Joshee, and S. Liu, "Utilization of hardwood in biorefinery: a kinetic interpretation of pilot-scale hot-water pretreatment of Paulownia elongata woodchips," *Journal of Biobased Materials and Bioenergy,* vol. 10, no. 5, pp. 339-348, 2016.
[129] E. Domínguez, A. Romaní, L. Domingues, and G. Garrote, "Evaluation of strategies for second generation bioethanol production from fast growing biomass Paulownia within a biorefinery scheme," *Applied Energy,* vol. 187, pp. 777-789, 2017.

[130] G. Pablo, B. Gullón, A. Romaní, and G. Garrote, "Fast-growing Paulownia wood fractionation by microwave-assisted hydrothermal treatment: A kinetic assessment," *Bioresource Technology,* vol. 338, pp. 125535, 2021.
[131] S. Caparrós, M. Díaz, J. Ariza, F. López, and L. Jiménez, "New perspectives for Paulownia fortunei L. valorisation of the autohydrolysis and pulping processes," *Bioresource technology,* vol. 99, no. 4, pp. 741-749, 2008.
[132] G. Pablo, A. Pérez-Pérez, G. Garrote, and B. Gullón, "Manufacturing of hemicellulosic oligosaccharides from fast-growing Paulownia wood via autohydrolysis: Microwave versus conventional heating," *Industrial Crops and Products,* vol. 187, pp. 115313, 2022.
[133] E. Domínguez, T. Nóvoa, G. Pablo, G. Garrote, and A. Romaní, "Sequential two-stage autohydrolysis biorefinery for the production of bioethanol from fast-growing Paulownia biomass," *Energy Conversion and Management,* vol. 226, pp. 113517, 2020.
[134] E. Domínguez, P. G. d. Río, A. Romaní, G. Garrote, and L. Domingues, "Hemicellulosic bioethanol production from fast-growing Paulownia biomass," *Processes,* vol. 9, no. 1, pp. 173, 2021.
[135] G. Pablo *et al.*, "Comparative study of biorefinery processes for the valorization of fast-growing Paulownia wood," *Bioresource Technology,* vol. 314, pp. 123722, 2020.
[136] H. Wang, N. Chen, F. Xie, E. Verkasalo, and J. Chu, "Structural properties and hydrolysability of paulownia elongate: the effects of pretreatment methods based on acetic acid and its combination with sodium sulfite or sodium sulfite," *International Journal of Molecular Sciences,* vol. 23, no. 10, pp. 5775, 2022.
[137] P. Sun, M. Heng, S. Sun, and J. Chen, "Direct liquefaction of paulownia in hot compressed water: Influence of catalysts," *Energy,* vol. 35, no. 12, pp. 5421-5429, 2010.
[138] J. Tao *et al.*, "Multi-step separation of different chemical groups from the heavy fraction in biomass fast pyrolysis oil," *Fuel Processing Technology,* vol. 202, pp. 106366, 2020.
[139] L. Haurie, M. P. Giraldo, A. M. Lacasta, J. Montón, and R. Sonnier, "Influence of different parameters in the fire behaviour of seven hardwood species," *Fire safety journal,* vol. 107, pp. 193-201, 2019.
[140] M. Islam, L. Chen, J. Sisler, and K. Tam, "Cellulose nanocrystal (CNC)–inorganic hybrid systems: synthesis, properties and applications," *Journal of Materials Chemistry B,* vol. 6, no. 6, pp. 864-883, 2018.
[141] J. Li, Q. H. Xu, and L. Q. Jin, "Research development on hydrophobic modification of cellulose nanofibrils," *Advanced Materials Research*, vol. 785, pp. 440-443, 2013.
[142] M. Henriksson, G. Henriksson, L. Berglund, and T. Lindström, "An environmentally friendly method for enzyme-assisted preparation of microfibrillated cellulose (MFC) nanofibers," *European Polymer Journal,* vol. 43, no. 8, pp. 3434-3441, 2007.
[143] T. I. Shaheen and H. E. Emam, "Sono-chemical synthesis of cellulose nanocrystals from wood sawdust using acid hydrolysis," *International journal of biological macromolecules,* vol. 107, pp. 1599-1606, 2018.
[144] C. Olsson and G. Westman, "Direct dissolution of cellulose: background, means and applications," *Cellulose-Fundamental Aspects,* vol. 10, pp. 52144, 2013.
[145] R. Bodvik *et al.*, "Aggregation and network formation of aqueous methylcellulose and hydroxypropylmethylcellulose solutions," *Colloids and Surfaces A: Physicochemical and Engineering Aspects,* vol. 354, no. 1-3, pp. 162-171, 2010.
[146] B. Lindman, G. Karlström, and L. Stigsson, "On the mechanism of dissolution of cellulose," *Journal of molecular liquids,* vol. 156, no. 1, pp. 76-81, 2010.
[147] O. A. El Seoud, A. Koschella, L. C. Fidale, S. Dorn, and T. Heinze, "Applications of ionic liquids in carbohydrate chemistry: a window of opportunities," *Biomacromolecules,* vol. 8, no. 9, pp. 2629-2647, 2007.

[148] K. Perepelkin, "Lyocell fibres based on direct dissolution of cellulose in N-methylmorpholine N-oxide: development and prospects," *Fibre Chemistry,* vol. 39, no. 2, pp. 163-172, 2007.
[149] L. Yan and Z. Gao, "Dissolving of cellulose in PEG/NaOH aqueous solution," *Cellulose,* vol. 15, no. 6, pp. 789, 2008.
[150] S. Liu and L. Zhang, "Effects of polymer concentration and coagulation temperature on the properties of regenerated cellulose films prepared from LiOH/urea solution," *Cellulose,* vol. 16, no. 2, pp. 189-198, 2009.
[151] E. Bialik *et al.*, "Ionization of cellobiose in aqueous alkali and the mechanism of cellulose dissolution," *The Journal of Physical Chemistry Letters,* vol. 7, no. 24, pp. 5044-5048, 2016.
[152] L. Alves, B. Medronho, F. E. Antunes, D. Topgaard, and B. Lindman, "Dissolution state of cellulose in aqueous systems. 2. Acidic solvents," *Carbohydrate polymers,* vol. 151, pp. 707-715, 2016.
[153] L. Alves, B. Medronho, F. E. Antunes, D. Topgaard, and B. Lindman, "Dissolution state of cellulose in aqueous systems. 1. Alkaline solvents," *Cellulose,* vol. 23, pp. 247-258, 2016.
[154] R. Alén, "Structure and chemical composition of wood," *Forest products chemistry,* vol. 3, pp. 11-57, 2000.
[155] A. Sundberg and B. Holmbom, "Wood and fibre chemistry," *Laboratory of Forest Products Chemistry, Faculty of Chemical Engeneering, Åbo Akademi University, Åbo,* 2002.
[156] F. Bertaud, A. Sundberg, and B. Holmbom, "Evaluation of acid methanolysis for analysis of wood hemicelluloses and pectins," *Carbohydrate Polymers,* vol. 48, no. 3, pp. 319-324, 2002.
[157] H. Nimz, "Chemistry of potential chromophoric groups in beech lignin," 1973.
[158] C. Cao, L. Xu, Y. He, L. Guo, H. Jin, and Z. Huo, "High-efficiency gasification of wheat straw black liquor in supercritical water at high temperatures for hydrogen production," *Energy & Fuels,* vol. 31, no. 4, pp. 3970-3978, 2017.
[159] R. Oliveira, M. Mateus, and D. Santos, "Chronoamperometric and chronopotentiometric investigation of Kraft black liquor," *International Journal of Hydrogen Energy,* vol. 43, no. 35, pp. 16817-16823, 2018.
[160] H. R. Ghatak, P. Kundu, and S. Kumar, "Thermochemical comparison of lignin separated by electrolysis and acid precipitation from soda black liquor of agricultural residues," *Thermochimica acta,* vol. 502, no. 1-2, pp. 85-89, 2010.
[161] M. Lawoko, G. Henriksson, and G. Gellerstedt, "Characterisation of lignin-carbohydrate complexes (LCCs) of spruce wood (Picea abies L.) isolated with two methods," 2006.
[162] A. Björkman, "Finely divided wood. III. Extraction of lignincarbohydrate complexes with neutral solvents," *Svensk Papperstidning,* vol. 60, pp. 243-251, 1957.
[163] S. Collinson and W. Thielemans, "The catalytic oxidation of biomass to new materials focusing on starch, cellulose and lignin," *Coordination chemistry reviews,* vol. 254, no. 15-16, pp. 1854-1870, 2010.
[164] W. Den, V. K. Sharma, M. Lee, G. Nadadur, and R. S. Varma, "Lignocellulosic biomass transformations via greener oxidative pretreatment processes: access to energy and value-added chemicals," *Frontiers in chemistry,* vol. 6, pp. 141, 2018.
[165] T. A. Elizabeth, K. O. Julius, N. D. Ekaette, S. B. Sudipta, S. Das, and M. Barooah, "Influence of different substrates on lignolytic enzyme production in improved strains of wood ear mushroom (Auricularia species)," 2016.
[166] H. Chen *et al.*, "A review on the pretreatment of lignocellulose for high-value chemicals," *Fuel Processing Technology,* vol. 160, pp. 196-206, 2017.

[167] J. Singh, M. Suhag, and A. Dhaka, "Augmented digestion of lignocellulose by steam explosion, acid and alkaline pretreatment methods: a review," *Carbohydrate polymers,* vol. 117, pp. 624-631, 2015.
[168] E. Shirkavand, S. Baroutian, D. J. Gapes, and B. R. Young, "Combination of fungal and physicochemical processes for lignocellulosic biomass pretreatment–a review," *Renewable and Sustainable Energy Reviews,* vol. 54, pp. 217-234, 2016.
[169] S. S. Hassan, G. A. Williams, and A. K. Jaiswal, "Emerging technologies for the pretreatment of lignocellulosic biomass," *Bioresource technology,* vol. 262, pp. 310-318, 2018.
[170] S. H. Mood *et al.*, "Lignocellulosic biomass to bioethanol, a comprehensive review with a focus on pretreatment," *Renewable and sustainable energy reviews,* vol. 27, pp. 77-93, 2013.
[171] Y. Gao, J. Remón, and A. S. Matharu, "Microwave-assisted hydrothermal treatments for biomass valorisation: a critical review," *Green Chemistry,* vol. 23, no. 10, pp. 3502-3525, 2021.
[172] J. Mata-Alvarez, *Biomethanization of the organic fraction of municipal solid wastes*. IWA publishing, 2002.
[173] H. Hartmann, I. Angelidaki, and B. K. Ahring, "Increase of anaerobic degradation of particulate organic matter in full-scale biogas plants by mechanical maceration," *Water Science and Technology,* vol. 41, no. 3, pp. 145-153, 2000.
[174] V. S. Chang and M. T. Holtzapple, "Fundamental factors affecting biomass enzymatic reactivity," *Twenty-first symposium on biotechnology for fuels and chemicals*, pp. 5-37, 2000.
[175] W. Kenealy, E. Horn, and C. Houtman, "Vapor-phase diethyl oxalate pretreatment of wood chips: Part 1. Energy savings and improved pulps," 2007.
[176] J. Zhu and X. Pan, "Woody biomass pretreatment for cellulosic ethanol production: technology and energy consumption evaluation," *Bioresource technology,* vol. 101, no. 13, pp. 4992-5002, 2010.
[177] A. Barakat, C. Mayer-Laigle, A. Solhy, R. A. Arancon, H. De Vries, and R. Luque, "Mechanical pretreatments of lignocellulosic biomass: towards facile and environmentally sound technologies for biofuels production," *Rsc Advances,* vol. 4, no. 89, pp. 48109-48127, 2014.
[178] M. J. Bussemaker and D. Zhang, "Effect of ultrasound on lignocellulosic biomass as a pretreatment for biorefinery and biofuel applications," *Industrial & Engineering Chemistry Research,* vol. 52, no. 10, pp. 3563-3580, 2013.
[179] F. Yue, W. Lan, A. Zhang, C. Liu, R. Sun, and J. Ye, "Dissolution of holocellulose in ionic liquid assisted with ball-milling pretreatment and ultrasound irradiation," *BioResources,* vol. 7, no. 2, pp. 2199-2208, 2012.
[180] Z. Hu and Z. Wen, "Enhancing enzymatic digestibility of switchgrass by microwave-assisted alkali pretreatment," *Biochemical Engineering Journal,* vol. 38, no. 3, pp. 369-378, 2008.
[181] R. Kumar and C. E. Wyman, "Effects of cellulase and xylanase enzymes on the deconstruction of solids from pretreatment of poplar by leading technologies," *Biotechnology progress,* vol. 25, no. 2, pp. 302-314, 2009.
[182] R. Amirta, T. Tanabe, T. Watanabe, Y. Honda, M. Kuwahara, and T. Watanabe, "Methane fermentation of Japanese cedar wood pretreated with a white rot fungus, Ceriporiopsis subvermispora," *Journal of biotechnology,* vol. 123, no. 1, pp. 71-77, 2006.
[183] T. J. McDonough, "The chemistry of organosolv delignification," 1992.
[184] M. Papatheofanous, E. Billa, D. Koullas, B. Monties, and E. Koukios, "Two-stage acid-catalyzed fractionation of lignocellulosic biomass in aqueous ethanol systems at low temperatures," *Bioresource Technology,* vol. 54, no. 3, pp. 305-310, 1995.

[185] S. Mirmohamadsadeghi, K. Karimi, A. Zamani, H. Amiri, and I. S. Horváth, "Enhanced solid-state biogas production from lignocellulosic biomass by organosolv pretreatment," *BioMed research international,* vol. 2014, 2014.
[186] Y. Sun and J. Cheng, "Hydrolysis of lignocellulosic materials for ethanol production: a review," *Bioresource technology,* vol. 83, no. 1, pp. 1-11, 2002.
[187] E. A. Monyoncho, T. K. Woo, and E. A. Baranova, "Ethanol electrooxidation reaction in alkaline media for direct ethanol fuel cells," 2018.
[188] J. Zhu, X. Pan, G. Wang, and R. Gleisner, "Sulfite pretreatment (SPORL) for robust enzymatic saccharification of spruce and red pine," *Bioresource technology,* vol. 100, no. 8, pp. 2411-2418, 2009.
[189] T. Heinze, K. Schwikal, and S. Barthel, "Ionic liquids as reaction medium in cellulose functionalization," *Macromolecular bioscience,* vol. 5, no. 6, pp. 520-525, 2005.
[190] T.-A. D. Nguyen *et al.*, "Pretreatment of rice straw with ammonia and ionic liquid for lignocellulose conversion to fermentable sugars," *Bioresource Technology,* vol. 101, no. 19, pp. 7432-7438, 2010.
[191] A. Hendriks and G. Zeeman, "Pretreatments to enhance the digestibility of lignocellulosic biomass," *Bioresource technology,* vol. 100, no. 1, pp. 10-18, 2009.
[192] J. D. McMillan, "Pretreatment of lignocellulosic biomass," ACS Publications, 1994.
[193] M. Feng, R. Qu, Z. Wei, L. Wang, P. Sun, and Z. Wang, "Characterization of the thermolysis products of Nafion membrane: A potential source of perfluorinated compounds in the environment," *Scientific reports,* vol. 5, pp. 9859, 2015.
[194] S. L. James *et al.*, "Mechanochemistry: opportunities for new and cleaner synthesis," *Chemical Society Reviews,* vol. 41, no. 1, pp. 413-447, 2012.
[195] S. M. Hick *et al.*, "Mechanocatalysis for biomass-derived chemicals and fuels," *Green Chemistry,* vol. 12, no. 3, pp. 468-474, 2010.
[196] R. A. Sheldon, "Green solvents for sustainable organic synthesis: state of the art," *Green Chemistry,* vol. 7, no. 5, pp. 267-278, 2005.
[197] H. Kobayashi, M. Yabushita, T. Komanoya, K. Hara, I. Fujita, and A. Fukuoka, "High-yielding one-pot synthesis of glucose from cellulose using simple activated carbons and trace hydrochloric acid," *Acs Catalysis,* vol. 3, no. 4, pp. 581-587, 2013.
[198] N. Meine, R. Rinaldi, and F. Schüth, "Solvent‐Free Catalytic Depolymerization of Cellulose to Water‐Soluble Oligosaccharides," *ChemSusChem,* vol. 5, no. 8, pp. 1449-1454, 2012.
[199] E. Sjöman, M. Mänttäri, M. Nyström, H. Koivikko, and H. Heikkilä, "Separation of xylose from glucose by nanofiltration from concentrated monosaccharide solutions," *Journal of Membrane Science,* vol. 292, no. 1-2, pp. 106-115, 2007.
[200] L. Schneider, J. Haverinen, M. Jaakkola, and U. Lassi, "Solid acid-catalyzed depolymerization of barley straw driven by ball milling," *Bioresource technology,* vol. 206, pp. 204-210, 2016.
[201] T. Kleine, J. Buendia, and C. Bolm, "Mechanochemical degradation of lignin and wood by solvent-free grinding in a reactive medium," *Green chemistry,* vol. 15, no. 1, pp. 160-166, 2013.
[202] W.-H. Chen, Y.-Y. Xu, W.-S. Hwang, and J.-B. Wang, "Pretreatment of rice straw using an extrusion/extraction process at bench-scale for producing cellulosic ethanol," *Bioresource Technology,* vol. 102, no. 22, pp. 10451-10458, 2011.
[203] M. Carr and W. Doane, "Modification of wheat straw in a high‐shear mixer," *Biotechnology and bioengineering,* vol. 26, no. 10, pp. 1252-1257, 1984.
[204] S. Zhang, D. R. Keshwani, Y. Xu, and M. A. Hanna, "Alkali combined extrusion pretreatment of corn stover to enhance enzyme saccharification," *Industrial Crops and Products,* vol. 37, no. 1, pp. 352-357, 2012.

[205] K. CHINNADURAI and K. MUTHUKUMARAPPAN, "Combined Effect of Alkali Soaking and Extrusion Conditions on Fermentable Sugar Yields from Switchgrass and Prairie Cord Grass," *Reno, Nevada,* pp. 1, 2009.
[206] C. Karunanithy and K. Muthukumarappan, "Optimization of alkali, big bluestem particle size, and extruder parameters for maximum enzymatic sugar recovery using response surface methodology," *BioResources,* vol. 6, no. 1, pp. 762-790, 2011.
[207] B. E. Dale, J. Weaver, and F. M. Byers, "Extrusion processing for ammonia fiber explosion (AFEX)," *Applied Biochemistry and Biotechnology,* vol. 77, pp. 35-45, 1999.
[208] A. S. A. Da Silva, R. S. S. Teixeira, T. Endo, E. P. Bon, and S.-H. Lee, "Continuous pretreatment of sugarcane bagasse at high loading in an ionic liquid using a twin-screw extruder," *Green Chemistry,* vol. 15, no. 7, pp. 1991-2001, 2013.
[209] S. Miller and R. Hester, "Concentrated acid conversion of pine sawdust to sugars. Part II: High-temperature batch reactor kinetics of pretreated pine sawdust," *Chemical Engineering Communications,* vol. 194, no. 1, pp. 103-116, 2007.
[210] S. N'Diaye, L. Rigal, P. Larocque, and P. Vidal, "Extraction of hemicelluloses from poplar, Populus tremuloides, using an extruder-type twin-screw reactor: a feasibility study," *Bioresource Technology,* vol. 57, no. 1, pp. 61-67, 1996.
[211] F. Shen *et al.*, "Recent advances in mechanochemical production of chemicals and carbon materials from sustainable biomass resources," *Renewable and sustainable energy reviews,* vol. 130, pp. 109944, 2020.
[212] H. Tarkow and W. C. FEIST, "A mechanism for improving the digestibility of lignocellulosic materials with dilute alkali and liquid ammonia," ACS Publications, 1969.
[213] A. Gollakota, N. Kishore, and S. Gu, "A review on hydrothermal liquefaction of biomass," *Renewable and Sustainable Energy Reviews,* vol. 81, pp. 1378-1392, 2018.
[214] F. Jin and H. Enomoto, "Rapid and highly selective conversion of biomass into value-added products in hydrothermal conditions: chemistry of acid/base-catalysed and oxidation reactions," *Energy & Environmental Science,* vol. 4, no. 2, pp. 382-397, 2011.
[215] K. Byrappa and M. Yoshimura, *Handbook of hydrothermal technology*. William Andrew, 2012.
[216] F. J. Wolfaardt, L. G. L. Fernandes, S. K. C. Oliveira, X. Duret, J. F. Görgens, and J.-M. Lavoie, "Recovery approaches for sulfuric acid from the concentrated acid hydrolysis of lignocellulosic feedstocks: A mini-review," *Energy Conversion and Management: X,* vol. 10, pp. 100074, 2021.
[217] A. G. Demesa, A. Laari, M. Sillanpää, and T. Koiranen, "Valorization of lignin by partial wet oxidation using sustainable heteropoly acid catalysts," *Molecules,* vol. 22, no. 10, pp. 1625, 2017.
[218] S. Mallik, K. Parida, and S. Dash, "Studies on heteropoly acid supported zirconia: III: Oxidative bromination of phenol using phosphotungstic acid supported on zirconia," *Journal of Molecular Catalysis A: Chemical,* vol. 261, no. 2, pp. 172-179, 2007.
[219] Z. Zhou, D. Liu, and X. Zhao, "Conversion of lignocellulose to biofuels and chemicals via sugar platform: an updated review on chemistry and mechanisms of acid hydrolysis of lignocellulose," *Renewable and Sustainable Energy Reviews,* vol. 146, pp. 111169, 2021.
[220] F. K. Kazi *et al.*, "Techno-economic comparison of process technologies for biochemical ethanol production from corn stover," *Fuel,* vol. 89, pp. S20-S28, 2010.
[221] S. C. Yat, A. Berger, and D. R. Shonnard, "Kinetic characterization for dilute sulfuric acid hydrolysis of timber varieties and switchgrass," *Bioresource technology,* vol. 99, no. 9, pp. 3855-3863, 2008.
[222] Y. H. Jung, I. J. Kim, H. K. Kim, and K. H. Kim, "Dilute acid pretreatment of lignocellulose for whole slurry ethanol fermentation," *Bioresource technology,* vol. 132, pp. 109-114, 2013.

[223] B.-Y. Cai, J.-P. Ge, H.-Z. Ling, K.-K. Cheng, and W.-X. Ping, "Statistical optimization of dilute sulfuric acid pretreatment of corncob for xylose recovery and ethanol production," *Biomass and Bioenergy,* vol. 36, pp. 250-257, 2012.
[224] X. Yang, N. Li, X. Lin, X. Pan, and Y. Zhou, "Selective cleavage of the aryl ether bonds in lignin for depolymerization by acidic lithium bromide molten salt hydrate under mild conditions," *Journal of agricultural and food chemistry,* vol. 64, no. 44, pp. 8379-8387, 2016.
[225] C. Li, Q. Wang, and Z. K. Zhao, "Acid in ionic liquid: An efficient system for hydrolysis of lignocellulose," *Green chemistry,* vol. 10, no. 2, pp. 177-182, 2008.
[226] J. B. Binder and R. T. Raines, "Fermentable sugars by chemical hydrolysis of biomass," *Proceedings of the National Academy of Sciences,* vol. 107, no. 10, pp. 4516-4521, 2010.
[227] K.-i. Shimizu, H. Furukawa, N. Kobayashi, Y. Itaya, and A. Satsuma, "Effects of Brønsted and Lewis acidities on activity and selectivity of heteropolyacid-based catalysts for hydrolysis of cellobiose and cellulose," *Green Chemistry,* vol. 11, no. 10, pp. 1627-1632, 2009.
[228] Y. Ogasawara, S. Itagaki, K. Yamaguchi, and N. Mizuno, "Saccharification of natural lignocellulose biomass and polysaccharides by highly negatively charged heteropolyacids in concentrated aqueous solution," *ChemSusChem,* vol. 4, no. 4, pp. 519-525, 2011.
[229] X. Li, Y. Jiang, L. Wang, L. Meng, W. Wang, and X. Mu, "Effective low-temperature hydrolysis of cellulose catalyzed by concentrated H 3 PW 12 O 40 under microwave irradiation," *Rsc Advances,* vol. 2, no. 17, pp. 6921-6925, 2012.
[230] I. Kurnia *et al.*, "Hydrolysis of cellulose and woody biomass over sustainable weak-acid carbon catalysts from alkaline lignin," *Fuel Processing Technology,* vol. 196, pp. 106175, 2019.
[231] S. Li, Z. Gu, B. E. Bjornson, and A. Muthukumarappan, "Biochar based solid acid catalyst hydrolyze biomass," *Journal of Environmental Chemical Engineering,* vol. 1, no. 4, pp. 1174-1181, 2013.
[232] S. Suganuma *et al.*, "Hydrolysis of cellulose by amorphous carbon bearing SO3H, COOH, and OH groups," *Journal of the American Chemical Society,* vol. 130, no. 38, pp. 12787-12793, 2008.
[233] D.-m. Lai, L. Deng, Q.-x. Guo, and Y. Fu, "Hydrolysis of biomass by magnetic solid acid," *Energy & Environmental Science,* vol. 4, no. 9, pp. 3552-3557, 2011.
[234] D. Beneroso, T. Monti, E. Kostas, and J. Robinson, "Microwave pyrolysis of biomass for bio-oil production: scalable processing concepts," *Chemical Engineering Journal,* vol. 316, pp. 481-498, 2017.
[235] A. Hasna, "Microwave processing applications in chemical engineering: cost analysis," *Journal of Applied Sciences,* vol. 11, no. 21, pp. 3613-3618, 2011.
[236] H. Li, Y. Qu, Y. Yang, S. Chang, and J. Xu, "Microwave irradiation–A green and efficient way to pretreat biomass," *Bioresource technology,* vol. 199, pp. 34-41, 2016.
[237] P. G. Del Rio, B. Gullón, A. Romaní, and G. Garrote, "Fast-growing Paulownia wood fractionation by microwave-assisted hydrothermal treatment: A kinetic assessment," *Bioresource Technology,* vol. 338, pp. 125535, 2021.
[238] Z. Zhu *et al.*, "Efficient sugar production from sugarcane bagasse by microwave assisted acid and alkali pretreatment," *Biomass and Bioenergy,* vol. 93, pp. 269-278, 2016.
[239] H. B. Sharma, A. K. Sarmah, and B. Dubey, "Hydrothermal carbonization of renewable waste biomass for solid biofuel production: A discussion on process mechanism, the influence of process parameters, environmental performance and fuel properties of hydrochar," *Renewable and sustainable energy reviews,* vol. 123, pp. 109761, 2020.
[240] H. A. Ruiz, M. H. Thomsen, and H. L. Trajano, "Hydrothermal processing in biorefineries," *Production of bioethanol and high added-value compounds of second and third generation biomass,* 2017.

[241] S. Kumar and F. Barla, *Sub-and supercritical hydrothermal technology: industrial applications*. CRC Press, 2019.
[242] D. Dallinger and C. O. Kappe, "Microwave-assisted synthesis in water as solvent," *Chemical reviews,* vol. 107, no. 6, pp. 2563-2591, 2007.
[243] S. Nizamuddin *et al.*, "Upgradation of chemical, fuel, thermal, and structural properties of rice husk through microwave-assisted hydrothermal carbonization," *Environmental Science and Pollution Research,* vol. 25, pp. 17529-17539, 2018.
[244] A. Lorente, J. Remón, V. L. Budarin, P. Sánchez-Verdú, A. Moreno, and J. H. Clark, "Analysis and optimisation of a novel “bio-brewery” approach: Production of bio-fuels and bio-chemicals by microwave-assisted, hydrothermal liquefaction of brewers’ spent grains," *Energy Conversion and Management,* vol. 185, pp. 410-430, 2019.
[245] B. Zhang, B. K. Biswal, J. Zhang, and R. Balasubramanian, "Hydrothermal Treatment of Biomass Feedstocks for Sustainable Production of Chemicals, Fuels, and Materials: Progress and Perspectives," *Chemical Reviews,* 2023.
[246] P. Intanakul, M. Krairiksh, and P. Kitchaiya, "Enhancement of enzymatic hydrolysis of lignocellulosic wastes by microwave pretreatment under atmospheric pressure," *Journal of wood chemistry and technology,* vol. 23, no. 2, pp. 217-225, 2003.
[247] J. Bian, P. Peng, F. Peng, X. Xiao, F. Xu, and R.-C. Sun, "Microwave-assisted acid hydrolysis to produce xylooligosaccharides from sugarcane bagasse hemicelluloses," *Food chemistry,* vol. 156, pp. 7-13, 2014.
[248] P. Binod, K. Satyanagalakshmi, R. Sindhu, K. U. Janu, R. K. Sukumaran, and A. Pandey, "Short duration microwave assisted pretreatment enhances the enzymatic saccharification and fermentable sugar yield from sugarcane bagasse," *Renewable Energy,* vol. 37, no. 1, pp. 109-116, 2012.
[249] Y. Shao *et al.*, "Acidic seawater improved 5-hydroxymethylfurfural yield from sugarcane bagasse under microwave hydrothermal liquefaction," *Environmental Research,* vol. 184, pp. 109340, 2020.
[250] C. Sasaki, A. Kiyokawa, C. Asada, and Y. Nakamura, "Glucose and valuable chemicals production from cotton waste using hydrothermal method," *Waste and biomass valorization,* vol. 10, pp. 599-607, 2019.
[251] C. Sasaki, H. Negoro, C. Asada, and Y. Nakamura, "Microwave-assisted glucose production from bode (Styrax tonkinensis) woody biomass for bioethanol production," *Journal of Material Cycles and Waste Management,* vol. 21, pp. 201-204, 2019.
[252] J.-K. Xu, J.-H. Chen, and R.-C. Sun, "Hydrothermal microwave valorization of eucalyptus using acidic ionic liquid as catalyst toward a green biorefinery scenario," *Bioresource technology,* vol. 193, pp. 119-127, 2015.
[253] C. Xu, J. Lan, J. Ye, Y. Yang, K. Huang, and H. Zhu, "Design of continuous-flow microwave reactor based on a leaky waveguide," *Chemical Engineering Journal,* vol. 452, pp. 139690, 2023.
[254] R. LeRoy, "Industrial water electrolysis: present and future," *International Journal of Hydrogen Energy,* vol. 8, no. 6, pp. 401-417, 1983.
[255] J. Wang, F. Xu, H. Jin, Y. Chen, and Y. Wang, "Non‐noble metal‐based carbon composites in hydrogen evolution reaction: fundamentals to applications," *Advanced materials,* vol. 29, no. 14, pp. 1605838, 2017.
[256] J. O. M. Bockris and T. N. Veziroglu, "Estimates of the price of hydrogen as a medium for wind and solar sources," *International Journal of Hydrogen Energy,* vol. 32, no. 12, pp. 1605-1610, 2007.
[257] R. F. De Souza, J. C. Padilha, R. S. Gonçalves, M. O. De Souza, and J. Rault-Berthelot, "Electrochemical hydrogen production from water electrolysis using ionic liquid as electrolytes: towards the best device," *Journal of Power Sources,* vol. 164, no. 2, pp. 792-798, 2007.

[258] E. Pomerantseva, C. Resini, K. Kovnir, and Y. V. Kolen'ko, "Emerging nanostructured electrode materials for water electrolysis and rechargeable beyond Li-ion batteries," *Advances in Physics: X,* vol. 2, no. 2, pp. 211-253, 2017.
[259] D. M. Santos, C. A. Sequeira, and J. L. Figueiredo, "Hydrogen production by alkaline water electrolysis," *Química Nova,* vol. 36, no. 8, pp. 1176-1193, 2013.
[260] M. Fang, G. Dong, R. Wei, and J. C. Ho, "Hierarchical nanostructures: design for sustainable water splitting," *Advanced Energy Materials,* vol. 7, no. 23, pp. 1700559, 2017.
[261] I. C. Man *et al.*, "Universality in oxygen evolution electrocatalysis on oxide surfaces," *ChemCatChem,* vol. 3, no. 7, pp. 1159-1165, 2011.
[262] Z. W. Seh, J. Kibsgaard, C. F. Dickens, I. Chorkendorff, J. K. Nørskov, and T. F. Jaramillo, "Combining theory and experiment in electrocatalysis: Insights into materials design," *Science,* vol. 355, no. 6321, 2017.
[263] M. Tahir *et al.*, "Electrocatalytic oxygen evolution reaction for energy conversion and storage: a comprehensive review," *Nano Energy,* vol. 37, pp. 136-157, 2017.
[264] P. Yu *et al.*, "Earth abundant materials beyond transition metal dichalcogenides: a focus on electrocatalyzing hydrogen evolution reaction," *Nano Energy,* vol. 58, pp. 244-276, 2019.
[265] D. Antipin and M. Risch, "Trends of epitaxial perovskite oxide films catalyzing the oxygen evolution reaction in alkaline media," *Journal of Physics: Energy,* vol. 2, no. 3, pp. 032003, 2020.
[266] Y. Sugano, M. d. Vestergaard, H. Yoshikawa, M. Saito, and E. Tamiya, "Direct Electrochemical Oxidation of Cellulose: A Cellulose‐Based Fuel Cell System," *Electroanalysis,* vol. 22, no. 15, pp. 1688-1694, 2010.
[267] O. Movil, M. Garlock, and J. A. Staser, "Non-precious metal nanoparticle electrocatalysts for electrochemical modification of lignin for low-energy and cost-effective production of hydrogen," *International Journal of Hydrogen Energy,* vol. 40, no. 13, pp. 4519-4530, 2015.
[268] A. Isogai and R. Atalla, "Dissolution of cellulose in aqueous NaOH solutions," *Cellulose,* vol. 5, pp. 309-319, 1998.
[269] L. Yan and X. Qi, "Degradation of cellulose to organic acids in its homogeneous alkaline aqueous solution," *ACS Sustainable Chemistry & Engineering,* vol. 2, no. 4, pp. 897-901, 2014.
[270] P. Parpot, A. Bettencourt, A. Carvalho, and E. Belgsir, "Biomass conversion: attempted electrooxidation of lignin for vanillin production," *Journal of applied electrochemistry,* vol. 30, pp. 727-731, 2000.
[271] T. Hibino, K. Kobayashi, M. Nagao, and S. Teranishi, "Hydrogen production by direct lignin electrolysis at intermediate temperatures," *ChemElectroChem,* vol. 4, no. 12, pp. 3032-3036, 2017.
[272] M. Rafiee, M. Alherech, S. D. Karlen, and S. S. Stahl, "Electrochemical aminoxyl-mediated oxidation of primary alcohols in lignin to carboxylic acids: Polymer modification and depolymerization," *Journal of the American Chemical Society,* vol. 141, no. 38, pp. 15266-15276, 2019.
[273] S. Li and X. Song, "Study on the preparation and production factors of a direct lignocellulose biomass fuel cell," *Journal of Electroanalytical Chemistry,* vol. 810, pp. 55-61, 2018.
[274] H. Xiao, M. Wu, and G. Zhao, "Electrocatalytic oxidation of cellulose to gluconate on carbon aerogel supported gold nanoparticles anode in alkaline medium," *Catalysts,* vol. 6, no. 1, pp. 5, 2015.
[275] X. Tan, W. Deng, M. Liu, Q. Zhang, and Y. Wang, "Carbon nanotube-supported gold nanoparticles as efficient catalysts for selective oxidation of cellobiose into gluconic acid in aqueous medium," *Chemical communications,* no. 46, pp. 7179-7181, 2009.

[276] D. An, A. Ye, W. Deng, Q. Zhang, and Y. Wang, "Selective conversion of cellobiose and cellulose into gluconic acid in water in the presence of oxygen, catalyzed by polyoxometalate-supported gold nanoparticles," *Chemistry–A European Journal,* vol. 18, no. 10, pp. 2938-2947, 2012.
[277] M. Wu, Y. Jin, G. Zhao, M. Li, and D. Li, "Electrosorption-promoted photodegradation of opaque wastewater on a novel TiO2/carbon aerogel electrode," *Environmental science & technology,* vol. 44, no. 5, pp. 1780-1785, 2010.
[278] C. Ma, W. Xue, J. Li, W. Xing, and Z. Hao, "Mesoporous carbon-confined Au catalysts with superior activity for selective oxidation of glucose to gluconic acid," *Green Chemistry,* vol. 15, no. 4, pp. 1035-1041, 2013.
[279] Y. Sugano *et al.*, "Specific electrocatalytic oxidation of cellulose at carbon electrodes modified by gold nanoparticles," *ChemCatChem,* vol. 8, no. 14, pp. 2401-2405, 2016.
[280] D. Meng, G. Li, Z. Liu, and F. Yang, "Study of depolymerization of cotton cellulose by Pb/PbO2 anode electrochemical catalysis in sulfuric acid solution," *Polymer degradation and stability,* vol. 96, no. 7, pp. 1173-1178, 2011.
[281] A. J. Domb, J. Kost, and D. Wiseman, *Handbook of biodegradable polymers*. CRC press, 1998.
[282] H. T. Brown, "XX.—On the electrolysis of sugar solutions.(Preliminary notice)," *Journal of the Chemical Society,* vol. 25, pp. 578-579, 1872.
[283] R. Zółtaszek, M. Hanausek, Z. M. Kiliańska, and Z. Walaszek, "The biological role of D-glucaric acid and its derivatives: potential use in medicine," *Postepy higieny i medycyny doswiadczalnej (Online),* vol. 62, pp. 451-462, 2008.
[284] T. Werpy and G. Petersen, "Top value added chemicals from biomass: volume I--results of screening for potential candidates from sugars and synthesis gas," National Renewable Energy Lab., Golden, CO (US), 2004.
[285] T. Mehtiö, M. Toivari, M. G. Wiebe, A. Harlin, M. Penttilä, and A. Koivula, "Production and applications of carbohydrate-derived sugar acids as generic biobased chemicals," *Critical reviews in biotechnology,* vol. 36, no. 5, pp. 904-916, 2016.
[286] T. N. Smith, K. Hash, C.-L. Davey, H. Mills, H. Williams, and D. E. Kiely, "Modifications in the nitric acid oxidation of D-glucose," *Carbohydrate research,* vol. 350, pp. 6-13, 2012.
[287] W. Hou and J. Bao, "Evaluation of cement retarding performance of cellulosic sugar acids," *Construction and Building Materials,* vol. 202, pp. 522-527, 2019.
[288] S. Ramachandran, P. Fontanille, A. Pandey, and C. Larroche, "Gluconic acid: properties, applications and microbial production," *Food Technology & Biotechnology,* vol. 44, no. 2, 2006.
[289] G. C. Hayes and C. R. Becer, "Levulinic acid: A sustainable platform chemical for novel polymer architectures," *Polymer Chemistry,* vol. 11, no. 25, pp. 4068-4077, 2020.
[290] J. J. Bozell *et al.*, "Production of levulinic acid and use as a platform chemical for derived products," *Resources, conservation and recycling,* vol. 28, no. 3-4, pp. 227-239, 2000.
[291] J. Lewkowski, "Synthesis, chemistry and applications of 5-hydroxymethylfurfural and its derivatives," *Arkivoc,* vol. 1, pp. 17-54, 2001.
[292] D. Bin *et al.*, "Controllable oxidation of glucose to gluconic acid and glucaric acid using an electrocatalytic reactor," *Electrochimica Acta,* vol. 130, pp. 170-178, 2014.
[293] S. Solmi, C. Morreale, F. Ospitali, S. Agnoli, and F. Cavani, "Oxidation of d-Glucose to Glucaric Acid Using Au/C Catalysts," *ChemCatChem,* vol. 9, no. 14, pp. 2797-2806, 2017.
[294] G. Moggia, T. Kenis, N. Daems, and T. Breugelmans, "Electrochemical oxidation of d-glucose in alkaline medium: Impact of oxidation potential and chemical side reactions on the selectivity to d-gluconic and d-glucaric acid," *ChemElectroChem,* vol. 7, no. 1, pp. 86-95, 2020.

[295] A. A. Marianou, C. M. Michailof, A. Pineda, E. F. Iliopoulou, K. S. Triantafyllidis, and A. A. Lappas, "Glucose to fructose isomerization in aqueous media over homogeneous and heterogeneous catalysts," *ChemCatChem,* vol. 8, no. 6, pp. 1100-1110, 2016.

[296] G. Moggia, J. Schalck, N. Daems, and T. Breugelmans, "Two-steps synthesis of D-glucaric acid via D-gluconic acid by electrocatalytic oxidation of D-glucose on gold electrode: Influence of operational parameters," *Electrochimica Acta,* vol. 374, pp. 137852, 2021.

[297] M. Tominaga, T. Shimazoe, M. Nagashima, and I. Taniguchi, "Electrocatalytic oxidation of glucose at gold nanoparticle-modified carbon electrodes in alkaline and neutral solutions," *Electrochemistry Communications,* vol. 7, no. 2, pp. 189-193, 2005.

[298] W.-J. Liu *et al.*, "Efficient electrochemical production of glucaric acid and H2 via glucose electrolysis," *Nature communications,* vol. 11, no. 1, pp. 265, 2020.

[299] N. Neha, B. Kouamé, T. Rafaïdeen, S. Baranton, and C. Coutanceau, "Remarkably efficient carbon-supported nanostructured platinum-bismuth catalysts for the selective electrooxidation of glucose and methyl-glucoside," *Electrocatalysis,* vol. 12, pp. 1-14, 2021.

[300] J. Rao, G. Richter, F. Von Sturm, and E. Weidlich, "The performance of glucose electrodes and the characteristics of different biofuel cell constructions," *Bioelectrochemistry and Bioenergetics,* vol. 3, no. 1, pp. 139-150, 1976.

[301] N. Poulopoulou *et al.*, "Sustainable plastics from biomass: Blends of polyesters based on 2, 5-furandicarboxylic acid," *Polymers,* vol. 12, no. 1, pp. 225, 2020.

[302] P. B. Smith, "Bio-based sources for terephthalic acid," *Green polymer chemistry: Biobased materials and biocatalysis*, pp. 453-469, 2015.

[303] S. Rajendran *et al.*, "Programmed photodegradation of polymeric/oligomeric materials derived from renewable bioresources," *Angewandte Chemie,* vol. 127, no. 4, pp. 1175-1179, 2015.

[304] M. Sajid, X. Zhao, and D. Liu, "Production of 2, 5-furandicarboxylic acid (FDCA) from 5-hydroxymethylfurfural (HMF): recent progress focusing on the chemical-catalytic routes," *Green chemistry,* vol. 20, no. 24, pp. 5427-5453, 2018.

[305] W.-J. Liu, L. Dang, Z. Xu, H.-Q. Yu, S. Jin, and G. W. Huber, "Electrochemical oxidation of 5-hydroxymethylfurfural with NiFe layered double hydroxide (LDH) nanosheet catalysts," *ACS Catalysis,* vol. 8, no. 6, pp. 5533-5541, 2018.

[306] J. Weidner *et al.*, "Cobalt–metalloid alloys for electrochemical oxidation of 5-hydroxymethylfurfural as an alternative anode reaction in lieu of oxygen evolution during water splitting," *Beilstein journal of organic chemistry,* vol. 14, no. 1, pp. 1436-1445, 2018.

[307] D.-H. Nam, B. J. Taitt, and K.-S. Choi, "Copper-based catalytic anodes to produce 2, 5-furandicarboxylic acid, a biomass-derived alternative to terephthalic acid," *Acs Catalysis,* vol. 8, no. 2, pp. 1197-1206, 2018.

[308] B. J. Taitt, D.-H. Nam, and K.-S. Choi, "A comparative study of nickel, cobalt, and iron oxyhydroxide anodes for the electrochemical oxidation of 5-hydroxymethylfurfural to 2, 5-furandicarboxylic acid," *Acs Catalysis,* vol. 9, no. 1, pp. 660-670, 2018.

[309] M. J. Kang, H. Park, J. Jegal, S. Y. Hwang, Y. S. Kang, and H. G. Cha, "Electrocatalysis of 5-hydroxymethylfurfural at cobalt based spinel catalysts with filamentous nanoarchitecture in alkaline media," *Applied Catalysis B: Environmental,* vol. 242, pp. 85-91, 2019.

[310] M. Cai, S. Ding, B. Gibbons, X. Yang, M. C. Kessinger, and A. J. Morris, "Nickel (ii)-modified covalent-organic framework film for electrocatalytic oxidation of 5-hydroxymethylfurfural (HMF)," *Chemical Communications,* vol. 56, no. 92, pp. 14361-14364, 2020.

[311] X. Huang *et al.*, "Enhancing the electrocatalytic activity of CoO for the oxidation of 5-hydroxymethylfurfural by introducing oxygen vacancies," *Green Chemistry,* vol. 22, no. 3, pp. 843-849, 2020.
[312] K. Hu, M. Zhang, B. Liu, Z. Yang, R. Li, and K. Yan, "Efficient electrochemical oxidation of 5-hydroxymethylfurfural to 2, 5-furandicarboxylic acid using the facilely synthesized 3D porous WO3/Ni electrode," *Molecular Catalysis,* vol. 504, pp. 111459, 2021.
[313] W. Wang, F. Kong, Z. Zhang, L. Yang, and M. Wang, "Sulfidation of nickel foam with enhanced electrocatalytic oxidation of 5-hydroxymethylfurfural to 2, 5-furandicarboxylic acid," *Dalton Transactions,* vol. 50, no. 31, pp. 10922-10927, 2021.
[314] S. R. Kubota and K. S. Choi, "Electrochemical Oxidation of 5‐Hydroxymethylfurfural to 2, 5‐Furandicarboxylic Acid (FDCA) in Acidic Media Enabling Spontaneous FDCA Separation," *ChemSusChem,* vol. 11, no. 13, pp. 2138-2145, 2018.
[315] T. R. dos Santos, P. Nilges, W. Sauter, F. Harnisch, and U. Schröder, "Electrochemistry for the generation of renewable chemicals: electrochemical conversion of levulinic acid," *Rsc Advances,* vol. 5, no. 34, pp. 26634-26643, 2015.
[316] M. Simões, S. Baranton, and C. Coutanceau, "Electrochemical valorisation of glycerol," *ChemSusChem,* vol. 5, no. 11, pp. 2106-2124, 2012.
[317] L. Du, Y. Shao, J. Sun, G. Yin, C. Du, and Y. Wang, "Electrocatalytic valorisation of biomass derived chemicals," *Catalysis Science & Technology,* vol. 8, no. 13, pp. 3216-3232, 2018.
[318] S. A. N. M. Rahim *et al.*, "A review of recent developments on kinetics parameters for glycerol electrochemical conversion–A by-product of biodiesel," *Science of the Total Environment,* vol. 705, pp. 135137, 2020.
[319] C. Liu, M. Hirohara, T. Maekawa, R. Chang, T. Hayashi, and C.-Y. Chiang, "Selective electro-oxidation of glycerol to dihydroxyacetone by a non-precious electrocatalyst–CuO," *Applied Catalysis B: Environmental,* vol. 265, pp. 118543, 2020.
[320] B. Katryniok *et al.*, "Selective catalytic oxidation of glycerol: perspectives for high value chemicals," *Green Chemistry,* vol. 13, no. 8, pp. 1960-1979, 2011.
[321] T.-G. Vo, P.-Y. Ho, and C.-Y. Chiang, "Operando mechanistic studies of selective oxidation of glycerol to dihydroxyacetone over amorphous cobalt oxide," *Applied Catalysis B: Environmental,* vol. 300, pp. 120723, 2022.
[322] Y. Kwon, E. de Jong, J. K. van der Waal, and M. T. Koper, "Selective electrocatalytic oxidation of sorbitol to fructose and sorbose," *ChemSusChem,* vol. 8, no. 6, pp. 970-973, 2015.
[323] J. Döbereiner, "Ueber die medicinische und chemische Anwendung und die vortheilhafte Darstellung der Ameisensäure," *Annalen der Pharmacie,* vol. 3, no. 2, pp. 141-146, 1832.
[324] P. Nilges and U. Schröder, "Electrochemistry for biofuel generation: production of furans by electrocatalytic hydrogenation of furfurals," *Energy & Environmental Science,* vol. 6, no. 10, pp. 2925-2931, 2013.
[325] S. R. Kubota and K.-S. Choi, "Electrochemical valorization of furfural to maleic acid," *ACS Sustainable Chemistry & Engineering,* vol. 6, no. 8, pp. 9596-9600, 2018.
[326] A. M. Román, N. Agrawal, J. C. Hasse, M. J. Janik, J. W. Medlin, and A. Holewinski, "Electro-oxidation of furfural on gold is limited by furoate self-assembly," *Journal of Catalysis,* vol. 391, pp. 327-335, 2020.
[327] F. Yang, Q. Zhang, H.-X. Fan, Y. Li, and G. Li, "Electrochemical control of the conversion of cellulose oligosaccharides into glucose," *Journal of Industrial and Engineering Chemistry,* vol. 20, no. 5, pp. 3487-3492, 2014.
[328] Y. Kwon, E. de Jong, S. Raoufmoghaddam, and M. T. Koper, "Electrocatalytic Hydrogenation of 5‐Hydroxymethylfurfural in the Absence and Presence of Glucose," *ChemSusChem,* vol. 6, no. 9, pp. 1659-1667, 2013.

[329] Y. Kwon, Y. Y. Birdja, S. Raoufmoghaddam, and M. T. Koper, "Electrocatalytic hydrogenation of 5-hydroxymethylfurfural in acidic solution," *ChemSusChem,* vol. 8, no. 10, pp. 1745-1751, 2015.

[330] G. Tian, R. Daniel, H. Li, H. Xu, S. Shuai, and P. Richards, "Laminar burning velocities of 2, 5-dimethylfuran compared with ethanol and gasoline," *Energy & Fuels,* vol. 24, no. 7, pp. 3898-3905, 2010.

[331] Y.-R. Zhang, B.-X. Wang, L. Qin, Q. Li, and Y.-M. Fan, "A non-noble bimetallic alloy in the highly selective electrochemical synthesis of the biofuel 2, 5-dimethylfuran from 5-hydroxymethylfurfural," *Green Chemistry,* vol. 21, no. 5, pp. 1108-1113, 2019.

[332] X. H. Chadderdon, D. J. Chadderdon, T. Pfennig, B. H. Shanks, and W. Li, "Paired electrocatalytic hydrogenation and oxidation of 5-(hydroxymethyl) furfural for efficient production of biomass-derived monomers," *Green Chemistry,* vol. 21, no. 22, pp. 6210-6219, 2019.

[333] H. Liu, T.-H. Lee, Y. Chen, E. W. Cochran, and W. Li, "Paired electrolysis of 5-(hydroxymethyl) furfural in flow cells with a high-performance oxide-derived silver cathode," *Green Chemistry,* vol. 23, no. 14, pp. 5056-5063, 2021.

[334] C. Moreau, M. N. Belgacem, and A. Gandini, "Recent Catalytic Advances in the Chemistry of Substituted Furans from Carbohydrates and in the Ensuing Polymers," *Topics in Catalysis,* vol. 27, 2004.

[335] L. Xin *et al.*, "Electricity Storage in Biofuels: Selective Electrocatalytic Reduction of Levulinic Acid to Valeric Acid or γ-Valerolactone," *ChemSusChem,* vol. 6, no. 4, pp. 674-686, 2013.

[336] Y. Du, X. Chen, J. Qi, P. Wang, and C. Liang, "Synthesis of valeric acid by selective electrocatalytic hydrogenation of biomass-derived levulinic acid," *Catalysts,* vol. 10, no. 6, pp. 692, 2020.

[337] P. Nilges, T. R. dos Santos, F. Harnisch, and U. Schröder, "Electrochemistry for biofuel generation: Electrochemical conversion of levulinic acid to octane," *Energy & Environmental Science,* vol. 5, no. 1, pp. 5231-5235, 2012.

[338] P. Du, J. Zhang, Y. Liu, and M. Huang, "Hydrogen generation from catalytic glucose oxidation by Fe-based electrocatalysts," *Electrochemistry Communications,* vol. 83, pp. 11-15, 2017.

[339] T. Rafaïdeen, S. Baranton, and C. Coutanceau, "Highly efficient and selective electrooxidation of glucose and xylose in alkaline medium at carbon supported alloyed PdAu nanocatalysts," *Applied Catalysis B: Environmental,* vol. 243, pp. 641-656, 2019.

[340] T. Rafaïdeen, N. Neha, B. R. S. Kouamé, S. Baranton, and C. Coutanceau, "Electroreforming of Glucose and Xylose in Alkaline Medium at Carbon Supported Alloyed Pd3Au7 Nanocatalysts: Effect of Aldose Concentration and Electrolysis Cell Voltage," *Clean Technologies,* vol. 2, no. 2, pp. 13, 2020.

[341] C. Lin *et al.*, "Engineered porous Co–Ni alloy on carbon cloth as an efficient bifunctional electrocatalyst for glucose electrolysis in alkaline environment," *Journal of Alloys and Compounds,* vol. 823, pp. 153784, 2020.

[342] C. Lin *et al.*, "Boosting water electrolysis with anodic glucose oxidation reaction over engineered cobalt nickel hydroxide nanosheet on carbon cloth," *Journal of Electroanalytical Chemistry,* vol. 861, pp. 113946, 2020.

[343] X. Liu, P. Cai, G. Wang, and Z. Wen, "Nickel doped MoS2 nanoparticles as precious-metal free bifunctional electrocatalysts for glucose assisted electrolytic H2 generation," *International Journal of Hydrogen Energy,* vol. 45, no. 58, pp. 32940-32948, 2020.

[344] D. Zheng *et al.*, "Three-birds-with-one-stone electrolysis for energy-efficiency production of gluconate and hydrogen," *Applied Catalysis B: Environmental,* vol. 277, pp. 119178, 2020.

[345] Y. Ding, M. Greiner, R. Schlögl, and S. Heumann, "A Metal‐Free Electrode: From Biomass‐Derived Carbon to Hydrogen," *ChemSusChem,* vol. 13, no. 16, pp. 4064-4068, 2020.
[346] C. Yang *et al.*, "Refining d-band center in Ni0. 85Se by Mo doping: A strategy for boosting hydrogen generation via coupling electrocatalytic oxidation 5-hydroxymethylfurfural," *Chemical Engineering Journal,* vol. 422, pp. 130125, 2021.
[347] N. Jiang, B. You, R. Boonstra, I. M. Terrero Rodriguez, and Y. Sun, "Integrating electrocatalytic 5-hydroxymethylfurfural oxidation and hydrogen production via Co–P-derived electrocatalysts," *ACS Energy Letters,* vol. 1, no. 2, pp. 386-390, 2016.
[348] K. Fan *et al.*, "Nickel–vanadium monolayer double hydroxide for efficient electrochemical water oxidation," *Nature communications,* vol. 7, no. 1, pp. 1-9, 2016.
[349] S. Liang *et al.*, "Ni3N-V2O3 enables highly efficient 5-(Hydroxymethyl) furfural oxidation enabling membrane free hydrogen production," *Chemical Engineering Journal,* vol. 415, pp. 128864, 2021.
[350] N. Kurig, J. r. m. Meyers, F. J. Holzhäuser, S. Palkovits, and R. Palkovits, "(Non-) Kolbe Chemistry Going with the Flow: The Continuous Electrolysis of Biogenic Acids," *ACS Sustainable Chemistry & Engineering,* vol. 9, no. 3, pp. 1229-1234, 2020.
[351] B. You, N. Jiang, M. Sheng, M. W. Bhushan, and Y. Sun, "Hierarchically Porous Urchin-Like Ni2P Superstructures Supported on Nickel Foam as Efficient Bifunctional Electrocatalysts for Overall Water Splitting," *ACS Catalysis,* vol. 6, no. 2, pp. 714-721, 2016.
[352] H. K. Goering and P. J. Van Soest, *Forage fiber analyses (apparatus, reagents, procedures, and some applications)* (no. 379). US Agricultural Research Service, 1970.
[353] P. v. Van Soest, J. B. Robertson, and B. A. Lewis, "Methods for dietary fiber, neutral detergent fiber, and nonstarch polysaccharides in relation to animal nutrition," *Journal of dairy science,* vol. 74, no. 10, pp. 3583-3597, 1991.
[354] D. Mertens, "Critical conditions in determining detergent fibers," *Proceedings of the forage analysis workshop*, pp. C1-C8, 1992.
[355] A. Sluiter *et al.*, "Determination of structural carbohydrates and lignin in biomass," *Laboratory analytical procedure,* vol. 1617, no. 1, pp. 1-16, 2008.
[356] C. Kuchelmeister and S. Bauer, "Rapid small-scale determination of extractives in biomass," *BioEnergy Research,* vol. 8, pp. 68-76, 2015.
[357] W. Ni *et al.*, "Hierarchical foam of exposed ultrathin nickel nanosheets supported on chainlike Ni-nanowires and the derivative chalcogenide for enhanced pseudocapacitance," *Nanoscale,* vol. 6, no. 5, pp. 2618-2623, 2014.
[358] A. S. Zaky, N. Pensupa, Á. Andrade-Eiroa, G. A. Tucker, and C. Du, "A new HPLC method for simultaneously measuring chloride, sugars, organic acids and alcohols in food samples," *Journal of Food Composition and Analysis,* vol. 56, pp. 25-33, 2017.
[359] I. ISO, "14040," *Environmental management—life cycle assessment—principles and framework,* pp. 235-248, 2006.
[360] M. Finkbeiner, A. Inaba, R. Tan, K. Christiansen, and H.-J. Klüppel, "The new international standards for life cycle assessment: ISO 14040 and ISO 14044," *The international journal of life cycle assessment,* vol. 11, pp. 80-85, 2006.
[361] W. A. Pippo, C. A. Luengo, L. A. M. Alberteris, P. Garzone, and G. Cornacchia, "Energy recovery from sugarcane-trash in the light of 2nd generation biofuels. Part 1: current situation and environmental aspects," *Waste and Biomass Valorization,* vol. 2, no. 1, pp. 1-16, 2011.
[362] P. Chindaprasirt and U. Rattanasak, "Eco-production of silica from sugarcane bagasse ash for use as a photochromic pigment filler," *Scientific Reports,* vol. 10, no. 1, pp. 9890, 2020.

[363] "Sphera Solutions GmbH, GaBi LCA Database Documentation." https://gabi.sphera.com/databases/gabi-data-search/ (accessed 12-12, 2022).
[364] G. Wernet, C. Bauer, B. Steubing, J. Reinhard, E. Moreno-Ruiz, and B. Weidema, "The ecoinvent database version 3 (part I): overview and methodology," *The International Journal of Life Cycle Assessment,* vol. 21, pp. 1218-1230, 2016.
[365] C. Schulze, S. Thiede, and C. Herrmann, "Life cycle assessment of industrial cooling towers," *Progress in Life Cycle Assessment,* pp. 135-146, 2019.
[366] M. M. Parascanu, M. Kaltschmitt, A. Rödl, G. Soreanu, and L. Sánchez-Silva, "Life cycle assessment of electricity generation from combustion and gasification of biomass in Mexico," *Sustainable production and consumption,* vol. 27, pp. 72-85, 2021.
[367] G. Tchobanoglous, *Integrated solid waste managementengineering principles and management issues*, no. 628 T3, 1993.
[368] S. H. Ko and C. P. Grigoropoulos, *Hierarchical nanostructures for energy devices*. Royal Society of Chemistry, 2014.
[369] H. Sun, Y. Ye, Z. Tian, S. Wu, J. Liu, and C. Liang, "Ni^{3+} doped cobalt–nickel layered double hydroxides as high-performance electrode materials for supercapacitors," *RSC advances,* vol. 7, no. 77, pp. 49010-49014, 2017.
[370] A. P. Grosvenor, M. C. Biesinger, R. S. C. Smart, and N. S. McIntyre, "New interpretations of XPS spectra of nickel metal and oxides," *Surface Science,* vol. 600, no. 9, pp. 1771-1779, 2006.
[371] N. Weidler *et al.*, "X-ray photoelectron spectroscopic investigation of plasma-enhanced chemical vapor deposited NiOx, NiOx(OH)y, and CoNiOx(OH)y: influence of the chemical composition on the catalytic activity for the oxygen evolution reaction," *The Journal of Physical Chemistry C,* vol. 121, no. 12, pp. 6455-6463, 2017.
[372] M. Pan *et al.*, "Low-crystalline Ni/Co-oxyhydroxides nanoarrays on carbon cloth with high mass loading and hierarchical structure as cathode for supercapacitors," *Electrochimica Acta,* vol. 357, pp. 136886, 2020.
[373] K. O. Iwu, A. Lombardo, R. Sanz, S. Scirè, and S. Mirabella, "Facile synthesis of Ni nanofoam for flexible and low-cost non-enzymatic glucose sensing," *Sensors and Actuators B: Chemical,* vol. 224, pp. 764-771, 2016.
[374] H. Liu, X. Wu, B. Yang, Z. Li, L. Lei, and X. Zhang, "Three-dimensional porous NiO nanosheets vertically grown on graphite disks for enhanced performance non-enzymatic glucose sensor," *Electrochimica Acta,* vol. 174, pp. 745-752, 2015.
[375] Y. Wu, H. Wang, S. Ji, B. G. Pollet, X. Wang, and R. Wang, "Engineered porous Ni 2 P-nanoparticle/Ni 2 P-nanosheet arrays via the Kirkendall effect and Ostwald ripening towards efficient overall water splitting," *Nano Research,* vol. 13, pp. 2098-2105, 2020.
[376] G. D. Brown, J. Bauer, H. M. Osborn, and R. Kuemmerle, "A solution NMR approach to determine the chemical structures of carbohydrates using the hydroxyl groups as starting points," *ACS omega,* vol. 3, no. 12, pp. 17957-17975, 2018.
[377] T. Runge and C. Zhang, "Two-stage acid-catalyzed conversion of carbohydrates into levulinic acid," *Industrial & engineering chemistry research,* vol. 51, no. 8, pp. 3265-3270, 2012.
[378] Z.-H. Liu *et al.*, "Synergistic maximization of the carbohydrate output and lignin processability by combinatorial pretreatment," *Green Chemistry,* vol. 19, no. 20, pp. 4939-4955, 2017.
[379] L. Xu, S.-J. Zhang, C. Zhong, B.-Z. Li, and Y.-J. Yuan, "Alkali-based pretreatment-facilitated lignin valorization: a review," *Industrial & Engineering Chemistry Research,* vol. 59, no. 39, pp. 16923-16938, 2020.
[380] K. W. Harrison, R. Remick, A. Hoskin, and G. Martin, "Hydrogen production: fundamentals and case study summaries," National Renewable Energy Lab.(NREL), Golden, CO (United States), 2010.

[381] B. Mondal *et al.*, "Unraveling the Mechanisms of Electrocatalytic Oxygenation and Dehydrogenation of Organic Molecules to Value‐Added Chemicals Over a Ni–Fe Oxide Catalyst," *Advanced Energy Materials,* vol. 11, no. 37, pp. 2101858, 2021.

[382] H. Luo *et al.*, "Role of Ni in PtNi Bimetallic Electrocatalysts for Hydrogen and Value-Added Chemicals Coproduction via Glycerol Electrooxidation," *ACS catalysis,* vol. 12, no. 23, pp. 14492-14506, 2022.

[383] M. Nakayama, K. Suzuki, and K. Fujii, "Single-ion catalyst of Ni^{2+} anchored in the interlayer space of layered MnO2 for electro-oxidation of ethanol in alkaline electrolyte," *Electrochemistry Communications,* vol. 105, pp. 106492, 2019.

[384] W. Chen *et al.*, "Unraveling the electrophilic oxygen-mediated mechanism for alcohol electrooxidation on NiO," *National Science Review,* vol. 10, no. 5, pp. nwad099, 2023.

[385] Y. Miao *et al.*, "Electrocatalysis and electroanalysis of nickel, its oxides, hydroxides and oxyhydroxides toward small molecules," *Biosensors and Bioelectronics,* vol. 53, pp. 428-439, 2014.

[386] S. Medway, C. Lucas, A. Kowal, R. Nichols, and D. Johnson, "In situ studies of the oxidation of nickel electrodes in alkaline solution," *Journal of Electroanalytical Chemistry,* vol. 587, no. 1, pp. 172-181, 2006.

[387] Q. Xiang, Y. Y. Lee, and R. W. Torget, "Kinetics of glucose decomposition during dilute-acid hydrolysis of lignocellulosic biomass," *Proceedings of the Twenty-Fifth Symposium on Biotechnology for Fuels and Chemicals Held May 4–7, 2003, in Breckenridge, CO*, pp. 1127-1138, 2004.

[388] M. Shamsipur, M. Najafi, and M.-R. M. Hosseini, "Highly improved electrooxidation of glucose at a nickel (II) oxide/multi-walled carbon nanotube modified glassy carbon electrode," *Bioelectrochemistry,* vol. 77, no. 2, pp. 120-124, 2010.

[389] I. Danaee, M. Jafarian, F. Forouzandeh, F. Gobal, and M. Mahjani, "Impedance spectroscopy analysis of glucose electro-oxidation on Ni-modified glassy carbon electrode," *Electrochimica acta,* vol. 53, no. 22, pp. 6602-6609, 2008.

[390] P. Parpot, K. Servat, A. Bettencourt, H. Huser, and K. Kokoh, "TEMPO mediated oxidation of carbohydrates using electrochemical methods," *Cellulose,* vol. 17, pp. 815-824, 2010.

[391] T. Hibino, K. Kobayashi, P. Lv, M. Nagao, and S. Teranishi, "High performance anode for direct cellulosic biomass fuel cells operating at intermediate temperatures," *Bulletin of the Chemical Society of Japan,* vol. 90, no. 9, pp. 1017-1026, 2017.

[392] V. Muiuane, M. Ferreira, P. Bignet, A. Bettencourt, and P. Parpot, "Production of formic acid from biomass-based compounds using a filter press type electrolyzer," *Journal of Environmental Chemical Engineering,* vol. 1, no. 4, pp. 1237-1244, 2013.

[393] A. Lasia, "Electrochemical impedance spectroscopy and its applications," *Modern aspects of electrochemistry*, pp. 143-248, 2002.

[394] S. Cheng, J. Zhang, M. Zhao, and C. Cao, "Electrochemical impedance spectroscopy study of Ni/MH batteries," *Journal of alloys and compounds,* vol. 293, pp. 814-820, 1999.

[395] W. Zheng, Y. Li, and L. Y. S. Lee, "Insights into the transition metal ion-mediated electrooxidation of glucose in alkaline electrolyte," *Electrochimica Acta,* vol. 308, pp. 9-19, 2019.

[396] M. Tominaga *et al.*, "Electrocatalytic oxidation of glucose at gold–silver alloy, silver and gold nanoparticles in an alkaline solution," *Journal of Electroanalytical Chemistry,* vol. 590, no. 1, pp. 37-46, 2006.

[397] J. M. Macleod and L. R. Schroeder, "Alkaline Degradation of Cellobiose, 3.6-Anhydro-4-O-(β-D-Gluc0pyranosyl)-D-Glucose, 3, 6-Anhydr0-4-0-Methyl-D-Glucose, and D-Glucose1," *Journal of Wood Chemistry and Technology,* vol. 2, no. 2, pp. 187-205, 1982.

[398] J. De Bruijn, A. Kieboom, and H. Van Bekkum, "Alkaline degradation of monosaccharides V: Kinetics of the alkaline isomerization and degradation of

monosaccharides," *Recueil des Travaux Chimiques des Pays‐Bas,* vol. 106, no. 2, pp. 35-43, 1987.
[399] A. Takagaki, W. Obata, and T. Ishihara, "Oxidative conversion of glucose to formic acid as a renewable hydrogen source using an abundant solid base catalyst," *ChemistryOpen,* vol. 10, no. 10, pp. 954-959, 2021.
[400] J. F. Mendicino, "Effect of borate on the alkali-catalyzed isomerization of sugars1," *Journal of the American Chemical Society,* vol. 82, no. 18, pp. 4975-4979, 1960.
[401] J. C. Speck Jr, "The lobry de Bruyn-Alberda van Ekenstein transformation," *Advances in carbohydrate chemistry*, vol. 13, pp. 63-103, 1958.
[402] V. Raeva and O. Gromova, "Separation of water–formic acid–acetic acid mixtures in the presence of sulfolane," *Fine Chemical Technologies,* vol. 14, no. 4, pp. 24-32, 2019.
[403] J. Feng *et al.*, "Selective catalytic conversion of waste lignocellulosic biomass for renewable value-added chemicals via directional microwave-assisted liquefaction," *Sustainable Energy & Fuels,* vol. 2, no. 5, pp. 1035-1047, 2018.
[404] C. Schädel, A. Blöchl, A. Richter, and G. Hoch, "Quantification and monosaccharide composition of hemicelluloses from different plant functional types," *Plant physiology and Biochemistry,* vol. 48, no. 1, pp. 1-8, 2010.
[405] H. Chen, C. Ferrari, M. Angiuli, J. Yao, C. Raspi, and E. Bramanti, "Qualitative and quantitative analysis of wood samples by Fourier transform infrared spectroscopy and multivariate analysis," *Carbohydrate polymers,* vol. 82, no. 3, pp. 772-778, 2010.
[406] R. Weingarten, J. Cho, W. C. Conner Jr, and G. W. Huber, "Kinetics of furfural production by dehydration of xylose in a biphasic reactor with microwave heating," *Green Chemistry,* vol. 12, no. 8, pp. 1423-1429, 2010.
[407] X. Qi, M. Watanabe, T. M. Aida, and R. L. Smith Jr, "Catalytic dehydration of fructose into 5-hydroxymethylfurfural by ion-exchange resin in mixed-aqueous system by microwave heating," *Green Chemistry,* vol. 10, no. 7, pp. 799-805, 2008.
[408] H. Li, A. Saeed, M. S. Jahan, Y. Ni, and A. van Heiningen, "Hemicellulose removal from hardwood chips in the pre-hydrolysis step of the kraft-based dissolving pulp production process," *Journal of Wood Chemistry and Technology,* vol. 30, no. 1, pp. 48-60, 2010.
[409] M. Orazov and M. E. Davis, "Tandem catalysis for the production of alkyl lactates from ketohexoses at moderate temperatures," *Proceedings of the National Academy of Sciences,* vol. 112, no. 38, pp. 11777-11782, 2015.
[410] P. Fongarland, N. Essayem, and F. Rataboul, "Noncatalyzed liquefaction of celluloses in hydrothermal conditions: Influence of reactant physicochemical characteristics and modeling studies," *Industrial & Engineering Chemistry Research,* vol. 56, no. 1, pp. 126-134, 2017.
[411] J. Li *et al.*, "Biochar from microwave pyrolysis of biomass: A review," *Biomass and Bioenergy,* vol. 94, pp. 228-244, 2016.
[412] D. Fuerstenau and A.-Z. Abouzeid, "The energy efficiency of ball milling in comminution," *International Journal of Mineral Processing,* vol. 67, no. 1-4, pp. 161-185, 2002.
[413] N. Katsu, T. Endo, and Y. Teramoto, "Evaluation of the average state of carbohydrate/lignin coexistence in wood by analysis of molecular motion," *Cellulose,* vol. 27, pp. 41-56, 2020.
[414] N. Terinte, R. Ibbett, and K. C. Schuster, "Overview on native cellulose and microcrystalline cellulose I structure studied by X-ray diffraction (WAXD): Comparison between measurement techniques," *Lenzinger Berichte,* vol. 89, no. 1, pp. 118-131, 2011.
[415] D. Ciolacu, F. Ciolacu, and V. I. Popa, "Amorphous cellulose—structure and characterization," *Cellulose chemistry and technology,* vol. 45, no.1, pp. 13, 2011.

[416] K. Chandrasekhar, Y.-J. Lee, and D.-W. Lee, "Biohydrogen production: strategies to improve process efficiency through microbial routes," *International journal of molecular sciences,* vol. 16, no. 4, pp. 8266-8293, 2015.
[417] X. Hu *et al.*, "Acid-catalyzed conversion of mono-and poly-sugars into platform chemicals: Effects of molecular structure of sugar substrate," *Bioresource technology,* vol. 133, pp. 469-474, 2013.
[418] T. W. Ching, V. Haritos, and A. Tanksale, "Microwave assisted conversion of microcrystalline cellulose into value added chemicals using dilute acid catalyst," *Carbohydrate polymers,* vol. 157, pp. 1794-1800, 2017.
[419] M. Österberg, M. H. Sipponen, B. D. Mattos, and O. J. Rojas, "Spherical lignin particles: A review on their sustainability and applications," *Green Chemistry,* vol. 22, no. 9, pp. 2712-2733, 2020.
[420] C. Zhang and T. Runge, "Fractionating pentosans and hexosans in hybrid poplar," *Industrial & engineering chemistry research,* vol. 51, no. 1, pp. 133-139, 2012.
[421] I. Dávila, P. Gullón, and J. Labidi, "Influence of the heating mechanism during the aqueous processing of vine shoots for the obtaining of hemicellulosic oligosaccharides," *Waste Management,* vol. 120, pp. 146-155, 2021.
[422] B. Y. Yang and R. Montgomery, "Alkaline degradation of invert sugar from molasses," *Bioresource technology,* vol. 98, no. 16, pp. 3084-3089, 2007.
[423] C. M. Brands and M. A. van Boekel, "Reactions of monosaccharides during heating of sugar− casein systems: Building of a reaction network model," *Journal of Agricultural and Food Chemistry,* vol. 49, no. 10, pp. 4667-4675, 2001.
[424] S. Raharja, L. Rigal, L. Barre, and P. Vidal, "Design of a continuous process for the alkaline treatment of xylose into lactic acid," *The Canadian journal of chemical engineering,* vol. 75, no. 5, pp. 913-920, 1997.
[425] Z. Shen *et al.*, "Effect of alkaline catalysts on hydrothermal conversion of glycerin into lactic acid," *Industrial & Engineering Chemistry Research,* vol. 48, no. 19, pp. 8920-8925, 2009.
[426] P. Abba, J. Gongwala, S. Laminsi, and J. Brisset, "The effect of the humid air plasma on the conductivity of distilled water: contribution of ions," *International Journal of Research in Chemistry and Environment (IJRCE),* vol. 4, no. 1, pp. 25-30, 2014.
[427] R. Gilliam, J. Graydon, D. Kirk, and S. Thorpe, "A review of specific conductivities of potassium hydroxide solutions for various concentrations and temperatures," *International Journal of Hydrogen Energy,* vol. 32, no. 3, pp. 359-364, 2007.
[428] Z. K. Goldsmith *et al.*, "Characterization of NiFe oxyhydroxide electrocatalysts by integrated electronic structure calculations and spectroelectrochemistry," *Proceedings of the National Academy of Sciences,* vol. 114, no. 12, pp. 3050-3055, 2017.
[429] R. W. Truss, B. Wood, and R. Rasch, "Quantitative surface analysis of hemp fibers using XPS, conventional and low voltage in‐lens SEM," *Journal of Applied Polymer Science,* vol. 133, no. 8, 2016.
[430] A. Shchukarev, B. Sundberg, E. Mellerowicz, and P. Persson, "XPS study of living tree," *Surface and Interface Analysis: An International Journal devoted to the development and application of techniques for the analysis of surfaces, interfaces and thin films,* vol. 34, no. 1, pp. 284-288, 2002.
[431] D. Sedan *et al.*, "Effect of calcium rich and alkaline solutions on the chemical behaviour of hemp fibres," *Journal of Materials Science,* vol. 42, pp. 9336-9342, 2007.
[432] X. Zhang *et al.*, "Large-scale synthesis of three-dimensional reduced graphene oxide/nitrogen-doped carbon nanotube heteronanostructures as highly efficient electromagnetic wave absorbing materials," *ACS applied materials & interfaces,* vol. 11, no. 42, pp. 39100-39108, 2019.

[433] H. Guo *et al.*, "Engineering phase transformation of MoS2/RGO by N-doping as an excellent microwave absorber," *ACS applied materials & interfaces,* vol. 12, no. 14, pp. 16831-16840, 2020.
[434] E. Domínguez, T. Nóvoa, P. G. del Río, G. Garrote, and A. Romaní, "Sequential two-stage autohydrolysis biorefinery for the production of bioethanol from fast-growing Paulownia biomass," *Energy Conversion and Management,* vol. 226, pp. 113517, 2020.
[435] P. G. del Río, A. Pérez-Pérez, G. Garrote, and B. Gullón, "Manufacturing of hemicellulosic oligosaccharides from fast-growing Paulownia wood via autohydrolysis: Microwave versus conventional heating," *Industrial Crops and Products,* vol. 187, pp. 115313, 2022.
[436] F. Rego, A. P. S. Dias, M. Casquilho, F. C. Rosa, and A. Rodrigues, "Fast determination of lignocellulosic composition of poplar biomass by thermogravimetry," *Biomass and bioenergy,* vol. 122, pp. 375-380, 2019.
[437] P.-L. Tang, P. M. Abdul, N. S. Engliman, and O. Hassan, "Effects of pretreatment and enzyme cocktail composition on the sugars production from oil palm empty fruit bunch fiber (OPEFBF)," *Cellulose,* vol. 25, pp. 4677-4694, 2018.
[438] O. Dahlman, A. Jacobs, and J. Sjöberg, "Molecular properties of hemicelluloses located in the surface and inner layers of hardwood and softwood pulps," *Cellulose,* vol. 10, pp. 325-334, 2003.
[439] S. Zhou, Y. Xue, A. Sharma, and X. Bai, "Lignin valorization through thermochemical conversion: comparison of hardwood, softwood and herbaceous lignin," *ACS Sustainable Chemistry & Engineering,* vol. 4, no. 12, pp. 6608-6617, 2016.
[440] Y. Li, X. Zhang, Z. Li, J. Song, and X. Wang, "Full Utilization of Lignocellulose with Ionic Liquid Polyoxometalates in a One - Pot Three - Step Conversion," *ChemSusChem,* vol. 12, no. 22, pp. 4936-4945, 2019.
[441] Y. Jia *et al.*, "Electrocatalytic degradation of rice straw lignin in alkaline solution through oxidation on a Ti/SnO 2–Sb 2 O 3/α-PbO 2/β-PbO 2 anode and reduction on an iron or tin doped titanium cathode," *Catalysis Science & Technology,* vol. 8, no. 18, pp. 4665-4677, 2018.
[442] R. Ghahremani, F. Farales, F. Bateni, and J. A. Staser, "Simultaneous hydrogen evolution and lignin depolymerization using NiSn electrocatalysts in a biomass-depolarized electrolyzer," *Journal of The Electrochemical Society,* vol. 167, no. 4, pp. 043502, 2020.
[443] D. Di Marino *et al.*, "Carboxylic acids production via electrochemical depolymerization of lignin," *ChemElectroChem,* vol. 6, no. 5, pp. 1434-1442, 2019.
[444] C. Lan, H. Fan, Y. Shang, D. Shen, and G. Li, "Electrochemically catalyzed conversion of cornstalk lignin to aromatic compounds: an integrated process of anodic oxidation of a Pb/PbO 2 electrode and hydrogenation of a nickel cathode in sodium hydroxide solution," *Sustainable Energy & Fuels,* vol. 4, no. 4, pp. 1828-1836, 2020.
[445] T. Renders, S. Van den Bosch, S.-F. Koelewijn, W. Schutyser, and B. Sels, "Lignin-first biomass fractionation: the advent of active stabilisation strategies," *Energy & environmental science,* vol. 10, no. 7, pp. 1551-1557, 2017.
[446] X. Luo, Z. Gong, G. Yang, L. Huang, L. Chen, and L. Shuai, "In-situ oxidation/reduction facilitates one-pot conversion of lignocellulosic biomass to bulk chemicals in alkaline solution," *Chemical Engineering Journal,* vol. 429, pp. 132365, 2022.
[447] L. Ostervold, S. I. P. Bakovic, J. Hestekin, and L. F. Greenlee, "Electrochemical biomass upgrading: degradation of glucose to lactic acid on a copper (II) electrode," *RSC advances,* vol. 11, no. 50, pp. 31208-31218, 2021.
[448] N. A. Ahmed, M. Miyatake, and A. Al-Othman, "Power fluctuations suppression of stand-alone hybrid generation combining solar photovoltaic/wind turbine and fuel cell systems," *Energy Conversion and management,* vol. 49, no. 10, pp. 2711-2719, 2008.

[449] W. Zhang, Y. Wang, P. Xu, D. Li, and B. Liu, "DC-bus voltage balancing control for 3-level DC/DC converters in renewable generation systems," *Energy Reports,* vol. 9, pp. 210-217, 2023.
[450] Y. Qin *et al.*, "Lithium-ion batteries under pulsed current operation to stabilize future grids," *Cell Reports Physical Science,* vol. 3, no. 1, 2022.
[451] Y. Holade *et al.*, "Recent advances in the electrooxidation of biomass-based organic molecules for energy, chemicals and hydrogen production," *Catalysis Science & Technology,* vol. 10, no. 10, pp. 3071-3112, 2020.
[452] R. Latsuzbaia *et al.*, "Continuous electrochemical oxidation of biomass derived 5-(hydroxymethyl) furfural into 2, 5-furandicarboxylic acid," *Journal of Applied Electrochemistry,* vol. 48, pp. 611-626, 2018.
[453] H. Zhou *et al.*, "Scalable electrosynthesis of commodity chemicals from biomass by suppressing non-Faradaic transformations," *Nature Communications,* vol. 14, no. 1, pp. 5621, 2023.
[454] L. Lin, X. Han, B. Han, and S. Yang, "Emerging heterogeneous catalysts for biomass conversion: studies of the reaction mechanism," *Chemical Society Reviews,* vol. 50, no. 20, pp. 11270-11292, 2021.
[455] G. R. Akien, L. Qi, and I. T. Horváth, "Molecular mapping of the acid catalysed dehydration of fructose," *Chemical Communications,* vol. 48, no. 47, pp. 5850-5852, 2012.
[456] T. Blasco, "Insights into reaction mechanisms in heterogeneous catalysis revealed by in situ NMR spectroscopy," *Chemical Society Reviews,* vol. 39, no. 12, pp. 4685-4702, 2010.
[457] B. T. W. Lo, L. Ye, and S. C. E. Tsang, "The contribution of synchrotron X-ray powder diffraction to modern zeolite applications: a mini-review and prospects," *Chem,* vol. 4, no. 8, pp. 1778-1808, 2018.
[458] M. A. Newton and W. van Beek, "Combining synchrotron-based X-ray techniques with vibrational spectroscopies for the in situ study of heterogeneous catalysts: a view from a bridge," *Chemical Society Reviews,* vol. 39, no. 12, pp. 4845-4863, 2010.
[459] L. Lin *et al.*, "Quantitative production of butenes from biomass-derived γ-valerolactone catalysed by hetero-atomic MFI zeolite," *Nature materials,* vol. 19, no. 1, pp. 86-93, 2020.
[460] S. Zhou, K. Jin, and M. J. Buehler, "Understanding plant biomass via computational modeling," *Advanced Materials,* vol. 33, no. 28, pp. 2003206, 2021.
[461] D. Xu *et al.*, "Microwave pyrolysis of biomass model compounds for bio-oil: Formation mechanisms of the nitrogenous chemicals and DFT calculations," *Energy Conversion and Management,* vol. 262, pp. 115676, 2022.
[462] T.-I. Lafka, V. Sinanoglou, and E. S. Lazos, "On the extraction and antioxidant activity of phenolic compounds from winery wastes," *Food chemistry,* vol. 104, no. 3, pp. 1206-1214, 2007.
[463] D. Yalcin, O. Ozcalik, E. Altiok, and O. Bayraktar, "Characterization and recovery of tartaric acid from wastes of wine and grape juice industries," *Journal of thermal analysis and calorimetry,* vol. 94, no. 3, pp. 767-771, 2008.
[464] J. A. Mendes, A. M. Xavier, D. V. Evtuguin, and L. P. Lopes, "Integrated utilization of grape skins from white grape pomaces," *Industrial crops and products,* vol. 49, pp. 286-291, 2013.
[465] R. A. Muhlack, R. Potumarthi, and D. W. Jeffery, "Sustainable wineries through waste valorisation: A review of grape marc utilisation for value-added products," *Waste management,* vol. 72, pp. 99-118, 2018.